uOttawa

L'Université canadienne
Canada's university

FACULTÉ DES ÉTUDES SUPÉRIEURES ET POSTOCTORALES

uOttawa

L'Université canadienne
Canada's university

FACULTY OF GRADUATE AND POSDOCTORAL STUDIES

Sébastien Monfette
AUTEUR DE LA THÈSE / AUTHOR OF THESIS

Ph.D. (Chemistry)
GRADE / DEGREE

Department of Chemistry
FACULTÉ, ÉCOLE, DÉPARTEMENT / FACULTY, SCHOOL, DEPARTMENT

Exploration of Ligand Effects, Substrate Effects and Reactor Effects on Macrocyclization via Ring-Closing Metathesis: A Rational Approach to Efficient Cyclization

TITRE DE LA THÈSE / TITLE OF THESIS

Deryn Fogg
DIRECTEUR (DIRECTRICE) DE LA THÈSE / THESIS SUPERVISOR

CO-DIRECTEUR (CO-DIRECTRICE) DE LA THÈSE / THESIS CO-SUPERVISOR

Tom Baker

Robert Crutchley

SonBinh Nguyen
Northwestern University

Sandro Gambarotta

Gary W. Slater
Le Doyen de la Faculté des études supérieures et postdoctorales / Dean of the Faculty of Graduate and Postdoctoral Studies

Exploration of Ligand Effects, Substrate Effects and Reactor Effects on Macrocyclization via Ring-Closing Metathesis: A Rational Approach to Efficient Cyclization

Sebastien Monfette

Thesis submitted to the
Faculty of Graduate and Postdoctoral Studies
In partial fulfillment of the requirements for the degree of

Doctor of Philosophy

Ottawa-Carleton Chemistry Institute
Faculty of Science
University of Ottawa

Your file Votre référence
ISBN: 978-0-494-79726-6
Our file Notre référence
ISBN: 978-0-494-79726-6

Table of contents

List of figures

Chapter 1

Chapter 2

Chapter 3

Chapter 5

Chapter 6

Appendix B

List of schemes

Chapter 1

Chapter 3

Chapter 4

Chapter 5

Chapter 6

List of charts

Chapter 1

Chapter 3

Chapter 4

Chapter 5

Chapter 6

List of tables

Chapter 2

Chapter 3

Chapter 4

Chapter 5

Chapter 6

Appendix A

Abstract

Olefin metathesis is credited with having transformed the way chemists think about the manipulation of C=C bonds, the success-story of which culminated in the highest of accolades to Schrock, Grubbs and Chauvin in 2005. It is, however, difficult to reconcile the groundbreaking effect that olefin metathesis had on organic synthesis, with its limited industrial applications. Nearly twenty years following the publication of the first well-defined Ru metathesis catalyst, the RCM reaction remains largely confined to the research setting. The low turnover numbers achieved by the Grubbs catalyst is the chief limiting factor preventing industrial uptake. Clearly, more efficient catalysts and reaction methodologies are needed to render RCM industrially viable. This thesis describes various approaches towards this goal.

As macrocyclic targets are highly prized in the industry, a mechanistic investigation of their formation by the Grubbs and pseudohalide catalysts was performed. This study revealed that different reaction pathways are operative for different catalysts. While the first-generation catalyst effects RCM macrocyclization by the traditional, direct path, the second-generation catalysts afford macrocyclic products through a concentration dependent oligomerization-backbiting pathway.

The second approach employs structure-activity relationship to examine the effect of the anionic ligands on metathesis activity. This study unambiguously showed, for the first time, that activity correlates with the electron-donating capacity of the anionic ligands. Therefore, incorporation of less electron-withdrawing anionic ligands was sought and the synthesis of nitrogen-bound pseudohalide catalysts was carried out. Gratifyingly, the isocyanate catalyst showed remarkable reactivity at room temperature. Polymers of well-defined chain length and low polydispersity could also be obtained with this catalyst, a task that has so far eluded all of the *O*-bound pseudohalide catalysts.

Lastly, an examination of the effect of the reactor on RCM macrocyclization efficiency was performed. An appropriate choice of continuous-flow reactor resulted in the transformation of RCM efficiency. Much faster reaction kinetics were obtained using continuous-flow reactors. Furthermore, the attainable turnover numbers are one order of magnitude higher than those using the traditional batch setup.

Acknowledgements

First and foremost, the biggest of thanks goes to my supervisor Prof. Deryn Fogg. I can never repay you enough for deciding to ship me over to Victoria, already six years ago. You gave me the bug for research, which you kept strongly alive with your infinite enthusiasm and excitement at the sound of new research results. It was an absolute pleasure to work with you, even when it meant spending 36 hours straight in your office to finalize a certain review. I must thank all my very close friends: Mathieu, Melanie, Dominique, Lyne, Philippe, Olivier, Vincent, Marianne, Julien and Genevieve for keeping me entertained enough so I stayed sane (at least I think so). Miss Blacquiere, you impersonated the closest thing I have to a counterion. I will be forever indebted to your sound judgment and wisdom. I always knew I would get an honest and valuable answer when bouncing any ideas (stupid or not) off you. Dr. Jay Conrad deserves credit for showing me the ropes in the Fogg group as well as...getting me addicted to coffee. The nights at the Acadia House are carved in my memory... and probably on my liver too. To Ken and Heather: thank you for lending me your inflatable mattress on all those nights where driving home was out of the question. Listening to Iron Maiden with Ken before passing out will be remembered for a long time. Big thanks to all the other "Foggies": Nick, Justin, Debbie, Adrien and Matt who made waking up and coming to work fun. Prof. Gorelsky, your commitment to excellence in all aspect of the chemistry (including ethanol-fueled discussions) is a model to follow. Mr. Flood and the staff of the Black Tomato are acknowledged for supplying beverages during those sessions aimed at answering the comments of referee 3. You guys most likely prevented a few fires. Dan Harrison and Prof. Lisa Rosenberg deserve credit for giving me a solid first-lab experience. To the LONZA team: Dr. Dominique Roberge, Markus, Michi and Craig, thank you so much for making my stay in Visp a fantastic learning experience. Nights in downtown Sierre with Dominique and Craig will be hard to forget. As well, I must acknowledge the invaluable experience of Glenn Facey (NMR) as well Scott Dalgarno and Robert McDonald for X-ray analysis. To Dan and Bob of the undergraduate lab, your good nature (and Nutella toasts) made the TA sessions that much more enjoyable. Last but certainly not least, I would like to thank my parents and younger brother for giving me the will and encouragement to go as far as I wanted.

List of abbreviations

ADMET	Acyclic diene metathesis
COD	Cyclooctadiene
CF	Continuous-flow
CM	Cross-metathesis
CMC	Critical monomer concentration
COSY	Correlation spectroscopy
CSTR	Continuous stirred-tank reactor
CT	Charge transfer
DeDAM	Diethyl diallyl malonate
DFT	Density functional theory
DME	1,2-Dimethoxyethane
DMF	*N*,*N*-dimethylformamide
DMSO	Dimethyl sulfoxide
ΔE_{elec}	Electrostatic attractive energy
ΔE_{E}	Total electronic bond energy
ΔE_{orb}	Orbital interaction energy
ΔE_{Pauli}	Electronic repulsion energy
ΔE_{st}	Total steric interaction energy
EDA	Energy decomposition analysis
EM_k	Effective molarity (kinetic)
EM_T	Effective molarity (thermodynamic)
equiv	equivalent
ESI	Electrospray ionization
EtOH	Ethanol
EtOAc	Ethyl acetate
Et_2O	Diethyl ether
FID	Flame-ionization detector
GC	Gas chromatography
GPC	Gel-permeation chromatography
H_2IMes	1,3-bis-(2,4,6-trimethylphenyl)imidazolin-2-ylidene

HMBC	Heteronuclear multiple bond coherence
HMQC	Heteronuclear multiple quantum coherence
HPLC	High-performance liquid chromatography
HR-MS	High-resolution mass spectrometry
IMes	1,3-bis-(2,4,6-trimethylphenyl)imidazol-2-ylidene
IPr	1,3-bis-(2,6-diisopropylphenyl)imidazol-2-ylidene
IR	Infrared
MALDI	Matrix-assisted laser desorption ionization
MeCN	Acetonitrile
MS	Mass spectrometry
NBE	Norbornene
NHC	*N*-heterocyclic carbene
NMR	Nuclear magnetic resonance
PDI	Polydispersity index
ppm	parts per million ($\mu g\ g^{-1}$)
PFR	Plug-flow reactor
py	pyridine
RCM	Ring-closing metathesis
ROM	Ring-opening metathesis
ROMP	Ring-opening metathesis polymerization
R_f	Retention factor
[S]	Substrate concentration
TD-DFT	Time-dependent density functional theory
THF	Tetrahydrofuran
THN	1,2,3,4-Tetrahydronaphthalene
TLC	Thin-layer chromatography
TOF	Turnover frequency
TON	Turnover number
Ts	*p*-Toluene sulfonate
XRD	X-ray diffraction

List of compounds

Organic compounds

1	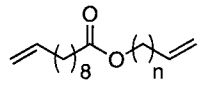 **a** n = 8, **b** n = 4, **c** n = 2	**2**	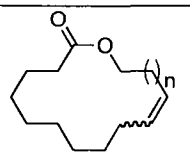 **a** n = 7, **b** n = 3, **c** n = 1
3	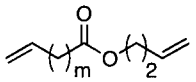 **a** m = 1, **b** m = 4 **c** m = 2	**4**	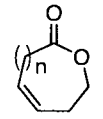 **a** n = 1, **b** n = 4
[4]$_2$	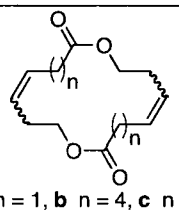 **a** n = 1, **b** n = 4, **c** n = 2	**5**	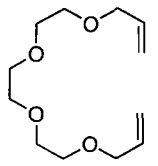
6	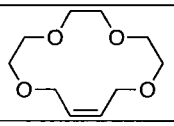	**7**	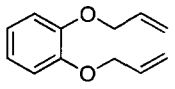
8	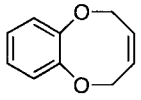	**9**	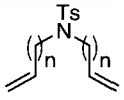 **a** n = 1, **b** n = 2, **c** n = 4
10	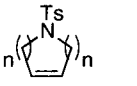 **a** n = 1, **b** n = 2, **c** n = 4	**11**	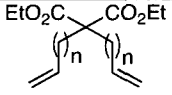 **a** n = 1, **b** n = 2
12	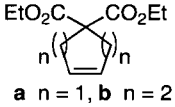 **a** n = 1, **b** n = 2	**13**	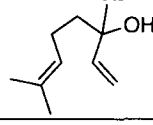
14	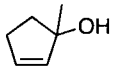	**15**	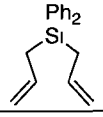
16		**17**	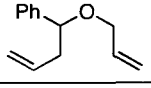
18	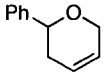	**19**	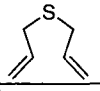
20		**21**	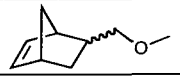

22	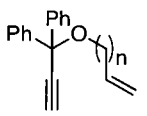 **a**: n = 1; **b**: n = 3	**23**	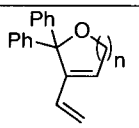 **a**: n = 1 **b**: n = 3
24	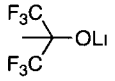	**25**	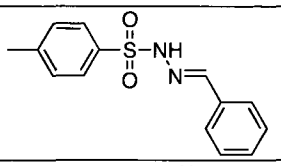
26	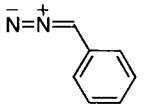	**27**	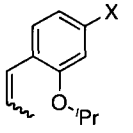 **a**: X = H **b**: X = NO_2
28	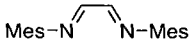	**29**	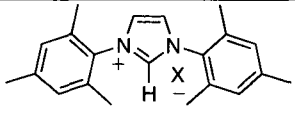 **a**: X = Cl; **b**: X = BF_4
30	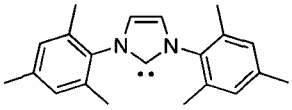	**31**	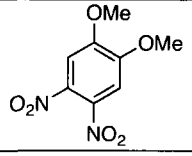
32	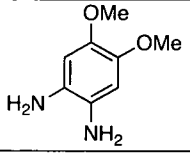	**33**	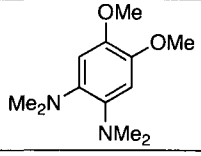
34	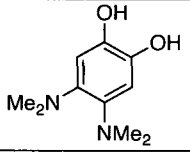	**35**	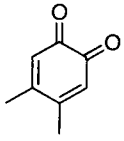
36	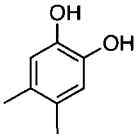	**37**	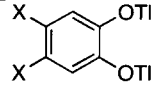 X = **a**: NMe_2; **b**: Me; **c**: Cl; **d**: Br
38	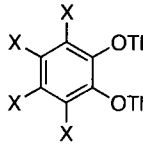 X = **a**: H; **b**: F; **c**: Cl; **d**: Br	**39**	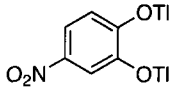
40	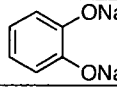		

Organometallic complexes

Ag-1	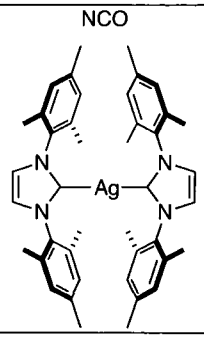	**Mo-1**	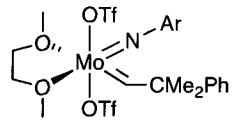 Ar = 2,6-diisopropylphenyl
Mo-2	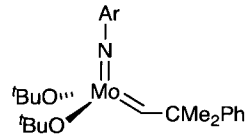 Ar = 2,6-diisopropylphenyl	**Mo-3**	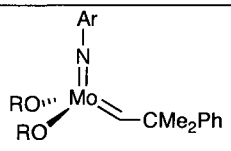 Ar = 2,6-diisopropylphenyl R = $C(CH_3)(CF_3)_2$
Ru-1	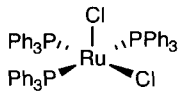	**Ru-2**	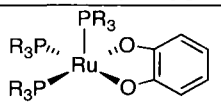 **a** R = Ph **b** R = Me
Ru-3	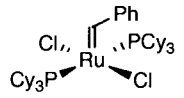	**Ru-4**	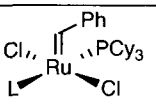 **a** L = IMes **b** L = H_2IMes
Ru-5	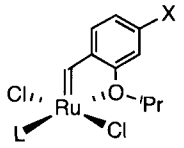 **a** L = IMes, X = H **b** L = H_2IMes, X = H **c** L = H_2IMes, X = NO_2	**Ru-6**	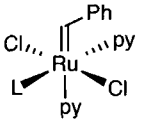 **a** L = IMes **b** L = H_2IMes
Ru-7	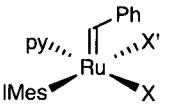 **a** X = X' = OC_6F_5 **b** X = Cl, X' = OC_6Br_5	**Ru-8**	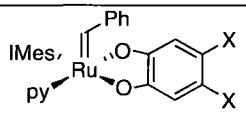 **a** X = Me **b** X = Cl **c** X = Br
Ru-9	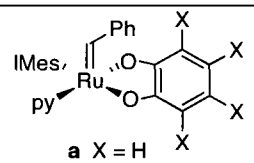 **a** X = H **b** X = F **c** X = Cl **d** X = Br	**Ru-10**	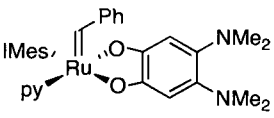

Ru-11	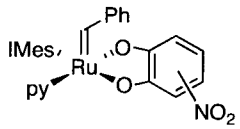	**Ru-12**	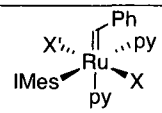 **a**: X = X' = NCS **b**. X = X' = NCO **c**: X = Cl; X' = NCO
Ru-13	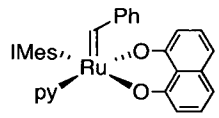	**Ru-14**	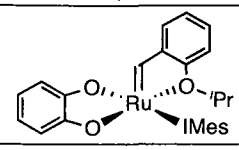

1. Introduction

1.1 Background

Chemistry has a profound impact on our everyday lives.[1] This science supplies the modern world with energy, medicines, foodstuffs and new materials. Despite this, the chemical industry has a very poor public image, due largely to its hazardous and polluting nature.[1] Safer, more energy-efficient, cleaner chemical processes are essential. Reflecting the need for a dramatic change in the chemical industry, the term "Green Chemistry" was coined in 1993 by Anastas of the United States Environmental Protection Agency.[2] The unifying philosophy of green chemistry, "seek prevention, not cure",[1] is now an accepted ideal in both academia and industry. Central to the Twelve Principles of Green Chemistry is the design and development of highly efficient catalytic methodologies.[2] "Greening" industrial processes through catalysis offers compelling potential to significantly reduce waste, relative to traditional stoichiometric processes characterized by large *E* factors (E = kg waste / kg product).[3] Catalysis can also reduce energy requirements for the desired transformations.

Catalytic reactions have been employed for millennia. Over 5,000 years ago, malt enzymes were used to ferment grain into alcohol. The contemporary history of catalysis begins in the mid-18th century.[4] In 1750, it was recognized that nitric acid helped in the synthesis of sulfuric acid, obtained by burning sulfur in humid air. Forty years later, Clement and Desormes discovered that the proportion of nitric acid required could be much reduced by allowing additional air to enter the reactor. The role of nitric acid in catalyzing the reaction was not then understood. Indeed, chemical reactions were thought to occur only when the reactants showed a mutual "affinity" (a term corresponding with fair accuracy to the free energy of reaction). The concept of affinity did not, however, account for the empirical observation that certain reactions only proceeded by addition of specific substances – normally transition metals.

In 1835, the Swedish chemist Jöns Jacob Berzelius reviewed the recent work of Faraday, Thenard, Fusinieri and Davy, all of whom had described reactions that could not be explained by affinity.[4] Berzelius proposed that a previously unrecognized force promoted the decomposition and re-assembly of compounds, and coined for it the term "catalytic force" (from the Greek *kata*, "down", and *lyein*, "loosen"), to describe how reactions occurred by

simple contact between substances. As the concept of reaction rates at the molecular level was not then current, the net effect of the catalytic force was not understood. It is now understood as the ability of a catalyst to lower the activation barrier of a reaction (Figure 1a) without being consumed, thus accelerating reaction rates relative to the corresponding non-catalyzed reaction. Catalysis enables the synthesis of a vast body of molecules that would be unattainable by conventional means, owing to the energy barriers to bond formation.

From the use of malt enzymes to today's highly active and selective molecular catalysts, catalysis has fascinated the curious mind for millennia. Selected milestones in the modern history of catalysis are given in Figure 1b. One glimpse suffices to see the large diversity afforded by catalytic methodologies. Of these highly successful catalytic reactions, few have achieved the iconic status of olefin metathesis. Indeed, this reaction offers an element of diversity and selectivity rarely matched by the other transformations[5,6] and is the focus of this thesis.

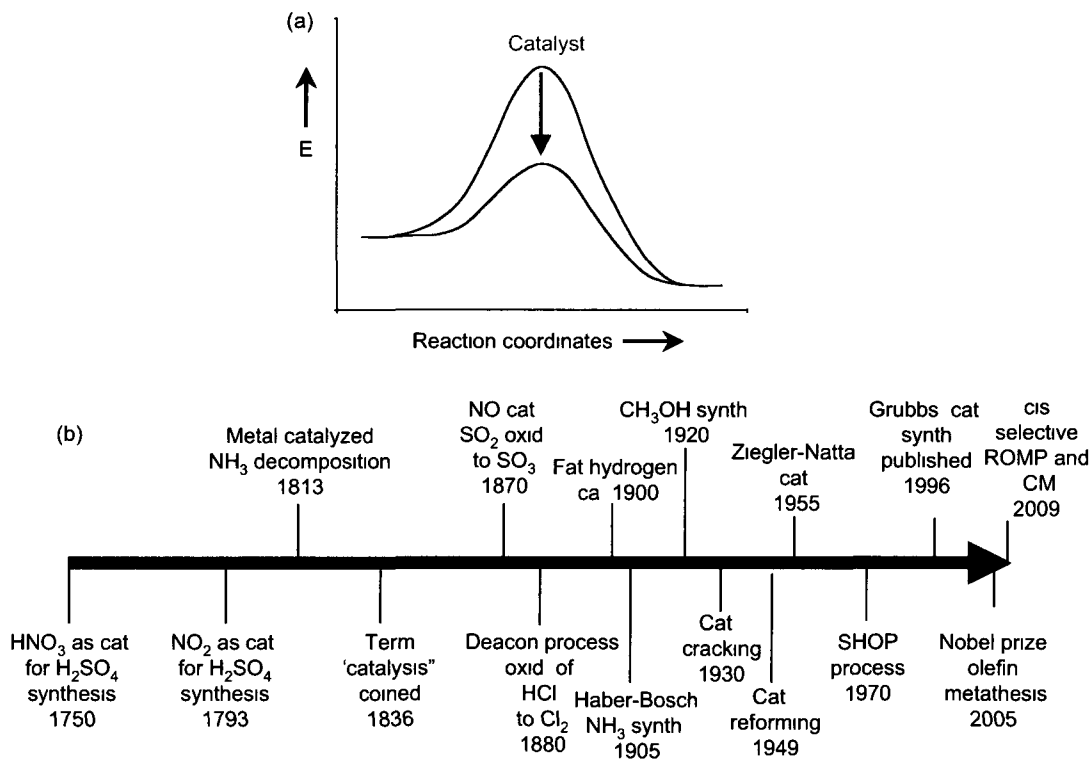

Figure 1. (a) A catalyst lowers the activation energy of a given reaction. (b) Summary of the modern history of catalysis and olefin metathesis.[4,7,8]

1.2 Olefin metathesis

1.2.1 The development of olefin metathesis

Olefin metathesis draws its name from Greek words that signify "transposition". The reaction involves the rearrangement of alkene functionalities in one or several molecules. The polymerization of norbornene, patented by Du Pont in 1955,[9] was one of the first example of the olefin metathesis reaction. This reaction employed an ill-defined catalyst system consisting of $TiCl_4$ and a reducing agent (EtMgBr or $LiAl(C_4H_9)_4$) to reduce the metal from Ti^{IV} to Ti^{II} (or lower).[9] Later years witnessed the development of other ill-defined catalysts including $WCl_6/EtOH/EtAlCl_2$,[10] $WCl_6/SnMe_4$.[11,12] and Re_2O_7/Al_2O_3.[13,14]

Despite enormous interest, the mechanism of olefin metathesis was not understood until 1970, when Chauvin proposed a sequence of [2+2] cycloadditions and cycloreversions between an alkene and a metal alkylidene.[15] The key intermediate in this mechanism is a metallacyclobutane species (Figure 2a). Grubbs later brought compelling evidence to the validity of the Chauvin mechanism through labeling studies.[16] Direct spectroscopic observation of this intermediate, for the ruthenium catalysts, by Piers and co-workers came 35 years following the Chauvin report.[17] (It may be noted, however, that the titanacyclobutane species, which represents the resting state in the Ti chemistry, was observed many decades ago).[5]

Several distinct reactions are mediated by the Chauvin mechanism (Figure 2b). Olefin cross-metathesis (CM) involves exchange of R groups between two different alkenes. Intramolecular CM generates in each turnover one cyclic and one acyclic olefin, a process central to ring-closing metathesis (RCM). Intermolecular reaction between two acyclic dienes ("acyclic diene metathesis", ADMET) yields polymers of ill-defined chain length. Ring-opening metathesis polymerization (ROMP) transforms strained cyclic olefins into polymers that – depending on the ring strain of the contributing monomers – can be synthesized with highly precise control over molecular weights (i.e. chain lengths) and molecular weight distributions. Indeed, such processes are now central to materials design.[18] Olefin metathesis can be extended to substrates bearing alkyne functionalities. For example, alkene-alkyne (enyne) metathesis leads to 1,3 conjugated dienes, while di-ynes can be induced to undergo cyclopolymerization to give conjugated polymers.[19]

References page 21

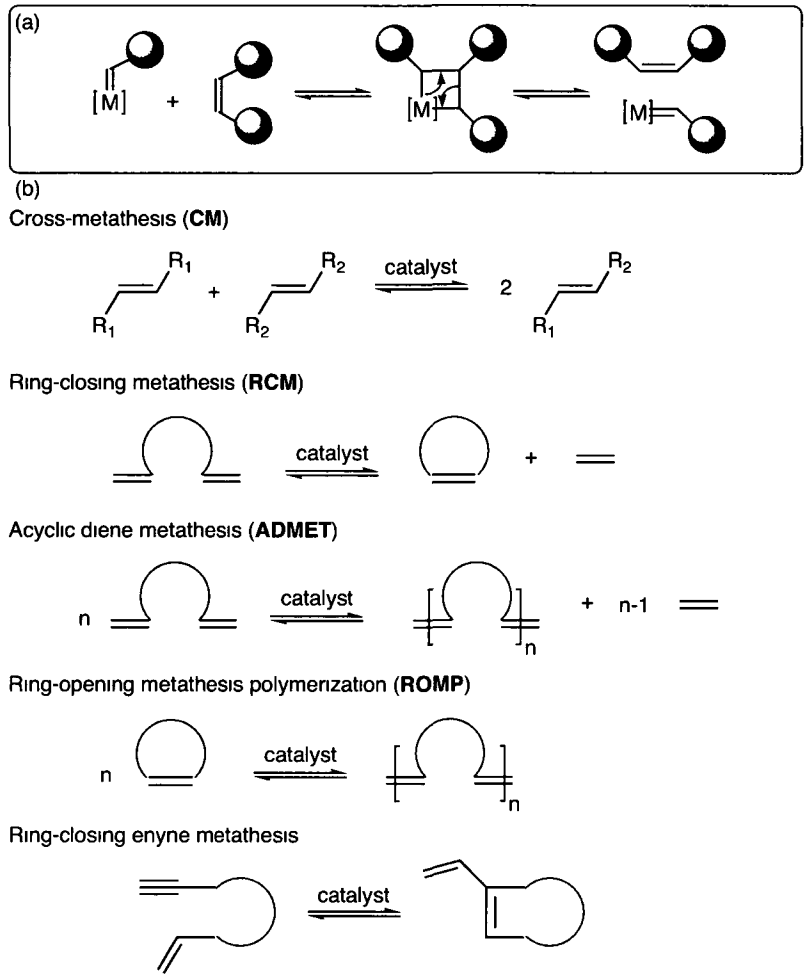

Figure 2. (a) The Chauvin mechanism for olefin metathesis. (b) Types of metathesis reactions.

The reversibility in the reactions of Figure 2 suggests an equilibrium distribution of products. However, this is not always true in practice. ROMP reactions, for example, are driven by the release of ring strain within (e.g.) a norbornene derivative, and the reverse reaction can thus be inhibited kinetically and thermodynamically, although low-strain cyclic oligomers may be generated by backbiting.[20] Similarly, CM, ADMET and RCM reactions are often accompanied by liberation of small alkenes such as ethylene, volatilization of which can impede the reverse reaction.

The power of olefin metathesis was first realized in ROMP, and a number of industrial processes employ this reaction. These include ROMP of dicyclopentadiene (to afford Telene®, Metton® and Pentam®), norbornene (Norsonex®) and cyclooctene (Vestenamer®).[6] All of these processes operate using ill-defined catalysts.[21] While these

catalytic mixtures are reactive enough to effect ROMP, they lack the activity and stability required for the other metathesis reactions of Figure 2b. Realization of the potential of olefin metathesis thus required the development of alternative catalytic systems. Chauvin's advance in elucidating the mechanism of olefin metathesis was central to the rational design of well-defined metal alkylidene complexes. Such catalysts, initially centered on Ta and Nb,[22-24] W[25,26] and Mo[27] (advances in group 6 complexes being spearheaded by Schrock, in particular), were followed by advances in Ru chemistry, most notably by Grubbs.[28,29] These alkylidene complexes laid the foundation for expansion of metathesis into the realm of organic synthesis.

Despite the large variety of metals capable of executing the olefin metathesis reaction, ruthenium catalysts are the most prized in organic synthesis. This stems chiefly from the significantly higher tolerance of these catalysts toward functional groups. This claim needs to be taken cautiously, however. While it is true that the Grubbs catalysts tolerate water and trace of air in the reaction, which contributes to their much easier handling relative to the group 6 catalysts, substrates bearing protic functionalities and aldehydes remain problematic for the ruthenium catalysts.[30-32] In contrast, this crucial requirement for broad applicability in organic synthesis is hardly met in the Schrock system, although these catalysts offer levels of chemo-[33,34] and enantioselectivity[35-37] unrivaled by the Grubbs ruthenium catalyst. Grubbs has proposed that the ability of the ruthenium catalysts to ignore most functional groups reflects a preferential reactivity with olefins.[38] In contrast, given their higher oxophilicity, early-metal catalysts favor reaction with carboxylic acid and aldehydes.[38] Since the discovery of the "user-friendly" Grubbs catalyst in 1992,[28] the olefin metathesis reaction has reached astonishing prominence in organic chemistry. Recent reviews describe its use in, inter alia, construction of synthetically valuable building blocks such as heterocyclic rings containing phosphorus,[39] sulfur,[39] oxygen,[40] or nitrogen,[40,41] including aromatic heterocycles;[42] spirocyclic,[43,44] cyclophane,[43] and polycyclic compounds;[43,44] compounds of biological and medicinal relevance such as peptidomimetics,[45,46] carbohydrate derivatives,[46-49] alkaloids,[46,50-54] bio-active cyclic molecules[55,56] and polycyclic ethers,[57] including macrocyclic aza-crown ethers,[58] and topologically interesting molecules and "molecular machines".[59,60] The immense potential of the olefin metathesis reaction led to the 2005 Nobel Prize in chemistry being awarded to the pioneers of metathesis chemistry: Chauvin, Schrock and Grubbs.[61-63]

References page 21

The many successes of olefin metathesis obscure the startlingly low industrial uptake of this reaction. Twenty years following the development of "robust" ruthenium catalysts, the scope of this reaction remains almost exclusively confined to the research setting. This is not because of a lack of industrial interest: on the contrary, great interest is evidenced by reports from Boehringer-Ingelheim Ltd.,[64-67] GlaxoSmithKline Inc.,[68,69] Merck & Co.,[70,71] Johnson & Johnson Inc.,[72] Pfizer Inc.[73] and Novartis Inc.[74] describing the assembly of various complex molecules by RCM (Chart 1). The absence of commercial processes employing RCM reflects their poor economics. Prohibitive costs stem from the large dose of catalyst required for satisfactory conversion to targets,[65] compounded by indirect expenditures associated with removal of metal impurities following metathesis. This is particularly problematic given the stringent limit of 5 ppm set for *combined* platinoid group metal (Ru, Os, Rh, Ir, Pd and Pt) contamination in active pharmaceutical ingredients (API).[75] For drugs prescribed to pregnant women, the acceptable limit is ten times lower (0.5 ppm).[75] Economical issues notwithstanding, two syntheses of commercially relevant targets have been scaled up to kilogram levels by Boehringer-Ingelheim[67] and GlaxoSmithKline.[68,69] In both cases, prolonged, iterative optimization was sought to achieve economic viability, and no plant process is on the horizon.

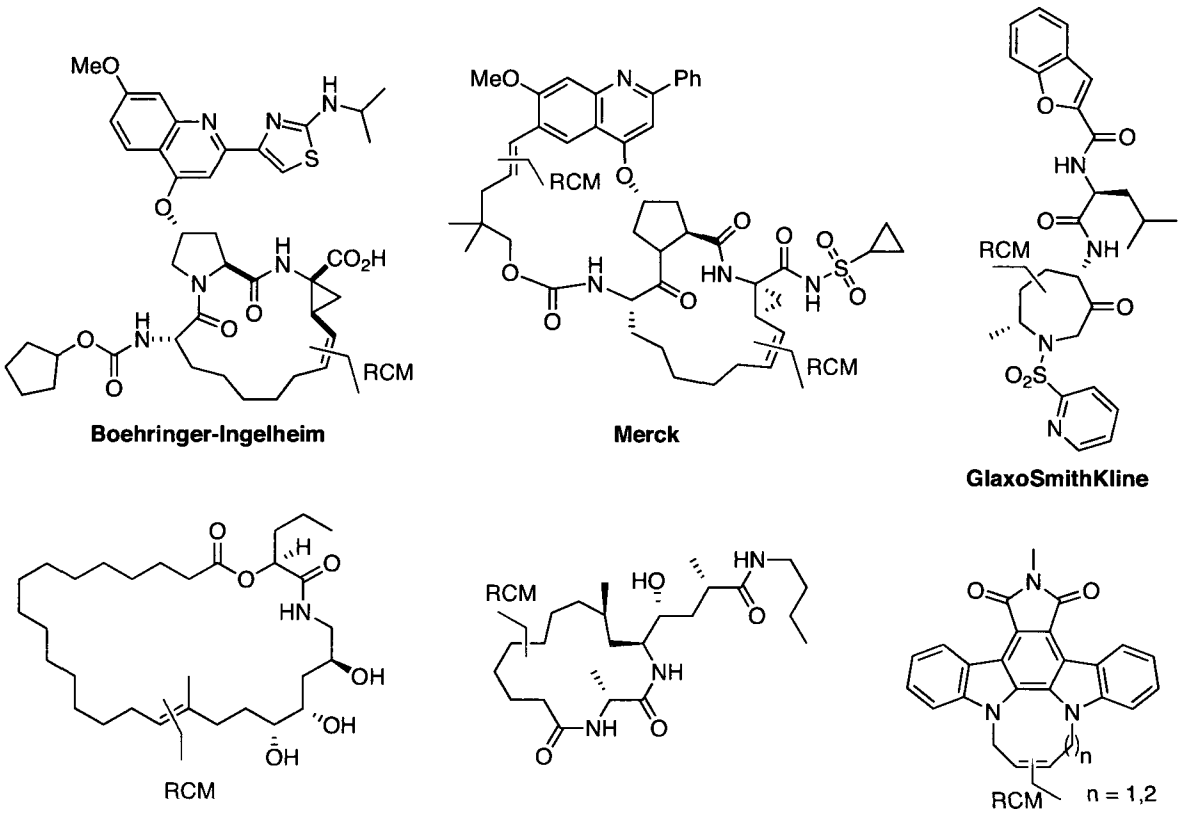

Chart 1. Value-added molecules synthesized via RCM in industrial contexts.[64-74]

Clearly, the future of RCM in the industry depends on the development of more active catalysts and suitable methodologies for efficient use of the catalyst dose. This thesis focuses on both aspects. The work presented herein takes as its starting point a review of current understanding in ruthenium-catalyzed olefin metathesis. The discussion below is organized into four sections: (1) the mechanism of Ru-catalyzed olefin metathesis, (2) the most recent developments in catalyst design, with a focus on consequences in terms of catalyst activity, selectivity and lifetime, (3) the energetic mapping of the metathesis cycle for Ru catalysts, and (4) the decomposition products of the Grubbs catalysts.

1.2.2 The mechanism of Ru-catalyzed olefin metathesis and nature of the intermediates.

Understanding the mechanism[76] by which ruthenium catalysts mediate metathesis is key to improvements. Irrespective of which Grubbs catalyst is employed, initiation (Figure 3a) requires formation of an empty coordination site cis to the Ru alkylidene.[76] This is normally

accomplished by loss of a neutral (L-donor) ligand, often PCy_3, from a basal site in the square pyramid. The resulting 14-electron complex, the active species, can re-coordinate the dissociated ligand (non-productive), or interact with an olefin (ethylene, in Figure 3a), enabling productive metathesis. In the latter case, the coordinated ethylene undergoes a [2+2] cycloaddition with the Ru alkylidene, generating a metallacyclobutane intermediate. Retro-cycloaddition affords a new olefin and regenerates the 14-electron complex. The ancillary ligands have a profound impact on the rates at each step. This interplay is discussed in Section 1.2.3.

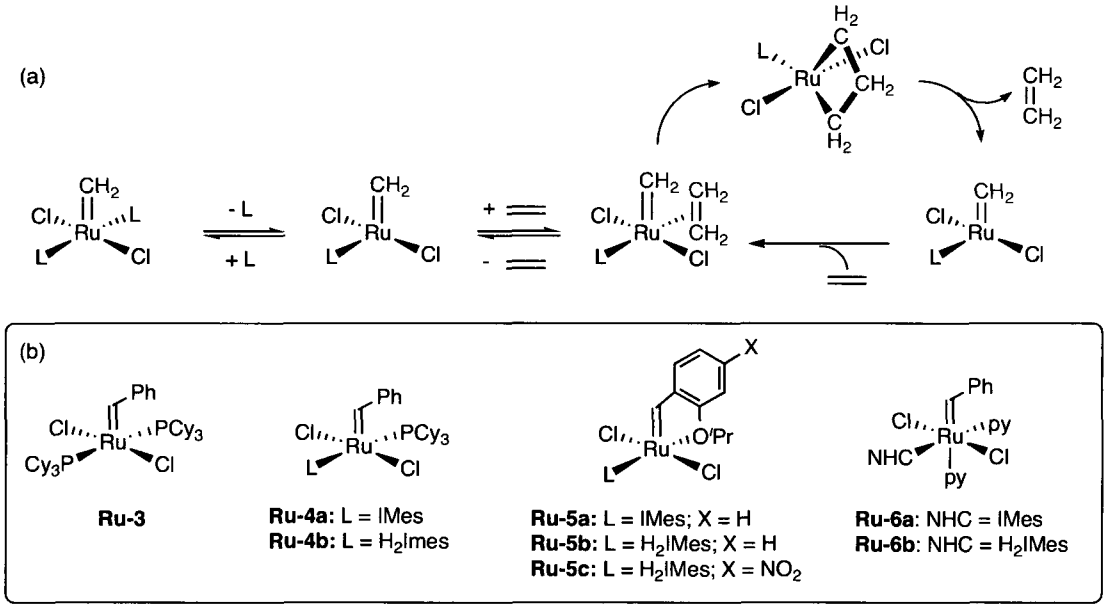

Figure 3. (a) Mechanism of Ru-catalyzed degenerate CM of ethylene. (b) Key Ru metathesis catalysts. IMes = *N,N'*-bis(mesityl)imidazoyl-2-ylidene; py = pyridine.

Various studies have sought identification and characterization of the proposed catalytic intermediates.[77-80] Most compelling of these is Piers direct (NMR) observation of the metallacyclobutane.[17] Proposed intermediates differ in their ligand arrangement. In both the Piers[17,81] and the Snapper[77] examples, a meridional arrangement of L, the alkylidene, and olefin is observed (Chart 2a). In contrast, Grubbs has reported a facial arrangement (Chart 2b).[78-80] The importance of either configuration is currently the subject of controversy. However, theoretical investigations suggest that the meridional arrangement may be lower in energy, and thus probable.[82-84] Interestingly, Goddard has suggested that the facial arrangement may increase selectivity.[82] He proposed that the higher energetic barriers between catalytic intermediates featuring such a ligand arrangement could retard or inhibit

secondary metathesis events[82] thought to contribute to formation of thermodynamic products.[20 85-87]

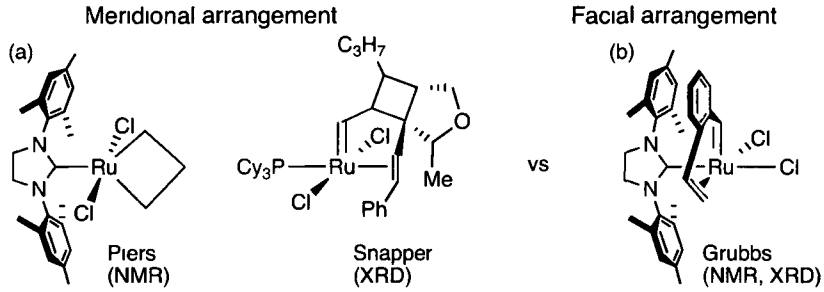

Chart 2. Characterized Ru complexes relevant to the metathesis cycle.[17 77-80]

1.2.3 The structure and function of the ligands on the Grubbs catalysts

Catalyst design has focused on modification of all of the ligands of the Grubbs catalysts (Figure 3b). While both neutral and anionic ligands have been targeted for study, most work has focused on redesign of the former, as discussed below. Discussion of work centered on the anionic ligands is deferred to Chapter 4.

Higher activity can be achieved for the Grubbs catalyst by varying the "placeholder" ligand, which dissociates from the metal to generate the vacant site required to initiate metathesis. Common placeholder ligands include PCy_3,[29,88,89] pyridine[90,91] or the "ether" moiety of styrenyl ether complexes (e.g. **Ru-5**).[92] Higher activity correlates well, if not exclusively, with the lability of the placeholder ligand.[76] For example, replacing the PCy_3 ligand in **Ru-4b** by PPh_3 increases initiation rates by two orders of magnitude.[76] Further improvements result from incorporation of pyridine (**Ru-6a/b**) or 3-bromopyridine[90,91] in place of phosphine. In the extreme, no placeholder ligand is present in Piers phosphonium catalysts, which are highly metathesis-active even at 0 °C.[93] Sanford and Grubbs have noted that the increased activity in these systems is due almost entirely to faster initiation, rates of propagation being essentially unaffected.[76] To achieve longer lifetime, faster propagation, and enhanced selectivity, modification of the ligands that remain bound throughout the catalytic cycle is essential, and has thus received much attention.

A breakthrough was achieved in 1998 by introduction of *N*-heterocyclic carbene (NHC) as ligand on the Grubbs catalyst.[88,94 95] These "second-generation" catalysts (e.g. **Ru-4b**) are characterized by dramatically higher metathesis activity, and heightened lifetime relative to their first-generation counterparts, at least in the precatalyst form (though it should be noted

that this is an artifact of low phosphine lability; vide infra). Unsurprisingly, NHCs remain the neutral ligand of choice within the Grubbs catalysts. Most commonly encountered within the Grubbs catalysts is the 1,3-dimesityl-4,5-dihydroimidazol-2-ylidene (H_2IMes) derivative, owing to the commercial availability of **Ru-4b**, and its consequently widespread use as a precursor in catalyst synthesis. Given the modular nature of the NHC ligand class,[96] however, variation of the steric and electronic properties of the NHC ligands has received much attention. Recent reviews by Grela[97] and Grubbs[98] report hundreds of ruthenium metathesis catalysts bearing various NHCs in conjunction with other ancillary ligands. Amongst the successes (and failures) described in these reviews, a consistent theme is the correlation between higher metathesis activity and strongly σ-donating NHCs, and an appropriate degree of steric protection (sufficient to retard decomposition but not so high as to impede substrate binding). Specifics are highlighted below. It should be acknowledged, however, that while it is self-evident that modification of the NHC (or other) ligands alters both steric and electronic properties,[99] correlations between catalytic activity and sometimes subtle stereoelectronic changes are not always obvious.

Removing bulk from the *N*-mesityl NHC to form *N*-*o*-tolyl[100-103] or *N*-phenyl[104] carbenes substantially improves yields in RCM or CM of sterically demanding olefins (**A-C**; Chart 3). However, this improved catalytic reactivity comes at a cost in catalyst lifetime, particularly when the ortho position of the NHC arms are not functionalized.[105-107] This result was rationalized on the basis of the easier rotation around the *N*-aryl bond when protons occupy the ortho positions, which brings the *o*-C-H bond closer to the Ru center and facilitates its activation (see Section 1.2.5). Ruthenium hydrides complexes are the expected product of this unwanted C-H activation and have indeed been observed as decomposition products from the Grubbs catalysts.[105,108] Improved catalyst stability, while retaining minimal functionalization of the ortho *N*-aryl positions, can be achieved by alkylating the imidazole ring backbone. Grubbs has proposed that this functionalization also limits the extent of rotation around the *N*-aryl bond.[104] Increasing the steric bulk of the NHC is not a viable alternative for catalyst stability. On the contrary, this promotes decomposition through C-H activation, while also retarding metathesis for steric reasons.[109] The *N*-adamantyl complex **D** (Chart 3), for example, is poorly reactive even for ROMP of norbornene,[109] one of the easiest metathesis reactions.

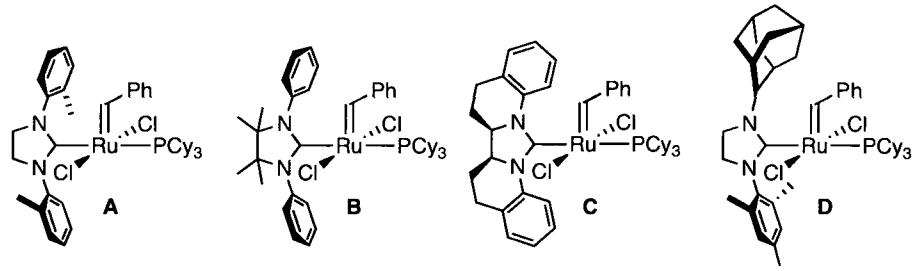

Chart 3. Selected examples of Ru metathesis catalysts featuring NHC ligands of varying steric bulk.

Incorporating different heteroatoms on the NHC ligands has a significant impact on catalytic activity. Examples of such ligands within the Grubbs framework include alkyl-amino,[110,111] thiazol-2-ylidene[112] and triazole[113] carbenes (**E-G**; Chart 4). Introduction of alkyl-amino and thiazole NHC ligands on the Grubbs catalyst was motivated by the stronger σ-donation and reduced steric bulk of these carbenes relative to H_2IMes.[110] However, no improvement in metathesis activity was achieved relative to the benchmark **Ru-4/5**. For the triazole NHC ligand, low metathesis activity stems from the short lifetime of the catalyst in solution. Grubbs proposed that this is due to fast decoordination of the triazole carbene from the Ru center.[114] The reduced bulk of the *N*-phenyl arms of the carbene in catalyst **G** appeared promising, and enabled metathesis of sterically demanding olefins despite short lifetime. In fact, catalyst **G** inspired the synthesis of *N*-tolyl and *N*-phenyl catalysts described above.[98] Chlorinated imidazole NHCs prepared by Furstner and co-workers afforded complexes with catalytic reactivity comparable to **Ru-4/5**.[113] This is surprising given the inductive effect of the halogen atoms, which reduces the σ-donating power of the NHC relative to H_2IMes, at least as judged by the higher ν(CO) stretch in the $Ni(CO)_3$(NHC) derivative.[99] These results imply that metathesis activity may depend less on the donor capacity of the carbene than its sterics.

References page 21

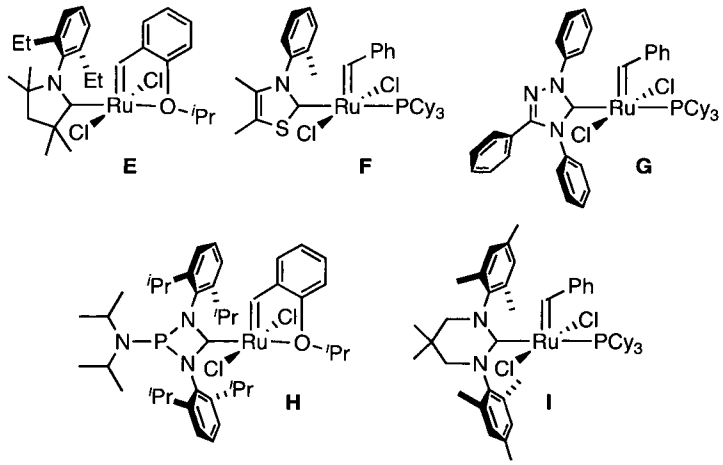

Chart 4. Selected examples of Ru complexes bearing heteroatom-substituted or 4- and 6-membered NHC ligands.

Ruthenium catalysts in which the NHC ligand contains a 4-[115] or 6-membered[116,117] heterocyclic ring (**H/I**; Chart 4) are characterized by metathesis rates inferior to the benchmark, imidazole-derived carbene. Based on the X-ray structure of **H**, Grubbs attributed the low reactivity of **H** to the increased steric demand of the NHC, which disfavors substrate binding.[117] For **I**, low metathesis activity was attributed to weaker σ-donation[115] arising from the bent geometry of the NHC core, and consequently limited overlap between the p orbitals of nitrogen and the carbene carbon. As the imidazole core offers the best compromise in terms of catalytic activity and stability, it remains the framework of choice for Ru-NHC complexes.

Modulation of the alkylidene moiety has also received much attention,[29,76,92,118] though such modifications only impact the metathesis activity of the *precatalyst* (initiation). Indeed, following one turnover, the starting alkylidene is replaced by another, the nature of which depends on the metathesis reaction. The first Grubbs catalyst contained a vinylidene moiety as the reactive site, and was reactive enough to catalyze ROMP of norbornene, as well as RCM of high effective-molarity (EM, see later) α,ω–dienes to afford common five, six and seven-membered rings.[28] During optimization of the alkylidene ligand, it was recognized that faster catalyst initiation correlates with large, electron-donating alkylidenes, which facilitate dissociation of the placeholder ligand.[29,76] Although alkylidene of type Ru=CHR (R = alkyl) afford fastest initiation, they are not the most stable.[119] The best compromise in terms of initiation rates and stability was obtained with Ru-benzylidenes (Ru=CHPh).[29] While the

rates of initiation of the first-generation benzylidene catalyst **Ru-3** are ca. 2× lower than its propylidene ($Ru=CHC_2H_5$) counterpart,[76] the half-life of the former is nearly 20× longer (8 days vs. 10 h).[119] As a result, the benzylidene moiety is very frequently encountered in the Grubbs catalysts.

As Ru-methylidene species ($Ru=CH_2$) are generated during most RCM and CM reactions, comparison of their initiation rates and lifetimes, vs. Ru-benzylidenes, is highly relevant. Initiation rates of second-generation Ru-benzylidene catalysts vary between 0.03 and 29 s^{-1} at 80 °C, depending on the NHC, halides and placeholder ligand present.[76] In contrast, initiation of $RuCl_2(H_2IMes)(PCy_3)(=CH_2)$ is too low to measure, even at 80 °C.[76] Compounding the low metathesis activity of the methylidene species is their short lifetime. The half-life of second-generation Ru-methylidene complexes is <6 h at 55 °C.[105] In contrast, the half-life of the corresponding benzylidene complex (**Ru-4b**) is over one month under the same conditions.[105] Thus, while the Ru-benzylidene *precatalysts* are highly metathesis-active and stable, the methylidene species is both much less reactive for metathesis, and very fragile. This point will be revisited later in this thesis.

Introduced in 1999 by Hoveyda and co-workers,[92] styrenyl ether catalysts (e.g. **Ru-5**; Figure 3b) have become nearly as common as their benzylidene counterpart.[97,98] These chelating alkylidene ligands improve the stability of the precatalysts relative to their benzylidene variants, as evidenced by their purification by silica gel chromatography in air using non-distilled solvents.[92,118] Catalyst stability comes at the expense of initiation rates, however, and high temperatures are generally required for use of such catalysts.[120] Electronic[118,121,122] or steric[123] deactivation of the chelate ring moiety effectively increases initiation rates; alternative approaches utilize additives such as organic[124,125] or Lewis acids.[124]

The potential for recycling styrenyl ether catalysts following reaction is highly attractive for the potential to limit catalyst costs.[126-128] The working hypothesis is that the free styrenyl ether ligand can recombine with the active species to regenerate the precatalyst. Work by Hoveyda,[92,129] Grela and Maudit[128,130] and Nolan[127,131] on these "boomerang" catalysts has suggested that catalyst recovery is indeed possible, albeit <60%,[131] but these claims are attended by much controversy. It remains unclear to what extent release-recapture takes place, vs. recovery of unactivated precatalyst. Moreover, the need to improve turnon

efficiency by destabilizing the ether chelate[118,121-123] will reduce re-uptake of the free styrenyl ether by the metal intermediate, limiting the efficiency of catalyst recovery.

Going beyond activity and lifetime, controlling the selectivity of the Grubbs catalysts is an active area of development. Given that the alkylidene and placeholder ligands are lost during the first turnover, achieving selectivity is generally sought through modification of ligands that remain bound during catalysis. Aspects of catalyst selectivity of greatest interest include asymmetric metathesis, control of olefin geometry (E vs. Z) and, very recently (as the result of work from this research group), the selectivity for cyclic, vs. oligomeric products in RCM of low-EM dienes. Among these, the first topic has received most attention.

Chiral Ru metathesis catalysts bearing C_2-[37,132,133] or C_1-[134-136] symmetry, or chelating[137-139] NHC ligands have been prepared (**J-L**; Chart 5a). Despite years of efforts focusing on NHC derivatization, the enantioselectivity of the ruthenium catalysts still lags behind that of the molybdenum catalysts. As well as NHC steric bulk, the nature of the halide ligands is important. Enantioselectivity for the usual chloride systems could be improved in some cases by use of LiBr or NaI additives,[132] presumably reflecting improved steric definition of the chiral pocket by the larger halogens. This comes, however, at the cost of metathesis activity.[140] Recent examples (e.g. **L**; Chart 5) show both high enantiomeric excess and high conversions without additives.[141] Substitution of the imidazole backbone is proposed to be critical.[132] Computational evidence supports chiral folding of the heterocyclic ring (Chart 5b), which is communicated to the *N*-bound aromatic groups, thus permitting transfer of chiral information to the substrate.[142] It will be noted, however, that all of these efforts rely on modification of a single, monodentate ligand. Strategies for synthesis of chiral Ru metathesis catalysts were expanded in recent work by Johanna Blacquiere of this research group, who succeeded for the first time in incorporating the binaphtholate (BINO) ligand motif into these systems.[143] The potential potency of this approach is clear from the advances with Schrock's BINO and biphenylate Mo systems. While further development is needed (particularly identification of appropriate 3,3'-substituents), this advance also opens the door to chiral matching/mismatching opportunities using the κ^2- *O,O* and NHC ligands.

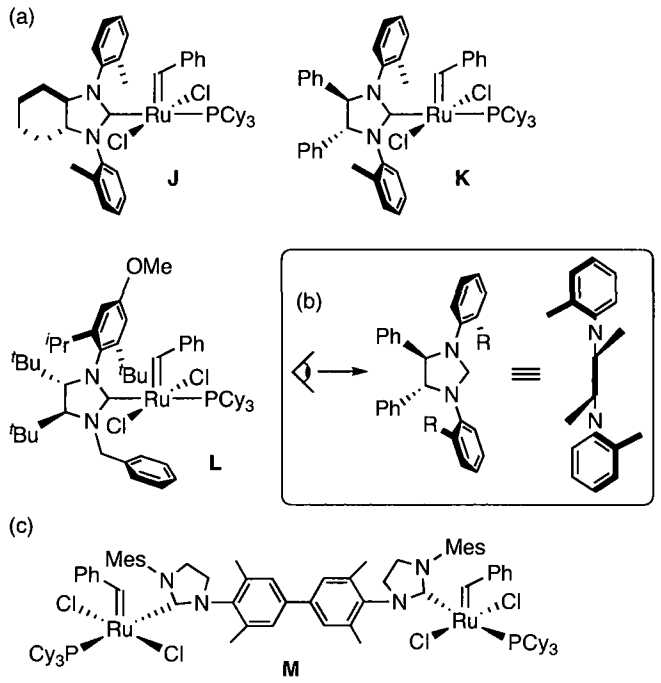

Chart 5. (a) Selected examples of chiral metathesis catalysts. (b) Origin of the chiral folding of the *N*-bound groups. (c) Catalyst showing selectivity for dimer formation.

The role of catalyst selectivity in controlling the balance between cyclic vs. oligomeric products in RCM construction of medium and large rings went long overlooked.[144] Competition between cyclization and oligomerization can severely reduce the yields of RCM targets, as discussed in detail in Chapter 3. While high dilution and elevated temperatures favor cyclization,[20,145] these conditions are detrimental to catalyst lifetime. Higher catalyst loadings are thus required. This is merely a nuisance in the research setting, owing to the need for laborious purification, but is a major problem in industrial practice. Development of catalysts exhibiting a bias toward cyclization is thus a major new target for selectivity in RCM catalysis. Work from our group first demonstrated the kinetic bias of an aryloxide catalyst toward RCM, over oligomerization, as described in Chapter 3.[144,146] Lemcoff and co-workers subsequently described a dimeric Ru catalyst with a bis-carbene linker ligand (**M**; Chart 5c) which exhibited selectivity for dimeric products over oligomers.[147] In contrast, the benchmark catalysts **Ru-4b** and **Ru-5b** showed the opposite selectivity. While selectivity for monocyclic products would be more generally useful, this example, as well as the aryloxide chemistry, highlights the potential for a design-based solution to this selectivity challenge.

References page 21

Selectivity over olefin geometry in metathesis is a long-sought goal. Metathesis normally yields a mixture of E and Z isomers (except for smaller rings), the ratio of which cannot be controlled.[148] Where a single isomer is desired, time-consuming separation is required. In a recent breakthrough, exclusive formation of the less stable Z olefin was obtained in ROMP and CM reactions using Mo-pyrrolide / monodentate alkoxide ligands (**N**, **O**; Chart 6a).[33,34] No such selectivity has so far been achieved in ruthenium catalysis. Selectivity for the less stable olefin is commonly undermined by secondary metathesis, which leads to formation of the thermodynamic product over time.[20,85-87] Interestingly, Ru complexes bearing thiazole NHC (e.g. **F**; Chart 4)[112] or acyclic *N*-heterocarbenes (**P**; Chart 6b)[85] are reported to show a slight preference toward the kinetic product during cross metathesis. It is unclear whether this reflects the incapacity of the catalyst to isomerize the olefinic products, or if decomposition occurs prior to secondary metathesis.

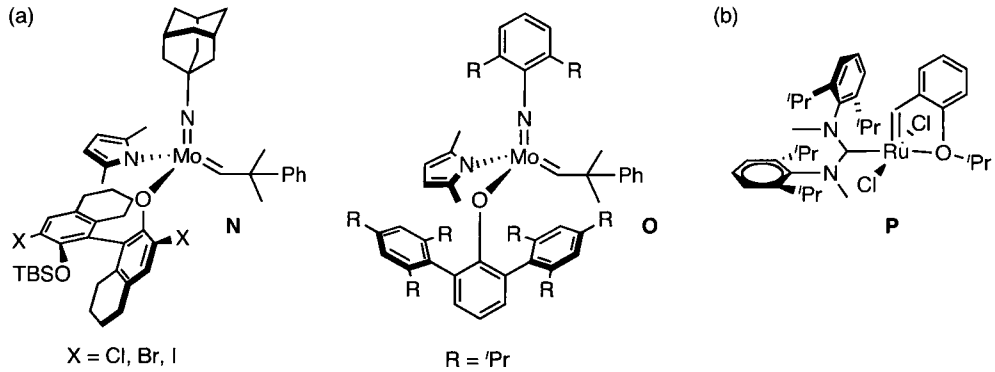

Chart 6. (a) Mo catalysts showing high selectivity for formation of Z olefins. (b) Ru catalyst bearing an acyclic NHC ligand.

1.2.4 Energetic mapping of the Ru-catalyzed olefin metathesis cycle

Since the 1992 discovery of the first well-defined ruthenium metathesis catalysts,[28] and despite the key importance of the ensuing systems, surprisingly little experimental thermodynamic data has been published that confers insight into the metathesis cycle. A seminal paper of Sanford and Grubbs, now nearly 10 years old, remains the key point of reference for the initiation step.[76] This paper revealed that – contrary to the initial[88,89,95,149] assertions – the lability of the phosphine ligand was *diminished* in second-generation Ru-NHC catalysts, despite apparently stronger σ-donation from the NHC vs. PCy_3 ligand. Loss of the PCy_3 ligand from second-generation **Ru-4a/b** was ca. 3 kcal mol^{-1} higher in energy than for first-generation **Ru-3** (ΔG° = 20 vs. 23 kcal mol^{-1}; both at 25 °C), translating into a

dissociation rate constant two orders of magnitude lower for **Ru-4a/b**.[76] A rationale for the slower initiation rates of the NHC complexes was proposed six years later by Kennepohl[150] in a combined DFT/X-ray absorption spectroscopy study. The metal center in the second-generation catalyst was shown to be more electron-deficient than in its first-generation counterpart,[150] owing to *poorer* charge donation from the NHC ligand, which slows dissociation of the placeholder ligand.

While the thermodynamics of initiation are well understood, measurement of thermodynamic data for ensuing steps is severely hampered under "real" catalytic conditions by the spectroscopic invisibility of intermediates present in minor amounts, and their decomposition at different rates. Thus only computational methods could be used to examine the energy profile of the entire metathesis cycle.[82-84,151-153] Recently, however, the Piers group published the first experimentally-determined free-energy diagram for a RCM reaction.[154] Key to success was the use of the Piers phosphonium catalyst **Q** (Scheme 1), which readily affords **R** by reaction with the cyclopentene ring formed by RCM of dimethyl diallyl malonate, in conjunction with $B(C_6F_5)_3$ to abstract the third, irrelevant chloride atom.[81] Because the phosphonium ion co-product is formed irreversibly, **R** can be observed by NMR analysis at low temperatures (ca. –78 °C).[81] Complex **R** can then react with ethylene to afford four-coordinate methylidene **T** (Scheme 1, path a), or the alternative metallacyclobutane product **S**. The latter was detected, although **T** was not.

Alternatively, **R** can undergo retro-cycloaddition to regenerate the starting cyclopentene, following which intermediate **T** can be trapped with ethylene to form **U** (Scheme 1, path b). By varying the ratios of added ethylene and cyclopentene, the equilibrium dynamics relating **R/S/U** could be examined by ^{1}H EXSY (exchange spectroscopy) correlation experiments at –73 °C. The relative rates of RCM and ring-opening metathesis were compared to establish an energy map for the catalytic cycle.[154] A surprisingly low barrier for cyclization reaction emerged; ca. 15.5 kcal mol^{-1}.[154] The reverse ring-opening process is likewise characterized by a low energy barrier (ca. 16.7 kcal mol^{-1}), consistent with the reversibility characteristic of many RCM reactions.[20] Importantly, the highest energy barrier observed is lower than that measured for the highly reactive Ti and W catalysts (25[155] and 21-26[156] kcal mol^{-1}, respectively), although different olefins were used for the group 4 and 6 catalysts (3,3-dimethyl-1-butene and ethylene respectively). It should be noted that the free energies of

reaction found in the Piers study should be extrapolated to higher temperatures only with caution, as the entropy of reaction will necessarily be affected.

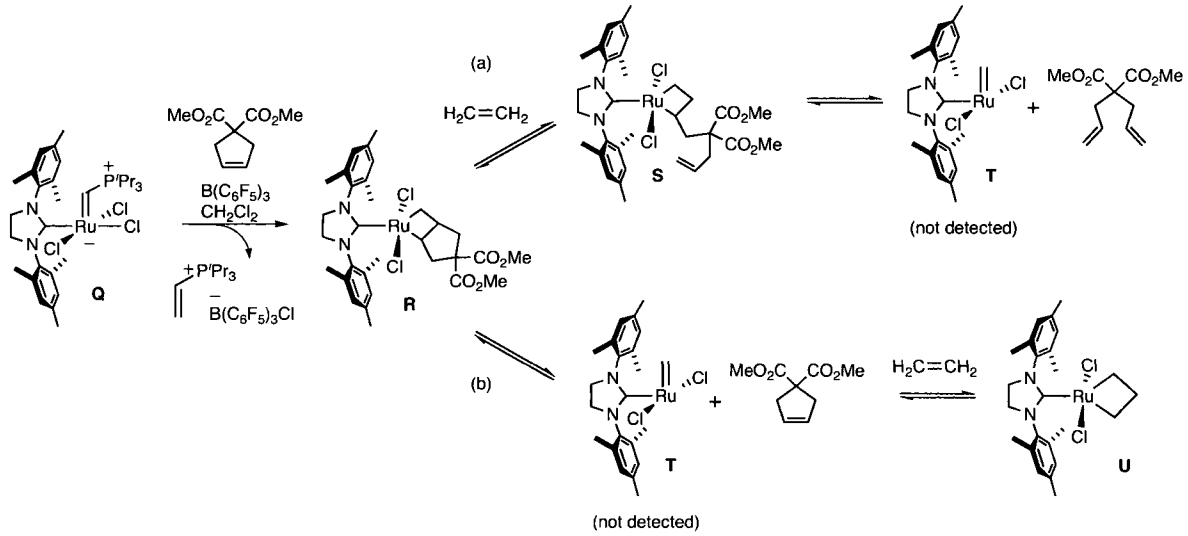

Scheme 1. (a) The ring-opening and (b) RCM of dimethyl diallyl malonate.[154]

1.2.5 Decomposition of the Grubbs catalysts

The foregoing highlights the enormous diversity of the Grubbs catalysts developed to date. This diversity masks, however, the remarkable similarity in reactive species. All of the most commonly employed Ru metathesis catalysts funnel toward an active species which differs solely in the nature of the L ligand (Figure 4). While key to metathesis, this species also mediates catalyst deactivation.[76,105,119] An influential kinetics study suggested that decomposition of the active methylidene species is unimolecular.[119] However, this model study was conducted in the absence of substrate for experimental simplicity, and it is therefore unclear whether unimolecular deactivation is indeed dominant under conditions of catalysis. More detailed decomposition studies under reaction conditions relevant to catalysis would therefore be valuable.

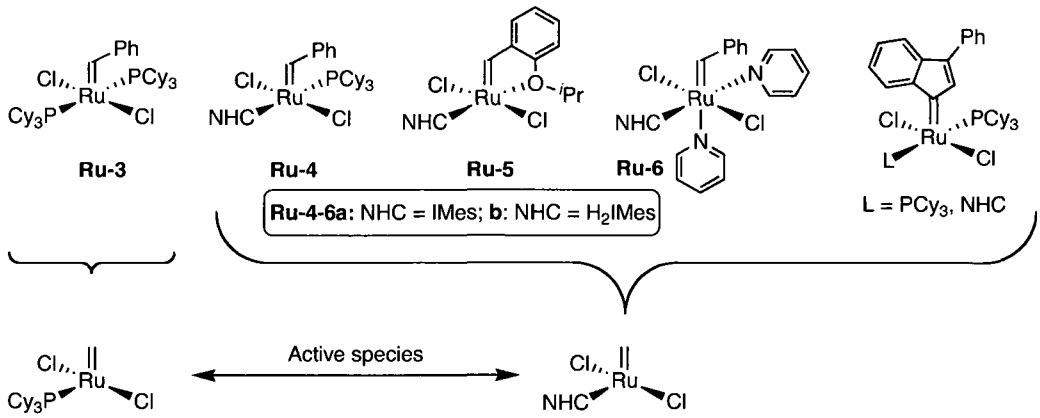

Figure 4. The various Grubbs catalysts converge toward a similar active species.

Chloride-bridged dimers are common deactivation products for both first- and second-generation catalysts, as originally pointed out by our group[157,158] (**V/W/X**; Chart 7).[105,158,159] Other decomposition products can reveal harmful reaction conditions or functionalities, notable among which is ethylene (**W**).[108,119,160,161] The detrimental effect of ethylene is a clear warning of problems inherent to (e.g.) CM with ethylene, RCM carried out in closed vessels in which the ethylene co-product cannot volatilize, etc. Other small molecules can also be problematic. Thus, Diver and co-workers showed complete loss of the Ru-benzylidene moiety on exposing second-generation catalysts to CO or aryl isocyanides.[162,163] Decomposition occurs via insertion of the alkylidene moiety in the neighboring mesityl ring, leading to **Y** (Chart 7).

As C-H bond activation[105-108,159] is a common decomposition pathway for crowded molecules (**W/X, Z-BB**; Chart 7), use of appropriately pruned *N*-aryl rings is sometimes undertaken to curb this process, as noted above. A styrenyl ether catalyst bearing *N*-phenyl substituents was shown by Blechert to undergo C-H activation during chromatography, leading to **Z**.[107] Despite the presence of an alkylidene moiety in **Z**, this complex is metathesis inactive. Blechert proposed that molecular oxygen is implicated in its formation, a clear hazard given the conventional reliance on aerobic chromatography to purify styrenyl ether catalysts, including **Ru-5**.[92,118]

Attempts to prepare a "third-generation" Ru-methylidene catalyst containing pyridine as placeholder ligand yielded tris-pyridine **CC**.[105] Interestingly, work by Renata Nunes of the dos Santos and Fogg groups revealed formation of the related IMes species during CM reaction of methyl vinyl ketone and **Ru-6a**.[164]

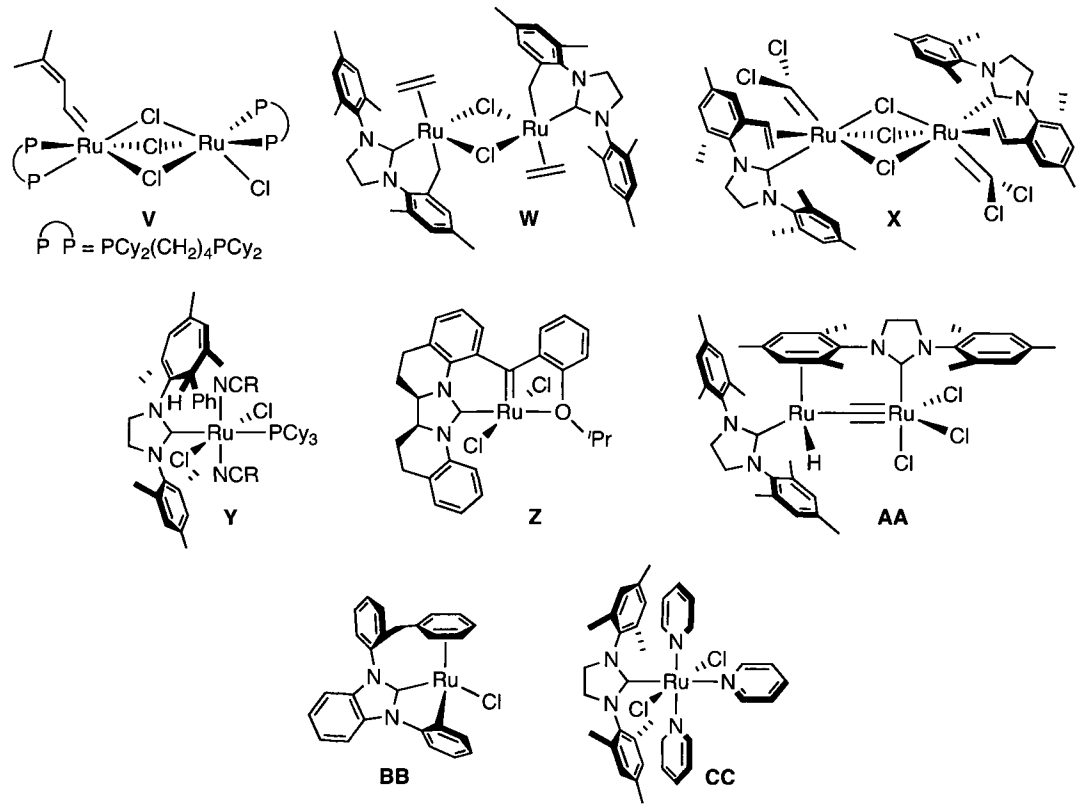

Chart 7. Selected, structurally characterized (XRD) decomposition products formed from the Grubbs catalysts.

1.3 Scope of this thesis

ROMP chemistry has held an important place in industry and academia for decades. In contrast, and despite their key potential for organic synthesis, ring-closing and cross-metathesis reactions are confined to the research setting. The inefficiencies of current catalytic methodologies have been a severe impediment to industrial uptake of these reactions. Understanding the factors that limit the success of this reaction is fundamental to developing economically and environmentally viable processes. This thesis addresses this challenge in the specific context of ruthenium-catalyzed RCM. Three key issues are explored.

First, as RCM macrocyclization is highly prized in pharma and elsewhere, the reaction profiles of the Grubbs and pseudohalide catalysts in this reaction were assessed (Chapter 3). Of particular importance is the extent to which different catalysts participate in, and influence, the ring-chain equilibria that control the thermodynamic balance between RCM and oligomeric products.

Second, a systematic analysis of the role of the anionic ligands on metathesis activity is undertaken. No reliable structure-activity relationship had previously been established for the anionic ligands in the Ru catalysts. Chapter 4 present the first such data. Chapter 5 builds on this knowledge to describe the synthesis and remarkable metathesis activity of a nitrogen-bound pseudohalide catalyst.

Chapter 6 turns to a fundamental aspect of synthetic chemistry that goes largely under-investigated in academia, in an examination of the influence of reactor configuration on RCM efficiency. The nature of the reactor emerges as critical to catalyst productivity, in ways that can be tied directly to the deeper understanding of the thermodynamics of RCM macrocyclization, and issues of poisoning, discussed in the earlier Chapters. These results hold great potential to advance the industrial viability of RCM assembly of large rings.

Finally, a summary of key findings, and suggestions for future work, are given in Chapter 7.

1.4 References

(1) Rothenberg, G., *Catalysis*. Wiley-VCH: Weinheim, 2008; p 279.
(2) Anastas, P. T.; Kirchhoff, M. M., *Acc. Chem. Res.* **2002**, *35*, 686-694.
(3) Sheldon, R. A., *Green Chem.* **2007**, *9*, 1273-1283.
(4) Robertson, A. J. B., *Platinum Met. Rev.* **1975**, *19*, 64-69.
(5) Ivin, K. J.; Mol, J. C., *Olefin Metathesis and Metathesis Polymerization*. Academic Press: New York, 1997.
(6) Grubbs, R. H., *Handbook of Metathesis*. Wiley-VCH: Weinheim, 2003.
(7) Sheldon, R. A., *Green Chem. and Catalysis*. Wiley-VCH: Chichester, 2007.
(8) Kieboom, A. P.; Moulijn, J. A.; Van Leeuwen, P. W. N. M.; Van Santen, R. A., History of Catalysis. In *Catalysis: an Integrated Approach*, Van Santen, R. A.; Van Leeuwen, P. W. N. M.; Moulijn, J. A.; Averill, B. A., Eds. Elsevier: Amsterdam, 1999; Vol. 123, pp 3-28.
(9) Anderson, A. W.; Merckling, N. G. Polymeric bicyclo[2.2.1]hept-2-ene. U.S. Patent No. 2721189, 1955.
(10) Calderon, N.; Ofstead, E. A.; Judy, W. A., *J. Polym. Sci., Part A-1* **1967**, *5*, 2209-2217.
(11) Höcker, H.; Reif, L.; Reimann, W.; Riebel, K., *Recl. Trav. Chim. Pays-Bas* **1977**, *96*, 47-53.
(12) Ast, W.; Rheinwald, G.; Kerber, R., *Recl. Trav. Chim. Pays-Bas* **1977**, *96*, 127-130.
(13) Warwel, S.; Kätker, H., *Synthesis* **1987**, 935-937.
(14) Warwel, S.; Kätker, H.; Rauenbusch, C., *Angew. Chem., Int. Ed. Engl.* **1987**, *26*, 702-703.
(15) Hérisson, J. L.; Chauvin, Y., *Makromol. Chem.* **1971**, *141*, 161-176.
(16) Grubbs, R. H.; Carr, D. D.; Hoppin, C.; Burk, P. L., *J. Am. Chem. Soc.* **1976**, *98*, 3478-3483.
(17) Romero, P. E.; Piers, W. E., *J. Am. Chem. Soc.* **2005**, *127*, 5032-5033.

(18) Fogg, D. E.; Foucault, H. M., Ring-Opening Metathesis Polymerization. In *Comprehensive Organometallic Chemistry III*, Crabtree, R. H.; Mingos, D. M. P., Eds. Elsevier: Oxford, 2007; Vol. 11, pp 623-652.
(19) Krause, J. O.; Nuyken, O.; Buchmeiser, M. R., *Chem. Eur. J.* **2004**, *10*, 2029-2035.
(20) Monfette, S.; Fogg, D. E., *Chem. Rev.* **2009**, *109*, 3783–3816.
(21) Mol, J. C., *J. Mol. Catal. A* **2004**, *213*, 39-45.
(22) Schrock, R. R., *Acc. Chem. Res.* **1979**, *12*, 98-104.
(23) Schrock, R. R., *J. Am. Chem. Soc.* **1974**, *96*, 6796-6797.
(24) Schrock, R.; Rocklage, S.; Wengrovius, J.; Rupprecht, G.; Fellmann, J., *J. Mol. Catal.* **1980**, *8*, 73-83.
(25) Wengrovius, J. H.; Schrock, R. R.; Churchill, M. R.; Missert, J. R.; Youngs, W. J., *J. Am. Chem. Soc.* **1980**, *102*, 4515-4516.
(26) Schrock, R. R.; DePue, R. T.; Feldman, J.; Schaverien, C. J.; Dewan, J. C.; Liu, A. H., *J. Am. Chem. Soc.* **1988**, *110*, 1423-1435.
(27) Schrock, R. R.; Murdzek, J. S.; Bazan, G. C.; Robbins, J.; DiMare, M.; O'Regan, M., *J. Am. Chem. Soc.* **1990**, *112*, 3875-3886.
(28) Nguyen, S. T.; Johnson, L. K.; Grubbs, R. H.; Ziller, J. W., *J. Am. Chem. Soc.* **1992**, *114*, 3974-3975.
(29) Schwab, P.; Grubbs, R. H.; Ziller, J. W., *J. Am. Chem. Soc.* **1996**, *118*, 100-110.
(30) Sheddan, N. A.; Arion, V. B.; Mulzer, J., *Tetrahedron Lett.* **2006**, *47*, 6689-6693.
(31) Young, D. G. J.; Burlison, J. A.; Peters, U., *J. Org. Chem.* **2003**, *68*, 3494-3497.
(32) Fu, G. C.; Nguyen, S. T.; Grubbs, R. H., *J. Am. Chem. Soc.* **1993**, *115*, 9856-9857.
(33) Ibrahem, I.; Yu, M.; Schrock, R. R.; Hoveyda, A. H., *J. Am. Chem. Soc.* **2009**, *131*, 3844-3845.
(34) Flook, M. M.; Jiang, A. J.; Schrock, R. R.; Muller, P.; Hoveyda, A. H., *J. Am. Chem. Soc.* **2009**, *131*, 7962-7963.
(35) Malcolmson, S. J.; Meek, S. J.; Sattely, E. S.; Schrock, R. R.; Hoveyda, A. H., *Nature* **2008**, *456*, 933-937.
(36) Cortez, G. A.; Baxter, C. A.; Schrock, R. R.; Hoveyda, A. H., *Org. Lett.* **2007**, *9*, 2871-2874.
(37) Funk, T. W.; Berlin, J. M.; Grubbs, R. H., *J. Am. Chem. Soc.* **2006**, *128*, 1840-1846.
(38) Trnka, T. M.; Grubbs, R. H., *Acc. Chem. Res.* **2001**, *34*, 18-29.
(39) McReynolds, M. D.; Dougherty, J. M.; Hanson, P. R., *Chem. Rev.* **2004**, *104*, 2239-2258.
(40) Deiters, A.; Martin, S. F., *Chem. Rev.* **2004**, *104*, 2199-2238.
(41) Collins, S. K., *J. Organomet. Chem.* **2006**, *691*, 5122-5128.
(42) Donohoe, T. J.; Fishlock, L. P.; Procopiou, P. A., *Chem. Eur. J.* **2008**, *14*, 5716-5726.
(43) Kotha, S.; Lahiri, K., *Synlett* **2007**, 2767-2784.
(44) Schmidt, B.; Hermanns, J., *Curr. Org. Chem.* **2006**, *10*, 1363-1396.
(45) Brik, A., *Adv. Synth. Catal.* **2008**, *350*, 1661-1675.
(46) Martin, W. H. C.; Blechert, S., *Curr. Top. Med. Chem.* **2005**, *5*, 1521-1540.
(47) Plumet, J.; Gomez, A. M.; Lopez, J. C., *Mini-Rev. Org. Chem.* **2007**, *4*, 201-216.
(48) Madsen, R., *Eur. J. Org. Chem.* **2007**, 399-415.
(49) Jorgensen, M.; Hadwiger, P.; Madsen, R.; Stutz, A. E.; Wrodnigg, T. M., *Curr. Org. Chem.* **2000**, *4*, 565-588.
(50) Arisawa, M.; Nishida, A.; Nakagawa, M., *J. Organomet. Chem.* **2006**, *691*, 5109-5121.

(51) Gaich, T.; Mulzer, J., *Curr. Top. Med. Chem.* **2005**, *5*, 1473-1494.
(52) Brenneman, J. B.; Martin, S. F., *Curr. Org. Chem.* **2005**, *9*, 1535-1549.
(53) Felpin, F.-X.; Lebreton, J., *Eur. J. Org. Chem.* **2003**, 3693-3712.
(54) Delgado, A., *Eur. J. Org. Chem.* **2008**, 3893-3906.
(55) Van de Weghe, P.; Eustache, J., *Curr. Top. Med. Chem.* **2005**, *5*, 1495-1519.
(56) Schall, A.; Reiser, O., *Eur. J. Org. Chem.* **2008**, 2353-2364.
(57) Clark, J. S., *Chem. Commun.* **2006**, 3571-3581.
(58) Ibrahim, Y. A., *J. Mol. Catal. A.* **2006**, *254*, 43-52.
(59) Collin, J. P.; Dietrich-Buchecker, C.; Hamann, C.; Jouvenot, D.; Kern, J. M.; Mobian, P.; Sauvage, J. P., *Compr. Coord. Chem. II* **2004**, *7*, 303-326.
(60) Champin, B.; Mobian, P.; Sauvage, J.-P., *Chem. Soc. Rev.* **2007**, *36*, 358-366.
(61) Chauvin, Y., *Angew. Chem., Int. Ed.* **2006**, *45*, 3741-3747.
(62) Schrock, R. R., *Angew. Chem., Int. Ed.* **2006**, *45*, 3748-3759.
(63) Grubbs, R. H., *Angew. Chem., Int. Ed.* **2006**, *45*, 3760-3765.
(64) Faucher, A. M.; Bailey, M. D.; Beaulieu, P. L.; Brochu, C.; Duceppe, J. S.; Ferland, J. M.; Ghiro, E.; Gorys, V.; Halmos, T.; Kawai, S. H.; Poirier, M.; Simoneau, B.; Tsantrizos, Y. S.; Llinas-Brunet, M., *Org. Lett.* **2004**, *6*, 2901-2904.
(65) Farina, V.; Shu, C.; Zeng, X.; Wei, X.; Han, Z.; Yee, N. K.; Senanayake, C. H., *Org. Process Res. Dev.* **2009**, *13*, 250-254.
(66) Yee, N. K.; Farina, V.; Houpis, I. N.; Haddad, N.; Frutos, R. P.; Gallou, F.; Wang, X.-J.; Wei, X.; Simpson, R. D.; Feng, X.; Fuchs, V.; Xu, Y.; Tan, J.; Zhang, L.; Xu, J.; Smith-Keenan, L. L.; Vitous, J.; Ridges, M. D.; Spinelli, E. M.; Johnson, M.; Donsbach, K.; Nicola, T.; Brenner, M.; Winter, E.; Kreye, P.; Samstag, W., *J. Org. Chem.* **2006**, *71*, 7133-7145.
(67) Nicola, T.; Brenner, M.; Donsbach, K.; Kreye, P., *Org. Process Res. Dev.* **2005**, *9*, 513-515.
(68) Wang, H.; Matsuhashi, H.; Doan, B. D.; Goodman, S. N.; Ouyang, X.; Clark, W. M., *Tetrahedron* **2009**, *65*, 6291-6303.
(69) Wang, H.; Goodman, S. N.; Dai, Q.; Stockdale, G. W.; Clark, W. M., *Org. Process Res. Dev.* **2008**, *12*, 226-234.
(70) Liverton, N. J.; Holloway, M. K.; McCauley, J. A.; Rudd, M. T.; Butcher, J. W.; Carroll, S. S.; DiMuzio, J.; Fandozzi, C.; Gilbert, K. F.; Mao, S.-S.; McIntyre, C. J.; Nguyen, K. T.; Romano, J. J.; Stahlhut, M.; Wan, B.-L.; Olsen, D. B.; Vacca, J. P., *J. Am. Chem. Soc.* **2008**, *130*, 4607-4609.
(71) McCauley, J. A.; Rudd, M. T.; Nguyen, K. T.; McIntyre, C. J.; Romano, J. J.; Bush, K. J.; Varga, S. L.; Ross, C. W., III; Carroll, S. S.; DiMuzio, J.; Stahlhut, M. W.; Olsen, D. B.; Lyle, T. A.; Vacca, J. P.; Liverton, N. J., *Angew. Chem., Int. Ed.* **2008**, *47*, 9104-9107.
(72) Wilson, L. J.; Malaviya, R.; Yang, C.; Argentieri, R.; Wang, B.; Chen, X.; Murray, W. V.; Cavender, D., *Bioorg. Med. Chem. Lett.* **2009**, *19*, 3333-3338.
(73) Content, S.; Dutton, C. J.; Roberts, L., *Bioorg. Med. Chem. Lett.* **2003**, *13*, 321-325.
(74) Machauer, R.; Veenstra, S.; Rondeau, J.-M.; Tintelnot-Blomley, M.; Betschart, C.; Neumann, U.; Paganetti, P., *Bioorg. Med. Chem. Lett.* **2009**, *19*, 1361-1365.
(75) Garrett, C. E.; Prasad, K., *Adv. Synth. Catal.* **2004**, *346*, 889-900.
(76) Sanford, M. S.; Love, J. A.; Grubbs, R. H., *J. Am. Chem. Soc.* **2001**, *123*, 6543-6554.
(77) Tallarico, J. A.; Bonitatebus, P. J., Jr.; Snapper, M. L., *J. Am. Chem. Soc.* **1997**, *119*, 7157-7158.

References page 21

(78) Anderson, D. R.; Hickstein, D. D.; O'Leary, D. J.; Grubbs, R. H., *J. Am. Chem. Soc.* **2006**, *128*, 8386-8387.
(79) Anderson, D. R.; O'Leary, D. J.; Grubbs, R. H., *Chem. Eur. J.* **2008**, *14*, 7536-7544.
(80) Stewart, I. C.; Benitez, D.; O'Leary, D. J.; Tkatchouk, E.; Day, M. W.; Goddard, W. A.; Grubbs, R. H., *J. Am. Chem. Soc.* **2009**, *131*, 1931-1938.
(81) van der Eide, E. F.; Romero, P. E.; Piers, W. E., *J. Am. Chem. Soc.* **2008**, *130*, 4485-4491.
(82) Benitez, D.; Tkatchouk, E.; Goddard, W. A., III, *Chem. Commun.* **2008**, 6194-6196.
(83) Correa, A.; Cavallo, L., *J. Am. Chem. Soc.* **2006**, *128*, 13352-13353.
(84) Straub, B. F., *Adv. Synth. Catal.* **2007**, *349*, 204-214.
(85) Rosen, E. L.; Sung, D. H.; Chen, Z.; Lynch, V. M.; Bielawski, C. W., *Organometallics* **2010**, *29*, 250-256.
(86) Allaert, B.; Ledoux, N.; Dieltiens, N.; Vander Mierde, H.; Stevens, C. V.; Van Der Voort, P.; Verpoort, F., *Catal. Commun.* **2008**, *9*, 1054-1059.
(87) Jordaan, M.; Vosloo, H. C. M., *Adv. Synth. Catal.* **2007**, *349*, 184-192.
(88) Huang, J.; Stevens, E. D.; Nolan, S. P.; Petersen, J. L., *J. Am. Chem. Soc.* **1999**, *121*, 2674-2678.
(89) Scholl, M.; Ding, S.; Lee, C. W.; Grubbs, R. H., *Org. Lett.* **1999**, *1*, 953-956.
(90) Sanford, M. S.; Love, J. A.; Grubbs, R. H., *Organometallics* **2001**, *20*, 5314-5318.
(91) Love, J. A.; Morgan, J. P.; Trnka, T. M.; Grubbs, R. H., *Angew. Chem., Int. Ed.* **2002**, *41*, 4035-4037.
(92) Kingsbury, J. S.; Harrity, J. P. A.; Bonitatebus, P. J.; Hoveyda, A. H., *J. Am. Chem. Soc.* **1999**, *121*, 791-799.
(93) Romero, P. E.; Piers, W. E.; McDonald, R., *Angew. Chem., Int. Ed.* **2004**, *43*, 6161-6165.
(94) Weskamp, T.; Schattenmann, W. C.; Spiegler, M.; Herrmann, W. A., *Angew. Chem., Int. Ed.* **1998**, *37*, 2490-2493.
(95) Scholl, M.; Trnka, T. M.; Morgan, J. P.; Grubbs, R. H., *Tetrahedron Lett.* **1999**, *40*, 2247-2250.
(96) Hirano, K.; Urban, S.; Wang, C.; Glorius, F., *Org. Lett.* **2009**, *11*, 1019-1022.
(97) Samojlowicz, C.; Bieniek, M.; Grela, K., *Chem. Rev.* **2009**, *109*, 3708-3742.
(98) Vougioukalakis, G. C.; Grubbs, R. H., *Chem. Rev.* **2010**, *110*, 1746-1787.
(99) Gusev, D. G., *Organometallics* **2009**, *28*, 6458-6461.
(100) Stewart, I. C.; Douglas, C. J.; Grubbs, R. H., *Org. Lett.* **2008**, *10*, 441-444.
(101) White, D. E.; Stewart, I. C.; Grubbs, R. H.; Stoltz, B. M., *J. Am. Chem. Soc.* **2008**, *130*, 810-811.
(102) Stewart, I. C.; Ung, T.; Pletnev, A. A.; Berlin, J. M.; Grubbs, R. H.; Schrodi, Y., *Org. Lett.* **2007**, *9*, 1589-1592.
(103) Berlin, J. M.; Campbell, K.; Ritter, T.; Funk, T. W.; Chlenov, A.; Grubbs, R. H., *Org. Lett.* **2007**, *9*, 1339-1342.
(104) Chung, C. K.; Grubbs, R. H., *Org. Lett.* **2008**, *10*, 2693-2696.
(105) Hong, S. H.; Wenzel, A. G.; Salguero, T. T.; Day, M. W.; Grubbs, R. H., *J. Am. Chem. Soc.* **2007**, *129*, 7961-7968.
(106) Hong, S. H.; Chlenov, A.; Day, M. W.; Grubbs, R. H., *Angew. Chem., Int. Ed.* **2007**, *46*, 5148-5151.
(107) Vehlow, K.; Gessler, S.; Blechert, S., *Angew. Chem., Int. Ed.* **2007**, *46*, 8082-8085.

References page 21

(108) Hong, S. H.; Day, M. W.; Grubbs, R. H., *J. Am. Chem. Soc.* **2004**, *126*, 7414-7415.
(109) Dinger, M. B.; Nieczypor, P.; Mol, J. C., *Organometallics* **2003**, *22*, 5291-5296.
(110) Anderson, D. R.; Lavallo, V.; O'Leary, D. J.; Bertrand, G.; Grubbs, R. H., *Angew. Chem., Int. Ed.* **2007**, *46*, 7262-7265.
(111) Anderson, D. R.; Ung, T.; Mkrtumyan, G.; Bertrand, G.; Grubbs, R. H.; Schrodi, Y., *Organometallics* **2008**, *27*, 563-566.
(112) Vougioukalakis, G. C.; Grubbs, R. H., *J. Am. Chem. Soc.* **2008**, *130*, 2234-2245.
(113) Fürstner, A.; Ackermann, L.; Gabor, B.; Goddard, R.; Lehmann, C. W.; Mynott, R.; Stelzer, F.; Thiel, O. R., *Chem. Eur. J.* **2001**, *7*, 3236-3253.
(114) Trnka, T. M.; Morgan, J. P.; Sanford, M. S.; Wilhelm, T. E.; Scholl, M.; Choi, T.-L.; Ding, S.; Day, M. W.; Grubbs, R. H., *J. Am. Chem. Soc.* **2003**, *125*, 2546-2558.
(115) Despagnet-Ayoub, E.; Grubbs, R. H., *Organometallics* **2005**, *24*, 338-340.
(116) Yang, L. R.; Mayr, M.; Wurst, K.; Buchmeiser, M. R., *Chem. Eur. J.* **2004**, *10*, 5761-5770.
(117) Yun, J.; Marinez, E. R.; Grubbs, R. H., *Organometallics* **2004**, *23*, 4172-4173.
(118) Michrowska, A.; Bujok, R.; Harutyunyan, S.; Sashuk, V.; Dolgonos, G.; Grela, K., *J. Am. Chem. Soc.* **2004**, *126*, 9318-9325.
(119) Ulman, M.; Grubbs, R. H., *J. Org. Chem.* **1999**, *64*, 7202-7207.
(120) Ben-Asuly, A.; Tzur, E.; Diesendruck, C. E.; Sigalov, M.; Goldberg, I.; Lemcoff, N. G., *Organometallics* **2008**, *27*, 811-813.
(121) Grela, K.; Harutyunyan, S.; Michrowska, A., *Angew. Chem., Int. Ed.* **2002**, *41*, 4038-4040.
(122) Zaja, M.; Connon, S. J.; Dunne, A. M.; Rivard, M.; Buschmann, N.; Jiricek, J.; Blechert, S., *Tetrahedron* **2003**, *59*, 6545-6558.
(123) Wakamatsu, H.; Blechert, S., *Angew. Chem., Int. Ed.* **2002**, *41*, 2403-2405.
(124) Gulajski, L.; Michrowska, A.; Bujok, R.; Grela, K., *J. Mol. Catal. A* **2006**, *254*, 118-123.
(125) Gawin, R.; Makal, A.; Wozniak, K.; Mauduit, M.; Grela, K., *Angew. Chem., Int. Ed.* **2007**, *46*, 7206-7209.
(126) Van Berlo, B.; Houthoofd, K.; Sels, B. F.; Jacobs, P. A., *Adv. Synth. Catal.* **2008**, *350*, 1949-1953.
(127) Clavier, H.; Nolan, S. P.; Mauduit, M., *Organometallics* **2008**, *27*, 2287-2292.
(128) Rix, D.; Caijo, F.; Laurent, I.; Gulajski, L.; Grela, K.; Mauduit, M., *Chem. Commun.* **2007**, 3771-3773.
(129) Garber, S. B.; Kingsbury, J. S.; Gray, B. L.; Hoveyda, A. H., *J. Am. Chem. Soc.* **2000**, *122*, 8168-8179.
(130) Rix, D.; Clavier, H.; Coutard, Y.; Gulajski, L.; Grela, K.; Mauduit, M., *J. Organomet. Chem.* **2006**, *691*, 5397-5405.
(131) Clavier, H.; Caijo, F.; Borre, E.; Rix, D.; Boeda, F.; Nolan, S. P.; Mauduit, M., *Eur. J. Org. Chem.* **2009**, 4254-4265.
(132) Seiders, T. J.; Ward, D. W.; Grubbs, R. H., *Org. Lett.* **2001**, *3*, 3225-3228.
(133) Berlin, J. M.; Goldberg, S. D.; Grubbs, R. H., *Angew. Chem., Int. Ed.* **2006**, *45*, 7591-7595.
(134) Fournier, P.-A.; Collins, S. K., *Organometallics* **2007**, *26*, 2945-2949.
(135) Fournier, P.-A.; Savoie, J.; Stenne, B.; Bedard, M.; Grandbois, A.; Collins, S. K., *Chem. Eur. J.* **2008**, *14*, 8690-8695.

References page 21

(136) Grisi, F.; Costabile, C.; Gallo, E.; Mariconda, A.; Tedesco, C.; Longo, P., *Organometallics* **2008**, *27*, 4649-4656.
(137) Van Veldhuizen, J. J.; Garber, S. B.; Kingsbury, J. S.; Hoveyda, A. H., *J. Am. Chem. Soc.* **2002**, *124*, 4954-4955.
(138) Van Veldhuizen, J. J.; Gillingham, D. G.; Garber, S. B.; Kataoka, O.; Hoveyda, A. H., *J. Am. Chem. Soc.* **2003**, *125*, 12502-12508.
(139) Gillingham, D. G.; Kataoka, O.; Garber, S. B.; Hoveyda, A. H., *J. Am. Chem. Soc.* **2004**, *126*, 12288-12290.
(140) Dias, E. L.; Nguyen, S. T.; Grubbs, R. H., *J. Am. Chem. Soc.* **1997**, *119*, 3887-3897.
(141) Stenne, B.; Timperio, J.; Savoie, J.; Dudding, T.; Collins, S. K., *Org. Lett.* **2010**, *12*, 2032-2035.
(142) Costabile, C.; Cavallo, L., *J. Am. Chem. Soc.* **2004**, *126*, 9592-9600.
(143) Blacquiere, J. M.; McDonald, R.; Fogg, D. E., *Angew. Chem., Int. Ed.* **2010**, *49*, 3807-3810.
(144) Conrad, J. C.; Fogg, D. E., *Curr. Org. Chem.* **2006**, *10*, 185-202.
(145) Gradillas, A.; Perez-Castells, J., *Angew. Chem., Int. Ed.* **2006**, *45*, 6086-6101.
(146) Conrad, J. C.; Eelman, M. D.; Duarte Silva, J. A.; Monfette, S.; Parnas, H. H.; Snelgrove, J. L.; Fogg, D. E., *J. Am. Chem. Soc.* **2007**, *129*, 1024-1025.
(147) Tzur, E.; Ben-Asuly, A.; Diesendruck, C. E.; Goldberg, I.; Lemcoff, N. G., *Angew. Chem., Int. Ed.* **2008**, *47*, 6422-6425.
(148) Fürstner, A.; Guth, O.; Rumbo, A.; Seidel, G., *J. Am. Chem. Soc.* **1999**, *121*, 11108-11113.
(149) Morgan, J. P.; Grubbs, R. H., *Org. Lett.* **2000**, *2*, 3153-3155.
(150) Getty, K.; Delgado-Jaime, M. U.; Kennepohl, P., *J. Am. Chem. Soc.* **2007**, *129*, 15774-15776.
(151) Cavallo, L., *J. Am. Chem. Soc.* **2002**, *124*, 8965-8973.
(152) Benitez, D.; Goddard, W. A., III, *J. Am. Chem. Soc.* **2005**, *127*, 12218-12219.
(153) Straub, B. F., *Angew. Chem., Int. Ed.* **2005**, *44*, 5974-5978.
(154) van der Eide, E. F.; Piers, W. E., *Nat. Chem.* **2010**, *2*, 571-576.
(155) Lee, J. B.; Ott, K. C.; Grubbs, R. H., *J. Am. Chem. Soc.* **1982**, *104*, 7491-7496.
(156) Feldman, J.; Davis, W. M.; Thomas, J. K.; Schrock, R. R., *Organometallics* **1990**, *9*, 2535-2548.
(157) Amoroso, D.; Snelgrove, J. L.; Conrad, J. C.; Drouin, S. D.; Yap, G. P. A.; Fogg, D. E., *Adv. Synth. Catal.* **2002**, *344*, 757-763.
(158) Amoroso, D.; Yap, G. P. A.; Fogg, D. E., *Organometallics* **2002**, *21*, 3335-3343.
(159) Leitao, E. M.; Dubberley, S. R.; Piers, W. E.; Wu, Q.; McDonald, R., *Chem. Eur. J.* **2008**, *14*, 11565-11572.
(160) Burdett, K. A.; Harris, L. D.; Margl, P.; Maughon, B. R.; Mokhtar-Zadeh, T.; Saucier, P. C.; Wasserman, E. P., *Organometallics* **2004**, *23*, 2027-2047.
(161) Lysenko, Z.; Maughon, B. R.; Mokhtar-Zadeh, T.; Tulchinsky, M. L., *J. Organomet. Chem.* **2006**, *691*, 5197-5203.
(162) Galan, B. R.; Pitak, M.; Gembicky, M.; Keister, J. B.; Diver, S. T., *J. Am. Chem. Soc.* **2009**, *131*, 6822-6832.
(163) Galan, B. R.; Gembicky, M.; Dominiak, P. M.; Keister, J. B.; Diver, S. T., *J. Am. Chem. Soc.* **2005**, *127*, 15702-15703.
(164) Nunes, R.; dos Santos, E. N.; Fogg, D. E., unpublished work.

2. Experimental methods

2.1 General procedures

2.1.1 Reaction conditions

Reactions were carried out under house N_2 (cryogenic boiloff, Linde) in an MBraun glovebox, or under argon (BOC gas, industrial grade) using standard double-manifold Schlenk techniques,[1] unless otherwise noted. The Ar stream was dried by passage through a column of activated (blue) Drierite. Glassware was oven-dried at 150 °C for at least 15 h before use, and allowed to cool under vacuum. Reactions involving silver salts were carried out in foil-wrapped glassware, in the dark as much as possible. Column chromatography was carried out in air by standard methods,[2] using silica gel (60 Å, Aldrich) as the stationary phase.

2.1.2 Solvents

Dry, oxygen-free benzene, toluene, hexanes, CH_2Cl_2, THF and diethyl ether (all HPLC grade, Fisher Scientifics) were obtained using a Glass Contour or Anhydrous Engineering solvent purification system, and stored over Linde 4 Å molecular sieves in the glovebox. All other solvents were distilled from an appropriate drying agent,[3] and stored over Linde 4 Å molecular sieves inside the glovebox.

2.1.3 Deuterated solvents

Deuterated solvents were purchased from Cambridge Isotope Laboratories Ltd. or from Aldrich Chemical Co., and used as received for NMR analysis of air-stable species. For oxygen- or moisture-sensitive compounds, ampoules of C_6D_6 or CD_2Cl_2 were opened inside the glovebox; $CDCl_3$ was distilled from CaH_2 and stored over Linde 4 Å molecular sieves in an amber bottle inside the drybox. To prevent contamination of the NMR solvents, the glovebox atmosphere was purged to remove solvent vapors prior to opening these storage vessels.

2.1.4 NMR analysis

^1H (300, 400 or 500 MHz), ^{13}C (75 or 125 MHz), ^{19}F (282 or 376 MHz) and ^{31}P (121 MHz) NMR spectra were recorded on Bruker Avance-300, Avance-400 or Avance-500 spectrometers at 23 °C. Chemical shifts for ^1H and ^{13}C are reported relative to

tetramethylsilane at 0 ppm, ^{31}P NMR spectra to 85% H_3PO_4 (in a sealed capillary within the solvent of interest) at 0 ppm, ^{19}F NMR spectra to trifluorotoluene at –63.72 ppm. Spectra of organometallic compounds were measured under anaerobic conditions in NMR tubes equipped with a J-Young valve.

2.1.5 Gas chromatography

GC-FID quantification was established using an Agilent 6890 chromatograph (equipped with an Agilent 7683 Series autosampler and a Varian CP-wax 52CB column with dimensions 30 m × 320 μm), or an Agilent 7890A instrument (equipped with an Agilent 7683B Series autosampler and a Agilent HP-5MS column with dimensions 30 m × 320 μm). Both instruments were set to an inlet split ratio of 10:1, and inlet and detector temperatures of 250 °C and 275 °C, respectively. Helium (UHP grade) was used as carrier gas, with flow rates of 1.1–1.6 mL min^{-1} depending on the substrate. An injection volume of 1 μL was used in all cases. The FID response was maintained between 100-2000 pA, using analyte concentrations of 0.5 to 5 mM. Retention times were confirmed with samples authenticated by MS and NMR analysis. Quantification involved (1) construction of calibration curves of peak area vs. concentration covering the relevant concentration regime, to correct for sample-dependent detector response (see section 2.12), and (2) use of 1,2,3,4-tetrahydronaphthalene (THN) as an internal integration standard. In RCM catalytic runs, for example, the diene:THN integration ratio was assessed in each sample relative to its value at time zero (t_o).

2.1.6 Other instrumentation

IR spectra were measured on a Bomem MB100 IR spectrometer graciously provided by the Gambarotta group, using NaCl salt plates. Liquids were analyzed neat, solid samples as Nujol mulls, made up in the glovebox for air-sensitive analytes.

Polymer molecular weights and polydispersities were measured by gel-permeation chromatography (GPC) in CH_2Cl_2 (flow rate 1.0 mL min^{-1}; samples 1-2 mg mL^{-1}) using a Wyatt DAWN light-scattering instrument equipped with Optilab DSP refractometer, HPLC system with a Waters model 515 pump, Rheodyne model 7725i injector with 200 μL injection loop, and Waters Styragel HR3 and HR4 columns in series.

Inert-atmosphere MALDI-TOF mass spectra were measured using a Bruker OmniFlex MALDI-TOF mass spectrometer equipped with an N_2 laser (337 nm), and interfaced to an MBraun glovebox. Spectra were collected in positive reflectron mode, with the accelerating voltage held at 20 kV, maintaining laser power at the minimum level required to observe a signal. For all samples, 300-400 laser shots were collected. Charge-transfer ionization[4] was employed, using pyrene or anthracene as matrix and CH_2Cl_2, C_6H_6 or THF as solvent. Matrix and analyte solutions were prepared at concentrations of 20 mg mL^{-1} and 1 mg mL^{-1}, respectively, mixed in a matrix:analyte ratio of 10:1 by volume, and spotted (1-3 μL) on the plate using the dried-droplet method. The mass spectrometer was calibrated externally before each use with *trans*-$RuCl_2(dppe)_2$, using the linear fit method. The most abundant isotope within the peak clusters for $[RuCl_2(dppe)_2]$ ($[M]^+$) and $[RuCl(dppe)_2]$ ($[M–Cl]^+$) were assigned *m/z* ratios of 968.11 and 933.14, respectively.

Electrospray analyses were performed by Dr. Clem Kazakoff of the uOttawa Mass Spectrometry Facility. Samples were prepared at concentrations of 1 mg mL^{-1} in MeCN or THF and filtering the solution through a glass-microfibre filter.

UV-Vis spectra were measured on a Varian Cary-50 spectrophotometer graciously provided by the Scaiano group, at a scan rate of 600 nm min^{-1}. Samples were prepared under N_2 inside the glovebox by filling a Hellma screw-top optical glass cell with 2 mL of a solution sufficiently dilute to avoid saturating the detector (typically 0.3 mM, though the specific concentration depends on the extinction coefficient of the analyte).

2.2 Synthesis of substrates

2.2.1 But-3-enyl but-3-enoate **3a**[5]

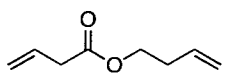

A 250 mL, 3-necked round-bottom flask equipped with a magnetic stirbar was loaded with 3-butenoic acid (5.3 g, 62 mmol), 3-buten-1-ol (4.7 g, 65 mmol), 4-dimethylaminopyridine (17.8 mg, 0.2 mmol), and anhydrous CH_2Cl_2 (150 mL). The colorless solution was cooled in an ice bath, and dicyclohexyl carbodiimide (15.3 g, 74 mmol) was added. Upon warming to room temperature, a white precipitate formed. The suspension was stirred for 24 h at room temperature, then filtered to remove the white urea by-product. The pale yellow filtrate was extracted with 5% aq. HCl (v/v, 100 mL), brine, then water. The combined organic layers were dried ($MgSO_4$), stripped, purified by column

chromatography (10% EtOAc in hexanes), and vacuum distillation (73-76 °C, 4 mm Hg). Yield: 4.6 g (53%). ^{1}H NMR ($CDCl_3$, 300 MHz): δ 5.97–5.69 (m, 2H, =C*H*), 5.18–5.03 (m, 4H, =CH_2), 4.13 (t, $^3J_{HH}$ = 6.6 Hz, 2H, OCH_2), 3.07 (dt, $^3J_{HH}$ = 6.9 Hz, $^4J_{HH}$ = 1.5 Hz, 2H, CH_2CO), 2.37 (qt, $^3J_{HH}$ = 6.9 Hz, $^4J_{HH}$ = 1.5 Hz, 2H, CH_2). ^{13}C{^{1}H} NMR ($CDCl_3$, 75 MHz): δ 171.4 (*C*=O), 133.8 (=*C*H), 130.2 (=*C*H), 118.4 (=*C*H_2), 117.2 (=*C*H_2), 63.6 (O*C*H_2), 39.1 (*C*H_2-CO), 33.0 (*C*H_2). IR (neat, cm^{-1}): ν 1740 (s) HR-MS (+EI): Calcd. for $C_5H_7O_2$, [M-C_3H_5]$^{+\bullet}$, *m/z* 99.0446. Found, *m/z* 99.0445.

2.2.2 But-3-enyl pent-4-enoate **3c**[5]

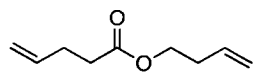

The procedure used to prepare **3a** was followed, using 4-pentenoic acid (4.04 g, 40 mmol) and 3-buten-1-ol (3.06 g, 42 mmol). Yield: 3.6 g (58%). ^{1}H NMR ($CDCl_3$, 300 MHz): δ 5.83–5.71 (m, 2H, =C*H*), 5.09–4.95 (m, 4H, =CH_2), 4.10 (t, $^3J_{HH}$ = 5.5 Hz, 2H, OCH_2), 2.39–2.33 (m, 6H, CH_2). ^{13}C{^{1}H} ($CDCl_3$, 125 MHz): δ 172.8 (*C*=O), 136.6 (=*C*H), 133.9 (=*C*H), 117.1 (=*C*H_2), 115.3 (=*C*H_2), 63.3 (O*C*H_2), 33.4 (*C*H_2), 33.0 (*C*H_2), 28.8 (*C*H_2). IR (neat, cm^{-1}): ν 1735 (s). HR-MS (+EI): Calcd. for $C_6H_9O_2$, [M-C_3H_5]$^{+\bullet}$, *m/z* 113.0603. Found, *m/z* 113.0603.

2.2.3 But-3-enyl hept-6-enoate **3b**[5]

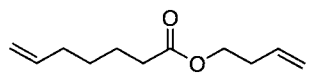

The procedure used to prepare **3a** was followed, using 6-heptanoic acid (2.01 g, 16 mmol) and 3-buten-1-ol (1.21 g, 17 mmol). Yield: 1.26 g (44%). ^{1}H NMR ($CDCl_3$, 300 MHz): δ 5.86–5.69 (m, 2H, =C*H*), 5.14–4.89 (m, 4H, =CH_2), 4.11 (t, $^3J_{HH}$ = 6.7 Hz, 2H, OCH_2), 2.41–2.25 (m, 4H, CH_2), 2.10–2.00 (m, 2H, CH_2), 1.69–1.56 (m, 2H, CH_2), 1.46–1.34 (m, 2H, CH_2). ^{13}C{^{1}H} ($CDCl_3$, 125 MHz): δ 173.6 (*C*=O), 138.3 (=*C*H), 134.0 (=*C*H), 117.1 (=*C*H_2), 114.6 (=*C*H_2), 63.2 (O*C*H_2), 34.1 (*C*H_2CO), 33.3 (*C*H_2), 33.1 (*C*H_2), 28.3 (*C*H_2), 24.4 (*C*H_2). IR (neat, cm^{-1}): ν 1736 (s). HR-MS (+EI): Calcd. for $C_7H_{11}O$, [M-C_4H_7O]$^{+\bullet}$, *m/z* 111.0810. Found, *m/z* 111.0808.

2.2.4 Dec-9-enyl undec-10-enoate **1a**[6]

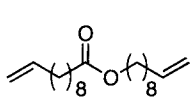

The procedure used to prepare **3a** was followed, using undec-10-enoic acid (10.01 g, 54 mmol) and 9-decen-1-ol (8.91 g, 57 mmol). Yield: 10.86 g (62%). ^{1}H and ^{13}C NMR values are in good agreement with those reported.[6] Due to the complexity of the aliphatic region for **1a**, only key ^{1}H NMR values are given here. ^{1}H NMR

($CDCl_3$, 300 MHz): δ 5.86-5.72 (m, 2H, =C*H*), 5.01-4.89 (m, 4H, =CH_2), 4.04 (t, $^3J_{HH}$ = 6.8 Hz, 2H, OCH_2).

2.2.5 Hex-5-enyl undec-10-enoate **1b**[7]

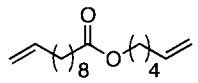

The procedure used to prepare **3a** was followed, using undec-10-enoic acid (4.34 g, 26 mmol) and 5-hexen-1-ol (2.73 g, 27 mmol). Yield: 3.32 g (53%). ^{1}H and ^{13}C NMR values are in good agreement with those reported.[7] Due to the complexity of the aliphatic region for **1b**, only key ^{1}H NMR values are given here. ^{1}H NMR ($CDCl_3$, 300 MHz): δ 5.86-5.71 (m, 2H, =C*H*), 5.04-4.89 (m, 4H, =CH_2), 4.05 (t, $^3J_{HH}$ = 6.6 Hz, 2H, OCH_2).

2.2.6 But-3-enyl undec-10-enoate **1c**[7]

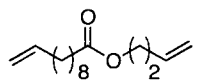

The procedure used to prepare **3a** was followed, using undec-10-enoic acid (4.65 g, 25 mmol) and 3-buten-1-ol (1.89 g, 26 mmol). Yield: 4.03 g (67%). ^{1}H and ^{13}C NMR values are in good agreement with those reported.[7] Due to the complexity of the aliphatic region for **1c**, only key ^{1}H NMR values are given here. ^{1}H NMR ($CDCl_3$, 300 MHz): δ 5.82-5.67 (m, 2H, =C*H*), 5.10-4.85 (m, 4H, =CH_2), 4.08 (t, $^3J_{HH}$ = 6.9 Hz, 2H, OCH_2).

2.2.7 *N,N*-diallyl-4-methylbenzenesulfonamide **9a**[8]

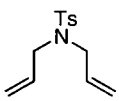

Method A. In an adaptation of a literature procedure,[8] a 100 mL round-bottom flask was charged with diallyl amine (2.00 g, 21 mmol), *p*-tosyl chloride (4.00 g, 21 mmol), triethylamine (2.19 g, 22 mmol) and CH_2Cl_2 (70 mL). The solution was stirred at 23 °C for 15 h hours to afford a white precipitate, which was filtered off, extracted with 10% aq. $KHSO_4$ (50 mL), saturated aq. $NaHCO_3$ (50 mL), and water (50 mL). The combined organic phases were dried ($MgSO_4$) and stripped to a yellow oil. Distillation under vacuum (bp. 188-192 °C, 9 mm Hg) afforded a colorless oil. Yield: 3.26 g (63%). **Method B**. In a modification of a literature procedure,[9] a 250 mL round-bottom flask was charged with *p*-tolylsulfonamide (3.05 g, 18 mmol), allyl bromide (6.61 g, 55 mmol), tetra-*n*-butylammonium iodide (6.60 g, 18 mmol), NaOH (3.64 g, 91 mmol), benzene (100 mL), and water (6 mL). The homogeneous yellow solution was refluxed for 2.5 h, at which time complete, clean formation of the desired product was evident (TLC: R_f = 0.66, 33% EtOAc in hexanes). The product was extracted with ethyl acetate (100 mL). The combined organic

fractions washed with brine (100 mL), then water (100 mL), dried (Na_2SO_4), and stripped to a yellow oil. Column chromatography (33% EtOAc in hexanes) and vacuum distillation (bp. 189-192 °C, 9 mm Hg) afforded a colorless oil. Yield: 2.80 g (63%). ^1H and ^{13}C NMR data agree with values reported.[8] As the literature NMR signals are incompletely assigned, full assignments are provided here. ^1H NMR ($CDCl_3$, 400 MHz): δ 7.70 (d, $^3J_{HH}$ = 8.1 Hz, 2H, Ts Ar C*H*), 7.29 (d, $^3J_{HH}$ = 8.1 Hz, 2H, Ts Ar C*H*), 5.65-5.56 (m, 2H, =C*H*), 5.16-5.11 (m, 4H, =CH_2), 3.80 (d, $^3J_{HH}$ = 6.3 Hz, 4H, NCH_2), 2,42 (s, 3H, Ts CH_3). $^{13}C\{^1H\}$ ($CDCl_3$, 101 MHz): δ 143.2 (Ts *C*CH_3), 137.4 (Ts *C*SO_2), 132.6 (=*C*H), 129.6 (Ts *C*H), 127.1 (Ts *C*H), 118.9 (=*C*H_2), 49.3 (N*C*H_2), 21.5 (Ts *C*H_3).

2.2.8 *N,N*-di(but-3-enyl)-4-methylbenzenesulfonamide **9b**[10]

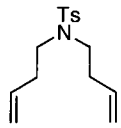

The compound was synthesized as described in Method B for **9a**, using *p*-tolylsulfonamide (1.84 g, 11 mmol), 4-bromobutene (2.90 g, 21 mmol), tetra-*n*-butylammonium iodide (3.29 g, 9 mmol), NaOH (1.43 g, 36 mmol), benzene (70 mL) and water (5 mL). This compound was pure enough to use without distillation. Yield: 1.20 g (40%). ^1H and ^{13}C NMR data agree with values reported.[10] As the literature NMR signals are incompletely assigned, full assignments are provided here. ^1H NMR ($CDCl_3$, 400 MHz): δ 7.68 (d, $^3J_{HH}$ = 8.3 Hz, 2H, Ts Ar C*H*), 7.28 (d, $^3J_{HH}$ = 8.6 Hz, 2H, Ts Ar C*H*), 5.75-5.64 (m, 2H, =C*H*), 5.07-4.99 (m, 4H, =CH_2), 3.19-3.16 (m, 4H, NCH_2), 2,40 (s, 3H, Ts CH_3), 2.31-2.25 (m, 4H, CH_2). $^{13}C\{^1H\}$ ($CDCl_3$, 101 MHz): δ 143.1 (Ts *C*CH_3), 136.9 (Ts *C*SO_2), 134.6 (=*C*H), 129.5 (Ts *C*H), 127.0 (Ts *C*H), 117.0 (=*C*H_2), 47.7 (N*C*H_2), 33.1 (CH_2-*C*H_2) 21.4 (Ts *C*H_3).

2.2.9 *N,N*-di(hex-5-enyl)-4-methylbenzenesulfonamide **9c**[9]

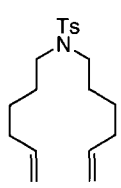

The compound was synthesized as described in Method B for **9a**, using *p*-tolylsulfonamide (1.03 g, 6 mmol), 6-bromohexene (1.63 g, 10 mmol), tetra-*n*-butylammonium iodide (1.85 g, 5 mmol), NaOH (0.80 g, 20 mmol), benzene (35 mL) and water (5 mL). This compound was pure enough to use without distillation. Yield: 1.77 g (58%). ^1H and ^{13}C NMR data agree with values reported.[9] As the literature NMR signals are incompletely assigned, full assignments are provided here. ^1H NMR ($CDCl_3$, 400 MHz): δ 7.68 (d, $^3J_{HH}$ = 8.4 Hz, 2H, Ts Ar C*H*), 7.29 (d, $^3J_{HH}$ = 8.4 Hz, 2H, Ts Ar C*H*), 5.82-5.69 (m, 2H, =C*H*), 5.02-4.92 (m, 4H, =CH_2), 3.09 (t, $^3J_{HH}$ = 7.4 Hz,

4H, NCH_2), 2,42 (s, 3H, Ts CH_3), 2.08-2.00 (m, 4H, CH_2CH=), 1.57-1.47 (m, 4H, NCH_2CH_2), 1.41-1.30 (m, 4H, CH_2CH_2CH=). $^{13}C\{^1H\}$ ($CDCl_3$, 101 MHz): δ 142.9 (Ts CSO_2), 138.3 (=CH), 137.1 (Ts CCH_3), 129.5 (Ts CH), 127.1 (Ts CH), 114.8 (=CH_2), 48.0 (NCH_2), 33.2 (CH_2CH=), 28.0 (NCH_2CH_2), 25.9 (CH_2CH_2CH=), 21.5 (Ts CH_3).

2.2.10 (1-(Allyloxy)prop-2-yne-1,1-diyl)dibenzene **22a** [10]

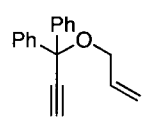

In a modification of a literature procedure,[10] a solution of 1,1-diphenyl-yn-1-ol (3.98 g, 19 mmol) in DMF (40 mL) was treated with NaH (0.56 g, 23 mmol). Vigorous bubbling and formation of an off-white solid was observed. The suspension was stirred for 1 h at 23 °C, then treated with allyl bromide (2.33 g, 19 mmol), warmed to 54 °C in an oil bath, and stirred for 13 h. The resulting homogeneous yellow solution was quenched with H_2O (20 mL) and extracted with diethyl ether (4 × 25 mL). The combined organic fractions were dried ($MgSO_4$) and stripped to yield a yellow oil, which was purified by column chromatography (10% EtOAc in hexanes). Yield: 3.04 g (64%). ^1H and ^{13}C NMR data agree with values reported.[10] As the literature NMR signals are incompletely assigned, full assignments are provided here. ^1H NMR ($CDCl_3$, 400 MHz): δ 7.78-7.73 (m, 4H, Ph *o*-C*H*), 7.47-7.34 (m, 6H, Ph *m*- and *p*-C*H*), 6.21-6.08 (m, 1H, =C*H*), 5.52 (dq, $^2J_{HH}$ (*gem*) ≈ $^4J_{HH}$ = 2.0 Hz, $^3J_{HH}$ = 17.4 Hz, 1H, *trans* =C*H*H), 5.32 (dq, $^2J_{HH}$ (*gem*) ≈ $^4J_{HH}$ = 2.0 Hz, $^3J_{HH}$ = 10.5 Hz, 1H, *cis* =C*H*H), 4.21 (dt, $^3J_{HH}$ = 5.1 Hz, $^4J_{HH}$ = 1.8 Hz, 2H, OCH_2), 2.98 (s, 1H, ≡C*H*). $^{13}C\{^1H\}$ ($CDCl_3$, 101 MHz): δ 143.1 (Ph *i*-*C*), 134.7 (=CH), 128.2 (Ph *m*-*C*H), 127.7 (Ph *p*-*C*H), 126.6 (Ph *o*-*C*H), 116.1 (=CH_2), 83.2 (HC≡*C*), 80.0 (*C*-$(Ph)_2$), 77.6 (H*C*≡), 65.9 (OCH_2).

2.2.11 (1-(Pent-4-enyloxy)prop-2-yne-1,1-diyl)dibenzene **22b**

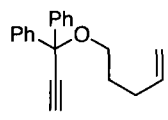

The procedure used to prepare **22a** was followed, using 1,1-diphenyl-yn-1-ol (2.79 g, 13 mmol), NaH (0.68 g, 28 mmol), 5-bromopentene (2.00 g, 13 mmol) and DMF (75 mL). Yield: 1.23 g (33%). ^1H NMR ($CDCl_3$, 400 MHz): δ 7.60-7.57 (m, 4H, Ph *o*-C*H*), 7.36-7.25 (m, 6H, Ph *m*- and *p*-C*H*), 5.91-5.81 (m, 1H, =C*H*), 5.05 (dq, $^2J_{HH}$ ≈ $^4J_{HH}$ = 2.0 Hz, $^3J_{HH}$ = 17.2 Hz, 1H, *trans* =C*H*H), 4.97 (dq, $^2J_{HH}$ ≈ $^4J_{HH}$ = 1.5 Hz, $^3J_{HH}$ = 10.2 Hz, 1H, *cis* =C*H*H), 3.52 (t, $^3J_{HH}$ = 6.4 Hz, 2H, OCH_2), 2.88 (s, 1H, ≡C*H*), 2.25-2.19 (m, 2H, OCH_2CH_2), 1.82-1.75 (m, 2H, CH_2CH=). $^{13}C\{^1H\}$ ($CDCl_3$, 101 MHz): δ 143.4 (Ph *i*-*C*), 138.5 (=CH), 128.1 (Ph *m*-*C*H), 127.6 (Ph *p*-*C*H), 126.6 (Ph *o*-*C*H), 114.6

(=CH_2), 83.5 (HC≡C), 79.8 (C(Ph)$_2$), 77.3 (HC≡), 64.0 (OCH_2), 30.5 (OCH_2CH_2), 29.2 (CH_2CH=). HR-MS (+EI): Calcd. for $C_{20}H_{20}O$, $[M]^{+\bullet}$, *m/z* 276.1514. Found, *m/z* 276.1511.

2.2.12 Diethyl 2,2-di(but-3-enyl)malonate **11**[5]

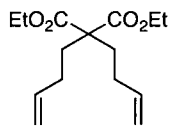

To a solution of sodium ethoxide (2.69 g, 40 mmol) in dry DMF (20 mL) was added diethyl malonate (2.11 g, 13 mmol). The solution was stirred for 9 h under N_2, after which 4-bromo-1-butene (944 mg, 7 mmol) was added and the reaction was stirred for a further 17 h. The mono-allyl adduct was isolated by quenching with 5% aq. HCl (25 mL) and extracting with Et_2O (4 × 20 mL). The combined organic phases were dried ($MgSO_4$), filtered, and stripped of solvent to give a brown oil, which was purified by chromatography on silica gel (10% EtOAc in hexanes). To a solution of the mono-allyl adduct (1.25 g, 6 mmol) in dry DMF (10 mL) was added solid NaH (280 mg, 12 mmol). The suspension was stirred for 1 h, after which 4-bromo-1-butene (945 mg, 7 mmol) was added and stirring continued at 80 °C for 20 h under N_2. The solution was worked up as above. Yield: 397 mg (25%). ^{1}H NMR ($CDCl_3$, 300 MHz): δ 5.85–5.70 (m, 2H, =CH), 5.08–4.92 (m, 4H, =CH_2), 4.20 (q, $^3J_{HH}$ = 7.1 Hz, 4H, CO_2CH_2), 2.04–1.90 (m, 8H, CH_2), 1.27 (t, $^3J_{HH}$ = 7.1 Hz, 6H, CH_3). ^{13}C{^{1}H} NMR ($CDCl_3$, 75 MHz): δ 171.9, 138.0, 115.4, 61.5, 57.4, 31.9, 28.8, 14.5. IR (neat, cm^{-1}): ν 1731 (s). HR-MS (+EI): Calcd. for $C_{13}H_{19}O_3$, $[M-C_2H_5O]^{+\bullet}$, *m/z* 223.1334. Found, *m/z* 223.1352.

2.2.13 4,7,10,13-Tetraoxahexadeca-1,15-diene **5**

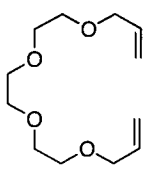

A 250 mL round-bottom flask was charged with triethylene glycol (4.54 g, 30 mmol) and DMF (150 mL) and cooled in an ice bath. NaH (1.80 g, 75 mmol) was added slowly to the colorless solution. Liberation of H_2 was observed along with the formation of a white solid. The solution was stirred at room temperature for 2 h after which allyl bromide (7.60 g, 62 mmol) was added. The solution was stirred for a further 24 h at room temperature. The white precipitate gradually disappeared and a yellow color emerged. The reaction was quenched with water (100 mL) and the product extracted with diethyl ether (3 × 75 mL). The combined organic layers were washed with brine then water, dried over Na_2SO_4 and stripped. The colorless oil was purified by column chromatography (60% Et_2O in hexanes). Yield: 4.75 g (68%). ^{1}H NMR ($CDCl_3$, 300 MHz): δ 5.95-5.82 (m, 2H, =CH), 5.28-5.12 (m, 4H, =CH_2), 3.99 (dt, $^3J_{HH}$ = 5.6 Hz, $^4J_{HH}$ = 1.3 Hz, 4H, CH_2CH=),

3.65-3.55 (m, 12H, CH_2). $^{13}C\{^1H\}$ NMR ($CDCl_3$, 75 MHz): δ 134.7 (=*C*H), 117.0 (=*C*H_2), 72.1 (*C*H_2CH=), 70.5 (*C*H_2), 69.3 (*C*H_2). HR-MS (+EI): Calcd. for $C_9H_{17}O_4$, $[M\text{-}C_3H_5]^{+\bullet}$, *m/z* 189.1127. Found, *m/z* 189.1126.

2.2.14 5-(Methoxymethyl)bicyclo[2.2.1]hept-2-ene **21**[11]

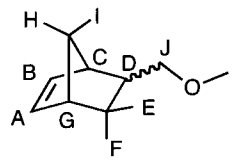

In a modification of a literature procedure,[11] a 250 mL round-bottom Schlenk flask was loaded with 5-norbornen-1-methanol (5.00 g, 40 mmol) and THF (100 mL). The colorless solution was cooled to 0 °C on the Schlenk line and solid NaH (1.18 g, 49 mmol) was slowly added against a flow of argon. Once bubbling of H_2 stopped, a clear, pale-yellow solution with a white suspension is obtained. Methyl iodide (6.97 g, 49 mmol) was then added against a flow of argon creating a mildly exothermic reaction. The resulting solution was left to stir under argon for 18 h at which point the homogeneous yellow solution was quenched with water (30 mL). The THF solvent was removed under reduced pressure and the resulting suspension was extracted with diethyl ether (4 × 50 mL). The combined organic fractions were dried over Na_2SO_4, stripped, purified by column chromatography (10% EtOAc in hexanes; R_f = 0.52) and vacuum distillation (bp. 85-90 °C, 70 mm Hg). Yield: 4.95 g (89%) of a 70:30 mixture of endo and exo isomers. ^{13}C NMR data agree with values reported.[11] As the literature ^{13}C NMR signals are incompletely assigned, full assignments are provided here (for numbering system, see structure). ^1H NMR ($CDCl_3$, 400 MHz): δ 6.11-6.02 (m, 1.42H, H_A endo and H_B exo), 6.04-6.01 (m, 0.42H, H_A exo), 5.92-5.90 (m, 1H, H_B endo), 3.39 (dd, J_{HH} = 9.2 Hz, J_{HH} = 6.3 Hz, 0.42H, H_J exo), 3.33 (s, 1.26 H, H_K exo), 3.29-3.27 (m, 3.42 H, H_K endo and H_J exo), 3.06 (dd, J_{HH} = 9.2 Hz, J_{HH} = 6.7 Hz, 1H, H_J endo), 2.98 (t, J_{HH} = 9.0 Hz, 1H, H_J endo), 2.87 (br s, $\omega_{1/2}$ = 8 Hz, 1H, H_C endo), 2.76 (br s, $\omega_{1/2}$ = 11.5 Hz, 1.42H, H_G endo and H_C exo), 2.70 (br s, $\omega_{1/2}$ = 6.5 Hz, 0.42H, H_G exo), 2.36-2.27 (m, 1H, H_D endo), 1.79 (ddd, J_{HH} = 11.7 Hz, J_{HH} = 8.5 Hz, J_{HH} = 3.9 Hz, 1H, H_F endo), 1.69-1.62 (m, 0.42H, H_D exo), 1.42-1.38 (m, 1H, H_H or H_I endo), 1.32-1.19 (m, 2.26H, H_H or H_I endo, H_H exo, H_I exo, H_E or H_F exo), 1.11-1.06 (m, 0.42H, H_E or H_F exo), 0.42 (ddd, J_{HH} = 11.6 Hz, J_{HH} = 4.5 Hz, J_{HH} = 2.7 HZ, 1H, H_E endo). $^{13}C\{^1H\}$ ($CDCl_3$, 101 MHz): δ 137.0 (C_A endo), 136.53 (C_A or C_B exo), 136.51 (C_A or C_B exo), 132.4 (C_B endo), 77.5 (C_J exo), 76.6 (C_J endo), 58.7 (C_K exo), 58.6 (C_K endo), 49.4 ($C_{H/I}$ endo), 45.0 ($C_{H/I}$ exo), 43.9 (C_C endo), 43.6 (C_G exo), 42.1 (C_G endo), 41.5 (C_C exo), 38.8 (C_D exo), 38.7 (C_D endo), 29.6 ($C_{E/F}$ exo), 29.1 ($C_{E/F}$ endo).

References page 70

2.2.15 1,2-Bis(allyloxy)benzene **7**[12]

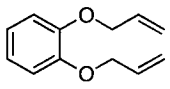

In a modification of a literature procedure,[12] a 250 mL round-bottom Schlenk flask was charged with catechol (4.40 g, 40 mmol) and anhydrous DMF (125 mL; added by cannula). The colorless solution was cooled to 0 °C in an ice bath, and solid NaH (2.10 g, 88 mmol) slowly added to produce a white suspension, which was treated with allyl bromide (9.94 g, 82 mmol) and left to stir for 18 h. The resulting yellow-green homogeneous solution was quenched with 5% aq. HCl (50 mL). The organics were extracted with diethyl ether (3 × 60 mL). The combined organic layers were washed with brine, then water (50 mL each), dried ($MgSO_4$), stripped, and purified by column chromatography (5% EtOAc in hexanes; R_f = 0.67). Yield: 6.47 g (85%). ^1H and ^{13}C NMR data agree with values reported.[12] As the literature NMR signals are incompletely assigned, full assignments are provided here. ^1H NMR ($CDCl_3$, 400 MHz): δ 6.93-6.88 (m, 4H, Ph C*H*), 6.14-6.04 (m, 2H, =C*H*), 5.42 (dq, $^3J_{HH}$ = 17.3 Hz, $^2J_{HH}$ (*gem*) ≈ $^4J_{HH}$ = 1.6 Hz, 2H, *trans* =C*H*H), 5.27 (dq, $^3J_{HH}$ = 10.6 Hz, $^2J_{HH}$ (*gem*) ≈ $^4J_{HH}$ = 1.5 Hz, 2H, *cis* =C*H*H), 4.61 (dt, $^3J_{HH}$ = 5.3 Hz, $^4J_{HH}$ = 1.6 Hz, OCH_2). $^{13}C\{^1H\}$ ($CDCl_3$, 101 MHz): δ 148.6 (Ph *C*O), 133.6 (=*C*H), 121.2 (Ph *m*-*C*H), 117.5 (=*C*H_2), 114.3 (Ph *o*-*C*H), 70.0 (O*C*H_2).

2.2.16 (1-(Allyloxy)but-3-enyl)benzene **17**[13]

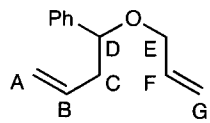

In a modification of a literature procedure,[13] a dry 100 mL Schlenk was loaded with 1-phenyl-3-butene-1-ol (2.02 g, 14 mmol) and anhydrous DMF (40 mL). The colorless solution was cooled in an ice bath. Solid NaH (0.41 g, 17 mmol) was added against a flow of Ar producing a color change to yellow. After stirring for 2 h at room temperature, allyl bromide (1.81 g, 15 mmol) was added creating a small exothermic reaction and formation of a white precipitate (presumably NaBr). The solution was stirred at room temperature for 16 h at which point water (25 mL) was added to quench the reaction. The product was extracted with diethyl ether (4 × 20 mL), dried ($MgSO_4$), and stripped. The resulting yellow oil was subsequently purified by column chromatography (5% EtOAc in hexanes; R_f = 0.71) and vacuum distillation (bp. 96-99 °C, 6 mm Hg). Yield: 1.62 g (63%). ^1H and ^{13}C NMR data agree with values reported.[13] As the literature NMR signals are incompletely assigned, full assignments are provided here (for numbering system, see structure). ^1H NMR ($CDCl_3$, 400 MHz): δ 7.32-7.20 (m, 5H, Ph C*H*), 5.89-5.80 (m, 1H, H_F), 5.79-5.68 (m, 1H, H_B), 5.19 (dq, $^3J_{HH}$ = 17.2 Hz, $^2J_{HH}$ (*gem*) ≈ $^4J_{HH}$ =

1.7 Hz, 1H, *trans* H_G), 5.10 (dq, $^3J_{HH}$ = 10.4 Hz, $^2J_{HH}$ (*gem*) ≈ $^4J_{HH}$ = 1.8 Hz, 1H, *cis* H_G), 5.02-4.94 (m, 2H, H_A), 4.29 (dd, $^3J_{HH}$ = 7.6 and 6.1 Hz, 1H, H_D), 3.88 (ddt, $^2J_{HH}$ (*gem*) = 12.8 Hz, $^3J_{HH}$ = 5.0 Hz, $^4J_{HH}$ = 1.6 Hz, 1H, H_E), 3.72 (ddt, $^2J_{HH}$ (*gem*) = 13.1 Hz, $^3J_{HH}$ = 6.08 Hz, $^4J_{HH}$ = 1.4 Hz, 1H, H_E), 2.59-2.52 (m, 1H, H_C), 2.41-2.34 (m, 1H, H_C). $^{13}C\{^1H\}$ ($CDCl_3$, 101 MHz): δ 141.9 (Ph *i*-*C*), 134.9 (C_B or C_F), 134.8 (C_B or C_F), 128.3 (Ph *m*-*C*H), 127.6 (Ph *p*-*C*H), 126.8 (Ph *o*-*C*H), 116.8 (C_A or C_G), 116.7 (C_A or C_G), 81.1 (C_D), 69.4 (C_E), 42.6 (C_C).

2.3 High-EM RCM products

2.3.1 General procedure

Inside the glovebox, a 50 mL Schlenk flask was loaded with the diene (60-300 mg), and diluted to a concentration of 100 mM with CH_2Cl_2. To the diene solution was added solid **Ru-6a** (1-5 mol%) from a stock solution in CH_2Cl_2, and the resulting solution was refluxed for 3 h under an argon atmosphere. Following reflux, a solution of Ktp (10 equiv vs. [Ru]) in THF was added to quench the catalyst. The main solution changes color from yellow to green over the course of 30 min. The resulting quenched solution was stripped off solvent and the green residue was purified by passing through a 4 cm plug of alumina using hexanes (20 mL) as eluent. Pure RCM products were isolated following removal of hexanes under reduced pressure. While the vast majority of these products are documented in the literature, NMR characterization is nevertheless given here to provide a useful reference point. They are ordered from the 5-membered rings to the 8-membered ring.

2.3.2 1-Tosyl-2,5-dihydro-1*H*-pyrrole **10a**[14]

Synthesized according to general protocol using **9a** (100 mg, 0.40 mmol) and **Ru-6a** (290 μL, 0.004 mmol, 10 mg mL^{-1}, CH_2Cl_2, 1 mol%) and Ktp (10 mg, 0.040 mmol). Yield: 79 mg (89%). ^1H NMR ($CDCl_3$, 400 MHz): δ 7.72 (d, $^3J_{HH}$ = 8.3 Hz, 2H, SO_2CCH), 7.32 (d, $^3J_{HH}$ = 8.3 Hz, 2H, CH_3CCH), 5.65 (s, 2H, =C*H*), 4.12 (s, 4H, NCH_2), 2.43 (s, 3H, CH_3). $^{13}C\{^1H\}$ ($CDCl_3$, 101 MHz): δ 143.4 (CCH_3), 134.3 (SO_2C), 129.7 (CH_3CCH), 127.4 (SO_2CCH), 125.4 (=*C*H), 54.8 (NCH_2), 21.5 (CH_3).

2.3.3 Diethyl cyclopent-3-ene-1,1-dicarboxylate **12a**[15]

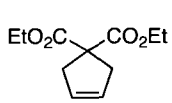

Synthesized according to general protocol using **11a** (100 mg, 0.42 mmol) and **Ru-6a** (300 μL, 0.004 mmol, 10 mg mL^{-1}, CH_2Cl_2, 1 mol%) and Ktp (11 mg,

0.043 mmol). Yield: 80 mg (91%). ^{1}H NMR ($CDCl_3$, 300 MHz): δ 5.60 (s, 2H, =C*H*), 4.19 (q, $^3J_{HH}$ = 7.2 Hz, 4H, OCH_2), 3.00 (s, 4H, CH_2), 1.24 (t, $^3J_{HH}$= 7.1 Hz, 6H, CH_3). ^{13}C{^{1}H} ($CDCl_3$, 75 MHz): δ 172.2 (*C*=O), 127.8 (=*C*H), 61.5 (O*C*H_2), 58.8 (*C*(CO_2Et)$_2$), 40.8 (*C*H_2), 14.0 (*C*H_3).

2.3.4 1-Methylcyclopent-2-enol **14**

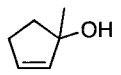

Synthesized according to general protocol using **13** (256 mg, 1.66 mmol) and **Ru-6a** (1 mL, 0.017 mmol, 12 mg mL^{-1}, CH_2Cl_2, 1 mol%) and Ktp (42 mg, 0.17 mmol). *Note: Diethyl ether was used as eluent for the purification stage (R_f = 0.71).* Yield: 80 mg (49%), limited by volatility. ^{1}H NMR ($CDCl_3$, 400 MHz): δ 5.82-5.79 (m, 1H, CH_2C*H*=), 5.70-5.67 (m, 1H, CC*H*=), 2.47-2.44 (m, 1H, =CHC*H*H), 2.34-2.31 (m, 1H, =CHC*H*H), 2.00-1.87 (m, 2H, CCH_2), 1.73 (br s, $\omega_{1/2}$ = 20 Hz, 1H, O*H*), 1.37 (m, 3H, CH_3). ^{13}C{^{1}H} ($CDCl_3$, 101 MHz): δ 137.8 (C*C*H=), 132.6 (CH_2*C*H=), 83.4 (*C*OH), 39.6 (C*C*H_2), 31.0 (*C*H_2CH=), 27.4 (*C*H_3). HR-MS (+EI): Calcd. for C_6H_9O, $[M-H]^{+\bullet}$, *m/z* 97.0653. Found, *m/z* 97.0651.

2.3.5 1,1-Diphenyl-2,5-dihydro-1*H*-silole **16**[16]

Synthesized according to general protocol using **15** (100 mg, 0.38 mmol) and **Ru-6a** (1 mL, 0.019 mmol, 14 mg mL^{-1}, CH_2Cl_2, 5 mol%) and Ktp (49 mg, 0.19 mmol). Yield: 76 mg (85%). ^{1}H NMR ($CDCl_3$, 400 MHz): δ 7.61 (d, $^3J_{HH}$ = 8.0 Hz, 4H, Ph *o*-C*H*), 7.45-7.39 (m, 6H, Ph *m*- and *p*-C*H*), 6.11 (s, 2H, =C*H*), 1.92 (s, 4H, CH_2). ^{13}C{^{1}H} ($CDCl_3$, 101 MHz): δ 135.7 (Ph, *i*-*C*H), 134.7 (Ph *o*-*C*H), 131.0 (Ph *m*-*C*H), 129.3 (Ph *p*-*C*H), 127.8 (=*C*H), 16.7 (*C*H_2).

2.3.6 2,5-Dihydrothiophene **20**[17]

Synthesized according to general protocol using **19** (300 mg, 2.6 mmol) and **Ru-6a** (1 mL, 0.014 mmol, 10 mg mL^{-1}, CH_2Cl_2, 0.5 mol%) and Ktp (40 mg, 0.16 mmol). Yield: 110 mg (49%) limited by volatility. ^{1}H NMR ($CDCl_3$, 300 MHz): δ 5.86 (s, 2H, =C*H*), 3.76 (s, 4H, CH_2). ^{13}C{^{1}H} ($CDCl_3$, 75 MHz): δ 128.6 (=*C*H), 39.0 (*C*H_2).

2.3.7 2,2-Diphenyl-3-vinyl-2,5-dihydrofuran **23a**[18]

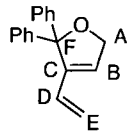

Synthesized according to general protocol using **22a** (100 mg, 0.40 mmol) and **Ru-6a** (292 μL, 0.004 mmol, 10 mg mL^{-1}, CH_2Cl_2, 1 mol%) and Ktp (10 mg, 0.04 mmol). Yield: 85 mg (86%). For numbering system, see structure. ^1H NMR ($CDCl_3$, 300 MHz): δ 7.35-7.21 (m, 10H, Ph C*H*), 6.24 (dd, $^3J_{HH}$ (*trans*) = 17.8 Hz, $^3J_{HH}$ (*cis*) = 11.3 Hz, 1H, H_D), 6.15 (m, 1H, H_B), 5.31 (dd, $^3J_{HH}$ (*trans*) = 17.8 Hz, $^2J_{HH}$ (*gem*) = 1.8 Hz, 1H, *trans* H_E , 5.11 (dd, $^3J_{HH}$ (*cis*) = 11.2 Hz, $^2J_{HH}$ (*gem*) = 1.8 Hz, 1H, *cis* H_E, 4.77 (s, 2H, CH_A). $^{13}C\{^1H\}$ ($CDCl_3$, 75 MHz): δ 143.7 (Ph *i-C*), 143.3 (C_D), 129.8 (C_B), 128.0 (Ph *m-C*H), 127.9 (Ph *o-C*H), 127.4 (Ph *p-C*H), 124.9 (C_C), 117.5 (C_E), 94.5 (C_F), 73.2 (C_A).

2.3.8 2-Phenyl-3,6-dihydro-2*H*-pyran **18**[19]

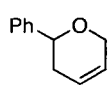

Synthesized according to general protocol using **17** (291 mg, 1.6 mmol) and **Ru-6a** (1.0 mL, 0.017 mmol, 12 mg mL^{-1}, CH_2Cl_2, 1 mol%) and Ktp (42 mg, 0.17 mmol). Yield: 196 mg (79%). ^1H NMR ($CDCl_3$, 400 MHz): δ 7.41-7.35 (m, 4H, Ph *o*-C*H* and Ph *m*-C*H*). 7.31-7.27 (m, 1H, Ph *p*-C*H*), 5.97-5.91 (m, 1H, $CHCH_2CH$=), 5.85-5.81 (m, 1H, OCH_2CH=), 4.57 (dd, $^3J_{HH}$ = 10.3 Hz, 3.6 Hz, OC*H*Ph), 4.40-4.37 (m, 2H, OCH_2), 2.44-2.34 (m, 1H, $CHCH_2$), 2.31-2.23 (m, 1H, $CHCH_2$). $^{13}C\{^1H\}$ ($CDCl_3$, 101 MHz): δ 142.6 (Ph *i-C*), 128.4 (Ph *m-C*H), 127.5 (Ph *p-C*H), 126.4 (OCH_2CH=), 125.9 (Ph *o-C*H), 124.4 ($CHCH_2CH$=), 75.6 (O*C*H), 66.6 (OCH_2), 32.9 ($CHCH_2$).

2.3.9 (*Z*)-1-Tosyl-2,3,6,7-tetrahydro-1*H*-azepine **10b**[10]

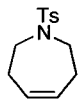

Synthesized according to general protocol using **9b** (60 mg, 0.21 mmol) and **Ru-6a** (152 μL, 0.002 mmol, 10 mg mL^{-1}, CH_2Cl_2, 1 mol%) and Ktp (5 mg, 0.02 mmol). Yield: 44 mg (82%) of a white crystalline solid. ^1H NMR ($CDCl_3$, 400 MHz): δ 7.67 (d, $^3J_{HH}$ = 8.3 Hz, 2H, SO_2CCH), 7.29 (d, $^3J_{HH}$ = 8.3 Hz, 2H, CH_3CCH), 5.75 (t, $^3J_{HH}$ = 3.3 Hz, 2H, =C*H*), 3.28-3.26 (m, 4H, NCH_2), 2.42 (s, 3H, Ts CH_3), 2.33-2.31 (m, 4H, $=CHCH_2$). $^{13}C\{^1H\}$ ($CDCl_3$, 101 MHz): δ 143.1 (CCH_3), 136.3 (SO_2C), 130.2 (=*C*H), 129.7 (CH_3CCH), 127.1 (SO_2CCH), 48.3 (NCH_2), 29.9 ($=CHCH_2$), 21.5 (CH_3).

2.3.10 (*Z*)-Diethyl cyclohept-4-ene-1,1-dicarboxylate **12b**[5]

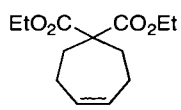

Synthesized according to general protocol using **11b** (100 mg, 0.37 mmol) and **Ru-6a** (206 μL, 0.0037 mmol, 13 mg mL^{-1}, CH_2Cl_2, 1 mol%) and Ktp (9 mg, 0.037 mmol). Yield: 75 mg (84%). ^1H NMR ($CDCl_3$, 400 MHz): δ 5.67 (t, $^3J_{HH}$ = 2.3 Hz, 2H, =C*H*), 4.18 (q, $^3J_{HH}$ = 7.0 Hz, 4H, COCH_2), 2.22-2.21 (m, 8H, CH_2), 1.24 (t, $^3J_{HH}$ = 7.1 Hz, 6H, CH_3). $^{13}C\{^1H\}$ ($CDCl_3$, 101 MHz): δ 172.3 (*C*=O), 130.9 (=*C*H), 61.1 (CO*C*H_2), 58.0 (*C*($CO_2Et)_2$) , 32.0 (C*C*H_2), 24.5 (=CH*C*H_2), 14.0 (*C*H_3).

2.3.11 (*Z*)-2,2-Diphenyl-3-vinyl-2,5,6,7-tetrahydrooxepine **23b**

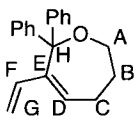

Synthesized according to general protocol using **22a** (100 mg, 0.36 mmol) and **Ru-6a** (260 μL, 0.0036 mmol, 10 mg mL^{-1}, CH_2Cl_2, 1 mol%) and Ktp (9 mg, 0.036 mmol). Yield: 80 mg (89%). For numbering system, see structure. ^1H NMR ($CDCl_3$, 400 MHz): δ 7.36-7.27 (m, 10H, Ph C*H*), 6.31 (t, $^3J_{HH}$ = 6.0 Hz, 1H, H_D), 5.73 (ddd, $^3J_{HH}$ (*trans*) = 16.9 Hz, $^3J_{HH}$ (*cis*) = 10.8 Hz, $^4J_{HH}$ = 0.9 Hz, 1H, H_F), 5.20 (dd, $^3J_{HH}$ (*trans*) = 17.1 Hz, $^2J_{HH}$ (*gem*) = 1.8 Hz, 1H, *trans* H_G, 4.67 (dd, $^3J_{HH}$ = 10.8 Hz, $^2J_{HH}$ (*gem*) = 1.8 Hz, 1H, *cis* H_G, 3.59 (t, $^3J_{HH}$ = 17.1 Hz, 2H, H_A), 2.48 (m, 2H, H_C), 1.68 (m, 2H, H_B). HR-MS (+EI): Calcd. for $C_{20}H_{20}O$, $[M]^{+\bullet}$, *m/z* 276.1514. Found, *m/z* 276.1511.

2.3.12 (*Z*)-2,5-Dihydrobenzo[*b*][1,4]dioxocine **8**[12]

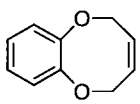

Synthesized according to general protocol using **7** (100 mg, 0.53 mmol) and **Ru-6a** (770 μL, 0.027 mmol, 25 mg mL^{-1}, CH_2Cl_2, 5 mol%) and Ktp (67 mg, 0.27 mmol). Yield: 71 mg (83%). ^1H NMR ($CDCl_3$, 300 MHz): δ 6.97 (s, 4H, Ph C*H*), 5.90-5.87 (m, 2H, =CH_2), 4.92-4.91 (m, 4H, OCH_2). ^{13}C NMR ($CDCl_3$, 75 MHz): δ 148.7 (Ph *C*O), 129.1 (=*C*H), 124.2 (Ph *m*-*C*H), 116.7 (Ph *o*-*C*H), 70.2 (OCH_2).

References page 70

2.4 Low-EM RCM products

2.4.1 Oxacycloicos-11-en-2-one **2a**[6]

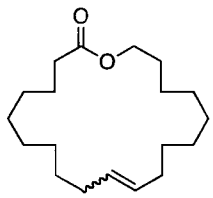

A solution of catalyst **Ru-3** (26 mg, 0.032 mmol) in 1 mL CH_2Cl_2 was added in one rapid dose to a solution of **1a** (200 mg, 0.62 mmol) in 620 mL CH_2Cl_2 in a 1 L round-bottom flask. The solution was heated to reflux for 24 h. After this time, a solution of Ktp (80 mg, 0.32 mmol) in THF (2 mL) was added to the yellow solution and stirred for a further hour at room temperature over which time the solution turned pale green. The solution was concentrated to ca. 1 mL and the product purified by chromatography on silica gel (10% EtOAc in hexanes) by taking the first eluent (R_f = 0.65; 10% EtOAc in hexanes). Evaporation of the solvent afforded **2a** as a colorless oil. Isolated yield: 113 mg (62%). Spectroscopic values match those for the published compound.[6]

2.4.2 Oxacyclohexadec-11-en-2-one **2b**[7]

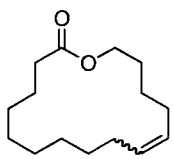

A solution of catalyst **Ru-3** (31 mg, 0.038 mmol) in 1 mL CH_2Cl_2 was added in one rapid dose to a solution of **1b** (200 mg, 0.75 mmol) in 150 mL CH_2Cl_2 in a 500 mL round-bottom flask. The solution was heated to reflux for 24 h. After this time, a solution of Ktp (95 mg, 0.38 mmol) in THF (2 mL) was added to the yellow solution and stirred for a further hour at room temperature over which time the solution turned pale green. The solution was concentrated to ca. 1 mL and the product purified by chromatography on silica gel (10% EtOAc in hexanes) by taking the first eluent (R_f = 0.63; 10% EtOAc in hexanes). Evaporation of the solvent afforded **2b** as a colorless oil. Isolated yield: 127 mg (71%). Spectroscopic values match those for the published compound.[7]

2.4.3 Oxacyclotetradec-11-en-2-one **2c**[7]

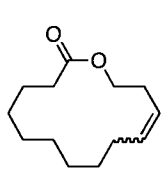

A solution of catalyst **Ru-4a** (35 mg, 0.043 mmol) in 1 mL CH_2Cl_2 was added in one rapid dose to a solution of **1c** (200 mg, 0.84 mmol) in 175 mL CH_2Cl_2 in a 500 mL round-bottom flask. The solution was heated to reflux for 24 h. After this time, a solution of Ktp (110 mg, 0.44 mmol) in THF (2 mL) was added to the yellow solution and stirred for a further hour at room temperature over which time the solution turned pale green. The solution was concentrated to ca. 1 mL and the

product purified by chromatography on silica gel (10% EtOAc in hexanes) by taking the first eluent (R_f = 0.52; 10% EtOAc in hexanes). Evaporation of the solvent afforded **2c** as a colorless oil. Isolated yield: 106 mg (60%). Spectroscopic values match those for the published compound.[7]

2.4.4 (*Z*)-6,7-Dihydrooxepin-2(*3H*)-one **4a**[5]

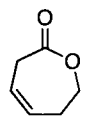

A solution of catalyst **Ru-4a** (43 mg, 0.051 mmol) in 2 mL CH_2Cl_2 was added in one rapid dose to a solution of **3a** (115 mg, 0.8 mmol) in 160 mL CH_2Cl_2 in a 250 mL Schlenk flask. The solution was heated to reflux for 24 h. After this time, a solution of Ktp (110 mg, 0.4 mmol) in THF (2 mL) was added to the yellow solution and stirred for a further hour at room temperature over which time the solution turned pale green. The solution was concentrated to ca. 1 mL and the product purified by chromatography on silica gel (gradient 10 to 30% EtOAc in hexanes) by taking the second eluent (R_f = 0.22; 30% EtOAc in hexanes). Evaporation of the solvent afforded **4a** as a colorless oil. Isolated yield: 23 mg (25%). ^{1}H NMR ($CDCl_3$, 300 MHz): δ 5.75–5.64 (m, 1H, =C*H*), 5.57–5.45 (m, 1H, C*H*), 4.39 (t, $^3J_{HH}$ = 5.6 Hz, 2H, OCH_2), 3.42–3.30 (m, 2H, CH_2), 2.53–2.42 (m, 2H, CH_2); ^{13}C{^{1}H} NMR ($CDCl_3$, 125 MHz): δ 173.5 (*C*=O), 129.3 (=*C*H), 118.8 (=*C*H), 65.8 (O*C*H_2), 33.7 (*C*H_2), 30.2 (*C*H_2). IR (neat, cm^{-1}): ν 1735 (s). HR-MS (+EI): Calcd. for $C_6H_8O_2$, $[M]^{+\bullet}$, *m/z* 112.0524. Found, *m/z* 112.0534.

2.4.5 1,8-Dioxacyclotetradeca-4,11-diene-2,9-dione [**4a**]$_2$

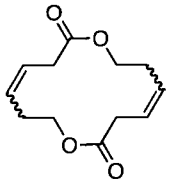

Compound [**4a**]$_2$ was isolated as secondary product during RCM of **3a** described above by taking the first eluent (R_f = 0.44; 30% EtOAc in hexanes) of the column. Evaporation of the solvent afforded **31** as a white, banana-smelling solid. Yield: 56 mg (61%). The isolated compound is present as a mixture of two isomers (presumably head-head and head-tail). No attempt to separate these isomers was undertaken. ^{1}H NMR ($CDCl_3$, 400 MHz): δ 5.77-5.36 (m, 2H, =C*H*), 4.25-4.15 (m, 2H, OCH_2), 3.11-2.99 (m, 2H, CH_2CO), 2.43-2.39 (m, 2H, CH_2CH=). ^{13}C{^{1}H} NMR ($CDCl_3$, 101 MHz): δ 171.3 (*C*=O, major isomer), 171.2 (*C*=O, minor isomer), 129.6 (OCH$_2$CH$_2$=*C*H, major isomer), 129.1 (OCH$_2$CH$_2$=*C*H, minor isomer), 126.0 (=*C*HCH$_2$CO, minor isomer), 125.2 (=*C*HCH$_2$CO, major isomer), 63.4 (O*C*H$_2$, minor isomer), 62.4 (O*C*H$_2$, major isomer), 39.4 (*C*H$_2$CO, major isomer), 38.8 (*C*H$_2$CO, minor

isomer), 31.9 (CH_2CH_2CH=, major isomer), 31.7 (CH_2CH_2CH=, minor isomer). IR (neat, cm^{-1}): ν 1734 (s). MS (+EI): 224.4 $[M]^{+\bullet}$

2.4.6 3,4,5,6,9,10-Hexahydrooxecin-2-one **4b**[5]

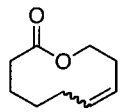

A solution of catalyst **Ru-3** (30 mg, 0.036 mmol) in 2 mL CH_2Cl_2 was added in one rapid dose to a stirred solution of **3b** (137 mg, 0.75 mmol) in 750 mL CH_2Cl_2 in a 1 L round-bottom flask. The solution was heated to reflux for 24 h. After this time, a solution of Ktp (90 mg, 0.36 mmol) in THF (2 mL) was added to the yellow solution and stirred for a further hour at room temperature over which time the solution turned pale green. The solution was concentrated to ca. 1 mL and the product purified by chromatography on silica gel (10% EtOAc in hexanes) by taking the first eluent (R_f = 0.52; 10% EtOAc in hexanes). Evaporation of the solvent afforded **33** as a colorless oil. Isolated yield: 99 mg (60%). ^{1}H NMR ($CDCl_3$, 300 MHz): δ 5.51–5.44 (m, 2H, =C*H*), 4.19–4.07 (m, 2H, OCH_2), 2.40–2.22 (m, 4H, CH_2CO and CH_2), 2.09–1.95 (m, 2H, CH_2), 1.82–1.72 (m, 2H, CH_2), 1.69–1.55 (m, 2H, CH_2). ^{13}C{^{1}H} NMR ($CDCl_3$, 125 MHz): δ 174.8 (*C*=O), 134.4 (=*C*H), 124.7 (=*C*H), 61.7 (OCH_2), 35.5 (CH_2CO), 28.6 (CH_2), 25.2 (CH_2), 24.8 (CH_2), 22.9 (CH_2). IR (neat, cm^{-1}): ν 1732 (s). HR-MS (+EI): Calcd. for $C_9H_{14}O_2$, $[M]^{+\bullet}$, *m/z* 154.0994. Found, *m/z* 154.0997.

2.4.7 1,11-Dioxacycloicosa-7,11-diene-2,12-dione $[\mathbf{4b}]_2$

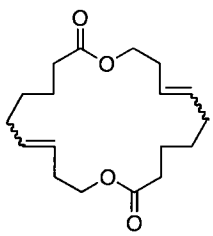

Compound $[\mathbf{4b}]_2$ was isolated as secondary product during RCM of **3b** described above by taking the second eluent (R_f = 0.27; 10% EtOAc in hexanes) of the column. Evaporation of the solvent afforded $[\mathbf{4b}]_2$ as a colorless sweet smelling oil. The isolated compound is present as a mixture of two isomers (presumably head-head and head-tail). No attempt to separate these isomers was undertaken. Yield: 36 mg (31%). ^{1}H NMR ($CDCl_3$, 300 MHz): δ 5.55-5.30 (m, 4H, =C*H*), 4.16-4.07 (m, 4H, OCH_2), 2.41-2.27 (m, 8H, CH_2CO and CH_2CH=), 2.08-1.97 (m, 4H, C$H_2(CH_2)_3$CO), 1.67-1.58 (m, 4H, CH_2CH_2CO), 1.44-1.32 (m, 4H, C$H_2(CH_2)_2$CO). ^{13}C NMR ($CDCl_3$, 125 MHz): δ 173.7 (*C*=O), 173.6 (*C*=O), 132.3 (=*C*H), 130.3 (=*C*H), 128.6 (=*C*H), 126.3 (=*C*H), 63.5 (OCH_2), 63.4 (OCH_2), 34.4 (CH_2), 34.2 (CH_2), 32.4 (CH_2), 32.1 (CH_2), 32.0 (CH_2), 31.8 (CH_2), 28.5 (CH_2), 24.4 (CH_2), 24.3 (CH_2). IR (neat, cm^{-1}): ν 1732 (s). MS (ESI): 331.5 $(M+Na)^{+\bullet}$

References page 70

2.4.8 1,9-Dioxacyclohexadeca-5,13-diene-2,10-dione $[\mathbf{4c}]_2$

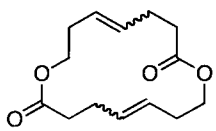

A solution of catalyst **Ru-4a** (36 mg, 0.042 mmol) in 2 mL CH_2Cl_2 was added in one rapid dose to a solution of **3c** (118 mg, 0.77 mmol) in 150 mL CH_2Cl_2 in a 250 mL Schlenk flask. The solution was heated to reflux for 24 h. After this time, a solution of Ktp (120 mg, 0.48 mmol) in THF (2 mL) was added to the yellow solution and stirred for a further hour at room temperature over which time the solution turned pale green. The solution was concentrated to ca. 1 mL and the product purified by chromatography on silica gel (gradient 10 to 20% EtOAc in hexanes) by taking the first eluent (R_f = 0.32; 20% EtOAc in hexanes). Evaporation of the solvent afforded $[\mathbf{4c}]_2$ as a colorless sweet smelling oil. Isolated yield: 66 mg (66%). The isolated compound is present as a mixture of two major isomers (presumably head-head and head-tail). No attempt to separate them was undertaken. ^{1}H NMR ($CDCl_3$, 400 MHz): δ 5.58-5.41 (m, 2H, =C*H*), 4.20-4.07 (m, 2H, OCH_2), 2.45-2.29 (m, 6H, CH_2CO and CH_2). ^{13}C{^{1}H} NMR ($CDCl_3$, 101 MHz): δ 173.1 (*C*=O), 173.0 (*C*=O), 130.2 (=*C*H), 129.2 (=*C*H), 128.6 (=*C*H), 127.2 (=*C*H), 64.2 (O*C*H_2), 64.0 (O*C*H_2), 34.1 (*C*H_2C=O), 33.8 (*C*H_2C=O), 31.7 (*C*H_2), 31.6 (*C*H_2), 27.52 (*C*H_2), 27.50 (*C*H_2). IR (neat, cm^{-1}): ν 1735 (s). MS (+EI): 252.2 $[M]^{+\bullet}$

2.4.9 (*Z*)-1,4,7,10-Tetraoxacyclotetradec-12-ene **6**[20]

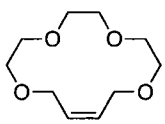

A solution of catalyst **Ru-4a** (10 mg, 0.012 mmol) in 1 mL CH_2Cl_2 was added in one rapid dose to a solution of **5** (50 mg, 0.22 mmol) in 450 mL CH_2Cl_2 in a 1 L round-bottom flask. The solution was heated to reflux for 24 h. After this time, a solution of Ktp (30 mg, 0.12 mmol) in THF (1 mL) was added to the yellow solution and stirred for a further hour at room temperature, over which time the solution turned pale green. The solution was concentrated to ca. 1 mL and the product purified by chromatography on silica gel (50% Et_2O in hexanes) by taking the first eluent (R_f = 0.4; 50% Et_2O in hexanes). Evaporation of the solvent afforded **6** as a colorless oil in pure Z isomer. Isolated yield: 14 mg (32%). ^{1}H NMR ($CDCl_3$, 300 MHz): δ 5.76 (t, $^3J_{HH}$ = 4.4 Hz, 2H, =C*H*), 4.30 (d, $^3J_{HH}$ = 4.9 Hz, 4H, =CHCH_2), 3.71-3.64 (m, 12H, CH_2). ^{13}C{^{1}H} NMR ($CDCl_3$, 75 MHz): δ 130.3 (=*C*H), 72.2 (*C*H_2), 70.6 (*C*H_2), 69.2 (*C*H_2), 67.2 (=CH*C*H_2). MS (ESI): 225.3 $(M+Na)^{+\bullet}$

References page 70

2.5 Synthesis of ligands

2.5.1 Lithium 1,1,1,3,3,3-hexafluoro-2-methylpropan-2-olate **24**

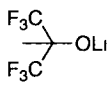

Inside the glovebox, a 50 mL round-bottom flask was charged with 1,1,1,3,3,3-hexafluoro-2-methyl-2-propanol (1.52 g, 8 mmol) and diethyl ether (20 mL). The colorless solution was cooled to –40 °C inside the glovebox freezer (ca. 2 h). It was then treated with 5.8 mL of BuLi (8 mmol) over 10 min creating a pale yellow solution and release of butane. (Titration of the commercially available 1.6 M BuLi solution in hexanes using 2,2-diphenylacetic acid[21] revealed a 1.44 M concentration of BuLi). The solution was stirred at room temperature for 2.5 h at which point the solvent was removed under vacuum affording a pale yellow gummy solid, which was subsequently suspended in cold hexanes and filtered. Yield: 1.43 g (91%). The compound was used without spectroscopic analysis.

2.5.2 *N*-tosylhydrazone **25**[22]

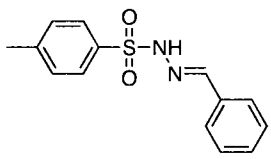

Reaction carried out in air. A scaled-up version of the published procedure is given here.[22] A 2 L round-bottom flask was equipped with an overhead stirrer and loaded with MeOH (750 mL) and 4-toluenesulfonehydrazine (200 g, 1.1 mol). The suspension was stirred until a clear, pale yellow solution was obtained. The solution was then cooled to 0 °C, and benzaldehyde (114.1 g, 1.1 mol) was added. The solution was allowed to warm to room temperature and a white precipitate formed within 5 min, which was collected by filtration. The filtrate was concentrated under reduced pressure to afford a second crop of the desired **25**. Trace of yellow color can be removed by reprecipitation from CH_2Cl_2:hexanes. Yield: 279 g (95%). Spectroscopic values match those for the published compound.[22]

2.5.3 Phenyl diazomethane **26**[22]

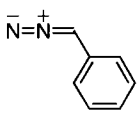

Reaction carried out in air, in the dark. Of note, the product was kept for a maximum of 3 h before use. In a modification of a literature procedure,[22] a 500 mL round-bottom flask was loaded with **25** (30.34 g, 0.11 mol) and triethylene glycol (250 mL). The suspension was warmed to 70 °C to completely dissolve **25** affording a clear, pale yellow solution. Upon addition of a solution of KOH (12.44 g, 0.22 mol) in water (50 mL), an immediate color change to red was observed. The solution was stirred at 70 °C for 5 min. Distilled water (100 mL) was added to form an orange, slushy solution. The

product was extracted with pentane (3 × 100 mL) and the combined organic fractions were washed once with water (100 mL). The organic fraction was dried with $MgSO_4$ and concentrated under vacuum to afford a thick red oil. *Importantly, exposure to vacuum should be maintained to a minimum duration to avoid loss of volatile* ***26***. Yield: 4.60 g (35%). Compound **26** was used as is, without spectroscopic analysis.

2.5.4 1-Allyl-2-isopropoxybenzene **27a**[23]

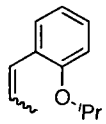

In a modification of a literature procedure,[23] a 50 mL round-bottom flask was loaded with 2-(prop-1-enyl)phenol (1.01 g, 7.53 mmol), acetone (15 mL) and distilled water (1 mL). Upon addition of NaOH (487 mg, 12.18 mmol), a color change to yellow then orange was observed. This solution was refluxed for 15 min and then allowed to cool to room temperature. Once cooled, 2-iodopropane (2.61 g, 15 mmol) and potassium carbonate (2.01 g, 14 mmol) were added. The suspension was refluxed for 15 h and turned yellow. Distilled water was added and the solution, and the acetone solvent removed under reduced pressure. The product was then extracted with diethyl ether (3 × 20 mL) and the combined organic layers were dried over Na_2SO_4. Compound **27a** was isolated as a viscous yellow oil following evaporation of the solvent under vacuum. Yield: 1.10 g (83%). Spectroscopic values match those for the published compound.[23]

2.5.5 Glyoxal-bis-(2,4,6-trimethylphenyl)imine **28**[24]

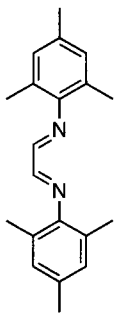

Reaction carried out in air. A scaled-up version of a literature procedure is presented here.[24] A 5 L round-bottom flask equipped with an overhead stirrer was charged with 2,4,6-trimethylaniline (500 g, 3.7 mol) methanol (1L) and glyoxal (270 mL, 40% solution in water, 1.9 mol). The solution was stirred and 1 mL of formic acid was added as a catalyst. A yellow precipitate formed within one minute; stirring was continued for 24 h at room temperature. The yellow product was collected by filtration using a 2 L Buchner funnel and was subsequently washed with methanol (500 mL) until colorless washings were obtained. The yellow fluffy solid was air-dried for several days in a large crystallization dish. *It is important to crush any agglomeration that may persist to allow efficient drying*. Yield: 505 g (93%). Spectroscopic values match those for the published compound.[24]

References page 70

2.5.6 1,3-Bis(2,4,6-trimethylphenyl)imidazolium chloride **29a**[24]

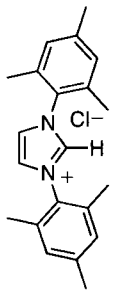

Reaction carried out in air. A scaled-up version of a literature procedure is presented here.[24] A 5 L round-bottom flask equipped with an overhead stirrer was charged with **28** (464 g, 1.6 mol), paraformaldehyde (62.2 g, 2.1 mol), and THF (2 L). A solution of HCl in dioxane (4 M, 430 mL, 1.7 mol) was slowly added to the stirred solution, while maintaining the temperature of the reaction below 30 °C. Following complete addition of the acid, the resulting brown solution was stirred for 24 h at room temperature, over which time a white solid formed. The off-white product was collected by filtration using a 2 L Buchner funnel, washed with THF (500 mL) until colorless washings are obtained, and air-dried for several days in a large crystallization dish. It is important to crush any agglomeration that may persist to allow efficient drying. Yield: 389 g (73%). Spectroscopic values match those for the published compound.[24]

2.5.7 1,3-Bis(2,4,6-trimethylphenyl)imidazolium tetrafluoroborate **29b**

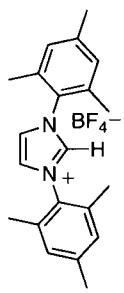

Reaction carried out in air. A 250 mL round-bottom flask was charged with **29a** (51.2 g, 0.15 mol) and the minimum volume of water to completely dissolve the salt (ca. 100 mL). To this yellowish solution was added HBF_4 (27.6 g, 48% in water, 0.15 mol) resulting in the immediate precipitation of a white solid. Stirring was continued for 20 min at room temperature at which point the suspension was poured into a 500 mL separatory funnel and extracted with CH_2Cl_2 (3 × 50 mL). The combined organic layers were dried ($MgSO_4$), and stripped to afford a fine white powder, which was dried under vacuum. Yield: 42.7 g (73%). ^{1}H NMR ($CDCl_3$, 300 MHz): δ 8.88 (t, $^4J_{HH}$ = 1.6 Hz, 1H, IMes NC*H*N), 7.56 (d, $^4J_{HH}$ = 1.6 Hz, 2H, IMes =C*H*), 7.03 (s, 4H, Mes =C*H*), 2.35 (s, 6H, Mes *p*-CCH_3), 2.11 (s, 12H, Mes *o*-CCH_3). ^{13}C{^{1}H} ($CDCl_3$, 75 MHz): δ 141.3 (IMes N*C*HN), 137.1 (Mes *p*-*C*), 134.0 (Mes *i*-*C*), 130.4 (Mes *o*-*C*), 129.8 (Mes =*C*H), 125.1 (IMes =*C*H), 21.1 (Mes *p*-*C*H_3), 17.1 (Mes *o*-*C*H_3).

2.5.8 1,3-Bis(2,4,6-trimethylphenyl)imidazol-2-ylidene **30**[24]

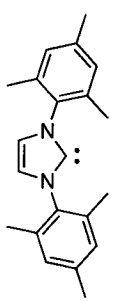

Inside the glovebox, a 500 mL round-bottom flask was charged with **29b** (15.0 g, 38.3 mmol), THF (300 mL), NaH (1.9 g, 77.5 mmol) and KO^{t}Bu (215 mg, 1.9 mmol, 5 mol%). The solution was stirred at room temperature for 3 h following which the solvent was removed under vacuum. The yellow residue was dissolved

in toluene (100 mL), filtered through Celite, and concentrated to ~5 mL under reduced pressure. Addition of hexanes (200 mL) and cooling to –35 °C yielded a white crystalline product, which was isolated by filtration and dried under vacuum for 6 h. Yield: 10.47 g (90%). Spectroscopic values match those for the published compound.[24]

2.5.9 1,2-Dimethoxy-4,5-dinitrobenzene **31**[25]

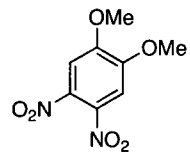

Reaction carried out in air. This compound was prepared by modification of a literature procedure.[26] *Note: Care must be taken as this synthesis releases nitric oxide (brown gas) as by-product*. A mixture of nitric acid (25 mL) and water (2.5 mL) was cooled to 0 °C in a 50 mL round-bottom flask. To this solution was added 1,2-dimethoxybenzene (10 mL, 79 mmol) by dropping funnel at a rate of 1 drop every 10 sec. An immediate color change to yellow (originally colorless) was observed; a yellow precipitate formed 20 min after addition of 1,2-dimethoxybenzene started. The solution was stirred at 0 °C until complete addition of 1,2-dimethoxybenzene (ca. 1 h). The reaction was then warmed to 60 °C in an oil bath for a further 3 h. The resulting yellow suspension was poured into 200 mL of ice-cold water, and the yellow product collected by filtration. The product was washed with 400 mL of a saturated $NaHCO_3$ solution in water and then by 300 mL of distilled water. Recrystallization from hot ethanol (ca. 200 mL) afforded yellow plates that were isolated by filtration. Yield: 9.5 g (53%). ^{1}H NMR ($CDCl_3$, 300 MHz): δ 7.33 (s, 2H, Ar C*H*), 4.01 (s, 6H, OCH_3). ^{13}C{^{1}H} ($CDCl_3$, 75 MHz): δ 152.3 (s, *C*OMe), 136.7 (s, *C*NO_2), 107.4 (s, *C*H), 57.5 (s, O*C*H_3).

2.5.10 4,5-Dimethoxybenzene-1,2-diamine **32**

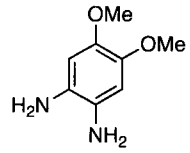

Reaction carried out in air. A 100 mL round-bottom flask was charged with **31** (2.01 g, 9 mmol), 10% Pd/C (83 mg) and absolute ethanol (50 mL). To this solution was added hydrazine monohydrate (4.4 mL, 90 mmol) over a period of 20 min leading to a color change to dark orange. The solution was then refluxed for 1.5 h over which time the color disappeared. The solution was filtered through Celite to remove the Pd/C, and the filtrate was stripped to afford a yellow solid. The solid was washed with 2-propanol (10 mL) and diethyl ether (20 mL) to afford an off-white crystalline solid that was recrystallized from hot THF. Yield: 1.08 g (73%). ^{1}H NMR (DMSO-d_6, 300 MHz): δ 6.26 (s, 2H, Ar C*H*), 4.08 (br s, $\omega_{1/2}$ = 15 Hz, 4H, NH_2), 3.58 (s, 6H, OCH_3). ^{13}C{^{1}H}

(DMSO-d_6, 75 MHz): δ 141.0 (s, *C*OMe), 128.6 (s, *C*NH_2), 103.0 (s, *C*H), 56.6 (s, O*C*H_3). MS (EI): *m/z* 168.1 (100%) $[M]^+$.

2.5.11 4,5-Dimethoxy-N^1,N^1,N^2,N^2-tetramethylbenzene-1,2-diamine **33**

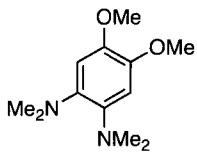

Reaction carried out in air. In an adaptation of a literature procedure,[27] a 250 mL round-bottom flask was charged with **32** (4.08 g, 24 mmol), formaldehyde (11.6 mL, 37% in water) and methanol (75 mL). Slow addition of a suspension of $NaBH_4CN$ (3.04 g, 48 mmol) and $ZnCl_2$ (3.30 g, 24 mmol) in methanol (75 mL) resulted in vigorous gas evolution along with dissolution of the solid. The reaction was stirred at room temperature for 24 h before it was quenched with 75 mL of a 0.1 M solution of aqueous NaOH. The methanol was removed under reduced pressure and the resulting solution was extracted with EtOAc (3 × 30 mL). The combined organic layers were concentrated, and the resulting brown residue was purified by vacuum distillation (bp. 65-66 °C, 2 mm Hg) to afford colorless oil. Yield: 2.6 g (48%). ^{1}H NMR ($CDCl_3$, 300 MHz): δ 6.62 (s, 2H, Ar C*H*), 3.87 (s, 6H, OCH_3), 2.75 (s, 12H, NCH_3). $^{13}C\{^1H\}$ ($CDCl_3$, 75 MHz): δ 144.2 (s, *C*O), 139.8 (s, *C*N), 104.9 (s, *C*H), 56.9 (s, O*C*H_3), 42.7 (s, N*C*H_3). MS (EI): *m/z* 224.1 (100%) $[M]^+$.

2.5.12 4,5-Bis(dimethylamino)benzene-1,2-diol **34**

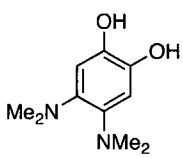

Reaction carried out in air. A 100 mL round-bottom flask was charged with **33** (2.60 g, 12 mmol) and CH_2Cl_2 (35 mL) and cooled to 0 °C in an ice bath. To this solution was added BBr_3 (26 mL, 26 mmol, 1M in CH_2Cl_2). Precipitation of an off-white solid occurred rapidly upon warming the solution to room temperature. This solid was collected by filtration, washed with CH_2Cl_2 (20 mL) and air-dried for 18 h. Yield: 1.27 g (56%). ^{1}H NMR ($CDCl_3$, 300 MHz): δ 8.81 (br s, $\omega_{1/2}$ = 120 Hz, 2H, O*H*), 7.06 (s, 2H, C*H*), 2.81 (s, 12H, NCH_3). $^{13}C\{^1H\}$ ($CDCl_3$, 75 MHz): δ 138.1 (*C*OH), 101.5 (=*C*H), 130.1 (*C*NMe_2), 40.6 (N*C*H_3). MS (EI): *m/z* 195.1 (13%) $[M-H]^+$.

2.5.13 4,5-Dimethylcyclohexa-3,5-diene-1,2-dione **35**[28]

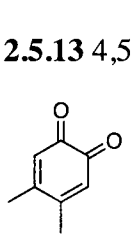

Reaction carried out in air. In a modification of a literature procedure,[28] a 1 L separatory funnel was charged with distilled water (550 mL), NaH_2PO_4 (1.7 g, 12 mmol) and $K_2[NO(SO_3)_2]$ (10 g, 37 mmol). The funnel was shaken to completely dissolve the inorganic radical. To the resulting purple solution was added a solution of 3,4-

dimethylphenol (1.78 g, 15 mmol) in diethyl ether (40 mL). The funnel was shaken for an additional 20 min at room temperature, over which time the solution turned red/brown. The resulting solution was extracted with chloroform (4 × 50 mL) following which the combined organic layers were dried with $MgSO_4$. The drying agent was removed by filtration and the filtrate stripped. Noteworthy, no water bath was used to accelerate evaporation of the solvent. The resulting red solid was washed with ice-cold diethyl ether (10 mL) and air-dried for 2 h. Yield: (1.21 g, 61%). ^{1}H NMR ($CDCl_3$, 300 MHz): δ 6.24 (s, 2H, Ar C*H*), 2.15 (s, 6H, CH_3). *Due to the instability of this quinone towards Diels-Alder dimerization,[28] it should be converted into the catechol derivative immediately following preparation.*

2.5.14 4,5-Dimethylbenzene-1,2-diol **36**[28]

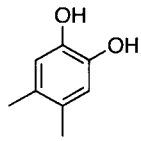

Reaction carried out in air. In a modification of a literature procedure,[28] a saturated solution of $Na_2S_2O_4$ in water (20 mL) was added to a rapidly stirred red solution of **35** (1.0 g, 7 mmol) in $CHCl_3$ (20 mL). An immediate color change to yellow was observed. After vigorous stirring at room temperature for 30 min, the resulting solution was extracted with water (2 × 20 mL). The combined organic layers were dried using $MgSO_4$. The drying agent was then removed by filtration and concentration of the filtrate under reduced pressure yielded a beige solid. Yield: 887 mg (87%). ^{1}H NMR ($CDCl_3$, 400 MHz): δ 6.66 (s, 2H, Ar C*H*), 4.85 (s, 2H, O*H*), 2.14 (s, 6H, CH_3). ^{13}C{^{1}H} ($CDCl_3$, 101 MHz): δ 141.0 (*C*OH), 129.0 (*C*CH_3), 116.9 (*C*H), 19.0 (CH_3). MS (EI): *m/z* 137.1 (100%) $[M-H]^{+\cdot}$

2.6 Thallium salts

2.6.1 General procedure

Note: The toxicity of thallium (particularly in the +1 oxidation state) is well established.[29] Care must be taken to prevent introduction into the body by inhalation, by ingestion via contaminated hands or gloves, or through the skin. All thallium reagents and wastes, including contaminated solvents, were handled using double-glove and secondary containment procedures, with separate disposal of all wastes in accordance with government regulations.

To a clear, colorless solution of catechol (566 mg, 5 mmol) in Et_2O (6 mL) was added a clear, colorless solution of TlOEt (2.58 g, 10 mmol) in Et_2O (2 mL). A yellow-orange solid

immediately began to precipitate. The solution was left to stir for 1 h, after which the precipitate was filtered off, washed with Et_2O, then hexanes (10 mL each) and dried under vacuum for 5 h. Yield: 2.30 g (86%).

Table 1. Summary of thallium salt yields and colors.

Structure	Yield (%)	Color	Structure	Yield (%)	Color
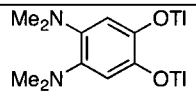 **37a**	70	Red	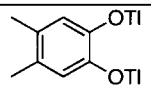 **37b**	90	Dark orange
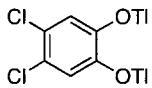 **37c**	94	Yellow	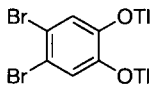 **37d**	90	Yellow
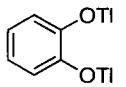 **38a**	86	Orange	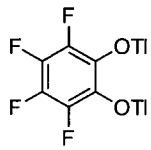 **38b**	87	Yellow
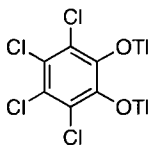 **38c**	92	Yellow	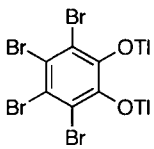 **38d**	97	Yellow
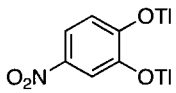 **39**	87	Purple			

2.7 Mo complexes

2.7.1 $Mo(CHCMe_2Ph)(NAr)(OSO_2CF_3)_2(dme)$ **Mo-1**[30]

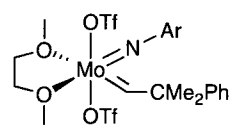

Ar = 2,6-diisopropylphenyl

Note: Secondary containment procedures were employed due to the highly corrosive nature of triflic acid. Synthesized according to a literature procedure[30] using $[Mo(NAr)_2(CH_2CMe_2Ph)_2]$ (7.9 g, 11 mmol), triflic acid (5 g, 33 mmol) and dimethoxyethane (150 mL). Yield: 5.55 g (63%). Spectroscopic values match those reported.[30]

2.7.2 $Mo(CHCMe_2Ph)(NAr)(O^tBu)_2$ **Mo-2**[30]

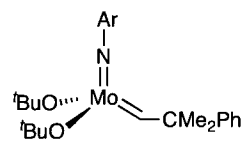

Ar = 2,6-diisopropylphenyl

Synthesized according to a literature procedure[30] using **Mo-1** (368 mg, 0.48 mmol), freshly-sublimed KO^tBu (107 mg, 0.96 mmol) and 10 mL anhydrous THF (10 mL). Pure **Mo-2** was obtained by cooling a

saturated hexanes solution to –35 °C for 14 h. Yield: 188 mg (74%). Spectroscopic values match those reported.[30]

2.7.3 $Mo(CHCMe_2Ph)(NAr)[OCMe(CF_3)_2]_2$ **Mo-3**[30]

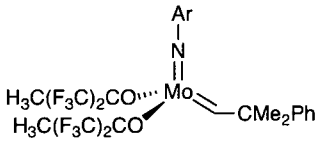

Ar = 2,6-diisopropylphenyl

The compound was prepared as for **Mo-2** using **Mo-1** (251 mg, 0.33 mmol) **24** (131 mg, 0.71 mmol) and THF (10 mL). Crystallization from hexanes at –35 °C afforded **Mo-3** as dark orange blocks. Yield: 169 mg (67%). Spectroscopic values match those reported.[30]

2.8 Ru complexes

2.8.1 $RuCl_2(PPh_3)_3$ **Ru-1**[31]

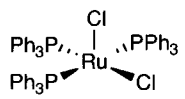

Synthesized according to a literature procedure[31] using $RuCl_3(H_2O)_x$ (5.01 g, 40-43% Ru, ca. 21 mmol), solid PPh_3 (32.93 g, 126 mmol) and methanol (250 mL). Removal of excess PPh_3 was performed by washing the brown product with Et_2O (250 mL). Yield: 17.32 g (88%). Spectroscopic values match those reported.[31]

2.8.2 $Ru(\kappa^2\text{-}O_2C_6H_4)(PPh_3)_3$ **Ru-2a**[32]

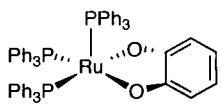

Solid **38a** (296 mg, 0.57 mmol) was added to a stirred solution of **Ru-1** (500 mg, 0.52 mmol) in 10 mL THF at room temperature. A color change from brown to blue took place over 1 h, and the solution became cloudy. The suspension was filtered through Celite to remove TlCl, and the filtrate stripped to dryness. Precipitation from THF-hexanes and washing with hexanes (3 × 5 mL) afforded deep blue **Ru-2**. Yield: 486 mg (94%). ^1H NMR (C_6D_6, 500 MHz): δ 7.39 (m, 2H, catechol COC*H*), 7.30 (m, 18H, PPh_3 *o*-C*H*), 7.02 (m, 2H, catechol C*H*), 6.90 (m, 9H, PPh_3 *p*-C*H*), 6.74 (m, 18H, PPh_3 *m*-C*H*). $^{13}C\{^1H\}$ NMR (C_6D_6, 125 MHz): δ 163.3 (s, catechol *C*O), 137.4-137.1 (m, PPh_3 *i*-*C*), 135.3-135.2 (m, PPh_3 *o*-*C*H), 128.9 (s, PPh_3 *p*-*C*H), 127.5-127.4 (m, PPh_3 *m*-*C*H), 117.6 (s, catechol *C*H), 117.5 (s, catechol *C*H). $^{31}P\{^1H\}$ NMR (C_6D_6, 121 MHz): δ 55.1 ppm (s); multiplicity unchanged down to –90 °C (C_7D_8). IR (Nujol, cm^{-1}): ν_{CO} 1270 (m). MALDI-MS, *m*/*z* (pyrene matrix): Calcd. for $[M\text{-}PPh_3]^{+\cdot}$ 734.1; Found, 734.4. Anal. Calcd. ($C_{60}H_{49}O_2P_3Ru$): C, 72.35; H, 4.96%. Found: C, 72.13; H, 4.87%.

2.8.3 $RuCl_2(CHPh)(PCy_3)_2$ **Ru-3**[33]

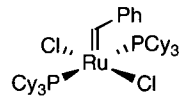

In an adaptation of a literature procedure,[33] a 500 mL round-bottom flask was loaded with **Ru-1** (7.01 g, 7 mmol) and CH_2Cl_2 (200 mL). The brown solution was cooled to –78 °C at which point a solution of **26** (1.76 g, 15 mmol) in hexanes (20 mL) was slowly added by cannula creating a color change to green-brown. The solution was stirred at –78 °C for an additional 20 min after complete addition of **26**. The solution was then warmed to 0 °C, stirred for a further 30 minutes after which the solution was finally allowed to warm to room temperature. A colorless solution of tricyclohexyl phosphine (4.51 g, 16 mmol) in toluene (50 mL) was added by cannula affording a gradual color change to dark red-purple over the course of 1.5 h. The volatiles were then removed under vacuum and the resulting dark red-purple residue was suspended in methanol (300 mL). The purple solid was filtered, washed with acetone (100 mL) and dried under vacuum. Yield: 4.2 g (70%). Spectroscopic values match those reported.[33]

2.8.4 $RuCl_2(CHPh)(IMes)(PCy_3)$ **Ru-4a**[34]

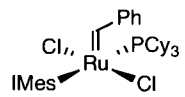

In an adaptation of a literature procedure,[34] a 500 mL round-bottom flask was loaded with **Ru-3** (20.76 g, 25 mmol) and toluene (350 mL). To the purple solution was added **30** (8.07 g, 27 mmol) as a solution in toluene (50 mL) affording a near immediate color change to red. The solution was stirred at room temperature for 2 h at which point all volatiles were removed under vacuum. The red foamy residue was then washed twice with hexanes (100 mL) at –78 °C to afford **Ru-4a** as a pink solid. Yield: 19.3 g (90%). Spectroscopic values match those reported.[34]

2.8.5 $RuCl_2(CHPh)(IMes)(py)_2$ **Ru-6a**[35]

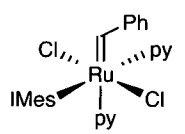

In an adaptation of a literature procedure,[35] pyridine (ca. 2 mL) was added to solid **Ru-4a** (2.1 g, 2.5 mmol) affording an immediate color change to green. The suspension was stirred for 15 min to ensure complete reaction. Hexanes (100 mL) was added to precipitate a green solid, which was collected by filtration, washed with hexanes (3 × 10 mL) and dried under vacuum. Yield: 1.79 g (>99%). Spectroscopic values match those reported.[35]

References page 70

2.8.6 $RuCl_2$(CH-2-O^{i}Pr-C_6H_4)(IMes) **Ru-5a**

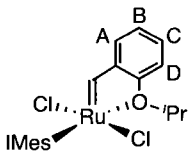

In an adaptation of a literature procedure,[36] a 100 mL round-bottom Schlenk was loaded with **Ru-4a** (2 g, 2.4 mmol) and CH_2Cl_2 (40 mL). To the resulting pink solution was added solid CuCl (230 mg, 2.4 mmol) and a solution of **27a** (415 mg, 2.4 mmol) in CH_2Cl_2 (40 mL). The solution was refluxed for 1 h, and the resulting green-brown solution was stripped to dryness. *All following manipulations were carried out in air using reagent grade solvents*. The residue was dissolved in the minimum amount of 1:1 CH_2Cl_2:pentane, and the insoluble $CuClPCy_3$ was removed by filtering through a plug of cotton wool. The filtrate was then evaporated to dryness, and the residue purified by column chromatography (30% EtOAc in hexanes, R_f = 0.43). Fractions containing the product were combined and the solvent evaporated to yield a green solid. For numbering system, see structure. Yield: 428 mg (25%). ^{1}H NMR (C_6D_6, 500 MHz): δ 16.84 (s, 1H, Ru=C*H*), 7.19 (d, $^3J_{HH}$=7.5 Hz, 1H, Ph H_A), 7.10 (t, $^3J_{HH}$ =7.5 Hz, 1H, Ph H_C), 6.89 (s, 4H, Mes C*H*), 6.68 (t, $^3J_{HH}$ =7.5 Hz, 1H, Ph H_B), 6.32 (d, $^3J_{HH}$ =7.9 Hz, 1H, Ph H_D), 6.25 (s, 2H, IMes =C*H*), 4.47 (sept, $^3J_{HH}$ = 6.1 Hz, 1H, OC*H*), 2.40 (s, 12H, Mes *o*-CH_3), 2.24 (s, 6H, Mes *p*-CH_3), 1.38 (d, $^3J_{HH}$ = 6.1 Hz, 6H, CHCH_3). ^{13}C NMR (C_6D_6, 125 MHz): δ 288.4 (Ru=*C*H), 177.6 (N*C*N), 152.8 (Ph *i*-*C*), 146.0 (Ph *C*O), 139.3 (Mes *p*-*C*CH_3), 138.4 (Mes *i*-*C*), 136.7 (Mes *o*-*C*CH_3), 129.3 (Mes *m*-*C*H), 128 (Ph C_C overlap with solvent), 124.5 (IMes =*C*H), 122.3 (Ph C_B), 121.9 (Ph C_A), 113.3 (Ph C_D), 75.2 (^{i}Pr O*C*H), 21.4 (^{i}Pr *C*H_3), 21.1 (Mes *p*-*C*H_3), 19.4 (Mes *o*-*C*H_3). MALDI-TOF MS, *m/z*: Calcd. for $[M]^{+\bullet}$ 624.1; found, 623.9. Anal. Calcd. ($C_{31}H_{36}Cl_2N_2ORu$): C, 59.61; H, 5.81; N, 4.48%. Found: C, 59.43; H, 5.98; N, 4.45 %.

2.8.7 $RuCl_2$(CH-2-O^{i}Pr-4-NO_2-C_6H_3)(H_2IMes) **Ru-5c**[36]

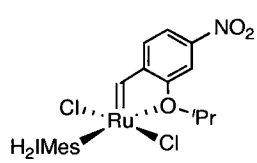

This compound was synthesized as for **Ru-5a** using **Ru-4b** (202 mg, 0.24 mmol), **27b** (60 mg, 0.27 mmol; graciously supplied by the Grela group), CuCl (28 mg, 0.28 mmol) and CH_2Cl_2 (20 mL). The product was purified by column chromatography using 40% EtOAc in hexanes as eluent. Upon evaporation of the fraction containing the green band, **Ru-5c** crystallized as dark green blocks. Yield: 103 mg (64%). Spectroscopic data matches those reported.[36]

2.8.8 Ru(κ^2-$O_2C_6H_2$-4,5-Me_2)(CHPh)(IMes)(py) **Ru-8a**[37]

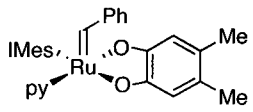

To a green solution of **Ru-6a** (300 mg, 0.41 mmol) in 5 mL THF was added solid, orange **37b** (228 mg, 0.42 mmol). The solution underwent a color change to brown within minutes. The suspension was stirred for 2 h, over which time the orange solid gradually disappeared, and a precipitate of TlCl deposited. The solution was filtered through Celite, and the filtrate stripped to a red residue. Reprecipitation from THF (<1 mL) by slow addition of hexanes yielded a brown solid. Yield after filtering off and drying under vacuum: 262 mg (89%). ^{1}H NMR (CD_2Cl_2, 500 MHz): δ 16.98 (s, 1H, Ru=C*H*), 8.28 (d, $^3J_{HH}$ = 5.0 Hz, 2H, py *o*-C*H*), 7.49 (t, $^3J_{HH}$ = 7.5 Hz, 1H, py *p*-C*H*), 7.30 (d, $^3J_{HH}$= 7.5 Hz, 2H, Ph *o*-C*H*), 7.21 (t, $^3J_{HH}$ = 7.0 Hz, 1H, Ph *p*-C*H*), 7.12 (s, 2H, IMes =C*H*), 6.96 (t, $^3J_{HH}$ = 7.0 Hz, 2H, py *m*-C*H*), 6.93 (t, $^3J_{HH}$ = 7.5 Hz, 2H, Ph *m*-C*H*), 6.88 (s, 2H, Mes =C*H*), 6.64 (s, 2H, Mes =C*H*), 6.36 (s, 1H, cat C*H*), 6.28 (s, 1H, cat C*H*), 2.24 (s, 6H, Mes *p*-CH_3), 2.14 (s, 6H, Mes *o*-CH_3), 2.06 (s, 3H, cat CH_3), 2.02 (s, 3H, cat CH_3), 1.90 (s, 6H, Mes *o*-CH_3). ^{13}C{^{1}H} (CD_2Cl_2, 125 MHz): δ 285.1 (Ru=*C*H), 189.7 (IMes N*C*N), 162.3 (cat *C*O), 158.9 (cat *C*O), 155.1 (py *o*-*C*H), 152.8 (Ph *i*-*C*), 139.4 (Mes *p*-*C*), 136.9 (Mes *i*-*C*), 135.9 (Mes *o*-*C*), 135.7 (Mes *o*-*C*), 134.7 (py *p*-*C*H), 129.5 (Mes *m*-*C*H), 129.3 (Mes *m*-*C*H), 128.5 (Ph *m*-*C*H), 127.5 (Ph *o*-*C*H), 126.6 (Ph *p*-*C*H), 124.6 (IMes =*C*H), 124.2 (py *m*-*C*H), 123.0 (cat *C*CH$_3$), 120.5 (cat *C*CH$_3$), 116.3 (cat =*C*H), 115.4 (cat =*C*H), 21.1 (Mes *p*-*C*H$_3$), 19.2 (cat *C*H$_3$), 19.1 (cat *C*H$_3$), 18.0 (Mes *o*-*C*H$_3$), 17.8 (Mes *o*-*C*H$_3$). IR (Nujol, cm^{-1}): ν_{CO} 1269 (m). MALDI-MS, *m/z*: Calcd. for [M-py]$^+$ 632.2; Found, 632.0. Anal. Calcd. ($C_{41}H_{43}N_3O_2Ru$): C, 69.27; H, 6.10; N, 5.91%. Found: C, 69.10; H, 6.39; N, 5.69 %.

2.8.9 Ru(κ^2-$O_2C_6H_2$-4,5-Cl_2)(CHPh)(IMes)(py) **Ru-8b**[37]

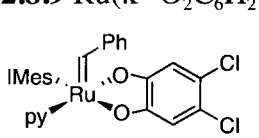

The procedure described for **Ru-8a** was followed using **Ru-6a** (460 mg, 0.63 mmol) and **37c** (378 mg, 0.65 mmol). Yield: 422 mg (88%). ^{1}H NMR ($CDCl_3$, 500 MHz): δ 17.08 (s, 1H, Ru=C*H*), 8.23 (d, $^3J_{HH}$ = 4.5 Hz, 2H, py *o*-C*H*), 7.45 (t, $^3J_{HH}$ = 7.3 Hz, 1H, py *p*-C*H*), 7.2 (d, $^3J_{HH}$ = 7.5 Hz, 2H, Ph *o*-C*H*), 7.07 (s, 2H, IMes =C*H*), 6.94-6.89 (m, 5H, py *m*-C*H*, Ph *m*-C*H*, Ph *p*-C*H*), 6.85 (s, 2H, Mes =C*H*), 6.65-6.64 (m, 2H, cat C*H*), 6.60 (s, 2H, Mes =C*H*), 2.31 (br s, 6H, Mes *p*-CH_3), 2.11 (br s, 6H, Mes *o*-CH_3), 1.79 (br s, 6H, Mes *o*-CH_3). ^{13}C{^{1}H} ($CDCl_3$, 125 MHz): δ 289.7 (Ru=*C*H), 188.4 (IMes N*C*N), 164.0 (cat *C*O), 160.7 (cat *C*O), 154.6 (py *o*-*C*H), 152.5 (Ph *i*-

C), 139.3 (Mes *p*-*C*), 136.5 (Mes *i*-*C*), 135.5 (Mes *o*-*C*), 134.8 (Mes *o*-*C*), 134.5 (py *p*-*C*H), 129.9 (Mes =*C*H), 129.2 (Mes =*C*H), 128.1 (Ph *m*-*C*H), 127.4 (Ph *o*-*C*H), 127.0 (Ph *p*-*C*H), 124.2 (IMes =*C*H), 123.9 (py *m*-*C*H), 117.2 (cat *C*Cl), 114.7 (cat *C*Cl), 114.5 (cat *C*H), 114.3 (cat *C*H), 21.0 (Mes *p*-*C*H_3), 17.7 (Mes *o*-*C*H_3), 17.6 (Mes *o*-*C*H_3). IR (Nujol, cm^{-1}): ν_{CO} 1260 (m). MALDI-MS, *m/z*: Calcd. for $[M]^+$ 751.1; Found 750.9. Anal. Calcd. ($C_{39}H_{37}Cl_2N_3O_2Ru$): C, 62.31; H, 4.96; N, 5.59%. Found C, 62.12 H, 5.28 N, 5.33%.

2.8.10 Ru(κ^2-$O_2C_6H_2$-4,5-Br_2)(CHPh)(IMes)(py) **Ru-8c**[37]

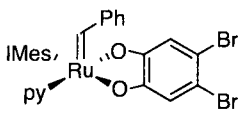

The procedure described for **Ru-8a** was followed, using **Ru-6a** (250 mg, 0.35 mmol) and **37d** (235 mg, 0.35 mmol). Yield: 264 mg (91%). ^{1}H NMR ($CDCl_3$, 500 MHz): δ 17.11 (s, 1H, Ru=C*H*), 8.24 (d, $^3J_{HH}$ = 5.2 Hz, 2H, py *o*-C*H*), 7.48 (t, $^3J_{HH}$ = 7.5 Hz, 1H, py *p*-C*H*), 7.21 (d, $^3J_{HH}$ = 7.9 Hz, 2H, Ph *o*-C*H*), 7.07 (s, 2H, IMes =C*H*), 6.99-6.83 (m, 9H, py *m*-C*H*, Ph *m*-C*H*, Ph *p*-C*H*, Mes =C*H*, cat C*H*), 6.62 (s, 2H, Mes =C*H*), 2.25 (br s, 6H, Mes *p*-CH_3), 2.13 (br s, 6H, Mes *o*-C*H*), 1.82 (br s, 6H, Mes *o*-C*H*). ^{13}C{^{1}H} ($CDCl_3$, 125 MHz): δ 290.5 (Ru=*C*H), 188.3 (IMes N*C*N), 164.9 (cat *C*O), 161.6 (cat *C*O), 154.6 (py *o*-*C*H), 152.5 (Ph *i*-*C*), 139.3 (Mes *p*-*C*), 136.5 (Mes *o*-*C*), 135.5 (Mes *o*-*C*), 134.8 (Mes *i*-*C*), 134.5 (py *p*-*C*H), 129.3 (Mes =*C*H), 128.1 (Mes =*C*H), 127.4 (Ph *o*-*C*H), 127.1 (Ph *p*-*C*H), 124.2 (IMes =*C*H), 123.9 (Ph *m*-*C*H), 117.8 (cat *C*H), 117.4 (cat *C*H), 108.7 (cat *C*Br), 105.8 (cat *C*Br), 21.0 (Mes *p*-*C*H_3), 17.7 (Mes *o*-*C*H_3), 17.6(Mes *o*-*C*H_3). IR (Nujol, cm^{-1}): ν_{CO} 1257 (m). MALDI-MS, *m/z*: Calcd. for $[M]^+$ 841.0; Found, 840.7. Anal. Calcd. ($C_{39}H_{37}Br_2N_3O_2Ru$): C, 55.72; H, 4.44; N, 5.00%. Found C, 56.06; H, 4.24; N, 5.00%.

2.8.11 Ru(κ^2-$O_2C_6H_4$)(CHPh)(IMes)(py) **Ru-9a**[38]

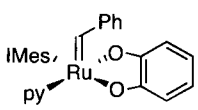

The procedure described for **Ru-8a** was followed, using **Ru-6a** (300 mg, 0.41 mmol) and **38a** (235 mg, 0.45 mmol). Yield: 218 mg (77%). ^{1}H NMR ($CDCl_3$, 300 MHz): δ 16.99 (s, 1H, Ru=C*H*), 8.36 (dd, $^3J_{HH}$ = 6.6 Hz, $^4J_{HH}$ = 1.6 Hz, 2H, py, *o*-C*H*), 7.45 (tt, $^3J_{HH}$ = 7.8 Hz, $^4J_{HH}$ = 1.6 Hz, 1H, py, *p*-C*H*), 7.28 (d, $^3J_{HH}$ = 7.0 Hz, 2H, Ph, *o*-C*H*), 7.17 (t, $^3J_{HH}$ = 7.5 Hz, 1H, Ph, *p*-C*H*), 7.08 (s, 2H, IMes =C*H*), 6.96-6.85 (m, 6H, Ph, *m*-C*H*; py, *m*-C*H*; Mes C*H*), 6.71 (dd, $^3J_{HH}$ = 7.0 Hz, $^4J_{HH}$ = 2.0 Hz, 1H, cat *o*-C*H*), 6.70 (dd, $^3J_{HH}$ = 7.0, $^4J_{HH}$ = 2.0 Hz, 1H, cat *o*-C*H*), 6.58 (br s, 2H, Mes C*H*), 6.49 (td, $^3J_{HH}$ = 7.0 Hz, $^4J_{HH}$ = 2.0 Hz, 1H, cat *m*-C*H*), 6.36 (td, $^3J_{HH}$ = 7.0 Hz, $^4J_{HH}$ = 2.0 Hz, 1H, cat

m-C*H*), 2.22 (s, 6H, Mes *p*-CH_3), 2.16 (s, 6H, Mes *o*-CH_3), 1.88 (s, 6H, Mes *o*-CH_3). $^{13}C\{^1H\}$ ($CDCl_3$, 75 MHz) : δ 287.4 (Ru=*C*H), 189.6 (IMes N*C*N), 164.1 (Ar, cat *C*O), 160.5 (Ar, cat *C*O), 154.7 (py, *o*-*C*H), 152.6 (Ph *i*-*C*), 139.0 (Mes *p*-*C*Me), 136.6 (Mes *o*-*C*Me), 135.2 (Mes *o*-*C*Me), 135.1 (Mes *i*-*C*), 134.0 (py *p*-*C*H), 129.1 (Mes *m*-*C*H), 128.0 (Ph *m*-*C*H), 127.7 (Ph *o*-*C*H), 126.5 (Ph *p*-*C*H), 124.0 (IMes =*C*H), 123.7 (py, *m*-*C*H), 116.1 (cat *C*H), 114.8 (cat *C*H), 114.2 (cat *C*H), 113.8 (cat *C*H), 21.1 (Mes *p*-C*C*H_3), 17.8 (Mes *o*-C*C*H_3), 17.7 (Mes *o*-C*C*H_3). IR (Nujol, cm^{-1}): ν_{CO} 1260 (m). Anal. Calcd. ($C_{39}H_{39}N_3O_2Ru$): C, 68.60; H, 5.76; N, 6.15%. Found C, 69.03; H, 5.38; N, 6.14%. MALDI-TOF MS, *m/z*: Calcd. for $[M\text{-py}]^+$ 604.2; Found, 604.1.

2.8.12 Ru(κ^2-$O_2C_6F_4$)(CHPh)(IMes)(py) **Ru-9b**[37]

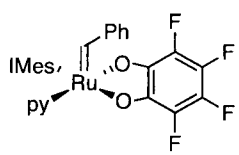

The procedure described for **Ru-9a** was followed, using **Ru-6a** (500 mg, 0.69 mmol) and **38b** (409 mg, 0.69 mmol). Yield: 453 mg (87%). ^1H NMR ($CDCl_3$, 300 MHz): δ 17.22 (s, 1H, Ru=C*H*), 8.23 (d, $^3J_{HH}$ = 5.1 Hz, 2H, py *o*-C*H*), 7.50 (t, $^3J_{HH}$ = 7.6 Hz, 1H, py *p*-C*H*), 7.22 (d, $^3J_{HH}$ = 6.7 Hz, 2H, Ph *o*-C*H*), 7.09 (s, 2H, IMes =C*H*), 6.97-6.90 (m, 5H, Ph *m*-C*H*, Ph *p*-C*H*, py *m*-C*H*), 6.84 (s, 2H, Mes =C*H*), 6.60 (s, 2H, Mes =C*H*), 2.23 (s, 6H, Mes *p*-CH_3), 2.11 (s, 6H, Mes *o*-CH_3), 1.83 (s, 6H, Mes *o*-CH_3). $^{13}C\{^1H\}$ ($CDCl_3$, 75 MHz): δ 292.3 (Ru=*C*H), 187.4 (IMes N*C*N), 154.0 (py *o*-*C*H), 152.0 (Ph *i*-*C*), 139.0 (Mes *o*-*C*), 135.2 (py *p*-*C*H), 135.0 (Mes *i*-*C*), 129.0 (Mes =*C*H), 128.6 (Ph *m*-*C*H), 128.4 (Ph *o*-*C*H), 127.0 (Ph *p*-*C*H), 125.0 (IMes =*C*H), 124.3 (Mes *p*-*C*), 124.0 (py *m*-*C*H), 21.2 (Mes *p*-*C*H_3), 18.0 (Mes *o*-*C*H_3). The quaternary ^{13}C resonances for the catechol ring could not be located, owing to their low intensity and splitting by the ^{19}F nuclei. $^{19}F\{^1H\}$ ($CDCl_3$, 282 MHz): δ -95.6 (ddd, $^3J_{FF}$ = 23.4 Hz, $^4J_{FF}$ = 8.5 Hz, $^5J_{FF}$ = 5.8 Hz, 1F, cat *o*-C*F*), -98.3 (ddd, $^3J_{FF}$ = 21.2 Hz, $^4J_{FF}$ = 9.2 Hz, $^5J_{FF}$ = 5.7 Hz, 1F, cat *o*-C*F*), -105.3 (td, $^3J_{FF}$ = 22.6 Hz, $^4J_{FF}$ = 8.9 Hz, 1F, cat *m*-C*F*), -107.4 (td, $^3J_{FF}$ = 22.9 Hz, $^4J_{FF}$ = 10.7 Hz, 1F, cat *m*-C*F*). IR (Nujol, cm^{-1}): ν_{CO} 1268 (m). MALDI-MS, *m/z*: Calcd. for $[M]^+$ 755.2; Found, 754.9. Anal. Calcd. ($C_{39}H_{35}F_4N_3O_2Ru$): C, 62.06; H, 4.67; N, 5.57%. Found C, 62.10; H, 4.43; N, 5.70%.

2.8.13 Ru(κ^2-$O_2C_6Cl_4$)(CHPh)(IMes)(py) **Ru-9c**[37]

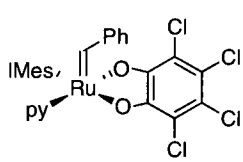

The procedure described for **Ru-9a** was followed using **Ru-6a** (300 mg, 0.41 mmol) and **38c** (274 mg, 0.42 mmol). Yield: 177 mg (52%). ^1H

NMR ($CDCl_3$, 500 MHz): δ 17.20 (s, 1H, Ru=C*H*), 8.38 (d, $^3J_{HH}$ = 4.9 Hz, 2H, py *o*-C*H*), 7.55 (t, $^3J_{HH}$ = 7.2 Hz, 1H, py *p*-C*H*), 7.31 (d, $^3J_{HH}$ = 7.2 Hz, 2H, Ph *o*-C*H*, Ph *p*-C*H*), 7.13 (br s, 2H, IMes =C*H*), 7.06 (t, $^3J_{HH}$ = 6.6 Hz, 2H, py *m*-C*H*), 6.96 (t, $^3J_{HH}$ = 8.2 Hz, 2H, Ph *m*-C*H*), 6.83 (br s, 2H, Mes =C*H*), 6.62 (br s, 2H, Mes =C*H*), 2.25 (br s, 12H, Mes *o*-CH_3), 2.11 (br s, 6H, Mes *p*-CH_3). Low solubility precluded location of the quaternary carbons. $^{13}C\{^1H\}$ ($CDCl_3$, 125 MHz): δ 292.5 (Ru=*C*H), 155.0 (py *o*-*C*H), 134.9 (py *p*-*C*H), 129.6 (Mes =*C*H), 129.2 (Mes =*C*H), 128.1 (Ph *m*-*C*H), 127.6 (Ph *o*-*C*H), 127.6 (Ph *p*-*C*H), 124.4 (IMes =*C*H), 124.1 (py *m*-*C*H), 21.0 (Mes *o*-CH_3), 17.8 (Mes *o*-CH_3), 17.5 (Mes *p*-CH_3). IR (Nujol, cm^{-1}): ν_{CO} 1261 (m). MALDI-MS, *m/z*: Calcd. for $[M\text{-py}]^+$ 740.0; Found, 740.1. Anal. Calcd. ($C_{39}H_{35}Cl_4N_3O_2Ru$): C, 57.08; H, 4.30; N, 5.12%. Found C, 56.77; H, 3.96; N, 4.71%.

2.8.14 Ru(κ^2-$O_2C_6Br_4$)(CHPh)(IMes)(py) **Ru-9d**[37]

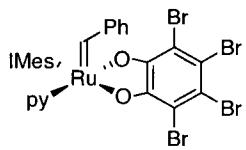

The procedure described for **Ru-9a** was followed using **Ru-6a** (100 mg, 0.14 mmol) and **38d** (117 mg, 0.14 mmol). Yield: 91 mg (66%). ^1H NMR ($CDCl_3$, 300 MHz): δ 17.15 (s, 1H, Ru=C*H*), 8.39 (d, $^3J_{HH}$ = 3.3 Hz, 2H, py *o*-C*H*), 7.55 (t, $^3J_{HH}$ = 8.5 Hz, 1H, py *p*-C*H*), 7.32 (d, $^3J_{HH}$ = 8.0 Hz, 2H, Ph *o*-C*H*), 7.12 (br s, 2H, IMes =C*H*), 7.06 (t, $^3J_{HH}$ = 7.0 Hz, 2H, py *m*-C*H*), 6.95 (t, $^3J_{HH}$ = 7.5 Hz, 2H, Ph *m*-C*H*), 6.81 (br s, 2H, Mes =C*H*), 6.61 (br s, 2H, Mes =C*H*), 2.25 (br s, 12H, Mes *o*-CH_3), 2.09 (br s, 6H, Mes *p*-CH_3). Low solubility precluded location of the quaternary carbons. $^{13}C\{^1H\}$ ($CDCl_3$, 125 MHz): δ 292.2 (Ru=*C*H), 155.2 (py *o*-*C*H), 134.8 (py *p*-*C*H), 129.3 (Mes =*C*H), 129.0 (Mes =*C*H), 128.4 (Ph *m*-*C*H), 127.6 (Ph *o*-*C*H), 127.5 (Ph *p*-*C*H), 125.0 (IMes =*C*H), 124.1 (py *m*-*C*H), 21.1 (Mes *o*-CH_3), 21.0 (Mes *o*-CH_3), 17.8 (Mes *p*-CH_3). IR (Nujol, cm^{-1}): ν_{CO} 1238 (m). MALDI-MS, *m/z*: Calcd. for $[M\text{-py}]^+$ 919.8; Found, 920.0. Anal. Calcd. ($C_{39}H_{35}Br_4N_3O_2Ru$): C, 46.92; H, 3.53; N, 4.21%. Found: C, 47.37; H, 3.56; N, 4.57%.

2.8.15 Ru(NCS-κ*N*)$_2$(CHPh)(IMes)(py)$_2$ **Ru-12a**

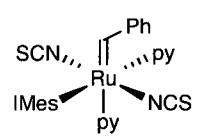

Solid Ag(SCN) (91.6 mg, 0.55 mmol) was added to a solution of **Ru-6a** (200 mg, 0.28 mmol) in toluene (20 mL). The suspension was stirred at room temperature for 16 h. No color change was apparent, but a suspension of AgCl formed, which was removed by filtration through Celite. The filtrate was

concentrated under vacuum and the green residue was precipitated from a minimum volume of benzene by addition of pentane. Yield after drying under vacuum for 15 h: 184 mg (97%). (*Note: ax. refers to the pyridine trans to the benzylidene moiety; eq. refers to the pyridine cis to the benzylidene moiety*). ^{1}H NMR ($CDCl_3$, 300 MHz): δ 18.05 (s, 1H, Ru=C*H*), 8.42 (d, $^3J_{HH}$ = 3.9 Hz, 2H, py ax. *o*-C*H*), 7.76 (d, $^3J_{HH}$ = 4.0 Hz, 2H, py eq. *o*-C*H*), 7.60 (br s, 2H, Ph *o*-C*H*), 7.41-7.30 (m, 2H, overlapping py ax. *p*-C*H*, Ph *p*-C*H*), 7.15-7.04 (m, 3H, overlapping py eq. *p*-C*H*, Ph *m*-C*H*), 6.93-6.90 (m, 4H, overlapping IMes =C*H*, py ax. *m*-C*H*), 6.65 (t, $^3J_{HH}$ = 6.2 Hz, 2H, py eq. *m*-C*H*), 6.50 (s, 4H, Mes C*H*), 2.15 (s, 12H, Mes *o*-CC*H*$_3$), 2.02 (s, 6H, Mes *p*-CC*H*$_3$). ^{13}C{^{1}H} ($CDCl_3$, 75 MHz): δ 324.6 (Ru*C*H), 180.7 (IMes N*C*N), 152.2 (Ph *i*-*C*), 151.1 (py eq. *o*-*C*H), 150.3 (py ax. *o*-*C*H), 139.4 (Mes *p*-*C*CH$_3$), 137.4 (N=*C*=S), 136.9 (2 overlapping signals, Mes *o*-*C*CH$_3$ and Mes *i*-*C*H), 136.7 (Ph *m*-*C*H), 135.4 (py eq. *p*-*C*H), 131.5 (py ax. *p*-*C*H), 130.9 (Ph *o*-*C*H), 129.3 (Mes *C*H), 128.7 (2 overlapping signals, IMes =*C*H and Ph *p*-*C*H), 128.5 (py ax. *m*-*C*H), 125.4 (IMes =*C*H), 124.4 (py eq. *m*-*C*H), 20.9 (Mes *p*-*C*H$_3$), 17.8 (Mes *o*-*C*H$_3$). IR (Nujol, cm^{-1}): ν_{NCS} 2089 (m). MALDI-MS, *m/z*: Calcd. for [M-2py]$^+$: 612.1; Found, 612.0. Anal. Calcd. ($C_{40}H_{40}N_6S_2Ru$): C, 62.39; H, 5.24; N, 10.91%. Found: C, 62.58; H, 4.84; N, 10.46 %.

2.8.16 Ru(NCO-κ*N*)$_2$(CHPh)(IMes)(py)$_2$ **Ru-12b**

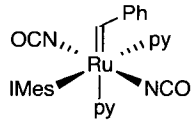

To a green solution of **Ru-6a** (302 mg, 0.42 mmol) in 10 mL benzene was added solid Ag(NCO) (139 mg, 0.93 mmol). The solution underwent a color change to emerald green within minutes, and a gray-brown precipitate deposited. The suspension was stirred for 45 min at which time an aliquot from the reaction mixture showed complete conversion to the desired **Ru-12b** (^{1}H NMR analysis). The solution was filtered through Celite, and the filtrate stripped to a green residue. Reprecipitation from THF (<1 mL) by slow addition of hexanes yielded an emerald green solid. Yield after filtering off and drying under vacuum: 282 mg (92%). (*Note: ax. refers to the pyridine trans to the benzylidene moiety; eq. refers to the pyridine cis to the benzylidene moiety*). ^{1}H NMR (CD_2Cl_2, 500 MHz): δ 18.72 (s, 1H, Ru=C*H*), 8.58 (br s, 2H, py ax. *o*-C*H*), 7.82 (br s, 2H, py eq. *o*-C*H*), 7.65 (d, $^3J_{HH}$ = 7.5 Hz, 2H, Ph *o*-C*H*), 7.48 (m, 1H, py ax. *p*-C*H*), 7.42 (t, $^3J_{HH}$ = 7.3 Hz, Ph *p*-C*H*), 7.29 (t, $^3J_{HH}$ = 7.8 Hz, 1H, py eq. *p*-C*H*), 7.07 (t, $^3J_{HH}$ = 7.6 Hz, 2H, Ph *m*-C*H*), 7.03 (s, 2H, IMes =C*H*), 7.00 (m, 2H, py ax. *m*-C*H*), 6.78 (m,

2H, py eq. *m*-C*H*), 6.70 (s, 4H, Mes C*H*), 2.17 (s, 6H, Mes *p*-CC*H*$_3$), 2.17 (s, 12H, Mes *o*-CC*H*$_3$). $^{13}C\{^1H\}$ (CD_2Cl_2, 125 MHz): δ 318.6 (Ru=*C*H), 183.7 (IMes N*C*N), 156.4 (Mes *i*-*C*), 152.3 (Ph *i*-*C*), 151.5 (py eq. *o*-*C*H), 150.2 (py ax. *o*-*C*H), 139.4 (Mes *p*-*C*CH$_3$), 137.0 (Mes *o*-*C*CH$_3$), 136.6 (2 overlapping signals, py eq. *p*-*C*H and N*C*O), 135.3 (py ax. *p*-*C*H), 130.1 (2 overlapping signals, Ph *o*-*C*H and *p*-*C*H), 129.3 (Mes *C*H), 128.4 (Ph *m*-*C*H), 124.9 (IMes =*C*H), 123.85 (2 overlapping signals, py ax. *m*-*C*H and py eq. *m*-*C*H), 21.1 (Mes *p*-*C*H$_3$), 18.0 (Mes *o*-*C*H$_3$). IR (Nujol, cm^{-1}): ν_{NCO} 2230 (m). MALDI-MS, *m/z*: Calcd. for [M-2py]$^+$ 580.1; Found, 580.0. Anal. Calcd. ($C_{40}H_{40}N_6O_2Ru$): C, 65.11; H, 5.46; N, 11.39%. Found: C, 64.95; H, 5.69; N, 11.19 %.

2.8.17 Attempted synthesis of Ru(κ^2-$O_2C_{10}H_6$)(CHPh)(IMes)(py) **Ru-13**

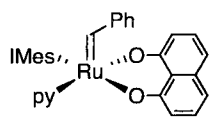

Yellow $Tl_2(O_2C_{10}H_4)$ (10 mg, 0.018 mmol) was added as a solid to a green solution of **Ru-6a** (10 mg, 0.014 mmol) in C_6D_6 (1 mL), causing a color change to brown within 5 min. The solution was allowed to stir at room temperature for 1 h, at which point a brown precipitate was visible. ^{1}H NMR analysis of the crude product revealed one new alkylidene singlet, and no visible signals in the 2.5-6.0 ppm window expected for π-bound aromatic rings. ^{1}H NMR (C_6D_6, 300 MHz): δ 18.13 (s). Attempts to isolate this new product led to decomposition, as deduced by disappearance of the alkylidene signal and degradation of the signal-to-noise ratio.

2.8.18 Attempted synthesis of Ru(κ^2-$O_2C_6H_4$)(CH-2-O^{i}Pr-C_6H_4)(IMes)(py) **Ru-14**

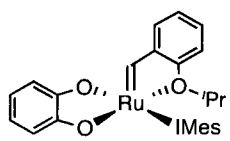

Addition of yellow **38a** (10 mg, 0.019 mmol) to a green solution of **Ru-5a** (13 mg, 0.019 mmol) in C_6D_6 (1 mL) caused a color change to brown within 5 min. The solution was allowed to stir at room temperature for 1 h, at which point a brown precipitate was evident. ^{1}H NMR analysis of the crude product revealed three new broad, poorly-resolved alkylidene singlets as well as two poorly-resolved hydride singlets. ^{1}H NMR (C_6D_6, 300 MHz): δ 17.52 (s), 16.38 (s), 15.76 (s), –4.19 (s), –12.41 (s). Ratio of these peaks: 1 : 0.19 : 0.37 : 1.82 : 0.68, respectively. This reaction was not pursued.

2.9 Ag complexes

2.9.1 $[Ag(IMes)_2][NCO]$ **Ag-1**

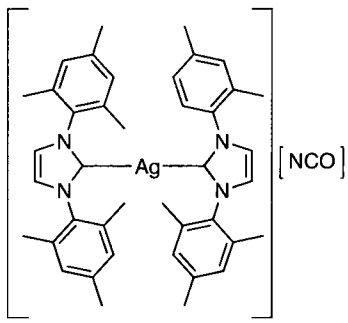

To a stirred suspension of Ag(NCO) (213 mg, 1.4 mmol) in acetone (1 mL) was added solid **30** (871 mg, 2.9 mmol). The reaction was stirred at room temperature for 1.5 h, then filtered through Celite. The red filtrate was stripped to dryness to afford an oily red residue, which afforded a cream-colored solid and a red supernatant upon addition of diethyl ether. The precipitate was filtered off, redissolved in a minimum volume of CH_2Cl_2, and treated with hexanes to afford a white powder. Yield: 674 mg (63%). ^{1}H NMR ($CDCl_3$, 300 MHz): δ 7.15 (d, $^4J_{HAg}$ = 1.5 Hz, 4H, IMes =C*H*), 6.90 (s, 8H, Mes C*H*), 2.43 (s, 12H, Mes *p*-CH_3), 1.72 (s, 24H, Mes *o*-CH_3). ^{13}C NMR ($CDCl_3$, 125 MHz): δ 182.0 (2 overlapping doublets, $^2J_{C107Ag}$ = 180 Hz; $^2J_{C109Ag}$ = 208 Hz, NC*N*), 139.8 (Mes *i*-*C*), 135.1 (N*C*O), 134.5 (Mes *p*-*C*CH_3), 129.6 (Mes *C*H), 122.8 (IMes =*C*H), 122.7 (Mes *o*-*C*CH_3), 21.1 (Mes *p*-*C*H_3), 17.6 (Mes *o*-*C*H_3). IR (Nujol, cm^{-1}): ν_{NCO} 2205 (m). MALDI-MS, *m/z*: positive ion mode: Calcd. for $[Ag(IMes)_2]^{+\cdot}$ 715.3; Found, 715.1.

2.10 Monitoring RCM and ROMP reactions

2.10.1 Representative procedure for the RCM of high-EM substrates at room temperature

In the glovebox, a 4-dram vial was charged with substrate **11a** (10 mg, 0.04 mmol) THN (internal standard for GC analysis; 5 mg, 0.04 mmol) and CH_2Cl_2 (8.3 mL, [**11a**] = 5 mM). A 1 mL aliquot was removed and analyzed (GC-FID) to establish the ratio of substrate to THN at t_0 (0% conversion). To the remaining substrate solution was added a stirbar and catalyst **Ru-12b** from a freshly prepared stock solution in CH_2Cl_2 (27 μL, 14 mM, 10 mg mL^{-1}). The reaction was stirred at room temperature (25 °C) and aliquots (1 mL) were periodically removed, quenched with Ktp[9] as a stock solution in THF (10 μL, 0.003 mmol, 70 mg mL^{-1}, ca. 8 equiv.) Each aliquot was then analyzed by GC-FID.

2.10.2 Representative procedure for the RCM of high-EM substrates at 40 °C, single time-point

The reactions were set up as in 2.10.1. Following addition of catalyst, the vials were capped, removed from the glovebox, and brought to reflux in an aluminum block maintained

at 40 °C. After 3 h, the vials were cooled to room temperature, opened to expose to air, and transferred to a GC vial in air by pipette. Conversions were measured by GC-FID as described above. The effectiveness of air as a quenching agent for the catecholate catalysts was confirmed by analysis of samples in duplicate, with one sample being analyzed immediately and the other left to queue for GC autosampling. No increase in conversion was observed over time in the GC queue.

2.10.3 Representative procedure for the RCM of high-EM substrates using high-throughput equipment, monitored over time

The protocol used was adapted from that developed by Johanna Blacquiere of this research group.[39] In a N_2-filled glovebox, toluene (425 μL) was added to 63 vials (capacity 1.5 mL) equipped with a magnetic stirbar, in an aluminum block, in seven rows of nine columns each (see Figure 1). Using a CAVRO automated liquid dispensing robot equipped with a 500 μL syringe, a solution of catalyst (25 μL, 0.013 μmol) was dispensed to each vial, with each row containing a different catalyst. No catalyst was added to column I of each row (used to assess the initial ratio of internal standard to substrate for GC analysis: see Section **2.1.5**). A solution of substrate and internal standard (50 μL, 2.5 μmol) was added to all vials, starting with vial A1. The substrate was added first to the least reactive catalyst (**Ru-9d**) to minimize any effect of the time lag for addition to vials A1–I7 (total 3 min). The vials were sealed with one Teflon and two rubber sheets, and screwed in place with an aluminum cover. The aluminum block was then heated to 60 °C, and rate profiles obtained by quenching at selected time intervals for GC analysis.[39]

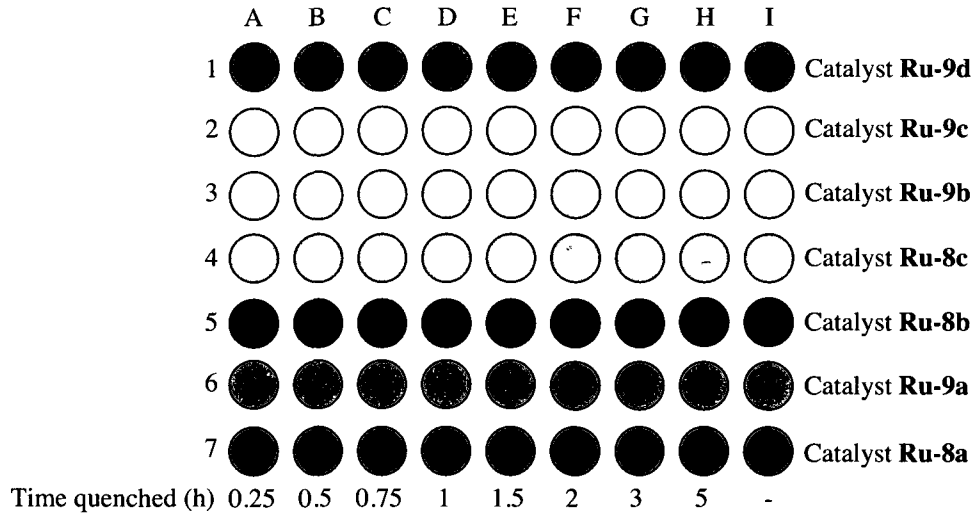

Figure 1. Plate design used to measure rate curves for the RCM of **9a** and **11a** with **Ru-8/9**.

2.10.4 Representative procedure for the RCM of low-EM substrates monitored over time, [S] = 5 mM

In a glovebox, a 4-dram vial was charged with **1a** (20 mg, 0.062 mmol), internal standard THN (10 mg), and CH_2Cl_2 to a concentration of 5 mM (12.4 mL). A 1 mL aliquot was removed for the t_0 reference, and the remaining solution was transferred to a 100 mL Schlenk flask containing a magnetic stirbar. RCM was initiated by adding 5 mol% **Ru-4a** from a stock solution (240 μL, 0.003 mmol, 10 mg mL^{-1}) by syringe. The solution was stirred vigorously at room temperature for 5 min to promote loss of ethylene, following which the Schlenk vessel was sealed, removed from the glovebox, fitted with a (previously Ar-filled) condenser under a flow of argon, and stirred at room temperature. After a period of 15 min from the addition of catalyst, the reaction was heated to reflux. Samples were removed at time intervals of 15, 30, and 45 min, 1, 1.5, 2 and 3 h (measured from the original catalyst charging). Aliquots were quenched immediately with a stock solution of Ktp in THF[39] (10 μL, 0.003 mmol, 70 mg mL^{-1}) and analyzed by GC-FID. Conversions were determined by the calibrated peak area response for diene and the RCM product, relative to values for the internal standard at t_0.

2.10.5 Representative procedure for the RCM of low-EM substrates monitored over time, [S] = 0.5 mM

In the glovebox, a 4-dram vial was charged with a solution of **3a** (10 mg, 0.055 mmol), internal standard THN (10 mg) and CH_2Cl_2 (1 mL). A 140 μL sample was removed and diluted to 0.5 mM with CH_2Cl_2 (15 mL). Another 10 μL aliquot was removed and diluted to 1.0 mL with CH_2Cl_2 ([**3a**] = 0.5 mM) for the t_0 reference. RCM was initiated by adding **Ru-4a** from a stock solution (20 μL, 0.004 mmol, 15 mg mL^{-1}), and carried out as in 2.10.4.

2.10.6 Representative procedure for the RCM of low-EM substrates monitored over time, [S] = 5 mM and addition of extra catalyst

RCM was carried out in a Schlenk vessel as in 2.10.4. Three hours after the first addition of catalyst, a 1 mL aliquot was removed and analyzed by GC to establish the extent of reaction. The remainder of the solution was allowed to cool to room temperature and carefully sent into the glovebox, where a fresh dose of **Ru-4b** (170 μL, 0.003 mmol, 13 mg mL^{-1}) was added. The solution was brought out of the glovebox for reflux under Ar, sampling and quenching as described above.

2.10.7 Representative procedure for the RCM of low-EM substrates monitored over time, initial [S] = 5 mM, followed by dilution to 0.5 mM

RCM was carried out in a Schlenk vessel as in 2.10.6. Following reintroduction into the glovebox, a 1.5 mL aliquot was removed and added to a second Schlenk vessel containing 13.5 mL CH_2Cl_2. The latter was brought out of the glovebox for reflux under Ar, sampling and quenching as described above.

2.10.8 Representative procedure for the measurement of ROMP kinetics

A solution of monomer **21** (116 mg, 0.84 mmol) in CH_2Cl_2 (8.4 mL) was added to a rapidly-stirred solution of **Ru-8a** (11 mg, 0.015 mmol) in CH_2Cl_2 (500 μL). Aliquots (1 mL) were removed periodically, quenched by addition of Ktp in THF (100 μL, 30 mg mL^{-1}, 119 mM, ca. 7 equiv), and stripped to dryness. Conversions were determined by ^1H NMR analysis in $CDCl_3$ by integrating the olefinic signals of **21** relative to those of the polymer.

2.10.9 Representative procedure for the synthesis of ROMP polymers

In the glovebox, a 1-dram vial was charged with **21** (97 mg, 0.70 mmol) and CH_2Cl_2 (1 mL). This solution was rapidly added to a green solution of **Ru-8a** (5.2 mg, 70 μmol, 1 mol%) in CH_2Cl_2 (6 mL). The solution was stirred vigorously until ROMP was complete, as indicated by ^1H NMR analysis. The metal end-group was cleaved by addition of 0.5 mL ethyl vinyl ether and the resulting solution was stripped of solvent to yield a gummy residue. Following reprecipitation from CH_2Cl_2-methanol, the rubbery polymer was dried under vacuum, weighed, and analyzed by light-scattering GPC.

2.11 Continuous-flow experiments

2.11.1 Equipment for continuous-flow experiments (carried out at LONZA AG, Visp, Switzerland)

Two independent Teledyne ISCO D-Series pumps, one containing the catalyst solution and the other containing the diene solution, were used in parallel to drive the reactants through the system. Mixing was accomplished using a CPMM-V1.2 caterpillar mixer of internal structure R-1200 (internal volume 25 μL), manufactured by the Institute for Mikrotechnik Mainz (IMM). For PFR experiments, a stainless-steel coil (0.72 mm inner diameter, internal volume 2.87 or 11 mL) was used as the residence time module. For CSTR experiments, an Ismatec pump was used to maintain a constant volume in the tank.

2.11.2 Representative procedure for the RCM of **1b** using a plug-flow reactor (PFR)

Two 250 mL Schott borosilicate bottles were dried in a Salvis vacuum oven (80 °C, 25 mbar) for a minimum of 15 h before use, cooled under a flow of argon for 10 min, and capped. Substrate **1b** (464 mg, 1.7 mmol), decane (248 mg, 0.17 mmol) and toluene (175 mL) were added to the first bottle. A 0.75 mL aliquot was removed and diluted with toluene (0.75 mL) to assess the ratio of **1b**:decane before addition of catalyst by GC-FID. To the second bottle was added toluene (175 mL) and **Ru-4b** (74 mg, 0.087 mmol). The substrate and catalyst solutions were introduced into a syringe pump at a fill rate of 20 mL min^{-1}, from which they were pumped into the micromixer where the solutions were homogenized. The combined solution was sent to the residence time module (coil) immersed in a Julabo HC temperature-controlled silicon oil bath maintained at a temperature of 40 °C, 60 °C, or 80 °C (±0.1 °C). The effluent from the coil was sampled periodically by diverting an aliquot (1 mL) into a 4 mL vial containing Ktp (10 μL of a 258 mM stock solution in THF; 40 equiv vs. Ru). The quenched solution was then analyzed by GC-FID. *Note: The ethylene formed as a co-product during RCM escapes only on exit of the reactant/product "plug" from the coil.*

2.11.3 Construction of time profiles using the PFR

Reaction times were varied by controlling the flow rates through the system: each data-point in the rate curves thus corresponds to a separate experiment. For each, a 10 sec interval was allowed for the new flow rate to stabilize, followed by purging for 3τ (see Chapter 6 for the definition of τ) prior to collecting samples for analysis. The minimum flow rate is 0.1 mL min^{-1} (irrespective of coil volume). At slower rates, axial diffusion and upstream mixing can limit the reproducibility of the coil residence time. For τ = 0.03-28.7 min, the 2.87 mL coil was used. To gain access to longer reaction times (τ = 30-60 min), the 11.00 mL coil was used to maintain flow rates above the 0.1 mL min^{-1} threshold. Upon exit of the effluent from the coil, a 1 mL sample was quenched with Ktp as above. Of note, immediate quenching (essential to ensure that residence times are reproducible and accurate) was confirmed in control experiments in which Ktp was charged along with the substrate feed. The duration of sampling ranged from <1 sec at a flow rate of 96 mL min^{-1} (reaction time 0.03 min), to 10 min for flow rates of 0.1 mL min^{-1} (reaction time 1 h). The total residence time remains constant for each sub-zone in the reacting solution: that is, it is independent of the sampling time.

References page 70

2.11.4 Representative procedure for the RCM of **1b** using a continuous stirred-tank reactor (CSTR)

The reaction was set up as in 2.11.2 up to the point of transfer from the micromixer. Following homogenization, the reactant solution was driven through a fine Teflon tube (total internal volume 247 μL; selected for fast transfer, ≤2.5 min) into the bottom of the residence time module. The tank consisted of a 10 mL round-bottom flask containing toluene (5 mL) and a magnetic stirbar, immersed in an oil bath maintained at 80 °C. A second Teflon tube (total internal volume 3 mL), connected to a piston pump and positioned at the 5 mL mark of the round-bottom flask, was used to remove any volume of solution in excess of 5 mL. The speed of the piston pump was maintained at 40 mL min^{-1}, vs. a maximum of 5 mL min^{-1} for the upstream syringe pumps, to ensure a constant volume of 5 mL, and to minimize the time interval (maximum 5 sec) between removal of the reactant solution from the tank, and its addition to the quenching solution. This minimizes any run-on metathesis following exit from the tank, and has the added benefit of promoting exchange of the headspace gas. The system was purged with 50 mL of the substrate and catalyst solution (i.e. 10× the residence time) before sampling. Upon exit, samples were quenched and analyzed as above.

2.12 Measurement of response factors

Note: Response factors must be assessed with great care, using only analytically pure material weighed on the analytical balance, and solvents measured using volumetric pipettes. To minimize evaporation (particularly for volatile solvents like CH_2Cl_2), vials should be sealed as much as possible. Sample preparation was performed in air, at ambient temperature (23 °C).

Two 4-dram vials were loaded with THN as internal standard (10.0032 mg, 0.07567 mmol). To the first vial was added **1b** (10.0004 mg, 0.03754 mmol); to the second, **2b** (12.0012 mg, 0.05035 mmol). Using a volumetric pipette (10 ± 0.02 mL), 10.00 mL of CH_2Cl_2 was added to both vials. Aliquots of 1000, 800, 600, 400 and 200 μL (± 1 μL) were removed from each vial by syringe topped to a final volume of 1 mL (if necessary) and analyzed in triplicate by GC-FID. Response factors were determined from a plot of average GC peak area vs. analyte concentration, according to equation (1).

$$\frac{\dfrac{\text{Slope RCM}}{\text{Slope THN}}}{\dfrac{\text{Slope Diene}}{\text{Slope THN}}} = \frac{\text{Slope RCM}}{\text{Slope Diene}} = \text{Response factor} \qquad (1)$$

2.13 Crystallographic analysis

X-ray crystallography analyses were performed by Dr. Scott J. Dalgarno (Heriot-Watt University, Scotland) or Dr. Robert McDonald (University of Alberta).

For **Ru-2a**, **Ru-8c**, **Ru-9a** and **Ru-9b** (Dr. Dalgarno), data were collected on a Bruker SMART 1000 CCD diffractometer with Mo Kα radiation using the ω-scan mode. Single crystals were mounted on a thin glass fiber using paraffin oil and cooled to the collection temperature (173 K). Data were collected using the SADABS program (Bruker). Structure solutions in the appropriate space groups were performed using the Patterson methods, completed with difference Fourier syntheses, and refined by full-matrix least-squares procedures based on F^2 using the SHELX-97 software package. All non-hydrogen atoms were refined anisotropically; hydrogen atoms were placed at geometrically calculated positions and allowed to ride on their parent atoms.

For **Ru-12a**, data were collected on a Bruker AXS SMART 1000 CCD diffractometer with Mo Kα radiation using the ω-scan mode. Single crystals were mounted on a thin glass fiber using paraffin oil and cooled to the collection temperature (208 K). Structure solution in the appropriate space group was solved by direct methods, completed with difference Fourier syntheses and refined with full-matrix least-squares procedures based on F^2 using the SHEXTL 5.10 program. All non-hydrogen atoms were refined anisotropically; hydrogen atoms were treated as idealized contributions.

For **Ru-12b** (Dr. McDonald), data were collected on a Bruker D8/APEX II CCD diffractometer with Mo Kα radiation using the ω-scan mode. Single crystals were mounted on a thin glass fiber using paraffin oil and cooled to the collection temperature (208 K). Data were collected using the SADABS program (Bruker). Structure solutions in the appropriate space groups were performed using the Patterson methods, completed with difference Fourier syntheses, and refined by full-matrix least-squares procedures based on F^2 using the SHELX-97 software package. All non-hydrogen atoms were refined anisotropically;

hydrogen atoms were placed at geometrically calculated positions and allowed to ride on their parent atoms.

Table 2. Crystal data and structure refinement for structurally-characterized complexes

	Ru-2a	**Ru-8c**	**Ru-9a**
Crystallographer	Dalgarno	Dalgarno	Dalgarno
CCDC #	689209	-	-
Empirical formula	$C_{66}H_{55}O_2P_3Ru$	$C_{39}H_{37}Br_2N_3O_2Ru$	$C_{39}H_{39}N_3O_2Ru$
Color	blue	orange	green
Formula wt.	1074.08	840.61	682.80
Temp. K	173(2)	173(2)	173(2)
Wavelength, Å	0.71073	0.71073	0.71073
Crystal syst., space group	monoclinic $P2_1/c$	Orthorombic *Pbca*	Monoclinic $P2_1$
Unit cell dimens.			
a, Å	13.3727(13)	15.957(6)	9.1238(12)
α, deg	90	90	90
b, Å	17.1572(18)	16.591(4)	17.399(2)
β, deg	94.653(3)	90	98.714(4)
c, Å	23.022(2)	27.041(7)	11.2246(14)
γ, deg	90	90	90
V, Å^3	5264.7(9)	7159(4)	1761.3(4)
Z, calcd. density, mg/cm^3	4, 1.355	8, 1.56	2, 1.436
μ, mm^{-1}	0.435	2.708	1.617
F(000)	2224	3376	776
Cryst. size, mm	0.6 × 0.44 × 0.42	0.4 × 0.25 × 0.1	0.2 × 0.11 × 0.07
Θ range for data collecn., deg	1.48-27.07	1.92-27.09	1.84-27.16
Limiting indices	$-17 \le h \le 12$ $-17 \le k \le 21$ $-22 \le l \le 28$	$-20 \le h \le 20$ $-20 \le k \le 21$ $-34 \le l \le 31$	$-11 \le h \le 11$ $-14 \le k \le 22$ $-13 \le l \le 14$
No. of rflns. collected/unique	21,831 / 10,952 (R_{int} = 0.0224)	46,173 / 7,861 (R_{int} = 0.0694)	9,441 / 5782 (R_{int} = 0.0223)
Abs. cor.	Multi-scan	Multi-scan	Multi-scan
Detector	Bruker SMART 1000 CCD	Bruker SMART 1000 CCD	Bruker SMART 1000 CCD
Max, min transmission	0.8383, 0.7802	0.7734, 0.4105	0.8952, 0.7381
Refinement method	Full-matrix least-squares on F^2	Full-matrix least-squares on F^2	Full-matrix least-squares on F^2
Data/restraints/params.	10,952 / 0 / 649	7,861 / 0 / 430	5,782 / 1 / 216
Goodness of fit on F^2	1.032	1.124	0.741
Final *R* indices ($I > 2\sigma(I)$)	R_1 = 0.0286, wR_2 = 0.0716	R_1 = 0.0619, wR_2 = 0.1387	R_1 = 0.0371, wR_2 = 0.0929
R indices (all data)	R_1 = 0.0286, wR_2 = 0.0716	R_1 = 0.0966, wR_2 = 0.1538	R_1 = 0.0408, wR_2 = 0.0968
Largest diff. peak, hole, e/Å^3	0.558, -0.279	1.043, -1.737	0.848, 0.56

Table 2. (Continued)

	Ru-9b	**Ru-12a**	**Ru-12b**
Crystallographer	Dalgarno	McDonald	McDonald
CCDC #	-	791245	791246
Empirical formula	$C_{39}H_{35}F_4N_3O_2Ru$	$C_{42}H_{44}N_6O_{0.5}S_2Ru$	$C_{40}H_{40}N_6O_2Ru$
Color	orange	green	green
Formula wt.	754.77	806.02	737.85
Temp. K	173(2)	208(2)	208(2)
Wavelength, Å	0.71073	0.71073	0.71073
Crystal syst., space group	monoclinic $P2_1/c$	monoclinic, C2/c	tetragonal, $P4_12_12$ (No. 92)
Unit cell dimens.			
a, Å	8.1640(10)	35.989(4)	9.5752(8)
α, deg	90	90	90
b, Å	20.642(3)	10.5410(10)	9.5752(8)
β, deg	93.364(4)	118.082(2)	90
c, Å	20.137(3)	24.085(3)	39.106(3)
γ, deg	90	90	90
V, Å^3	3387.6(7)	8061.2(15)	3585.4(5)
Z, calcd density, mg/cm^3	4, 1.48	8, 1.328	4, 1.367
μ, mm^{-1}	0.524	0.531	0.481
F(000)	1544	3344	1528
Cryst. size, mm	0.35 × 0.22 × 0.21	0.40 × 0.20 × 0.08	0.30 × 0.29 × 0.23
Θ range for data collecn., deg	1.41-27.12	1.28-26.37	2.37-20.48
Limiting indices	$-7 \le h \le 10$ $-26 \le k \le 25$ $-25 \le l \le 25$	$-44 \le h \le 44$ $-13 \le k \le 13$ $-19 \le l \le 29$	$-11 \le h \le 11$ $-11 \le k \le 11$ $-47 \le l \le 47$
No. of rflns. collected/unique	24,086 / 7450 (R_{int} = 0.0311)	18,700 / 8,200 (R_{int} = 0.0729)	26,313 / 3,346 (R_{int} = 0.0464)
Abs. cor.	Multi-scan	Semi-empirical from equivalents	Gaussian integration (face-indexed)
Detector	Bruker SMART 1000 CCD	Bruker AXS SMART 1000 CCD	Bruker D8/Apex II CCD
Max, min transmission	0.8979, 0.8378	1.0, 0.76	0.8959, 0.8708
Refinement method	Full-matrix least-squares on F^2	Full-matrix least-squares on F^2	Full-matrix least-squares on F^2
Data/restraints/params.	7,450 / 0 / 448	8200 /9 / 467	3346 / 12 / 288
Goodness of fit on F^2	1.027	1.029	1.185
Final *R* indices ($I > 2\sigma(I)$)	R_1 = 0.0314, wR_2 = 0.0722	R_1 = 0.0633, wR_2 = 0.1268	R_1 = 0.0452, wR_2 = 0.1097
R indices (all data)	R_1 = 0.0426, wR_2 = 0.0767	R_1 = 0.1175, wR_2 = 0.1437	R_1 = 0.0633, wR_2 = 0.1268
Largest diff. peak, hole, e/Å^3	0.495, -0.68	0.689, -0.653	0.917, -0.507

2.14 DFT calculations

All calculations were performed by Dr. Serge Gorelsky of the uO Centre for Catalysis Research & Innovation. DFT calculations were performed using the Gaussian 03 package.[40] Stationary points on the potential energy surface were obtained using the B3LYP[41-43] exchange-correlation functional with the DZVP basis[44] for all atoms. Tight SCF convergence criteria (10^{-8} a.u.) were used for all calculations. The converged wave functions were tested to confirm that they correspond to the ground-state surface. Harmonic frequency calculations were used to determine the nature of the stationary points obtained. Bond order[45] analysis was carried out using the AOMix program.[46] For simulation of UV-Vis spectra, time-dependent DFT (TD-DFT) was used to calculate the energies and intensities of the lowest 30 singlet-singlet transitions. Absorption curves (i.e. the electronic spectra) were calculated by the method reported,[47] assuming a band width at half-height of 2,500 cm^{-1} (a typical value for electronic transitions for complexes of the type described). Pseudo-Voigt functions with 50% weight for contributing Gaussian and Lorentzian functions were used to simulate the absorption bands.

2.15 References

(1) Shriver, D. F.; Drezdzon, M. A., *The Manipulation of Air-Sensitive Compounds*. 2nd Ed. ed.; John Wiley & Sons: New York, 1986; p 326.
(2) Still, W. C.; Kahn, M.; Mitra, A., *J. Org. Chem.* **1978**, *43*, 2923-2925.
(3) Armarego, W. L. F.; Perrin, D. D., *Purification of Common Laboratory Chemicals*. 4th Ed. ed.; Butterworth-Heinemann: Oxford, 1997; p 529.
(4) Eelman, M. D.; Blacquiere, J. M.; Moriarty, M. M.; Fogg, D. E., *Angew. Chem., Int. Ed.* **2008**, *47*, 303-306.
(5) Conrad, J. C.; Eelman, M. D.; Duarte Silva, J. A.; Monfette, S.; Parnas, H. H.; Snelgrove, J. L.; Fogg, D. E., *J. Am. Chem. Soc.* **2007**, *129*, 1024-1025.
(6) Litinas, K. E.; Salteris, B. E., *J. Chem. Soc., Perkin Trans. 1* **1997**, 2869-2872.
(7) Fürstner, A.; Langemann, K., *Synthesis* **1997**, 792-803.
(8) Varray, S.; Lazaro, R.; Martinez, J.; Lamaty, F., *Organometallics* **2003**, *22*, 2426-2435.
(9) Arisawa, M.; Kato, C.; Kaneko, H.; Nishida, A.; Nakagawa, M., *Perkin 1* **2000**, 1873-1876.
(10) Clavier, H.; Nolan, S. P., *Chem. Eur. J.* **2007**, *13*, 8029-8036.
(11) Ivin, K. J.; Lam, L.-M.; Rooney, J. J., *Macromol. Chem. Phys.* **1994**, *195*, 1189-1197.
(12) Miller, S. J.; Kim, S.-H.; Chen, Z.-R.; Grubbs, R. H., *J. Am. Chem. Soc.* **1995**, *117*, 2108-2109.
(13) Schmidt, B., *J. Chem. Soc., Perkin Trans. 1* **1999**, 2627-2637.
(14) Terada, Y.; Arisawa, M.; Nishida, A., *Angew. Chem., Int. Ed.* **2004**, *43*, 4063-4067.
(15) Yao, Q. W.; Zhang, Y. L., *J. Am. Chem. Soc.* **2004**, *126*, 74-75.
(16) Schmidt, B.; Pohler, M.; Costisella, B., *J. Org. Chem.* **2004**, *69*, 1421-1424.
(17) Spagnol, G.; Heck, M.-P.; Nolan, S. P.; Mioskowski, C., *Org. Lett.* **2002**, *4*, 1767-1770.

(18) Fürstner, A.; Ackermann, L.; Gabor, B.; Goddard, R.; Lehmann, C. W.; Mynott, R.; Stelzer, F.; Thiel, O. R., *Chem. Eur. J.* **2001**, *7*, 3236-3253.
(19) Fu, G. C.; Nguyen, S. T.; Grubbs, R. H., *J. Am. Chem. Soc.* **1993**, *115*, 9856-9857.
(20) Marsella, M. J.; Maynard, H. D.; Grubbs, R. H., *Angew. Chem., Int. Ed. Engl.* **1997**, *36*, 1101-1103.
(21) Kofron, W. G.; Baclawski, L. M., *J. Org. Chem.* **1976**, *41*, 1879-1880.
(22) Creary, X., *Org. Synth.* **1986**, *64*, 207-216.
(23) Bujok, R.; Bieniek, M.; Masnyk, M.; Michrowska, A.; Sarosiek, A.; Stepowska, H.; Arlt, D.; Grela, K., *J. Org. Chem.* **2004**, *69*, 6894-6896.
(24) Arduengo, A. J.; Krafczyk, R.; Schmutzler, R.; Craig, H. A.; Goerlich, J. R.; Marshall, W. J.; Unverzagt, M., *Tetrahedron* **1999**, *55*, 14523-14534.
(25) Marquet, J.; Moreno-Manas, M.; Vallribera, A.; Virgili, A.; Bertran, J.; Gonzalez-Lafont, A.; Lluch, J. M., *Tetrahedron* **1987**, *43*, 351-360.
(26) Rosa, D. T.; Reynolds, R. A., III; Malinak, S. M.; Coucouvanis, D.; Ali, M.; MacDonnell, F. M., *Inorg. Synth.* **2002**, *33*, 112-119.
(27) Kim, S.; Oh, C. H.; Ko, J. S.; Ahn, K. H.; Kim, Y. J., *J. Org. Chem.* **1985**, *50*, 1927-1932.
(28) Teuber, H. J.; Staiger, G., *Chem. Ber.* **1955**, *88*, 802-827.
(29) Galvan-Arzate, S.; Santamaria, A., *Toxicol. Lett.* **1998**, *99*, 1-13.
(30) Schrock, R. R.; Murdzek, J. S.; Bazan, G. C.; Robbins, J.; DiMare, M.; O'Regan, M., *J. Am. Chem. Soc.* **1990**, *112*, 3875-3886.
(31) Hoffman, P. R.; Caulton, K. G., *J. Am. Chem. Soc.* **1975**, *97*, 4221-4228.
(32) Monfette, S.; Duarte Silva, J. A.; Gorelsky, S. I.; Dalgarno, S. J.; dos Santos, E. N.; Araujo, M. H.; Fogg, D. E., *Can. J. Chem.* **2009**, *87*, 361-367.
(33) Schwab, P.; Grubbs, R. H.; Ziller, J. W., *J. Am. Chem. Soc.* **1996**, *118*, 100-110.
(34) Huang, J.; Stevens, E. D.; Nolan, S. P.; Petersen, J. L., *J. Am. Chem. Soc.* **1999**, *121*, 2674-2678.
(35) Conrad, J. C.; Amoroso, D.; Czechura, P.; Yap, G. P. A.; Fogg, D. E., *Organometallics* **2003**, *22*, 3634-3636.
(36) Michrowska, A.; Bujok, R.; Harutyunyan, S.; Sashuk, V.; Dolgonos, G.; Grela, K., *J. Am. Chem. Soc.* **2004**, *126*, 9318-9325.
(37) Monfette, S.; Camm, K. D.; Gorelsky, S. I.; Fogg, D. E., *Organometallics* **2009**, *28*, 944-946.
(38) Monfette, S.; Fogg, D. E., *Organometallics* **2006**, *25*, 1940-1944.
(39) Blacquiere, J. M.; Jurca, T.; Weiss, J.; Fogg, D. E., *Adv. Synth. Catal.* **2008**, *350*, 2849-2855.
(40) Frisch, M. J.; Trucks, G. W.; Schlegel, H. B.; Scuseria, G. E.; Robb, M. A.; Cheeseman, J. R.; J. A. Montgomery, J.; Vreven, T.; Kudin, K. N.; Burant, J. C.; Millam, J. M.; Iyengar, S. S.; Tomasi, J.; Barone, V.; Mennucci, B.; Cossi, M.; Scalmani, G.; Rega, N.; Petersson, G. A.; Nakatsuji, H.; Hada, M.; Ehara, M.; Toyota, K.; Fukuda, R.; Hasegawa, J.; Ishida, M.; Nakajima, T.; Honda, Y.; Kitao, O.; Nakai, H.; Klene, M.; Li, X.; Knox, J. E.; Hratchian, H. P.; Cross, J. B.; Bakken, V.; Adamo, C.; Jaramillo, J.; Gomperts, R.; Stratmann, R. E.; Yazyev, O.; Austin, A. J.; Cammi, R.; Pomelli, C.; Ochterski, J. W.; Ayala, P. Y.; Morokuma, K.; Voth, G. A.; Salvador, P.; Dannenberg, J. J.; Zakrzewski, V. G.; Dapprich, S.; Daniels, A. D.; Strain, M. C.; Farkas, O.; Malick, D. K.; Rabuck, A. D.; Raghavachari, K.; Foresman, J. B.; Ortiz, J. V.; Cui, Q.; Baboul, A. G.; Clifford, S.; Cioslowski, J.;

Stefanov, B. B.; Liu, G.; Liashenko, A.; Piskorz, P.; Komaromi, I.; Martin, R. L.; Fox, D. J.; Keith, T.; Al-Laham, M. A.; Peng, C. Y.; Nanayakkara, A.; Challacombe, M.; Gill, P. M. W.; Johnson, B.; Chen, W.; Wong, M. W.; Gonzalez, C.; Pople, J. A. *Gaussian 03*, Revision C.02; Gaussian, Inc.: Wallingford, CT, 2003.
(41) Lee, C.; Yang, W.; Parr, R. G., *Phys. Rev. B* **1988**, *37*, 785-789.
(42) Miehlich, B.; Savin, A.; Stoll, H.; Preuss, H., *Chem. Phys. Lett.* **1989**, *157*, 200-206.
(43) Becke, A. D., *J. Chem. Phys.* **1993**, *98*, 5648-5652.
(44) Godbout, N.; Salahub, D. R.; Andzelm, J.; Wimmer, E., *Can. J. Chem.* **1992**, *70*, 560-571.
(45) Mayer, I., *Chem. Phys. Lett.* **1983**, *97*, 270-274.
(46) Gorelsky, S. I. *AOMix: Program for Molecular Orbital Analysis*, Version 6.42; University of Ottawa: Ottawa, Canada, 2009.
(47) Gorelsky, S. I.; Lever, A. B. P., *J. Organomet. Chem.* **2001**, *635*, 187-196.

3. Catalyst influence on RCM macrocyclization efficiency*

3.1 Introduction

Macrocyclic structures are abundant in natural products, and show immense potential as antitumor, antibiotic and antifungal agents.[1] The often high potency and selectivity of such structures are due in part to the capacity of the macrocyclic core to confer a high degree of structural pre-organization on key functional groups present as ring substituents, thus minimizing entropy losses upon docking at the binding site of a receptor.[1] The powerful biological effects and novel modes of action characteristic of many natural products, coupled with the challenge of sourcing them in the volumes required for testing,[2] motivate the search for efficient routes from robust chemical feedstocks.[2] Beyond medicinal purposes, macrocycles are of considerable value in a range of other applications, including perfumery agents[3] and cyclic polymers relevant to both advanced materials and chemical biology.[4,5]

Synthetic methodologies employed for construction of macrocyclic structures originated with classic stoichiometric reactions such as macrolactonization[6] and macrolactamization,[7] both of which have been used with success.[8] Activating agents are normally employed to promote these reactions. These include 2,2'-dipyridyl disulfide (**A**),[9] 1-methyl-2-chloropyridinium iodide (**B**),[10] 2,4,6-trichlorobenzoyl chloride (**C**),[11] and diethyl azodicarboxylate in conjunction with PPh_3 (**D**);[12] Chart 1. Synthetic strategies based on carbon-carbon bond formation have also proved successful. Selected examples include macroaldolization,[13] S_N2 cyclization,[14-16] Dieckmann condensation of diesters,[17-19] intramolecular Diels-Alder synthesis,[20-22] as well as various Wittig-type reactions.[23-25] Catalytic cyclizations using Pd,[26-29] Cu[30,31] and Au[28] have likewise been documented.

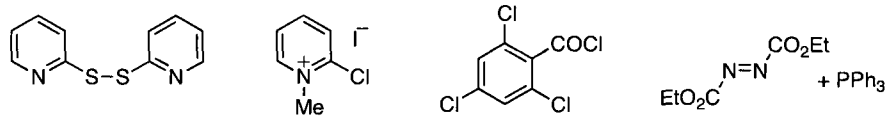

(**A**) (Corey-Nicolaou) (**B**) (Mukaiyama) (**C**) (Yamagushi) (**D**) (Mitsunobu)

Chart 1. Selected reagents used for macrolactonization.

---

* Part of the work described in this Chapter has been published, including a major review of the operation and implications of ring-chain equilibria in RCM (and ROMP). (a) Monfette, S.; Fogg, D. E., *Chem. Rev.* **2009**, *109*, 3783–3816; (b) Monfette, S.; Crane, A. K.; Duarte Silva, J. A.; Facey, G. A.; dos Santos, E. N.; Araujo, M. H.; Fogg, D. E., *Inorg. Chim. Acta* **2010**, *363*, 481-486; (c) Conrad, J. C.; Eelman, M. D.; Duarte Silva, J. A.; Monfette, S.; Parnas, H. H.; Snelgrove, J. L.; Fogg, D. E., *J. Am. Chem. Soc.* **2007**, *129*, 1024-1025.

References page 118

Despite this plethora of potential methodologies, relatively few are actually used in total synthesis, as Miller has noted.[2] This reflects the highly functionalized nature of many "macrocyclization precursors" found in synthesis campaigns, and their sensitivity to conventional cyclization reagents, owing to which high chemoselectivity and mild reaction conditions are essential. Ru-catalyzed ring-closing metathesis is attractive in this context, given the reasonable functional group tolerance of (e.g.) the Grubbs catalysts, their ease of handling, and their often-preferential reaction with olefins.[32] (This last is not invariable, although the hyperbole associated with market development regrettably tends to obscure this point: see Chapter 1). The power of the method withstands hyperbole, however, and reports from both academia and industry highlight the potential of RCM for the construction of macrocyclic structures.[8,33-36]

Common questions preceding deployment of RCM include the following: Which catalyst should be used? What conditions should be employed? Are Ziegler conditions required to curb formation of undesired oligomeric by-products? Answers remain few, however, and reactions are typically carried out by trial and error. A recent review by Gradillas and Perez-Castells provides some empirical indicators of the temperatures and dilutions often employed.[8] While such factors can be key to success, the nature and reactivity of the catalyst can also be critical.[33]

During the RCM synthesis of Herbarumin I and II, which feature a 10-membered cyclic core, Furstner and co-workers observed different E:Z ratios on use of the first- or second-generation Grubbs catalysts.[37] Other groups subsequently reported similar differences during synthesis of medium or large rings.[34,35,38-42] These empirical observations were attributed to different selectivity of the respective catalysts. Surprisingly, however, the underlying reaction mechanism was not examined until recently. Work on RCM macrocyclization, carried out by myself in collaboration with Jay Conrad and Joao Duarte Silva of this group, uncovered a previously unrecognized mechanistic pathway operative for the second-generation catalyst **Ru-4a**.[43] Rather than the expected, direct RCM pathway (Scheme 1, path a), diene oligomerization is kinetically dominant, as evidenced by the near complete disappearance of volatile constituents by GC-FID analysis. Subsequent backbiting (Scheme 1, path b) liberates the targeted macrocycle via a concentration-dependent equilibrium.[33] In contrast to the behaviour of the Grubbs catalyst **Ru-4a**, perbromophenoxide **Ru-7b** was

References page 118

found to generate this macrocycle without detectable oligomeric intermediates.[44] It was unclear whether direct cyclization (path a) is operative for this catalyst, or if backbiting is simply much faster. These two pathways, however, could account for the catalyst-dependent variation in E/Z ratios noted above.

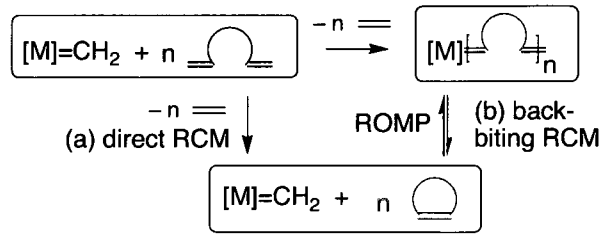

Scheme 1. Simplified metathesis manifolds involved in the formation of macrocyclic rings, showing (a) direct RCM and (b) RCM via the ring-chain (oligomerization-backbiting) equilibrium.

RCM reactions proceeding via the oligomerization-backbiting pathway are thermodynamically controlled: that is, RCM yields are determined by the equilibrium constant for the reaction. Conversely, for catalysts that operate by direct RCM, a kinetic product distribution is obtained. (Throughout the rest of this Chapter, RCM catalysts are classified as affording kinetic (K-class) or thermodynamic (T-class) product distributions). The preliminary study discussed above focused only on the Grubbs catalysts **Ru-4a** and **Ru-6a**, and perbromoaryloxide **Ru-7b**.[43,44] To gain insight into the behaviour of the more widely-used first- and second-generation catalysts **Ru-3**, **Ru-4b**, and the Hoveyda catalysts **Ru-5**, a more detailed analysis was undertaken.

This Chapter describes the first systematic comparison of cyclization efficiency for the most commonly employed ruthenium metathesis catalysts, for a range of substrates that function as precursors to large and medium rings. Four questions motivated this work: (1) Which metathesis catalysts, if any, share the kinetic bias of **Ru-4a** toward oligomerization? (2) Does the catalyst affect K_{eq} in the ring-chain equilibrium? That is, can the catalyst affect the thermodynamic ratio of cyclic vs. oligomeric products? (3) Is the oligomerization-backbiting pathway also operative during synthesis of medium rings, or is it inhibited by the higher ring strain? (4) What synthetic protocols can be used to promote the RCM of medium and large rings? It was hoped that answers to these questions would confer a deeper understanding of the thermodynamic factors that control the behavior of the Grubbs catalysts

in RCM macrocyclization, as well as practical insights into process optimization (e.g. guidance toward a rational choice of catalyst and experimental conditions). Additionally, establishing correlations between RCM yield and catalyst structure may uncover clues as to the underlying catalyst features that promote RCM. This last has tantalizing potential to promote uptake of RCM methodologies in pharmaceutical[34-36,45-50] and general industrial practice.

3.2 Ring-chain equilibria: theory

3.2.1 The Jacobson-Stockmayer theory

The challenges associated with the assembly of medium and large rings, irrespective of the specific reaction employed, have been recognized for nearly a century. In the early 1920s, the natural products muscone and civetone were found to feature, respectively, 15- and 17-membered cyclic cores.[16] Efforts to synthesize the macrocyclic ring led rapidly to the realization that intermolecular condensation limited yields. The underlying physical organic chemistry was therefore intensively studied by luminaries such as Ruggli, Ruzicka and Ziegler.

In 1950, Jacobson and Stockmayer proposed a theory (referred to below as the JS theory) that sought to predict the distribution of cyclic and linear polymers formed in concentrated solutions, from bifunctional precursors.[51] The JS theory assumed that: (1) all rings are strainless, generated without any heat of cyclization; (2) the end-to-end distances of linear chains obey Gaussian statistics; (3) the probability of cyclization is determined by the fraction of all configurations for which the chain ends coincide, and (4) the reactivity of chain ends is independent of chain length.[52] The JS theory predicts a critical monomer concentration (CMC) at equilibrium, below which a distribution of cyclic species is present, and above which the total concentration of cyclic oligomers remains constant, and linear chains emerge.[53] Because enthalpic effects are neglected (assumption 1), and because the change in entropy for the chain is treated as essentially independent of chain length, the macrocyclization equilibrium constant is determined solely by the change in configurational entropy associated with cyclization. The value of K_x (i.e. the critical monomer concentration, CMC) for the cyclic species C_x declines with increasing degree of polymerization x, and hence ring size, within a homologous series.

While the inverse relationship between K_x and the degree of polymerization x is in accord with experimental observations,[52] Kornfield noted that the JS theory requires an accurate distance between the reacting ends to precisely calculate K_x and hence product distributions.[52] Suter and Höcker improved on the original model by using the rotational isomeric state (RIS) model to estimate end-to-end chain distances. (This treatment considers the chemical structure of the chain in predicting the conformational behavior of macromolecules).[54] Values of K_x thus predicted agreed well with experimental values for macrocycles containing >30-40 backbone atoms.[55] Even once RIS assessments are incorporated, however, the JS theory tends to overestimate the cyclization equilibrium constant K_x for shorter chains, as the ring strain increases, and the assumption of zero enthalpy of cyclization becomes less tenable. The theory remains useful for assessing the equilibrium proportion of relatively strain-free cyclooligomers formed through polymer backbiting.

The limitations associated with considering solely entropic factors become more severe for medium rings, for which enthalpic factors are increasingly important (see Section 3.2.3). Kornfield's updated treatment, which calculates the enthalpy change through Monte Carlo methods,[52] marginally improved the accuracy of the distribution of cyclic and linear products obtained by ROMP of cycloolefins such as cyclobutene, cyclooctene and cyclododecene. Here the change in enthalpy is assumed to be due only to the strain energy, as the number of bonds and hence total bond energy in the ring-chain equilibrium remains constant, and intermolecular interactions are largely unaffected. However, even when ring-strain is calculated, the experimental and computed K_x still differs for rings of <25 atoms.[52] This disagreement in K_x could be due to one (or both) of the following: (1) the presence of the metal endgroup on the oligomeric chain, required for the ring-chain equilibrium to occur, is not taken into account in the Kornfield model. This may profoundly affect the enthalpy and entropy in the cyclic transition state. (2) The experimentally-determined "K_x" values may not be equilibrium values. A number of workers have noted that the observed product distributions depend on catalyst lifetime and/or activity.[56-58] Thorn-Csanyi, for example, commented on the wide range of values reported for the 1,5-cyclooctadiene system, and showed that full equilibrium had not been established in all cases.[57]

References page 118

Issues of predictability notwithstanding, the lasting message of the JS theory and its later incarnations is a qualitative prediction, based on entropic effects: that is, higher proportions of cyclic species will be found at lower concentration, with an increased bias in favor of smaller ring sizes as dilution increases.

3.2.2 The concept of effective molarity

The JS theory was developed for analysis of polymerization reactions (i.e. the "chain" side of the ring-chain equilibrium), but its fundamentals are equally applicable to the synthesis of cyclic targets (i.e. the "ring" side of the same equilibrium) providing that neither cyclization nor oligomerization is irreversible. However, for cyclization reactions, the CMC is not a useful metric, particularly for predicting the outcome of minimally exothermic reactions.[59] Furthermore, because it does not distinguish between rings of different sizes, this concept has little predictive value in organic synthesis, where selectivity for a single ring size is generally desired. More broadly used is the related concept of effective molarity (EM), originally developed to assess the ease of cyclization of bifunctional molecules,[15,16,60,61] and now widely used to evaluate the probability of self-assembly in many contexts.[62-68] A number of useful reviews, particularly by Mandolini, Ercolani and Illuminati, aid in tracing the evolution of EM concepts.[15,16,61,69] The thermodynamic or equilibrium EM value is in fact equivalent to the macrocyclization equilibrium constant K_x,[70] and is defined as the ratio K_{intra}/K_{inter} (intra- and intermolecular reactions).[61] The higher the value, the greater the ease of cyclization and, by extension, the higher the concentration that can be tolerated for synthesizing a given ring free from competing polymerization reactions. Few thermodynamic EM values have been described,[69] however, owing to the dominance of studies that focus on irreversible reactions. Much more common are kinetic EM values, in which the efficiency of cyclization is assessed from the ratio of the rate constants for the analogous intramolecular and intermolecular reactions under identical conditions (i.e. the kinetic EM value = k_{intra}/k_{inter}). Importantly, the EM values do not represent physically-real concentrations,[71] instead they should be viewed as an empirical predictor to assess the ease of cyclization reactions.

3.2.3 Thermodynamic considerations for RCM

In contrast to ROMP, where ring-opening of cyclic olefins is normally driven by release of ring strain, no enthalpic driver exists in RCM, barring strategies in which two reactions are coupled (e.g., ROM-RCM processes).[72-74] RCM is thus entropy-driven, and the enthalpic

costs that can be sustained are limited by the extent to which (in Gibbs-Helmholtz terms) the $T\Delta S$ term can be maximized. The entropic benefit associated with release and volatilization of ethylene on metathesis of vinylic α,ω–dienes is powerful but indiscriminate, promoting inter- and intramolecular reactions equally. The elevated temperatures (usually >40 °C)[8,75] characteristically used for RCM, generally regarded as a kinetic requirement, thus have an additional thermodynamic role in the ring-chain equilibrium. They favor cyclization by further reducing viscosity and maximizing thermal motion: they also serve to reinforce any entropic bias in the $T\Delta S$ term.

A key feature distinguishing the so-called common ring sizes (particularly those of five and six members) from larger rings is the high kinetic *and* thermodynamic bias toward their formation. The probability of encounter between reactive endgroups is inversely proportional to ring size, and is therefore at a maximum in this size regime, relative to larger systems. The higher translational and (overall) rotational mobility associated with molecules of smaller size likewise favor formation of common rings over larger rings, or acyclic oligomers, despite the loss in rotational and conformational flexibility. The cumulative effect is to render synthesis of common rings highly straightforward, to the extent that they are frequently accessible by direct RCM (Scheme 1, path a), and do not exhibit any tendency toward oligomerization under normal conditions of concentration and temperature. Appropriately substituted dienes can show a dramatically greater bias. A now-classic paper by Forbes and Wagener demonstrated that, where aided by the Thorpe-Ingold effect, RCM of such substrates can be achieved even in neat diene.[76] Under more conventional solution conditions, the "benchmark" substrate diethyl diallyl malonate showed no evidence of oligomerization at diene concentrations of 100 mM, in contrast to dienes that afford larger rings.[43] (It will be noted however that oligomers were reported during RCM of neat dimethyl diallyl malonate).[76]

Ring strain increases sharply in the medium-ring regime, owing principally to imperfect staggering and transannular strain between atoms forced into proximity from opposite sides of the ring.[16] The precise position of this maximum, with respect to ring size, depends on the nature, substitution, and hybridization of the ring atoms.[15] Of interest, given the greater degree of functionalization often characteristic of RCM substrates, is the finding that ΔG° for ROMP of common and medium rings becomes less favorable as ring substitution

increases.[53,77] This offers some promise for formation of medium-sized RCM targets, although the extent of strain will clearly be critical. Strain diminishes as ring size increases further, but remains higher than that present in the common rings. Because entropic gains offer the only means to pay this enthalpic penalty, cyclization is strongly affected by the extent to which the entropy term $T\Delta S$ can be biased in its favor. The relative weighting of the two key entropic factors, translational mobility (which favors small molecules) and conformational motion (which favors macromolecules), is sensitive to concentration, because translational mobility declines with increasing viscosity, while conformational motion is much less affected.[78] Maximizing dilution maximizes translational entropy, and hence the entropic bias toward RCM. Elevated temperatures can also favor cyclization, as noted above. Two experimental variables of particular importance in creating a thermodynamic bias toward cyclic products are thus high temperatures and high dilutions. It will be noted that the low temperature ceiling in refluxing CH_2Cl_2 limits the extent to which the $T\Delta S$ term can be weighted in this commonly-used RCM solvent. Use of higher temperatures offers advantages in this regard, but can adversely affect catalyst lifetimes, as noted in Chapter 1, Section 1.2.3.

The above highlights the thermodynamic importance of carrying out RCM reactions at appropriately high dilutions. This exacts a price in terms of reaction rates and productivity, however. The kinetic dependence on concentration of cyclization vs. oligomerization is less straightforward than in classic, stoichiometric cyclizations. In RCM, the initial reaction of substrate with catalyst is necessarily bimolecular, and dilution thus hampers both direct RCM, and oligomerization. Nevertheless, a higher-order kinetic dependence on diene concentration for the intermolecular reaction results as diene concentration is reduced. A recent review of the RCM macrocyclization literature points out that the standard range of substrate concentrations is 0.2-8.5 mM, with catalyst loadings of 2-10 mol%.[8] Operating at very high dilutions (<0.1 mM) is not generally practical. Apart from considerations of reaction time and solvent costs[79] (the latter now acquiring greater recognition as RCM methodologies enter the industrial arena),[35,80,81] competing catalyst decomposition becomes much more problematic. This increases the catalyst loadings required, and the burden of purification (see Chapter 6).

Additives can be used to perturb the free energy of cyclization, to the point where lower temperatures and higher substrate concentrations can be employed in the synthesis of

medium and large rings, without formation of oligomers. Such additives can be classified into templating or capping agents (Scheme 2). Templating agents that have proved effective in RCM range from simple alkali[82,83] or alkaline earth metals[84,85] to transition metal ions[85] or complexes,[86-95] and charged or neutral organic molecules.[96-101] Binding the template to a polar site of the substrate can increase the probability of intramolecular reaction by bringing the olefinic groups into close proximity. An added advantage can be the selective formation of Z-olefin geometries.[82,85] Capping agents also act via binding of a Lewis acid to polar sites of a substrate, thus limiting the conformational mobility of the diene.[102] While useful in specific cases, these methods are usually not generalizable.

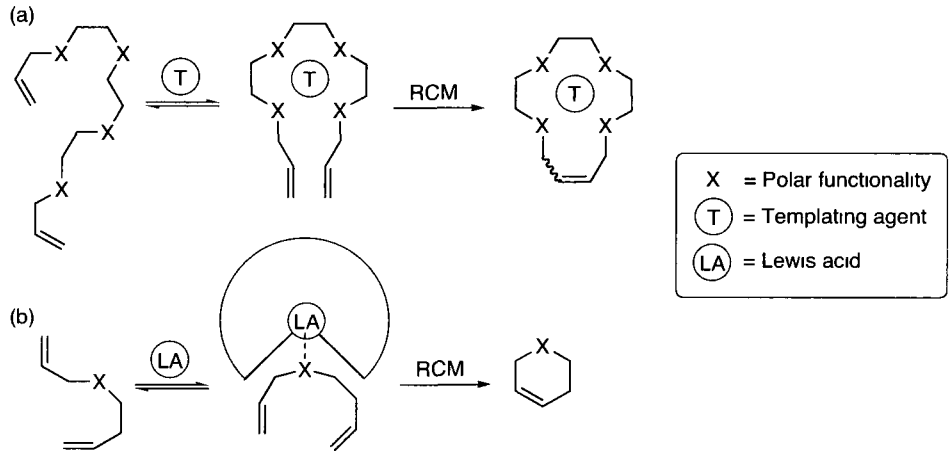

Scheme 2. Favoring RCM by using (a) templating agents and (b) capping agents.

3.2.4 Reversibility in RCM

Olefin metathesis is commonly represented as a fully reversible set of [2+2] cycloaddition-cycloreversion equilibria (Scheme 3a). In practice, complete reversibility is rare. Common restrictions include formation of products that cannot reenter the metathesis cycle by reason of efficient volatilization or low reactivity; inhibition of backbiting by rigidity, ring strain, or catalyst deactivation prior to establishment of equilibrium; low catalyst reactivity toward internal olefins, or non-metathetical reaction pathways. Of greatest importance to the extent of reversibility in the *initial* stages of RCM or oligomerization is the nature of the diene.

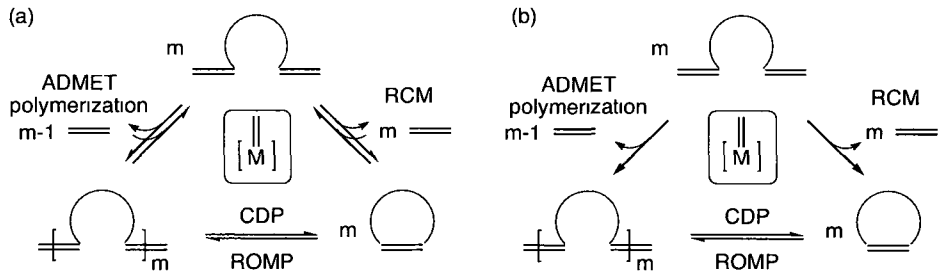

Scheme 3. (a) Conventional representation of olefin metathesis: equilibria relate all olefinic species. (b) Olefin metathesis pathways invoking irreversible loss of ethylene. ADMET = acyclic diene metathesis. CDP = cyclodepolymerization.

In contrast to ROMP, where the olefin remains subtended on the metal via the growing chain, RCM and ADMET proceed via release of the olefin, hence increasing the entropic driving force for these reactions. Where a vinylic α,ω–diene (still the vast majority of substrates) is involved, this driving force is significantly amplified, owing to the release and volatilization of ethylene as the olefinic co-product. Loss of ethylene is highly efficient for RCM under standard conditions: that is, at elevated temperatures, in a vessel open to an atmosphere of nitrogen or argon, in organic solvents in which ethylene is poorly soluble. This is especially true as temperatures increase (representative data for the solubility of ethylene in toluene under 1 atm of C_2H_4: at 40 °C, 8 mM; above 45 °C, <1 mM).[103] The initial metathesis reaction – whether RCM or oligomerization – is thus rapidly rendered irreversible. The entropic gain associated with volatilization of ethylene adds greatly to the driving force for *both* oligomerization and RCM. Once the ethylene has escaped, regeneration of the starting α,ω–diene is impossible, and the metathesis equilibria simplify to the pathways shown in Scheme 3b. The only equilibrium then still operative is that between oligomeric and RCM products (providing that the catalyst is competent to effect both ROMP and backbiting), and its concentration-dependence can be exploited to manipulate product ratios, as discussed below.[43]

It should be noted that loss of ethylene can be retarded by various factors, including use of sealed vessels with minimal headspace (a particular issue in high-throughput catalysis using small, sealed vials in 96-well plates). Where ethylene is retained in solution, metathesis productivity is adversely affected by unproductive metathetical exchange,[104,105] and by conversion of Ru-alkylidene species into shorter-lived and less metathesis-active methylidene species.[104,106,107] This point will be re-examined in Section 3.4.1, and in Chapter

6.

3.3 Monitoring RCM formation of medium and large rings

3.3.1 Background

To quantitatively assess the progress of RCM macrocyclization reactions, a suitable analytical method is necessary. Given the potential operation of the oligomerization-backbiting pathway (at least for second-generation **Ru-4a**), it is essential to monitor not only the rate of consumption of diene, but also the rate of evolution of the RCM product. However, this can be less straightforward than has been generally assumed. GC and ^{1}H NMR analysis are the most commonly encountered methods used to assess the RCM yields. The chief limitation of the former is the inability to report directly on involatile oligomers, which go unobserved and must be quantified by difference. Conventional 1D ^{1}H NMR analysis offers a versatile and potentially convenient alternative, attractive for its potential to quantify the various species present without the time-consuming calibration required by GC and related chromatographic methods. In fact, however, profound discrepancies between NMR-reported conversions and yields, and the self-consistent picture assembled from GC-FID, MS, and TLC data, indicate that NMR-based kinetics data for RCM should be viewed with extreme caution. A key issue is the similarity between the spectra of the oligomers, and the composite spectrum of starting diene and RCM product.[108] Scattered reports in the literature raise related points. Specifically, the Christoffers and Srikrishna groups have commented on the difficulty in discriminating between the ^{1}H and ^{13}C NMR signatures of certain cyclic dimers or trimers, vs. the desired medium-ring products (Chart 2).[109,110] Given the widespread reliance on simple ^{1}H NMR methods for analysis of RCM reactions, this points toward a potentially serious problem, examined in more detail below.

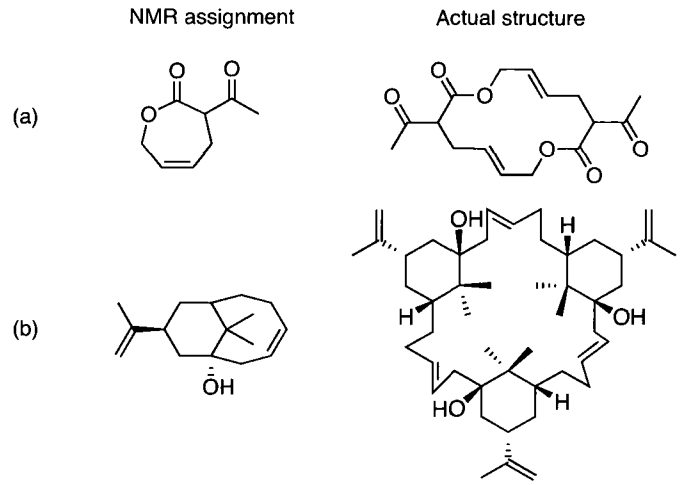

Chart 2. NMR assignment of RCM products, vs. actual structures determined using XRD by (a) Christoffers[109] and (b) Srikrishna.[110]

3.3.2 ^{1}H NMR analysis

The fundamental question at the outset of this study was to what extent ^{1}H NMR analysis can be used to distinguish oligomers from their parent dienes, the RCM products, and mixtures of the two. In turn, this determines whether it is possible to measure the rate of oligomerization, the rate of RCM via backbiting, or both. Presented here are case studies drawn from metathesis of the α,ω-dienes of Chart 3, for which the susceptibility to oligomerization had been separately established (with the exception of **9c**).[43] These are selected to cover a range of target ring sizes and functionalities, including 7-20-membered lactones, polyether, catechol ether, and amine rings. Throughout the discussion that follows, it should be recognized that oligomers are typically formed as mixtures of linear and cyclic species. Such mixtures are designated for convenience as multiples of the parent diene (e.g. **1b**, [**1b**]$_n$). More rarely, cyclic oligomers are formed as the sole products, particularly in the attempted synthesis of strained medium-ring products. These are identified from the absence of endgroups in the ^{1}H NMR spectrum. When unambiguously identified, these cyclic oligomers are designated as multiples of the RCM "cyclomonomer" (e.g. **2b**, [**2b**]$_n$).

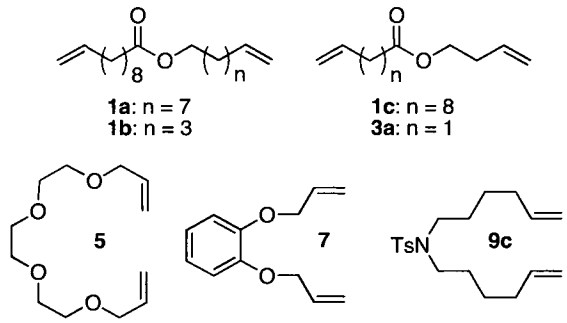

Chart 3. Substrates investigated in this NMR study.

Treatment of **1a/b** with the Ru-NHC catalysts **Ru-4a** or **Ru-6a** generates significant proportions of oligomers en route to the 20- and 16-membered lactone targets.[43] Using catalyst **Ru-4a**, for example, >50% oligomerization is observed for **1a** and **1b** at 15 min in CH_2Cl_2 at room temperature, at a diene concentration of 5 mM. The formation of oligomers was immediately apparent by GC analysis, from the sharp decline in the proportion of volatile constituents relative to the internal standard, and was confirmed by MALDI-TOF mass spectrometry.[43] In sharp contrast is the ambiguity in the corresponding ^{1}H NMR data (Figure 1), which juxtaposes the ^{1}H NMR spectra of the starting diene **1b** and its RCM product **2b**, with the spectrum of the *isolated* oligomer $[\mathbf{1b}]_n$.

Most obvious of the ^{1}H NMR markers for cyclization are the disappearance of the vinylic ABX signals in **1b**, and the emergence of the resonances due to the internal olefinic protons in **2b**. The pseudosymmetrical diene gives rise to two near-identical ABX patterns, for which the midpoint of the X multiplet (=C*H*) appears at ca. 5.80 ppm, and that of the AB multiplets (=CH_2) at 4.98 ppm. The multiplets for the internal E and Z olefinic protons of **2b** appear midway between these signals, with the E-C*H* signals being slightly downfield from the Z-C*H* multiplet. (The OCH_2 triplet at 4.08 ppm undergoes a very minor shift on cyclization, as do the remaining aliphatic protons: the latter are not shown in Figure 1).

The apparently diagnostic value of the chemical shifts for the olefinic protons in **2b**, vs. **1b**, does not survive comparison with the spectrum of oligomeric $[\mathbf{1b}]_n$ (Figure 1b), which closely resembles a composite of Figures 1a and 1c. That is, the spectrum of $[\mathbf{1b}]_n$ could readily be interpreted as revealing a mixture of the starting diene and the RCM product, in which the ratio of internal C*H* to terminal CH_2 signals suggests ca. 70 % conversion to **2b**. The only anomalous feature is the higher proportion of E-olefinic units present, relative to

References page 118

2b, a discrepancy that could be attributed to changes in the E:Z ratios over the timescale of metathesis[111] (a function of catalyst selectivity and/or reversibility).[112] Moreover, the change is less obvious for *mixtures* of $[\mathbf{1b}]_n$ and **2b**: the differences diminish steadily as the proportion of **2b** increases, and could therefore go unnoticed.

Where the presence of oligomeric constituents is recognized, and their signals correctly assigned, overlap with the resonances due to **1b** and **2b** remains problematic, as this impedes measurement of both the rate of oligomerization of **1b**, and the rate of cyclodepolymerization of $[\mathbf{1b}]_n$. Routine ^{1}H NMR analysis is therefore of little assistance in evaluating yields at intermediate stages of reaction, and thus monitoring the progress of RCM. The same limitation is found for substrates **1a/c**, precursors to 20- and 14-membered lactones.

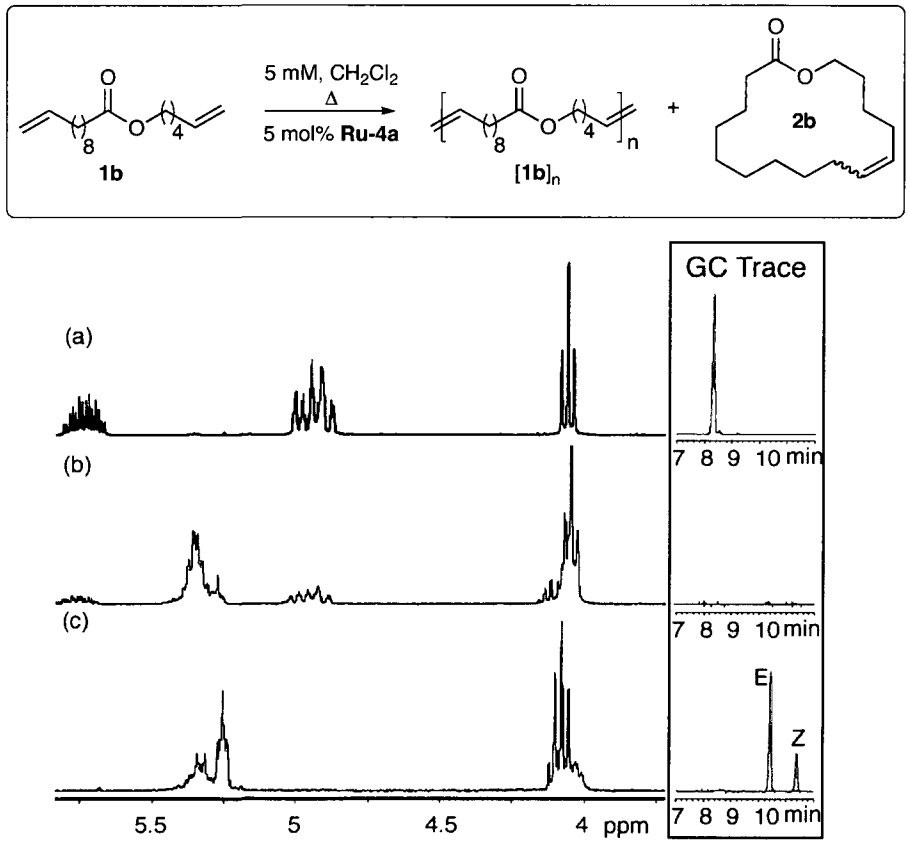

Figure 1. ^{1}H NMR spectra ($CDCl_3$, 300 MHz) of organic species present during RCM of **1b** (5 mM in CH_2Cl_2, Δ, 5 mol% **Ru-4a**). (a) Diene **1b**. (b) Isolated $[\mathbf{1b}]_n$. (c) RCM product **2b**. Inset at right shows the corresponding GC traces.

A different picture emerges from RCM of the smaller prolactone **3a**, again at a diene concentration of 5 mM. Here we find that ^{1}H NMR analysis can report accurately on the progress of reaction, because the oligomeric constituents are cyclic species with a unique

NMR signature. Figure 2 shows the spectra for starting **3a**, an aliquot from the reaction (removed after 30 min reaction), the isolated, 14-membered cyclodimer $[\mathbf{4a}]_2$, and the RCM product, β-unsaturated caprolactone **4a**. GC-MS analysis of the reaction aliquot at temperatures up to 320 °C revealed only **4a** and $[\mathbf{4a}]_2$, but small amounts of the cyclic tetramer $[\mathbf{4a}]_4$ were also detected by ESI-MS. No linear oligomers were observed, as also noted in an earlier report describing the formation of cyclomonomer, cyclodimer and cyclotrimer by Wittig routes.[25] Isolation of the cyclic dimer was undertaken in order to verify the NMR assignments for the crude reaction mixture. The isolated sample of $[\mathbf{4a}]_2$ is identified as the head-to-tail isomer on the basis of the pattern in the olefinic region. Of note, the methylene resonances for the cyclodimer appear consistently further upfield than the corresponding signals for **4a**, presumably reflecting the increased flexibility and thus lower torsional ring strain. A similar effect is key to monitoring the progress of ROMP of norbornene monomers, in which the olefinic resonances located at ca. 6.0 ppm in the strained bicyclic monomer shift upfield by ca. 0.4 ppm on ring-opening (see Chapters 4 and 5).

An additional feature in the spectrum of the crude reaction mixture (Figure 2b) illustrates the complexity that can emerge during in situ ^{1}H NMR analysis. As well as the signals for cyclooligomer $[\mathbf{4a}]_n$, RCM product **4a**, and a small amount of diene **3a**, multiple broad peaks are observed between 1-2 ppm. These are assigned to competing isomerization of **3a**. Isomerization appears to be particularly characteristic of the Ru-NHC catalysts,[113-115] and has been shown by Wagener and co-workers to occur concurrently with metathesis.[116,117] Disappearance of these signals on longer reaction times implies that ring-closing shifts the isomerization equilibrium in favor of the α,ω-diene **3a**. This has important implications for monitoring reaction. Because **3a** undergoes competing (if reversible) conversion to poorly-resolved isomeric species in addition to oligomeric intermediates, the rate of its disappearance is not straightforwardly related to metathesis. Rates of RCM can, however, be determined from the rate of appearance of product **4a**. Thus, for the lactone substrates studied, ^{1}H NMR analysis becomes practical as the target ring size shifts into the medium-ring regime. This is due to two factors: (a) preferential formation of cyclic oligomers, and (b) the presence of discrete signals for the "cyclomonomer" and cyclic oligomers.

References page 118

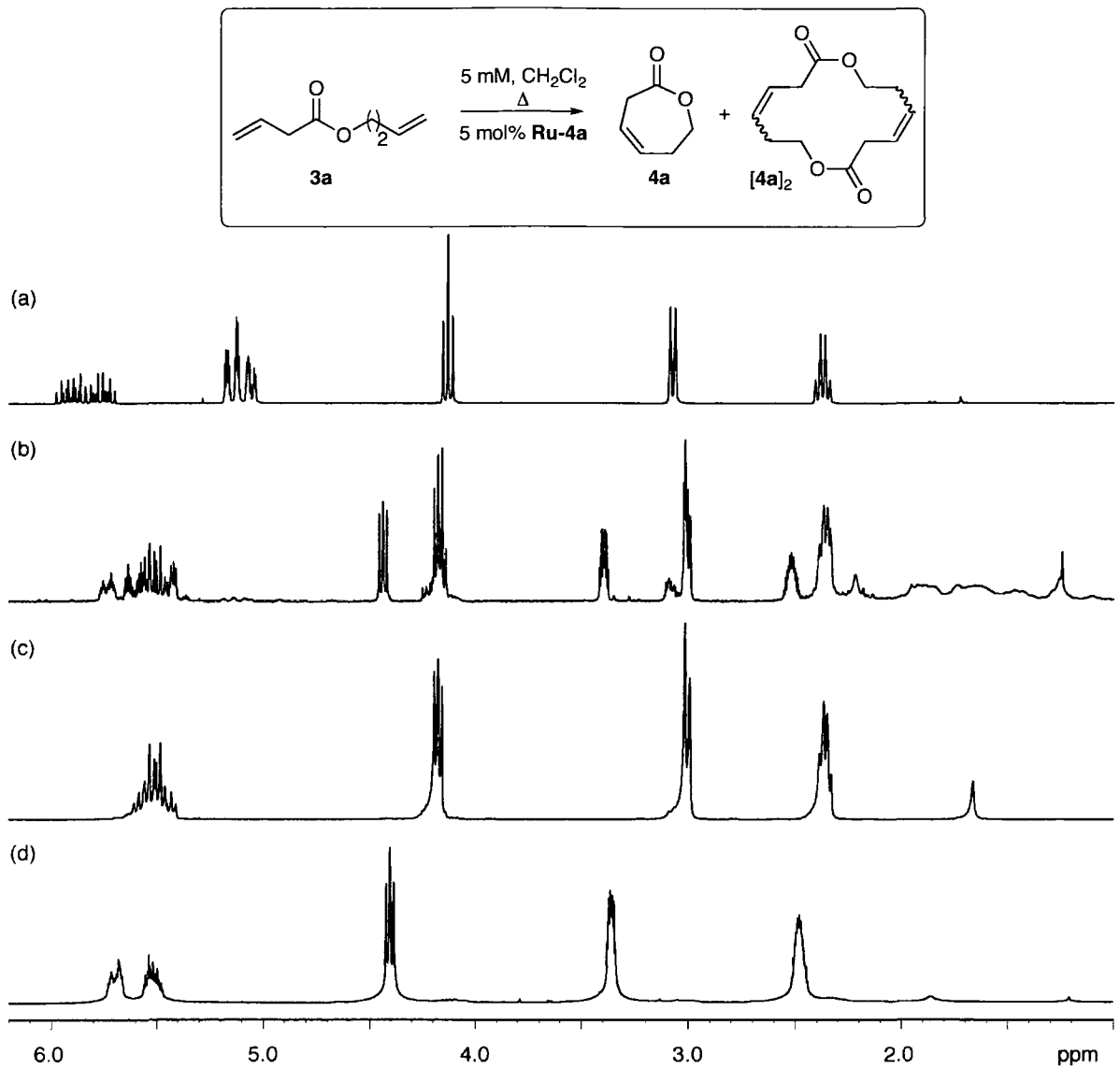

Figure 2. ^{1}H NMR spectra ($CDCl_3$, 300 MHz) showing stages in the RCM of **3a** (5 mM in CH_2Cl_2, Δ, 5 mol% **Ru-4a**). (a) Diene **3a**. (b) Aliquot from reaction mixture at 30 min, containing a mixture of oligomers and 38% **4a** (the latter identified by GC analysis). (c) Isolated cyclodimer **[4a]**$_2$. (d) Isolated **4a** (spectrum acquired by Joao Duarte Silva).

To assess the utility of ^{1}H NMR analysis in monitoring formation of other substrates, three additional dienes were examined: allylic polyether **5**, which undergoes RCM to yield a 14-membered crown ether analogue **6**, allylic catechol ether **7**, precursor to 8-membered **8**, and tosylate-protected amine **9c**, in principle a precursor to eleven-membered ring **10c**. These were deliberately chosen because the functionalities present would confer varying degrees of flexibility within the medium- and large-ring regime. Additionally, their C_2 symmetry eliminates unnecessary complications arising from head-head and head-tail mixtures of

oligomers.

Figure 3 shows the spectra of diene **5**, an aliquot from the reaction mixture at 15 min (consisting of $[\mathbf{5}]_n$ and – as indicated by GC-FID analysis – 3% **6**, with no remaining diene), and the isolated RCM product **6**. The vinylic signals for **5** and oligomeric $[\mathbf{5}]_n$ appear at closely corresponding chemical shifts, and cannot be independently integrated. Pseudo-crown ether **6** appears to be present as solely the Z-olefin,[82] despite the absence of an added templating agent. As before, the signals due to the internal olefinic protons for $[\mathbf{5}]_n$ and **6** appear between the vinylic =C*H* and =CH_2 multiplets, but they are less well-isolated than in the lactone examples. For **6**, they abut the range for the =C*H* methine multiplet, while for $[\mathbf{5}]_n$ they overlap with these signals. Similar limitations in chemical shift dispersion are observed for the catechol ether $[\mathbf{7}]_2$ (vide infra).

More readily distinguished is the doublet for the OCH_2CH= protons in **6**. This well-resolved signal appears at 4.3 ppm, ca. 0.3 ppm downfield from the corresponding signals for **5** or $[\mathbf{5}]_n$. The rate of formation of **6** can therefore be measured, although the rate of consumption of substrate **5** cannot, as no signals clearly distinguish the diene from its oligomer. The distinction between $[\mathbf{5}]_n$ and **6** is unexpected on the basis of the macrolactone precedents. It reflects the presence in **6** of a well-isolated reporter group consisting of a methylene group flanked by olefin and ether functionalities. The combined influence of these groups serves to shift the methylene doublet into a region devoid of other aliphatic signals.

References page 118

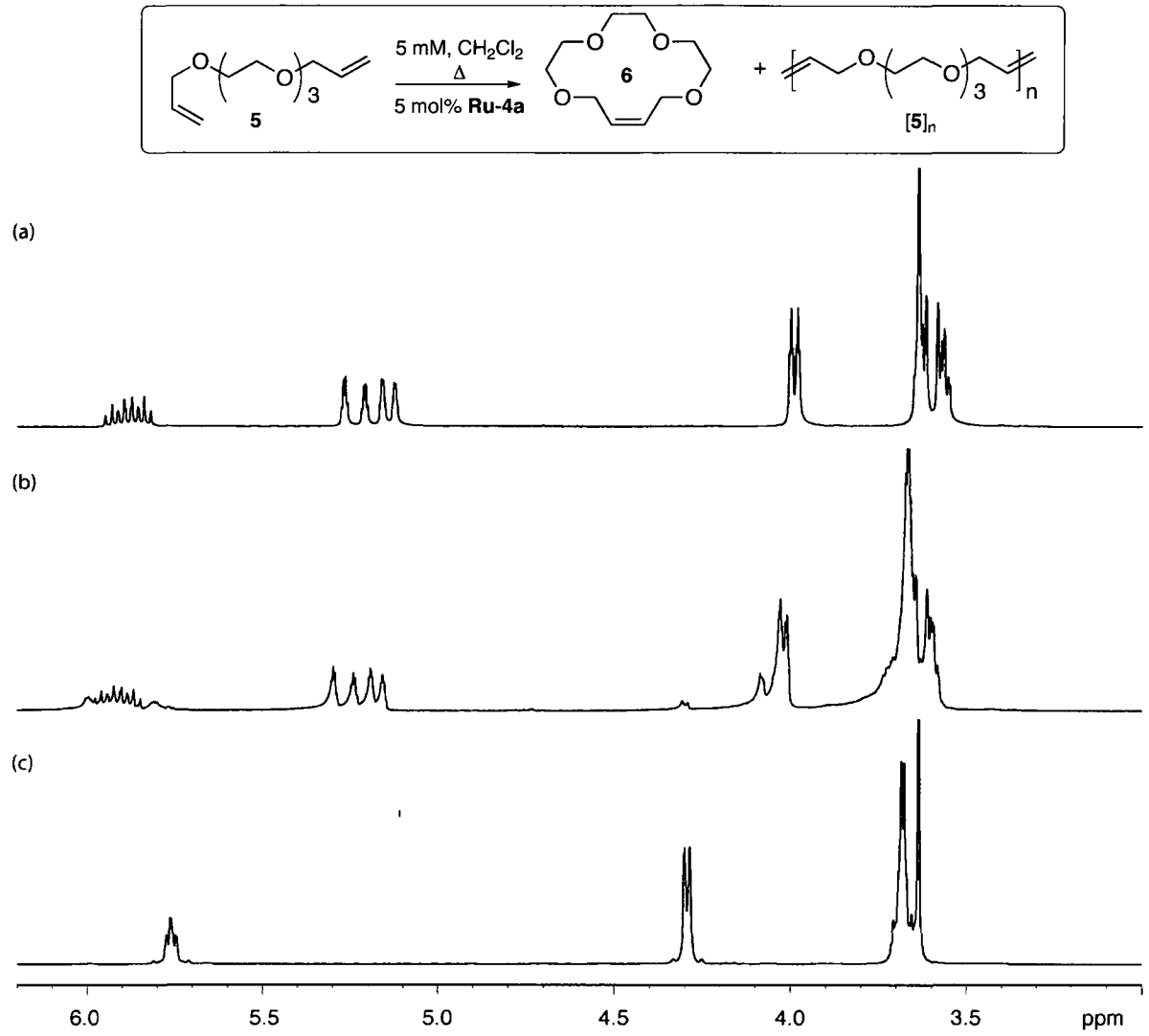

Figure 3. ^{1}H NMR spectra ($CDCl_3$, 300 MHz) showing stages in the RCM of diallyl polyether **5** (5 mM in CH_2Cl_2, Δ, 5 mol% **Ru-4a**). (a) Diene **5**. (b) Aliquot from reaction mixture at 15 min, containing $[\mathbf{5}]_n$, no remaining **5**, and 3% **6** (GC analysis). (c) Isolated RCM product **6**; Z isomer.

Diallyl catechol **7** exhibits a much stronger conformational bias toward cyclization than the dienes discussed above. RCM reactions carried out at the standard 5 mM concentration of diene show no tendency toward oligomerization, instead favoring direct RCM. That is, only signals for starting diene and/or the RCM product **8** are observed at all stages of reaction. Signals for oligomers emerge at higher concentrations, however. At 100 mM, an equilibrium is established between $[\mathbf{7}]_n$, $[\mathbf{8}]_n$, and **8**. Major constituents in the oligomeric fraction include linear and cyclic dimers and trimers, and linear tetramer and pentamer, most of which where

isolated by preparative TLC (carried out by Angela Crane of this research group) for independent ^{1}H NMR and ESI-MS analysis. Spectra for the starting diene **7**, an aliquot from the reaction mixture, and isolated **8** are shown in Figure 4a-c, with spectra for the isolated linear dimer $[\mathbf{7}]_2$ and cyclic trimer $[\mathbf{8}]_3$ in Figure 4d/e. Of note in Figure 4b is the marked degradation in resolution characteristic of aliquots from the reaction mixture, a reflection of the small but distinct differences in chemical shifts for the various species present.

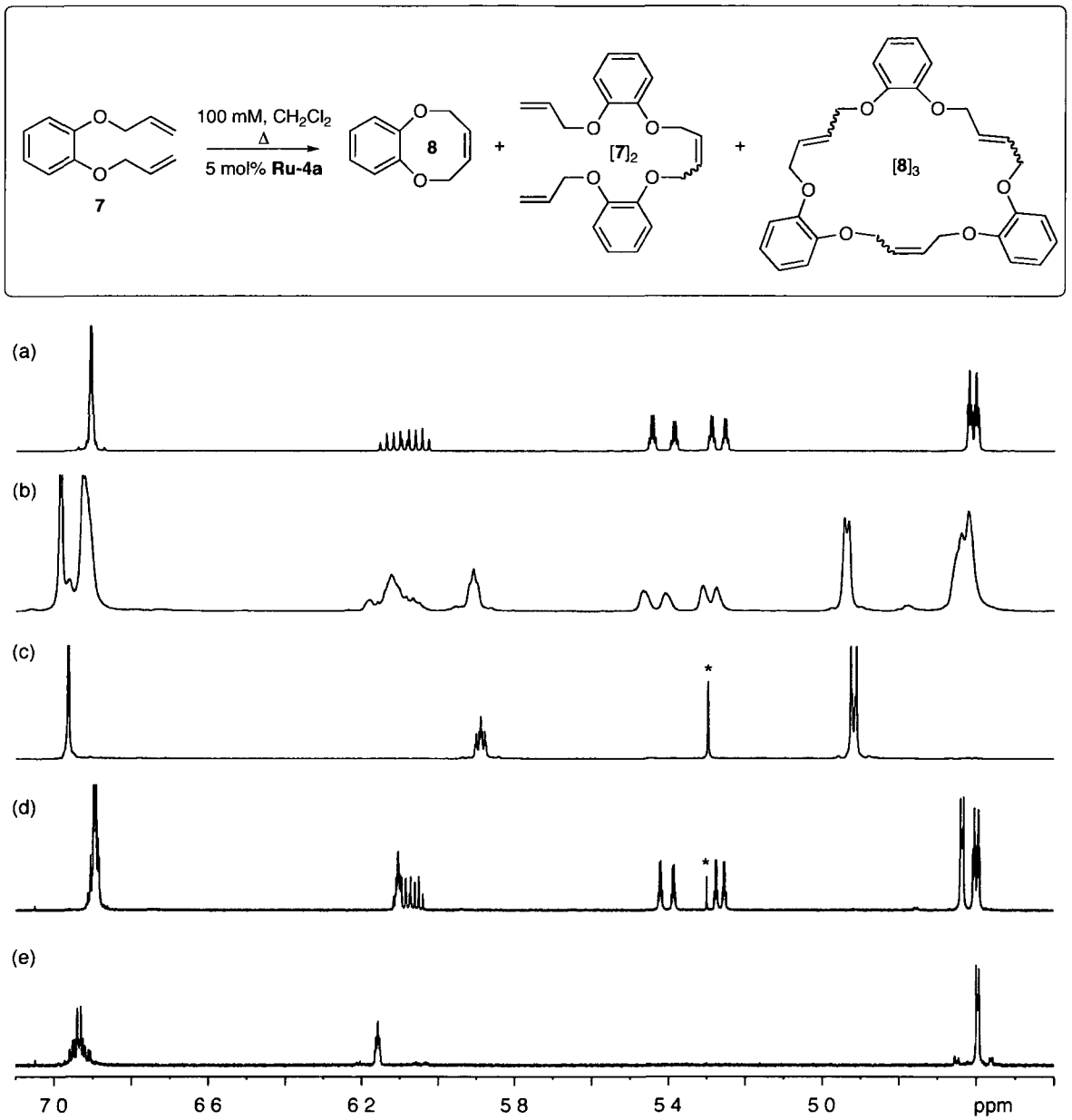

Figure 4. ^{1}H NMR spectra ($CDCl_3$, 300 MHz) showing stages in the RCM of catechol ether **7** (100 mM in CH_2Cl_2, Δ, 5 mol% **Ru-4a**). (a) Diene **7**. (b) Aliquot from reaction at 1 h, containing $[\mathbf{7}]_n$, $[\mathbf{8}]_n$, and 38% **8**; no **7** remains (GC analysis). (c) Isolated RCM product **8**; Z isomer. (d) Linear dimer $[\mathbf{7}]_2$. (e) Cyclic trimer $[\mathbf{8}]_3$. Asterisk indicates residual CH_2Cl_2.

The oligomers present in the crude reaction mixture cannot be distinguished from diene **7** by ^{1}H NMR analysis. Overlap between the signals for the vinylic proton (centered at ca. 6.1 ppm) and the internal olefinic protons means that the spectra of **7** and $[\mathbf{7}]_2$ offer no unique handles to facilitate independent quantification. The triplet due to the internal olefin in cyclic trimer $[\mathbf{8}]_3$, while better isolated, also shows a slight overlap with the vinylic proton envelope for **7**, and its OCH_2 multiplet (ca. 4.9 ppm) likewise overlaps with the corresponding signals for **7** and $[\mathbf{7}]_2$. In contrast, the signal due to the internal, Z-olefinic proton in **8** is isolated from the olefinic resonances for **7**, $[\mathbf{7}]_2$, and cyclotrimer $[\mathbf{8}]_3$. Thus, while the rate of oligomerization cannot be monitored, the overall progress of reaction can be gauged from the rate of appearance of product.

C_2-symmetric amine **9c** again exhibits a strong bias toward oligomerization at a 5 mM concentration of diene. In our hands, the oligomers could not be induced to undergo backbiting to yield azacycloundec-6-ene **10c**. (While this is consistent with the low effective molarity of such eleven-membered cycloalkanes,[15] Nakagawa and co-workers were reportedly successful in synthesizing **10c** via RCM using the first-generation Grubbs catalyst).[118] We were unable to establish rates of consumption of **9c** by ^{1}H NMR analysis, owing to overlap between the signals for **9c** and its oligomers (Figure 5). Both linear and cyclic oligomers are formed, as judged by ESI-MS analysis, which reveals cyclic and linear dimers, cyclic trimer, and cyclic tetramer, but not **10c**. The presence of linear $[\mathbf{9c}]_n$ is confirmed by the observation of vinylic endgroups in ^{1}H NMR spectra of aliquots from the reaction mixture. However, the proportion of the various cyclic oligomers present cannot be evaluated, owing to the near-perfect overlap of their signals. The spectrum for the isolated cyclic dimer $[\mathbf{10c}]_2$ (Figure 5c) agrees precisely with that reported for **10c**,[118,119] implying that ^{1}H NMR analysis is of no assistance in evaluating the progress of either the oligomerization or the backbiting reaction. This near identical ^{1}H NMR chemical shift of the olefinic signals of $[\mathbf{10c}]_2$ and those reported[118] for **10c** was unexpected given the precedent of caprolactone **4a** (Figure 2), where the strain of the RCM target was instrumental in providing the required chemical shift dispersion to resolve ^{1}H NMR signals between **4a** and $[\mathbf{4a}]_2$.

The findings noted above regarding the utility of ^{1}H NMR analysis for monitoring formation of these lactone, polyether, catechol ether, and amine rings are collected in Table 1. In no case, with the exception of **3a**, can the signals for diene and oligomers be

distinguished. The unique behavior of **3a** lies in the fact that it forms solely cyclic oligomers, which, unlike their linear counterparts, contain no vinylic endgroups, and are readily distinguished from the diene on this basis. As a corollary, wherever linear oligomers can be formed (as is generally the case), overlap between their vinylic signals and those of the parent diene means that the rate of disappearance of diene cannot be assessed by ^{1}H NMR observation.

The rate of appearance of the RCM product, in contrast, can sometimes be measured. The essential requirement is that at least one signal for the RCM target be distinct from those of linear and cyclic oligomers as well as starting diene. For the macrolactones, this requirement is not met. For several of the remaining cases examined, an illuminating distinction emerged. Overlap between signals for cyclic oligomers and "cyclic monomers" (i.e. RCM targets) is less problematic than was the case for linear oligomers and diene. For smaller rings, in which a degree of ring strain is present (as is the case for **4a** and **8**), the majority of the aliphatic ring signals may be shifted significantly downfield from the corresponding signals in the cyclic oligomers. Shifts in the olefinic signals are often less reliably distinct, though the tendency toward Z-olefinic configurations in smaller rings can aid by compressing the peak envelope. In special cases, as for pseudo-crown ether **6**, a unique NMR handle may be present that facilitates analysis, although this is difficult to predict a priori.[120]

Overlap between the signals for the RCM targets and *linear* oligomers follows the same pattern: any ring strain present in the RCM product reduces the probability of overlap between corresponding signals. The progress of backbiting for substrates can therefore be gauged from the rate of appearance of the ^{1}H NMR signals for the RCM targets.

References page 118

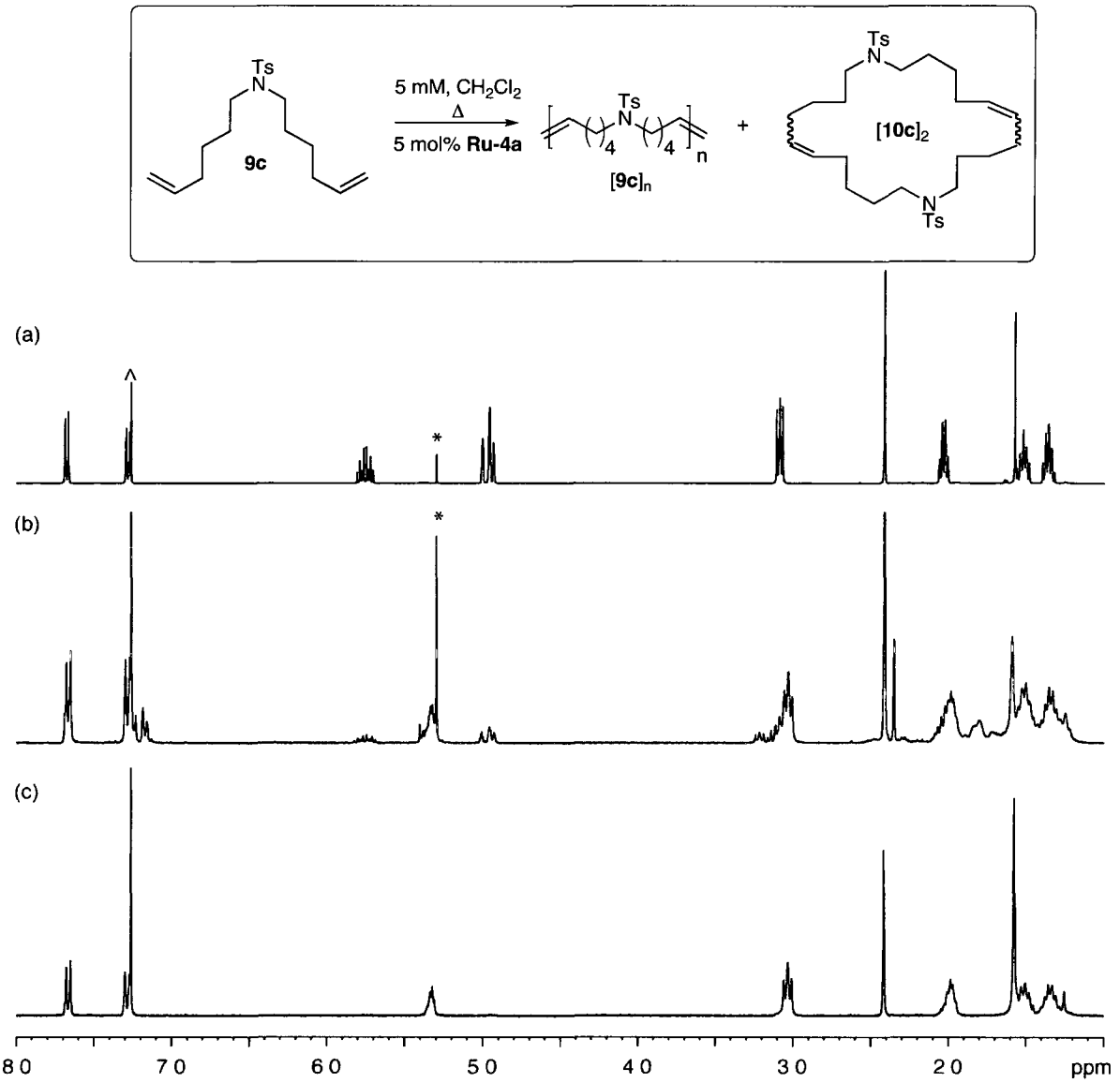

Figure 5. ^{1}H NMR (300 MHz; $CDCl_3$) spectra for the RCM of **9c** (5 mM in CH_2Cl_2, Δ, 5 mol% **Ru-4a**). (a) Diene **9c**. (b) Aliquot from reaction mixture, containing solely oligomers $[\mathbf{9c}]_n$. (c) Isolated cyclic dimer $[\mathbf{10c}]_2$. Solvent peaks indicated by ^ ($CHCl_3$); * (CH_2Cl_2). Spectra acquired by Angela Crane.

Table 1. Utility of ^{1}H NMR analysis for monitoring the RCM of the substrates of Chart 3.

RCM target	Ring size	Distinguishable signals		Observable rates
		diene, oligomers	oligomers, RCM target	
2	14-20	–	–	none
4a	7	x[a]	x	d[product]/dt
6	14	–	x	d[product]/dt
8	8	–	x	d[product]/dt
10c	11	–	N/A[b]	none

[a] The rate of consumption of diene is obscured by concurrent isomerization. [b] RCM target is not obtained.

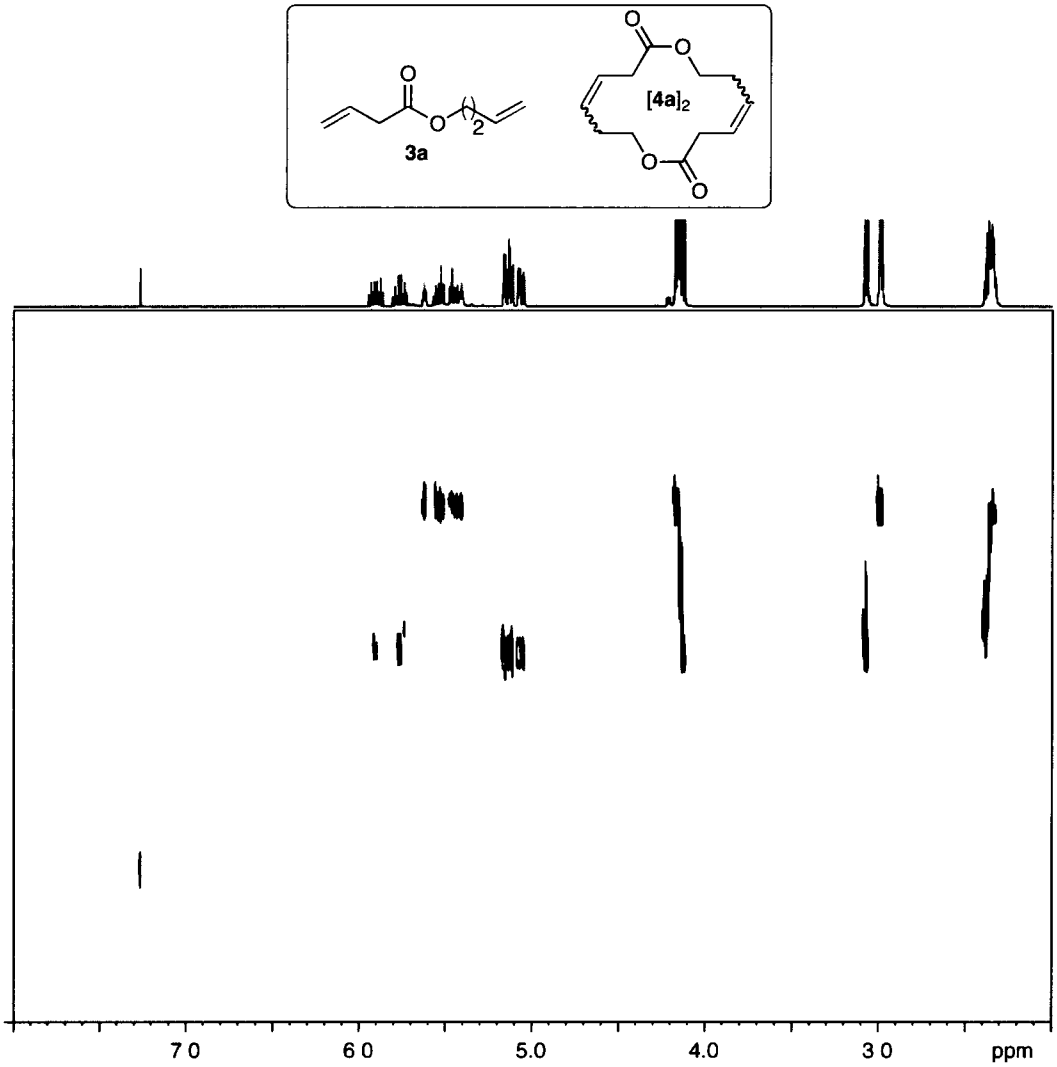

Figure 6. ^{1}H DOSY-NMR spectrum of a 1:1 mixture of **3a** and $[\mathbf{4a}]_2$ (500 MHz, $CDCl_3$). Well-isolated signals for **3a** are shown in blue; for $[\mathbf{4a}]_2$ are shown in red.

It will be clear from the foregoing that routine, 1D ^{1}H NMR analysis is not always reliable in reporting on the presence of oligomers formed during diene metathesis reactions. Mass spectrometric methods are invaluable as a tool for complementary, if often qualitative, assignment. Of interest as a means of deconvoluting the NMR assignments, and hence improving quantitation, is diffusion-ordered spectroscopy (DOSY), which enables "size-sorting" of signals on the basis of the different diffusion constants of molecules present in a mixture.[121-123] Signals for diene and/or RCM target can thus be distinguished from those due to oligomers. Shown in Figure 6, by way of illustration, is the DOSY spectrum for a 1:1 mixture of **3a** and [**4a**]$_2$ in $CDCl_3$. Fastest-diffusing of the constituents observed is $CHCl_3$ (for which the midpoint of the cross-peak is set to zero). Likewise, the cross-peaks for the vinylic signals of diene **3a** (in blue) indicate faster diffusion than that for the olefinic signals for [**4a**]$_2$ (in red). Of note, however, near-overlapping resonances such as the OCH_2 signals at ca. 4.2 ppm result in "smearing" of the cross-peak, the midpoint of which corresponds to the average for the two molecules. While qualitative, this elongation is nevertheless telling, and indicates overlap between two species of different size. For direct insight into molecular size, at least one peak within each constituent must be resolved. High field strengths are key to the necessary chemical shift dispersion.

3.3.3 Key findings

^{1}H NMR spectroscopy is widely used to evaluate the rate and in situ yields of RCM reactions. NMR analysis is valuable for monitoring RCM of substrates that possess a strong conformational bias toward cyclization, because the reaction is not complicated by formation of oligomers. Greater caution is required for dienes that function as precursors to medium-sized or macrocyclic rings, for which the oligomerization-backbiting pathway must be considered. The results described above illustrate the hazards involved in relying on unsupported NMR analysis to assess the extent and rate of RCM of such substrates. The fundamental problem is simply that deconvolution and quantification of the ^{1}H NMR signals for diene, oligomers and RCM product is frequently difficult. Overlap between signals for linear oligomers and diene is particularly troublesome. Differentiation between cyclic oligomers and diene is more straightforward, given the absence of vinylic signals in the former. Cyclic oligomers can sometimes be distinguished from their ''cyclomonomer" RCM targets, particularly where ring strain is present. Deconvolution and quantification of signals

for cyclic oligomers can be much more challenging. The NMR spectra of such species can be indistinguishable from those for the RCM targets, and other methods are then essential for quantitative analysis (e.g. HPLC).

3.4 The influence of the Ru metathesis catalyst on the ring-chain equilibrium

3.4.1 Methodology

This Section focuses on RCM of prolactones **1** and **3** (Chart 4a). These substrates were chosen for four reasons. (1) To facilitate comparison of RCM yields for different ring sizes, a consistent framework was required. As noted in Section 3.2.3, variation of functional groups and the position of sp^2 centers within a substrate affects EM values, and hence probability of cyclization.[15,16,124] (2) Prolactones **1** and **3** are readily obtained in high yield (>85%) via carbodiimide coupling between the appropriate carboxylic acid and alcohol. (3) The wealth of data reported by Illuminati and Mandolini for the cyclization of the saturated lactone analogs to **2** and **4** provides a valuable point of comparison with the unsaturated targets sought here.[15,16] (4) Our earlier work established that **1/3** undergo a ring-chain equilibrium with **Ru-4a**.[43] To maximize relevance for the organic chemist, the most commonly encountered Grubbs catalysts were used in this study. Also included was catalyst **Ru-5c**, which is not currently commercially available (June 2010), but is employed in Boehringer-Ingelheim's second-generation route to BILN 2061.[35] Additionally, two aryloxide catalysts (**Ru-7a/b**) were investigated, to further explore differences in RCM yields between the chloride and pseudohalide families.

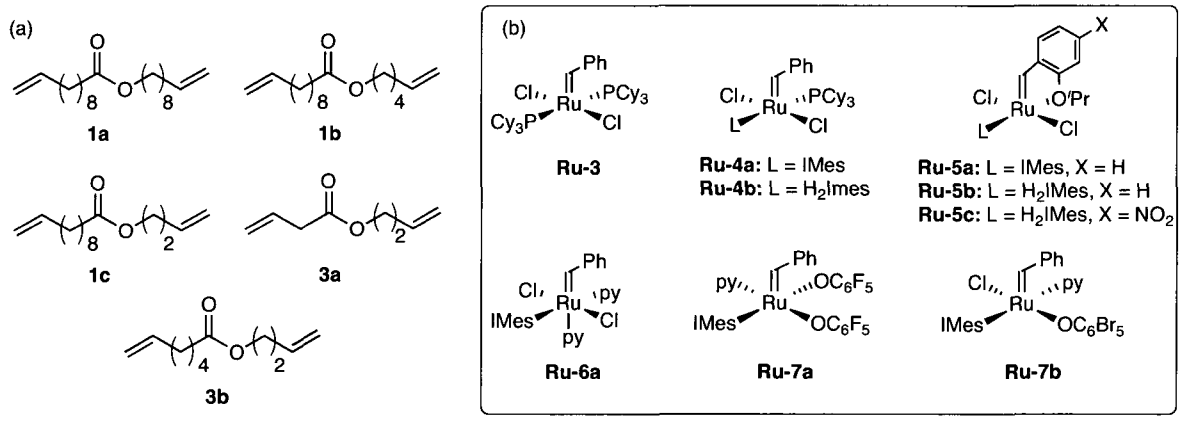

Chart 4. (a) Substrates and (b) catalysts employed in this Section.

Given the need to examine various substrate-catalyst combinations, this study began by exploring the capacity of high-throughput (HT) methodologies to streamline the process. Thus, rate profiles were compiled using automated equipment, in a procedure designed by Johanna Blacquiere of this group.[125] To test the method, conversions of substrate **1a** to the 20-membered macrocycle **2a** by representative catalysts **Ru-3**, **Ru-4a/b** and **Ru-5b** were monitored over time in duplicate, using an aluminum plate containing 96 1-mL vials immersed in a temperature-controlled bay. Each vial was charged with a desired amount of substrate, solvent (CH_2Cl_2) and then catalyst at a temperature of 20 °C using a CAVRO liquid-dispensing robot. The vials were sealed using two Teflon sheets, heated to 40 °C, stopped at a specified time by addition of a quenching agent, and analyzed (GC-FID). Of the various reagents used to terminate metathesis via the Grubbs catalysts,[107,126-132] potassium hydrotris(pyrazolyl) borate (Ktp) was most suitable in effecting near-immediate annihilation of activity, and was used throughout this study.

As can be seen from Figure 7a, consumption of starting **1a** is incomplete (ca. 15-18% remaining **1a**) for all catalysts studied, suggesting decomposition. Yields of **2a** reach a maximum at 30 min (54-58%), with no further increase over five hours. The difference indicates the presence of ca. 35% oligomers. In contrast, when RCM of **1a** is carried out at reflux in a system open to argon, but otherwise identical, complete consumption of **1a** is observed within 15 min. Incomplete consumption of **1a** using the HT method almost undoubtedly reflects entrapment of ethylene, and hence enhanced non-productive metathesis as well as ethylene-mediated deactivation of the catalyst.[104,106,107,133] (The detrimental effect of ethylene on catalyst lifetime will be revisited in Chapter 6). Moreover, regeneration of starting **1a** by cross-metathesis of **2a** with ethylene is also possible, as demonstrated by Furstner[134] and Weiler[135] for closely-related macrocycles. These results issue a clear warning that HT methods cannot be used to determine reliable rate profiles for RCM macrocyclization. Similar limitations can be inferred for a method proposed by the Grubbs group, in which RCM activity is assessed by measuring conversion profiles in sealed NMR tubes.[136] The acknowledged problem of ethylene build-up inside the tube[137] can have

profound consequences on the catalytic results.[136,137] Thus, this method may be limited to high-EM substrates for which cyclization is essentially irreversible.

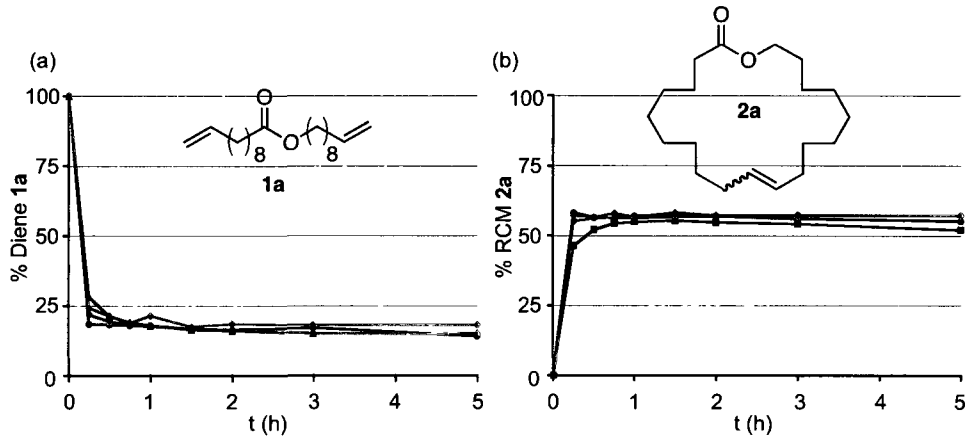

Figure 7. Automated measurement of (a) consumption of **1a** and (b) formation of **2a** as function of time. Conditions: 5 mM **1a** in CH_2Cl_2, Δ, 5 mol% [Ru]. Calibrated GC-FID analysis (±1% in replicate runs). **Ru-3** (◇), **Ru-4a** (■), **Ru-4b** (●) and **Ru-5b** (◉).

3.4.2 Generality of the kinetic bias toward oligomerization pathway

The tendency of **Ru-3-6** toward cyclization over oligomerization was next investigated. Within the 7- to 20-membered ring series, **1a** and **1b**, the precursor to 20- and 16-membered lactones, exhibit the lowest bias toward oligomerization (the saturated lactones are characterized by the highest and nearly identical EM values of the **2/4** series).[15,138] These substrates offer an excellent assay of the kinetic bias toward inter- vs. intramolecular metathesis.

Reactions were carried out in Schlenk glassware immersed in a water bath maintained at 20 °C. The headspace was swept with a stream of argon to promote volatilization of the ethylene co-product. A 10 min period was allowed for the reaction to equilibrate to the bath temperature, following which the catalyst (as a solution in CH_2Cl_2) was added by syringe. Reaction times varied from 30 sec to a maximum of 1 h. After this time, a consistent increase in the amount of oligomers was observed, presumably owing to evaporation of the solvent under the steam of argon. Nevertheless, a reaction time of one hour was sufficient to extract the required information.

Plots of the relative amount of oligomerization (% oligomers / % conversion) of substrates **1a/b** by catalysts **Ru-3-6** are shown in Figure 8. Percent conversion was chosen as the

independent variable to compensate for the varying activity of these catalysts at 20 °C. Importantly, at the earliest time point taken (30 sec), conversions were always ≥5%, enabling RCM products to be reliably detected and quantified, where present. For all catalysts, the initial rate of metathesis is very fast, but slows significantly after one minute, as expected given the superior reactivity of the benzylidene precatalyst relative to the methylidene propagating species.[107] Unexpectedly, however, it is within that initial period (<1 min) that almost all oligomerization occurs. This may indicate that the benzylidene precatalysts have a greater bias toward oligomerization compared to the methylidenes, and may represent a paradigm of a highly-reactive catalyst suffering from lower selectivity.

Consistent with our previous report with **Ru-4a**,[43] second-generation catalysts **Ru-4-6** afford a majority of oligomers in the early stages of the reaction with **1a** and **1b**. At 30 sec (ca. 5% conversion), the product distribution consists of a minimum of 80% oligomer for **1a**, and 67% oligomer for **1b**. The proportion of oligomers decreases as conversions of **1a/b** increase. At ca. 30% conv. (1 h), the proportion of oligomers is 50% for **1a**, and 20-40% oligomers for **1b**. Nevertheless, all of these catalysts follow the same trend: near-total initial formation of oligomers, with a decrease in their proportion as conversions increase. The second-generation catalysts **Ru-4-6** can thus be classified as thermodynamically-controlled (T-class). Interestingly, this kinetic tendency toward oligomerization is substantially reduced for the first-generation catalyst **Ru-3**, for which the initial proportion of oligomers is 50 and 28% for **1a** and **1b** respectively (cf. 80 and 67% for **1a** and **1b** using **Ru-4-6**). These values decrease to 30% and <2% at full conversion for **1a** and **1b** respectively. First-generation **Ru-3** is thus classified as kinetically controlled (K-class).

References page 118

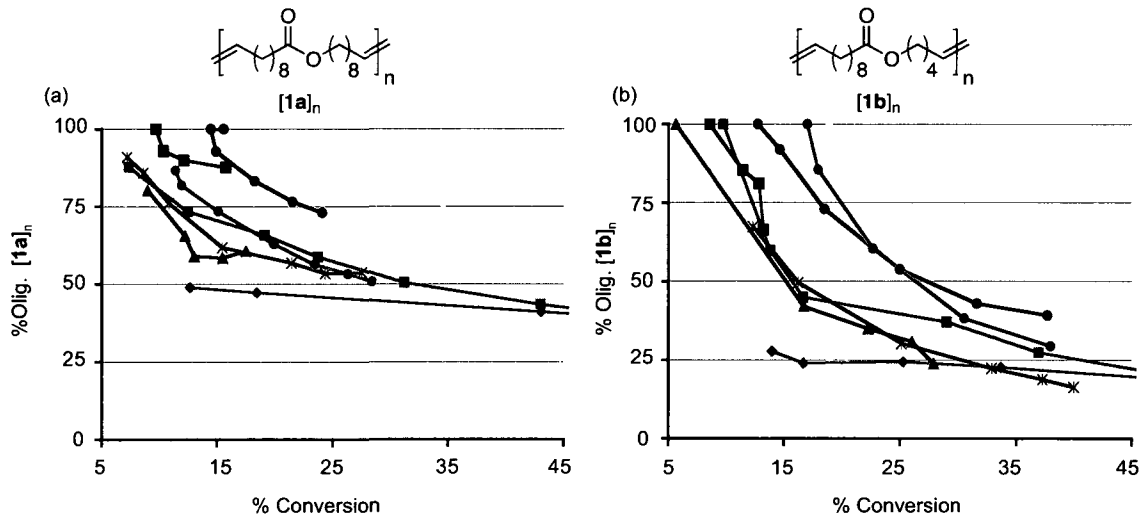

Figure 8. Proportion of oligomers (% oligomers / % conversion) as a function of conversion for (a) **1a** and (b) **1b**. Conditions: 5 mM **1a/b** in CH_2Cl_2, 20 °C, 5 mol% [Ru]. Calibrated GC-FID analysis (±1% in replicate runs). **Ru-3** (◆), **Ru-4a** (■), **Ru-4b** (●), **Ru-5a** (▲), **Ru-5b** (●), **Ru-5c** (■), **Ru-6a** (✶).

In context of macrocyclization, two important implications arise from this classification. First, yields of RCM products obtained using a K-class catalyst should be higher than those observed with a T-class catalyst. Indeed, EM_k are generally higher than the thermodynamic EM_t, especially where ring strain is present in the target.[15] Secondly, when oligomers do form, these are less likely to be converted into the desired cyclic product if a K-class catalyst is employed. Therefore, protocols designed to minimize formation of oligomers should be enforced when working with such a catalyst. To test the validity of these hypotheses, RCM of prolactones **1/3** via **Ru-3-6** was carried at a constant concentration, and the RCM yields compared.

3.4.3 Catalyst influence on cyclization of large rings

Cyclizations of prolactones **1a-c** were carried out as described above, but at reflux to accelerate reaction. A representative plot showing yields of 20-membered **2a** over time is presented in Figure 9. In accordance with the above hypothesis, maximum RCM yield of **2a** (94%) is achieved with first-generation **Ru-3**. A small proportion of oligomers (22%) is formed by **Ru-3** after 15 min, decreasing to 5% after 3 h. The slow depletion of oligomers is in accord with the low reactivity of **Ru-3** toward hindered olefins[139] and consistent with a report by Hodge and co-workers showing slow cyclodepolymerization (CDP) of unsaturated

polyesters using **Ru-3**.[140] Closely related to CDP, chain-transfer of ROMP polymers was also shown to be slower with **Ru-3** relative to **Ru-4b**.[141]

In contrast, over 80% oligomers are formed at 15 min using the T-class catalysts **Ru-4-6**. As expected from the similarity in the active species $RuCl_2(NHC)(=CH_2)$, backbiting proceeds at similar rates for the NHC catalysts, and equilibrium yields of **2a** are very close (51-57%). The remaining material consists of involatile oligomers. While molybdenum catalyst **Mo-2** effects slower consumption of **1a** relative to the ruthenium catalysts (3 h for **Mo-2** vs. 15 min for **Ru-3-6**), the yield of **2a** reached 81% at 3 h. No sign of backbiting RCM was evident for **Mo-2**. Given the high sensitivity of **Mo-2** toward water and oxygen as well as its thermal instability, the study of this catalyst is limited to diene **1a**.

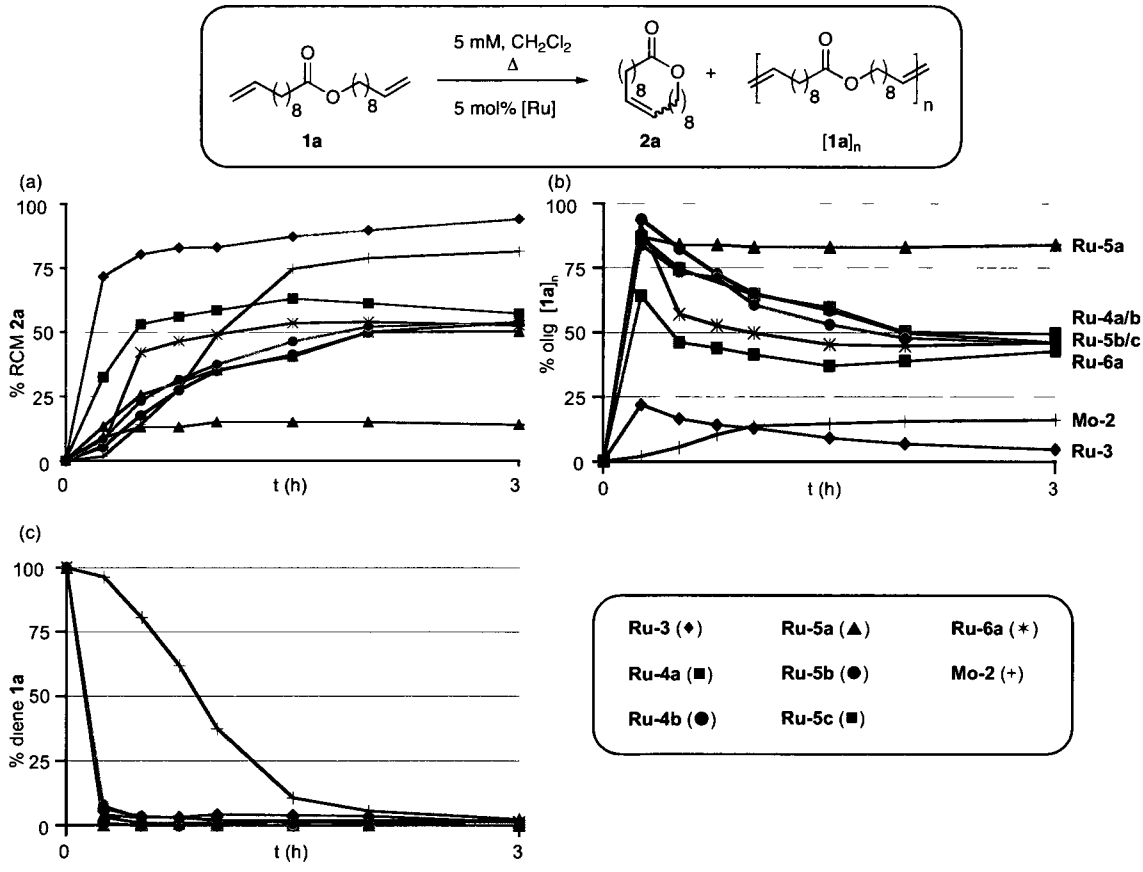

Figure 9. Yield of (a) **2a**, (b) oligomers and (c) consumption of **1a** over time. Conditions: 5 mM **1a** in CH_2Cl_2, Δ, 5 mol% [Ru]. Calibrated GC-FID analysis (±1% in replicate runs). **Ru-3** (♦), **Ru-4a** (■), **Ru-4b** (●), **Ru-5a** (▲), **Ru-5b** (●), **Ru-5c** (■), **Ru-6a** (✶) and **Mo-2** (+).

Strangely, styrenyl ether catalyst **Ru-5a** goes against the trend established for the other NHC catalysts, only yielding 14% **2a** after 3 h. GC-MS analysis of the crude reaction mixture reveals various olefinic products, the masses of which are lower than diene **1a**, RCM **2a** and the expected linear or cyclic oligomers. As olefin isomerization is thought to be particularly problematic for second-generation catalysts,[101,114,115,142] isomerization of starting **1a** followed by RCM or cross-metathesis could account for these side-products. Alternatively, isomerization of the olefinic functionalities within the oligomers[116,117,143-145] formed from **1a**, followed by backbiting could also lead to various olefinic products. Mechanistic issues aside, formation of the different olefin products will necessarily hamper establishment of equilibrium, and thus lower the yield of **2a**.

The significantly higher yield of **2a** attainable using first-generation **Ru-3** vs. **Ru-4-6** (94 vs. 51-57%) could be the result of kinetic vs. thermodynamic control, as suggested above. However, another possible explanation for the lower yield of **2a** with **Ru-4-6** is catalyst deactivation prior to complete backbiting. This possibility was examined by adding a fresh dose of catalyst (e.g. **Ru-4b**; Figure 10) to the reaction once the yield of **2a** reached a plateau (ca. 3 h). Fifteen minutes following the second addition of catalyst, a decrease in the proportion of **2a** (from 50 to 20%) is mirrored by a 30% increase in oligomers. Importantly, longer reaction times allow for the regeneration of **2a** through backbiting. The yield of **2a** was identical (within experimental error) before and after the second addition of **Ru-4b**, underscoring the futility of attempting to "push" these reactions by adding more catalyst once equilibrium is reached.

Contrariwise, diluting the reaction ten-fold after 3 h resulted in near-quantitative formation of **2a** after a further hour (96% **2a**; dilution from 5 mM to 0.5 mM; performed by Maureen Robinson, summer student in this research group). No extra catalyst was added to the reaction in this experiment, which provides convincing evidence that a sufficient amount of active catalyst is present after 3 h to effect backbiting. Consistent with the dilution experiment, near-quantitative formation of **2a** (>98%) can be obtained by RCM of **1a** via **Ru-4b** using a diene concentration of 0.5 mM at the outset but the reaction times are increased to 5 h (instead of 3 h at a diene concentration of 5 mM). Importantly, while RCM

is slower under more dilute conditions, the rate of decomposition of the methylidene[106,107,146] is unaffected. Thus, cyclization of **1a** at a diene concentration of 0.5 mM with the sensitive pyridine-ligated **Ru-6a** (5 mol%) results in catalyst decomposition prior to full consumption of the diene (20% remaining **1a**) whereas the same loading of this catalyst effects complete conversion of diene **1a** at a concentration of 5 mM. When 10 mol% **Ru-6a** is used at a diene concentration of 0.5 mM, however, diene **1a** is fully consumed and formation of **2a** reaches 96% at 3 h. It is worth noting that lowering reaction concentration (i.e. more solvent) may expose the catalyst to an increased proportion of trace noxious contaminants in the solvent, which could also participate in promoting catalyst decomposition.

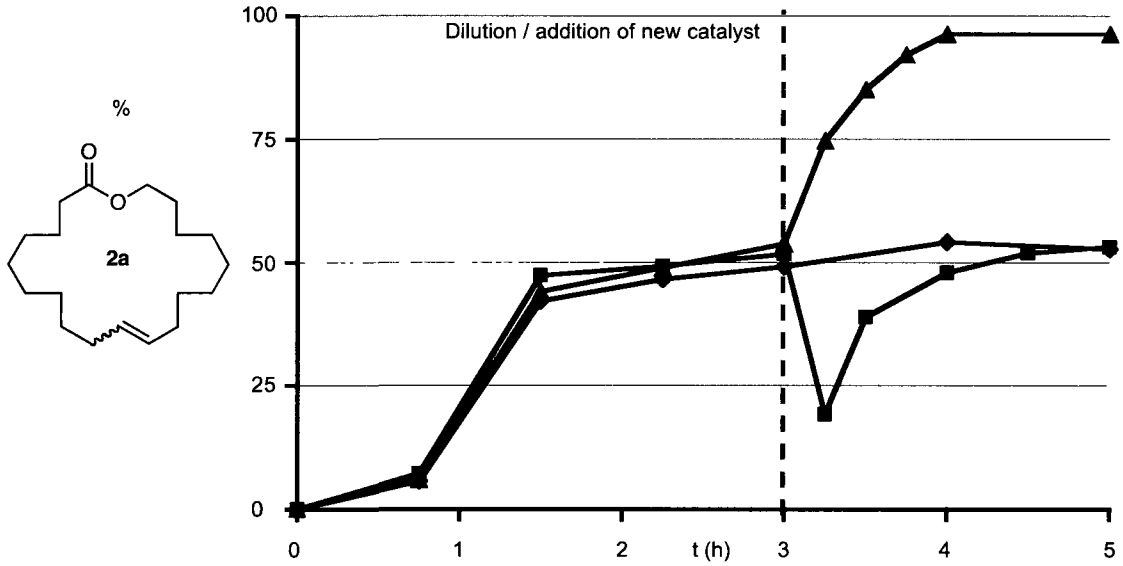

Figure 10. Formation of **2a** catalyzed by **Ru-4b** over time. Conditions: CH_2Cl_2, Δ, 5 mol% **Ru-4b**, (◆) 5 mM **1a**, (■) 5 mM **1a** and addition of fresh **Ru-4b** at 3 h, and (▲) 5 mM **1a** then dilution to 0.5 mM after 3 h. Calibrated GC-FID analysis (±1% in replicate runs).

The effect of ring size on RCM yields was analyzed for catalysts **Ru-3-6** with dienes (**1b/c**) that afford 16- and 14-membered lactones. For conciseness, complete rate profiles are given only in the Appendix; the RCM data are compiled in Table 2. For 16-membered **1b,** all catalysts studied afford quantitative formation of **2b** within 3 h (5 mM diene). As with **1a**, oligomerization is kinetically favoured, albeit to a lesser extent (ca. 60% at 15 min for **1b**, vs. ca. 90% for **1a**). Again, **Ru-3** affords least oligomerization (5%, vs. 44-60% for **Ru-4-6**). Importantly, the second-generation catalysts were capable of cyclodepolymerization of these

oligomers, which undergo complete conversion to **2b** over a total reaction time of 3 h. The small proportion of oligomer obtained with **Ru-3** (5% after 15 min) likewise disappears after 30 min.

For 14-membered **1c,** in comparison, **Ru-4-6** afford 83-87% of the RCM product **2c** within 3 h (5 mM diene). Again, the proportion of oligomers is at a maximum at 15 min (ca. 40%), dropping to ca. 15% over 3 h. In contrast to the results obtained with **1a**, for which the first-generation catalyst **Ru-3** gave highest RCM yield, this catalyst affords slightly lower yields of **2c** (76%) relative to the NHC complexes. A higher initial proportion of oligomers is present than was found for **1a/b** (24%), which does not decline over 3 h reaction. The absence of backbiting may indicate formation of cyclic oligomers, for which the reactivity **Ru-3** is insufficient to re-open, as required to initiate backbiting (vide infra). Consistent with this hypothesis, dropwise addition of **1c** to **Ru-3** in refluxing CH_2Cl_2 affords quantitative RCM at 1 h, without any observable oligomerization (see Section 3.4.6).

Table 2. RCM yields of **2a-c** obtained with **Ru-3-6**.[a]

Catalyst	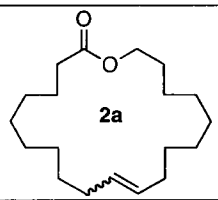 **2a**	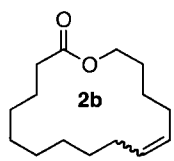 **2b**	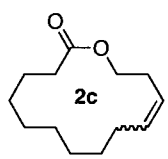 **2c**
Ru-3	94	>99	76 (>99)[b]
Ru-4a	50	>99	85
Ru-4b	54	>99	84
Ru-5a	15[c]	>99	83
Ru-5b	54	>99	87
Ru-5c	57	>99	86
Ru-6a	53	>99	84

[a] GC-FID analysis. [b] Dropwise addition of substrate over 1 h. [c] Isomerized material present. Conditions: 5 mM diene in CH_2Cl_2, Δ, 5 mol% [Ru]. Calibrated GC-FID analysis (±1% in replicate runs).

3.4.4 Catalyst influence on cyclization of medium rings.

The higher ring strain of medium rings renders them challenging synthetic targets. As noted in Section 3.2.3, the combination of imperfect staggering and transannular strain

reaches a maximum in the medium-ring regime.[16] Medium rings are thus characterized by very low EM values. They are consequently prone to formation of cyclic oligomers and their synthesis requires higher dilutions, relative to macrocycles. As the difference in ring strain between cyclomonomer (i.e. RCM target) and cyclic oligomers is particularly high for the medium rings, the tendency of the second-generation catalysts towards oligomerization may be highly detrimental to RCM yields if backbiting is not possible (due to ring strain).

The low EM values characteristic of medium rings is manifested during cyclization of **3b**, precursor to a 10-membered lactone. At a substrate concentration of 5 mM (as for macrocyclic **2a-c**), RCM yields of 10-membered **4b** never exceeded 30% and RCM of **3b** was thus carried at a diene concentration of 0.5 mM. Even at this concentration, oligomers are apparent in the early stages and throughout reaction (Figure 11). As with dienes **1a-c**, minimal formation of oligomers is found for first-generation **Ru-3** (maximum 6% vs. 40% for **Ru-4-6**). For this diene, however, negligible backbiting is found for *all* catalysts; the proportion of oligomers only grows over time. Catalyst **Ru-3** affords the highest amount of **4b** (>99% at 2 h) while catalysts **Ru-4-6** converge on ca. 60% yield of **4b** at 3 h (56-62%; Table 3); involatile oligomers account for the remaining material. Interestingly, a decrease in the yield of **4b** is observed over time for catalysts **Ru-4a/b**. The loss is small (ca. 7%), but outside the experimental error (±1%) for this reaction. It may indicate rapid formation of **4b** as the kinetic product, followed by ring-opening and oligomerization to afford the thermodynamic ratio of products in a step-wise mechanism.[56] Consistent with this explanation, isolation of **4b** requires efficient quenching of the catalyst prior to work-up. Failure to do so results in oligomerization of **4b** to (primarily) cyclic dimer, as determined by ESI-MS analysis. (Other unidentified side-products are also observed by GC). Precedents exist for the "decomposition" of the RCM products to oligomers during workup, particularly when styrenyl ether catalysts (**Ru-5**) are employed.[34,147]

References page 118

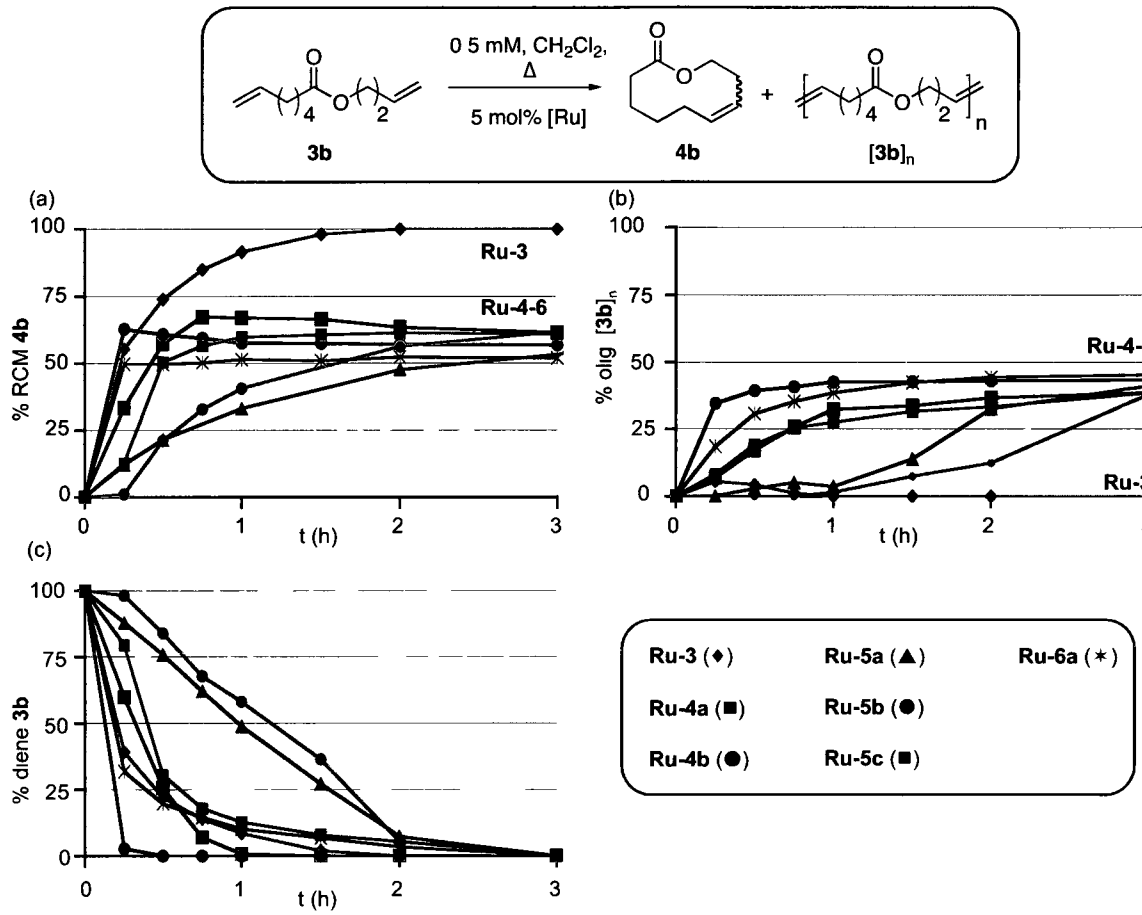

Figure 11. Proportion of (a) **4b**, (b) oligomers and (c) consumption of **3b** over time. Conditions: 0.5 mM **3b** in CH_2Cl_2, Δ, 5 mol% [Ru]. Calibrated GC-FID analysis (±1% in replicate runs). **Ru-3** (◆), **Ru-4a** (■), **Ru-4b** (●), **Ru-5a** (▲), **Ru-5b** (●), **Ru-5c** (■), **Ru-6a** (✶).

Table 3. RCM yields of **4a/b** obtained with **Ru-3-6**.[a]

Catalyst	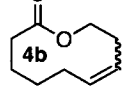	
Ru-3	>99	0
Ru-4a	62	63
Ru-4b	57	68
Ru-5a	59	67
Ru-5b	61[b]	66
Ru-5c	61	67
Ru-6a	56	68

[a] Conditions 0.5 mM diene in CH_2Cl_2, Δ, 5 mol% [Ru]. [b] After 6 h. Calibrated GC-FID analysis, ±1% in replicate runs. The RCM of **3a** was performed in part by Philippa Payne, a USRA student in the Fogg group.

Differences in the E:Z ratio of products obtained by RCM or CM reactions have long been attributed to kinetic or thermodynamic control, albeit with few specifics.[37,111,148] For macrocyclic **2a-c**, the observed ratios did not differ between catalysts (ca. 3:1 for **2a/b**; 9:1 for **2c**). However, in the case of 10-membered **4b**, significant variations in E:Z ratios were observed depending on which catalyst is employed. The NHC catalysts **Ru-4-6** afforded largely the Z isomer (>20:1 throughout the reaction; Figure 12), while **Ru-3** afforded a 1:2.5 E:Z mixture at 15 min, which evolves toward the thermodynamically favored Z isomer over time, and plateaus at a 1:4 ratio after 3 h. Preferential formation of the Z-olefin may originate from the higher stability of the Z-ester configuration (Scheme 4a).[102] Although the ca. 10 kcal mol^{-1} rotational barrier between E- and Z-esters implies free rotation at ambient temperature, the Z-configuration is favored by its ca. 5 kcal mol^{-1} lower ground state energy,[102] and will thus be present in a larger proportion.

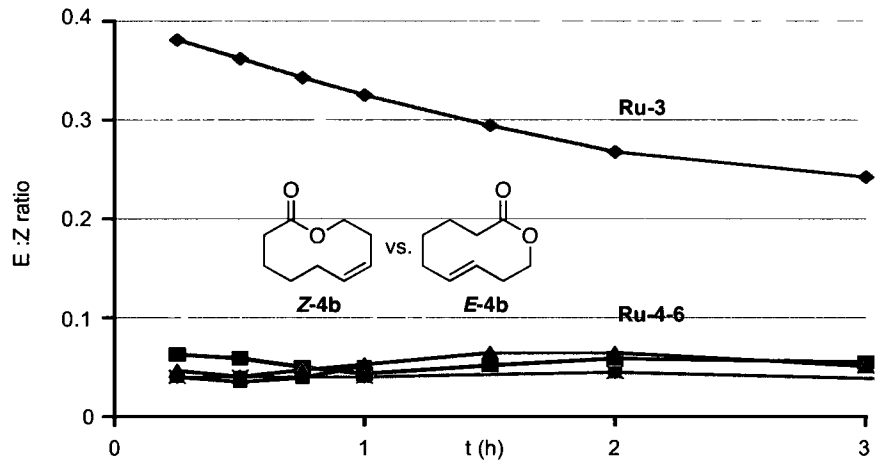

Figure 12. E:Z ratio of **4b** over time. Conditions: 0.5 mM **3b** in CH_2Cl_2, Δ, 5 mol% [Ru]. Calibrated GC-FID analysis (±1% in replicate runs). **Ru-3** (◆), **Ru-4a** (■), **Ru-4b** (●), **Ru-5a** (▲), **Ru-5b** (●), **Ru-5c** (■), **Ru-6a** (✶).

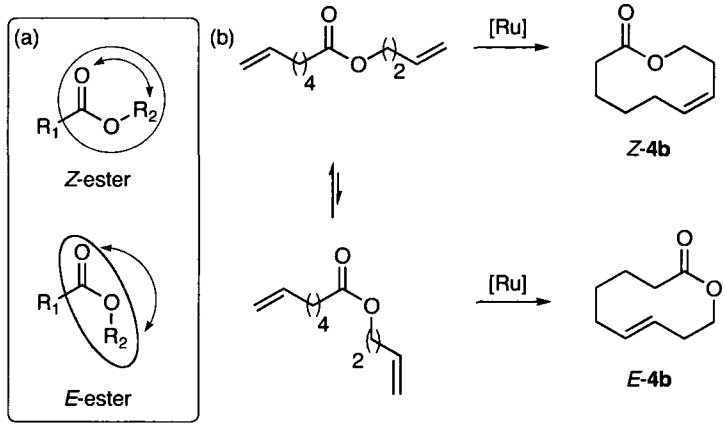

Scheme 4. (a) E and Z esters. (b) Rationale for the preferential formation of Z-**4b**.

While seven-membered rings are often readily accessible, and are hence classified among the common ring sizes, the sp^2 centers of the ester functionality of **3a** drastically lower the EM value for this substrate.[15] Thus, RCM of **3a** faces similar challenges as **3b**. As with 10-membered **4b**, the proportion of oligomers formed during RCM of **4a** does not disappear over time (See Appendix A for conversion profiles). While yields of **4a** obtained with NHC catalysts **Ru-4-6** at 0.5 mM diene are generally fair (63-68%), no RCM product was observable using first-generation **Ru-3**. Consumption of **3a** by **Ru-3** also remains incomplete; 60% residual diene remains after 3 h even at 5 mol% **Ru-3**. This is consistent with a report of Furstner showing that **Ru-3** is ineffective for RCM of four substrates bearing the 3-butenoate moiety.[149] Incomplete reaction may indicate catalyst poisoning by chelation of the carbonyl oxygen atom. A common solution to this problem is introduction of Lewis acids such as $Ti(O^iPr)_4$ to preferentially bind the polar functionalities of the substrate/product.[150-153] However, in our hands, $Ti(O^iPr)_4$ had no beneficial effect in RCM of **3a** by **Ru-3**. Even when 1 equiv. of this Lewis acid was added relative to the substrate, no RCM product could be detected, and a similar proportion (64%) of unreacted **3a** remained after 3 h.

The inability of first-generation **Ru-3** to carry out RCM of **3a** serves as a reminder of the limited substrate scope of this catalyst. Dienes bearing a sterically[112,139,154] or electronically[155-158] deactivated olefin are not amenable to cyclization by **Ru-3**, although they can often be dimerized at the more reactive olefinic site. The propensity of this catalyst to favor cyclization of medium and large rings, relative to second-generation **Ru-4-6**, thus comes at a

cost in terms of the range of dienes that can be subjected to RCM. A potential solution is the deliberate design of catalysts that combine the extended substrate scope of the second-generation catalysts with the bias of **Ru-3** toward cyclization. As noted in the introduction of this Chapter, preliminary results suggest that pseudohalide catalysts such as **Ru-7b** may fulfill this need. Examination and comparison of the macrocyclization rate profiles of the pseudohalide and Grubbs catalysts was thus undertaken.

3.4.5 RCM macrocyclization using pseudohalide catalysts

Macrocyclization using pseudohalide catalysts **Ru-7a/b** was performed using **1a** as substrate. This substrate was selected because the ca. 50% yield of 20-membered **2a** obtained with the second-generation catalysts **Ru-4-6** is ideal to identify differences in yield. Reactions were carried out exactly as described for **Ru-3-6** (Section 3.4.3); the conversion profiles for **Ru-7a/b** are shown in Figure 13. To rule out catalyst decomposition as the limiting factor of RCM yields, addition of a second dose of each catalyst was performed once the conversions reached a plateau.

For perfluorophenoxide **Ru-7a**, conversion to **2a** is slow, and limited to 10% at 1 h (3% **2a**, 7% oligomers). An induction period is apparent, with conversions increasing after 1 h., accompanied by a color change from green to yellow. The reaction plateaus at 5 h, with a proportion of 69% **2a** and 31% oligomers. Addition of fresh **Ru-7a** had no effect; the proportion of **2a** and oligomers remained constant for an additional period of 8.5 hours (Figure 14). The final product distribution obtained after, with or without addition of a second dose of **Ru-7a**, is only slightly higher than that obtained with the parent **Ru-6a** (53% **2a** and 47 oligomers; ±1% error). Thus, rates of RCM aside, replacing both chloride ligands with perfluorophenoxide has little effect on the yields of **2a**.

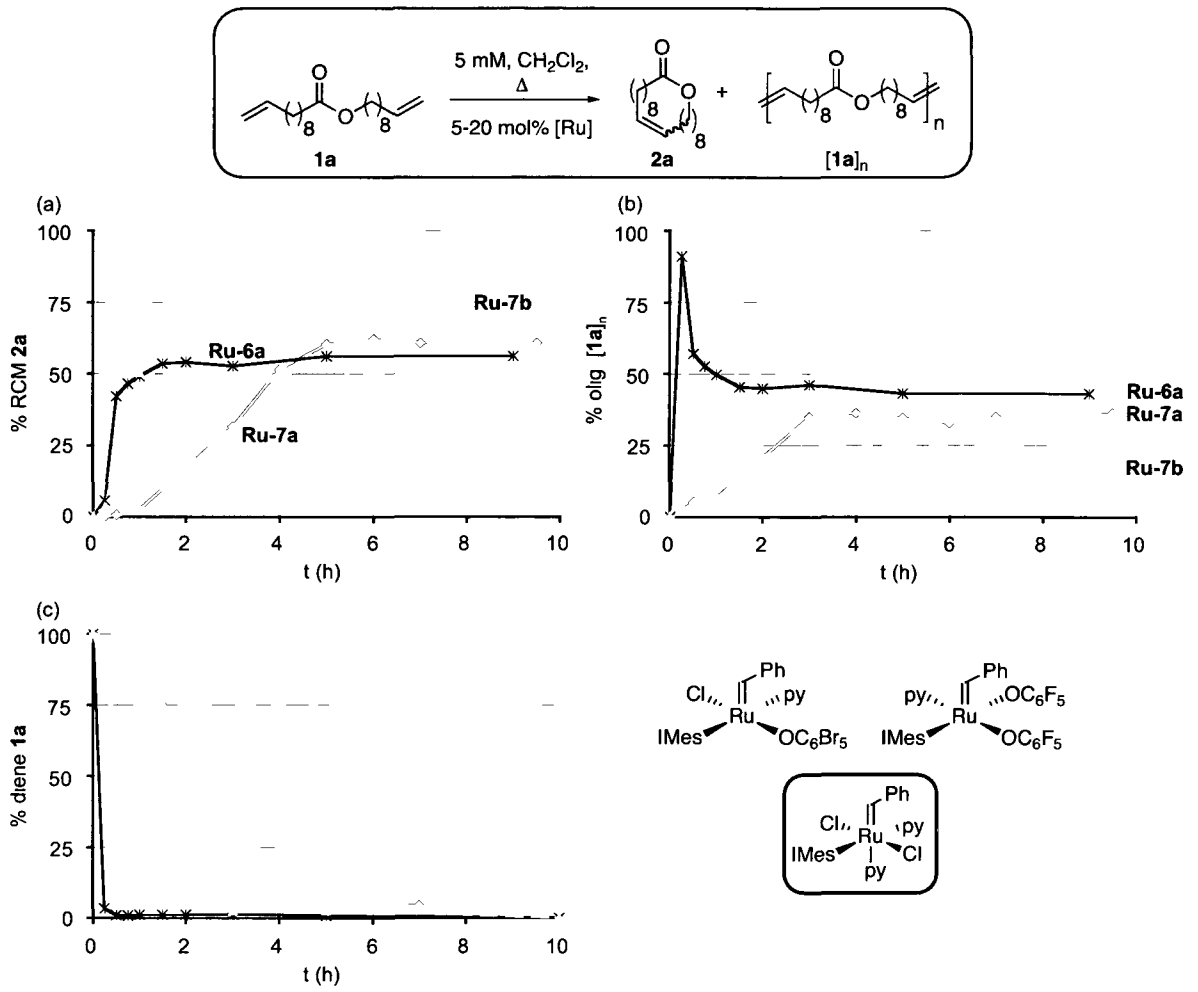

Figure 13. Proportion of (a) **2a**, (b) oligomers and (c) diene **1a** over time using aryloxide catalysts **Ru-7a/b**. Conditions: 5 mM **1a** in CH_2Cl_2, Δ, 5 mol% [Ru] unless otherwise specified. Calibrated GC-FID analysis (±2% in replicate runs). **Ru-7a** (◇), **Ru-7b** ( ); filled line = 5 mol%; dashed line = 20 mol% **Ru-7b**. Conversion profile for the dichloride parent **Ru-6a** (✶) included for comparison.

RCM of **1a** with perbromophenoxide **Ru-7b** was more complicated. Under the standard conditions (5 mM **1a** in refluxing CH_2Cl_2, 5 mol% [Ru]), **Ru-7b** decomposes prior to complete consumption of diene **1a**. After six hours, the product distribution consists of 51% **2a** with 29% oligomers and 20% unreacted **1a**. No change was observed on extended reaction (15 h). Interestingly, the 51% yield of **2a** observed at 6 h is similar to that found with **Ru-4-6** (50-57%), despite 20% unreacted diene, implying that the yields of **2a** could be as much as 20% higher with this catalyst if decomposition can be curbed. The observation of oligomeric species during RCM of **1a** contrasts with the prior report showing no detectable

oligomerization during RCM formation of 16-membered **1b** by **Ru-7b**.[44] This is in line with the greater proportion of oligomers formed at 15 min for **1a**, vs. **1b** (ca. 80%, vs. 60% respectively, Figure 9). It is also worth noting that dropwise addition of substrate was performed in earlier work, which could limit the extent of oligomerization.

As **Ru-7b** appears to decompose in refluxing CH_2Cl_2, dropwise addition of the catalyst was undertaken. Addition of **Ru-7b** (5 mol%) was performed by syringe pump, with addition times varying between 15 min to 2 h. This protocol did not afford good results, however. Final conversions were consistently lower relative to the original protocol, where **Ru-7b** is added all at once. Moreover, final conversions decreased as the addition time of **Ru-7b** was increased. For example, when **Ru-7b** is added over 15 min, final conversions, attained at 4 h, were 43% (29% **2a**; 14% oligomers) while addition over 2 h led to a maximum of 25% conversion (14% **2a**; 11% oligomers) after 2.5 h. Decomposition of **Ru-7b** by exposure to air at the syringe-needle junction is the probable culprit, as evidenced by the color change of the catalyst solution in the syringe, from pale green to dark green-yellow. Such a color change is observed when a CH_2Cl_2 solution of **Ru-7b** is deliberately exposed to air, but is not observed for the parent solution inside the glovebox (N_2 atmosphere).

Given the failure of the syringe pump protocol, RCM of **1a** using **Ru-7b** was performed using 20 mol% catalyst instead of the regular dosage of 5 mol%. All other reaction parameters remained constant (5 mM **1a**, CH_2Cl_2, Δ), however. Even at this elevated catalyst loading, complete consumption of **1a** requires 3 h (Figure 13). During the first 45 min of reaction, the rate of formation of **2a** and oligomers is similar; a proportion of 38% **2a** and 32% oligomer (30% remaining **1a**) is observed at that time. After 45 minutes, however, no further increase in oligomer formation is evident but the proportion of **2a** continues to climb. The yields of **2a** reach a plateau at 3 h (68% **2a**, 32% oligomers). Interestingly, the addition of a fresh dose of catalyst **Ru-7b** after 3 h (Figure 14) has a similar effect to that observed with **Ru-4b** (Figure 10). A decrease in the yield of **2a** (from 68 to 60%) is observed 15 min after addition of fresh **Ru-7b** but longer reaction time (six additional hours) results in the regeneration of **2a** to a final yield of 69%. This experiment proves that **Ru-7b** is sufficiently reactive to effect both ring-opening of **2a** and backbiting of the ensuing oligomers. Thus, the

nearly 20% higher yields of **2a** observed with **Ru-7b** cannot be attributed to the inability of this catalyst to participate in the ring-chain equilibrium. Importantly, a control experiment using 20 mol% **Ru-4b** and **Ru-5b** showed that the final yields of **2a** are unaffected by the higher catalyst loading (52% and 54% for **Ru-4b** and **Ru-5b** respectively; cf. 54% for both at a loading of 5 mol%).

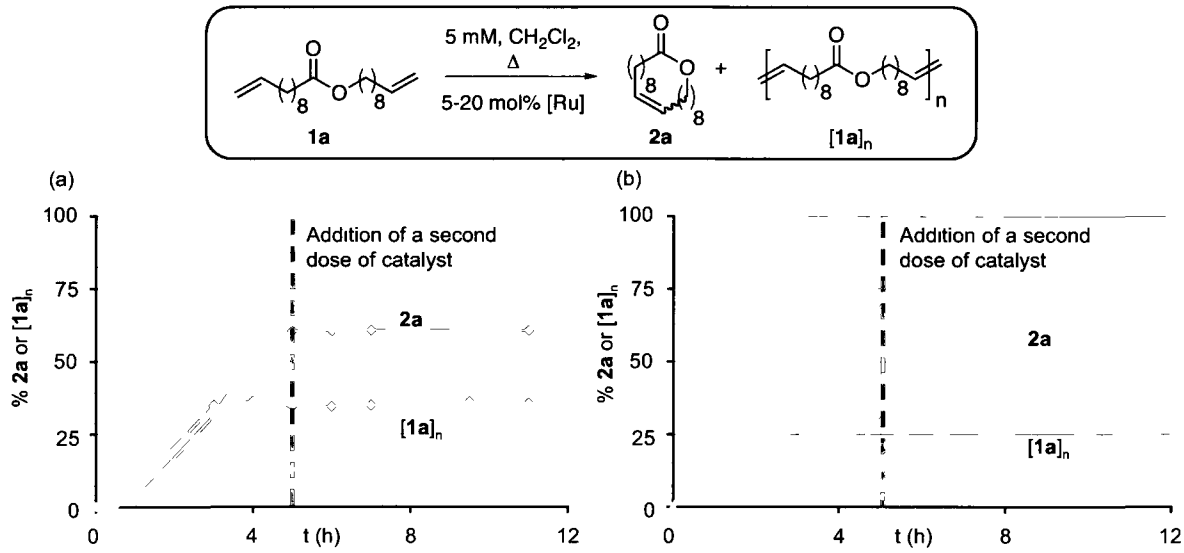

Figure 14. Effect of addition of a second dose of catalyst on the % RCM **2a** and % oligomers for (a) **Ru-7a** (◇) and (b) **Ru-7b** ( ). RCM = full line; Oligomers = dashed line. Conditions: 5 mM **1a** in CH_2Cl_2, Δ, 5 mol% **Ru-7a**, 20 mol% **Ru-7b**. Calibrated GC-FID analysis (±2% in replicate runs).

Clearly, the different stereo-electronic properties of the pentabromophenoxide vs. the chloride ligand must be responsible for the increased yield of 20-membered **2a** using aryloxide **Ru-7b**. Alternatively, however, the bias of **Ru-7b** toward cyclization of **1a** may be kinetic in origin, particularly given the short lifetime of this catalyst evident from the elevated catalyst loading of 20 mol% required to effect complete consumption of **1a** (Figure 13). Even when a second dose of catalyst is added, the high sensitivity of **Ru-7b** may lead to deactivation before equilibrium can be established. However, a change in product distribution would be expected upon addition of fresh catalyst, which is not the case. Regardless, this catalyst combines both the extended substrate scope[44] of the second-generation catalysts **Ru-4-6** with the higher tendency toward cyclization of **Ru-3**. Thus, by

curbing the deactivation of this catalyst, higher RCM yields may be obtained without resorting to dilution.

3.4.6 Exploiting the ring-chain equilibrium

The RCM literature is rife with reports of unwanted oligomerization.[33] The enhanced reactivity of the second-generation catalysts can allow "recycling" of oligomers into desired cyclic species, but this possibility is largely under-exploited. Scattered literature reports describe the conversion of oligomers into smaller cyclic products by using elevated temperatures[159] or more reactive catalysts.[112,154] Success depends on the ability of the catalyst to re-attach to the olefinic moiety of the oligomers. Conversion of linear oligomers containing accessible olefin endgroups into the desired RCM product is thus more common than conversion of cyclic oligomers, for which only internal olefins are present.[33] While the more reactive second-generation catalysts are expected to be better catalysts for conversion of oligomers to RCM products, as shown by Hodge and co-workers for CDP of polyesters using **Ru-4b**,[140] little systematic data exist for the remaining catalysts. To examine the competence of the first- and second-generation catalysts in cyclodepolymerization, the isolated cyclic dimer $[\mathbf{4b}]_2$ was subjected to backbiting RCM by representative catalysts **Ru-3**, **Ru-4b** and **Ru-5b/c**.

Dimeric $[\mathbf{4b}]_2$ was prepared in 71% yield by RCM of **3b** using 5 mol% of styrenyl ether **Ru-5b** as shown in Scheme 5. After quenching the catalyst with Ktp,[125] pure $[\mathbf{4b}]_2$ was isolated as a colorless, slightly odorant oil by flash chromatography. Cyclomonomer **4b** was isolated in 13% yield in the process.

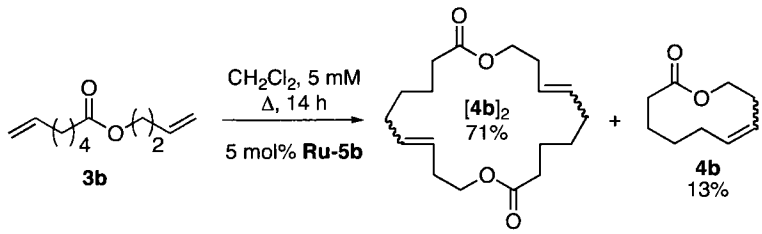

Scheme 5. Synthesis of $[\mathbf{4b}]_2$. Conditions: 5 mM **3b** in CH_2Cl_2, Δ, 14 h, 5 mol% **Ru-5b**.

The progress of the attempted CDP reaction is shown in Figure 15, which demonstrates the appearance of 10-membered **4b** via backbiting of cyclic dimer $[\mathbf{4b}]_2$ as function of time for

the four catalysts tested. For first-generation **Ru-3**, null formation of **4b** is observed over 5 h, and the proportion of $[\mathbf{4b}]_2$ remains constant. The failure of **Ru-3** to effect backbiting is not due to its inability to react with the olefins of $[\mathbf{4b}]_2$. Indeed, reaction of $[\mathbf{4b}]_2$ with 5 mol% **Ru-3** at an arbitrary substrate concentration of 1 M (CH_2Cl_2, 23 °C) affords >90% oligomers along with 9% remaining $[\mathbf{4b}]_2$ after 15 min. ^{1}H NMR examination of the crude (quenched) reaction mixture revealed no vinylic endgroups, implying that either solely cyclic oligomers are formed, or that the polymer obtained is too long for the endgroups to be detected. Irrespective of the nature of the oligomers, the null formation of **4b** from its cyclic dimer with **Ru-3** implies that backbiting is much slower than ring-opening of $[\mathbf{4b}]_2$. This also suggests that the rate of deactivation of **Ru-3** may be faster than backbiting.

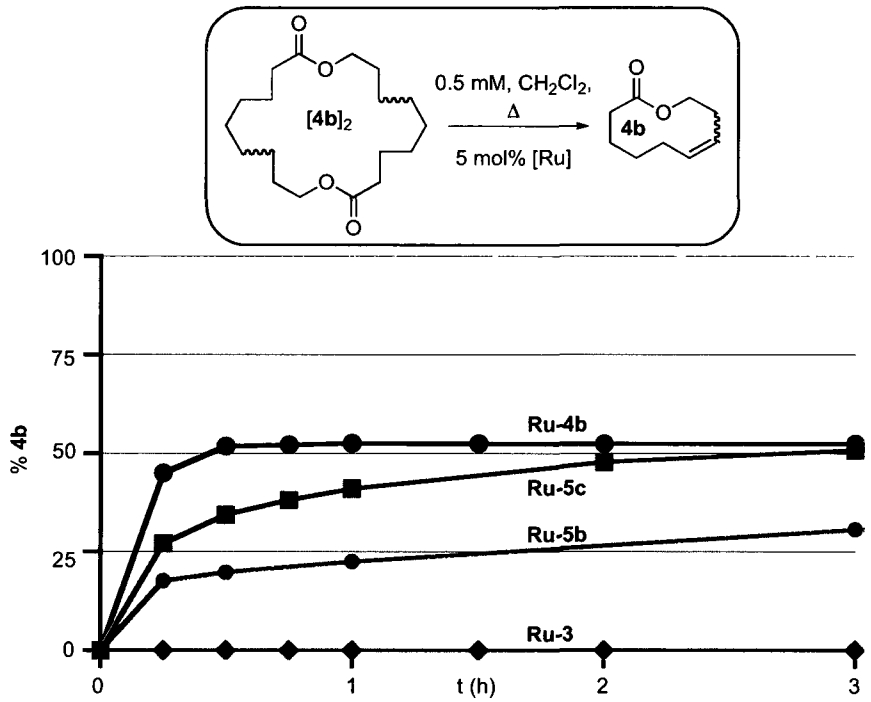

Figure 15. Formation of **4b** from isolated $[\mathbf{4b}]_2$ over time. Conditions: 0.5 mM $[\mathbf{4b}]_2$ in CH_2Cl_2, Δ, 5 mol% [Ru]. Calibrated GC-FID analysis (±1% in replicate runs). **Ru-3** (◆), **Ru-4b** (●), **Ru-5b** (●), **Ru-5c** (■).

In contrast, when second-generation **Ru-4b** is employed under the same conditions, 45% **4b** is formed after only 15 min at reflux. The proportion of **4b** plateaus at 52% at 45 min; the mass balance corresponds to residual $[\mathbf{4b}]_2$. Styrenyl ether catalysts **Ru-5b/c** were also competent at effecting this transformation, albeit at a slower rate. For unsubstituted **Ru-5b**,

18% **4b** is formed after 15 min. The reaction then slows, the yield of **4b** reaching 31% at 3 h. On prolonged reaction (18 h), **4b** is obtained in 55% yield. For the nitro-substituted styrenyl ether catalyst **Ru-5c**, reaction rates are intermediate between those of **Ru-4b** and **Ru-5b**. At 15 min, 25% **4b** is formed, plateauing at 55% **4b** after 8 h. Consistent with equilibrium control of the reaction, the yields of **4b** obtained from CDP of $[\mathbf{4b}]_2$ by second-generation **Ru-4b** and **Ru-5b/c** agree closely (51-55%) and that obtained from diene **3b** with the same catalysts (56-62%; Figure 11). Thus, barring issues of reaction rates, the choice of catalyst for converting oligomers into smaller cyclic species is largely inconsequential.

As a corollary, the poor performance of first-generation **Ru-3** in backbiting means that protocols designed to limit oligomerization are critical to maximizing RCM yields. An excellent example is found in RCM of **1c**, precursor to the 14-membered lactone **2c**. Under the standard conditions, second-generation **Ru-4-6** afford ca. 15% higher yield of **2c** relative to **Ru-3**. This was attributed to the inability of **Ru-3** to effect backbiting of the initial proportion of oligomers formed at 15 min. However, if substrate **1c** is added dropwise to a refluxing solution containing **Ru-3** (5 mM once addition of substrate is completed) over 1 h, no oligomer could be detected at any point, and formation of **2c** is quantitative after 65 min. This strongly suggests that oligomerization of **1c** by **Ru-3** is terminal and thus avoiding oligomerization is critical for maximizing RCM yields. With second-generation **Ru-4b**, the yield of **2c** was unaffected whether the diene was added dropwise or via the standard "one-shot" protocol (82% vs. 84%). This result is explained by higher propensity of this catalyst to effect ring-opening and subsequent oligomerization of the product once the equilibrium concentration of **2c** has been reached. Yamamoto and co-workers also commented on the futility of slow addition of catalyst **Ru-4b** in RCM macrocyclization.[158] Thus, unless catalyst lifetime is an issue, Ziegler-type protocols involving slow infusion of substrate to minimize oligomerization are not beneficial when T-class second-generation catalysts are employed.

3.5 Conclusions

This Chapter describes the first systematic evaluation of the kinetic and thermodynamic selectivity of the Grubbs catalysts in RCM cyclization of medium and, more particularly, macrocyclic rings. This study links the mechanistic aspects of RCM macrocyclization with the choice of catalyst and reaction conditions required to maximize RCM yields. The

questions that were asked at the outset of this study have now been answered. (1) All second-generation catalysts share the kinetic bias of **Ru-4a** for oligomerization of large rings while first-generation **Ru-3** does not. Of importance for sustainable metathesis, the use of kinetically-controlled first-generation **Ru-3** increases macrocyclization yields relative to other catalysts under the same conditions. However, this is only possible for dienes in which neither end is deactivated (this resulting in dimerization), or where stable cyclic oligomers do not form. Thermodynamically-controlled second-generation catalysts **Ru-4-6** permit a broader substrate scope but show a kinetic bias toward oligomerization. Higher dilutions are required to maximize RCM yields when using these NHC catalysts, because RCM is then operative under thermodynamic conditions, and the lower EM_T relative to EM_k factor comes into play. As a compensating factor, "recycling" of isolated oligomers to the desired RCM product is only possible with the second-generation catalysts. Importantly, the RCM yields furnished by the Grubbs second-generation catalysts are *equilibrium* yields. Attempting to "push" these reactions by addition of more catalyst is therefore useless. Conversely, simple dilution of the reaction shifts the equilibrium toward the smaller cyclic products. Furthermore, given the similarity between active species, essentially no difference in yield is observed when using any of the second-generation Grubbs catalysts (barring issues of catalyst lifetime).

(2) While useful in the research setting as a means of increasing RCM yields, the requirement for high dilutions is highly problematic in the industrial context, where solvent costs are a major contributor to process economics and waste. Much preferable would be development of catalysts with a broad substrate scope, which afford minimal proportion of oligomers. In this context, the so far unique ability of perbromoaryloxide **Ru-7b** to afford higher RCM yields relative to the Grubbs second-generation catalysts is very interesting. Up to 20% higher yield of a 20-membered **2a** was observed using **Ru-7b**. This result points towards an impact of the catalyst structure on K_{eq}. However, before any realistic application of this catalyst can be considered, the high sensitivity of **Ru-7b** will need to be addressed.

(3) For RCM of medium rings, all catalysts show a constant increase in the proportion of oligomeric species over the course of the reaction. Importantly, these oligomers are not

converted into RCM product (except when isolated cyclic oligomers are deliberately subjected to "RCM" conditions), as was the case for the macrocyclic rings. (4) This implies that much higher dilutions are required for suppressing the formation of oligomers when T-class catalysts are employed. Alternatively, for substrates compatible with first-generation **Ru-3**, dropwise addition of the diene to the reaction may be beneficial.

What causes the higher RCM yield observed with **Ru-7b** relative to **Ru-4-6**? Is it the differences in the ligand sterics, electronics or both, that favor cyclization? Answering these questions would prove invaluable for the design of the next generation of aryloxide catalysts. Theoretical approaches could potentially aid in calculating the energy difference for macrocyclization using (e.g.) the dichloride and aryloxide catalysts.

3.6 References

(1) Driggers, E. M.; Hale, S. P.; Lee, J.; Terrett, N. K., *Nat. Rev. Drug Discov.* **2008**, *7*, 608-624.
(2) Miller, A. K., *Angew. Chem., Int. Ed.* **2009**, *48*, 3221-3223.
(3) Kraft, P., Aroma Chemicals IV: Musks. In *Chemistry and Technology of Flavors and Fragrances*, Rowe, D. J., Ed. CRC Press: Boca Raton, 2005; pp 143-168.
(4) Bielawski, C. W.; Benitez, D.; Grubbs, R. H., *Science* **2002**, *297*, 2041-2044.
(5) Winnik, M. A., *Acc. Chem. Res.* **1985**, *18*, 73-79.
(6) Parenty, A.; Moreau, X.; Campagne, J. M., *Chem. Rev.* **2006**, *106*, 911-939.
(7) Cramer, N.; Buchweitz, M.; Laschat, S.; Frey, W.; Baro, A.; Mathieu, D.; Richter, C.; Schwalbe, H., *Chem. Eur. J.* **2006**, *12*, 2488-2503.
(8) Gradillas, A.; Perez-Castells, J., *Angew. Chem., Int. Ed.* **2006**, *45*, 6086-6101.
(9) Corey, E. J.; Nicolaou, K. C., *J. Am. Chem. Soc.* **1974**, *96*, 5614-5616.
(10) Mukaiyama, T.; Usui, M.; Saigo, K., *Chem. Lett.* **1976**, 49-50.
(11) Inanaga, J.; Hirata, K.; Saeki, H.; Katsuki, T.; Yamaguchi, M., *Bull. Chem. Soc. Jpn.* **1979**, *52*, 1989-1993.
(12) Kurihara, T.; Nakajima, Y.; Mitsunobu, O., *Tetrahedron Lett.* **1976**, 2455-2458.
(13) Meng, D.; Bertinato, P.; Balog, A.; Su, D.-S.; Kamenecka, T.; Sorensen, E.; Danishefsky, S. J., *J. Am. Chem. Soc.* **1997**, *119*, 10073-10092.
(14) McGowan, G.; Thomas, E. J., *Org. Biomol. Chem.* **2009**, *7*, 2576-2590.
(15) Galli, C.; Mandolini, L., *Eur. J. Org. Chem.* **2000**, 3117-3125.
(16) Illuminati, G.; Mandolini, L., *Acc. Chem. Res.* **1981**, *14*, 95-102.
(17) Vedejs, E.; Zajac, M. A., *Org. Lett.* **2001**, *3*, 2451-2454.
(18) Tse, B., *J. Am. Chem. Soc.* **1996**, *118*, 7094-7100.
(19) Roxburgh, C. J., *Tetrahedron* **1995**, *51*, 9767-9822.
(20) Nicolaou, K. C.; Tang, Y.; Wang, J., *Angew. Chem., Int. Ed.* **2009**, *48*, 3449-3453.
(21) Banert, K.; Schumann, P., *Synlett* **2008**, 535-538.
(22) Zapf, C. W.; Harrison, B. A.; Drahl, C.; Sorensen, E. J., *Angew. Chem., Int. Ed.* **2005**, *44*, 6533-6537.
(23) Menand, M.; Blais, J.-C.; Valery, J.-M.; Xie, J., *J. Org. Chem.* **2006**, *71*, 3295-3298.

(24) Smith, A. B., III; Safonov, I. G., *Org. Lett.* **2002**, *4*, 635-637.
(25) Yvergnaux, F.; Le Floch, Y.; Gree, R.; Toupet, L., *Tetrahedron Lett.* **1989**, *30*, 7393-7396.
(26) Shimamura, H.; Breazzano, S. P.; Garfunkle, J.; Kimball, F. S.; Trzupek, J. D.; Boger, D. L., *J. Am. Chem. Soc.* **2010**, *132*, 7776-7783.
(27) Li, P.; Li, J.; Arikan, F.; Ahlbrecht, W.; Dieckmann, M.; Menche, D., *J. Org. Chem.* **2010**, *75*, 2429-2444.
(28) Trost, B. M.; Dong, G., *Nature* **2008**, *456*, 485-488.
(29) Beaubien, S.; Deslongchamps, P., *Can. J. Chem.* **2006**, *84*, 29-48.
(30) Evano, G.; Toumi, M.; Coste, A., *Chem. Commun.* **2009**, 4166-4175.
(31) Pellico, D.; Gomez-Gallego, M.; Ramirez-Lopez, P.; Mancheno, M. J.; Sierra, M. A.; Torres, M. R., *Chem. Eur. J.* **2010**, *16*, 1592-1600.
(32) Trnka, T. M.; Grubbs, R. H., *Acc. Chem. Res.* **2001**, *34*, 18-29.
(33) Monfette, S.; Fogg, D. E., *Chem. Rev.* **2009**, *109*, 3783-3816.
(34) Yee, N. K.; Farina, V.; Houpis, I. N.; Haddad, N.; Frutos, R. P.; Gallou, F.; Wang, X.-J.; Wei, X.; Simpson, R. D.; Feng, X.; Fuchs, V.; Xu, Y.; Tan, J.; Zhang, L.; Xu, J.; Smith-Keenan, L. L.; Vitous, J.; Ridges, M. D.; Spinelli, E. M.; Johnson, M.; Donsbach, K.; Nicola, T.; Brenner, M.; Winter, E.; Kreye, P.; Samstag, W., *J. Org. Chem.* **2006**, *71*, 7133-7145.
(35) Farina, V.; Shu, C.; Zeng, X.; Wei, X.; Han, Z.; Yee, N. K.; Senanayake, C. H., *Org. Process Res. Dev.* **2009**, *13*, 250-254.
(36) Nicola, T.; Brenner, M.; Donsbach, K.; Kreye, P., *Org. Process Res. Dev.* **2005**, *9*, 513-515.
(37) Fürstner, A.; Radkowski, K.; Wirtz, C.; Goddard, R.; Lehmann, C. W.; Mynott, R., *J. Am. Chem. Soc.* **2002**, *124*, 7061-7069.
(38) Maysuya, Y.; Takayanagi, S.-i.; Nemoto, H., *Chem. Eur. J.* **2008**, *14*, 5275-5281.
(39) Fürstner, A.; Mueller, C., *Chem. Commun.* **2005**, 5583-5585.
(40) Castoldi, D.; Caggiano, L.; Panigada, L.; Sharon, O.; Costa, A. M.; Gennari, C., *Chem. Eur. J.* **2005**, *12*, 51-62.
(41) Castoldi, D.; Caggiano, L.; Panigada, L.; Sharon, O.; Costa, A. M.; Gennari, C., *Angew. Chem., Int. Ed.* **2005**, *44*, 588-591.
(42) Vyboishchikov, S. F.; Thiel, W., *Chem. Eur. J.* **2005**, *11*, 3921-3935.
(43) Conrad, J. C.; Eelman, M. D.; Duarte Silva, J. A.; Monfette, S.; Parnas, H. H.; Snelgrove, J. L.; Fogg, D. E., *J. Am. Chem. Soc.* **2007**, *129*, 1024-1025.
(44) Conrad, J. C.; Parnas, H. H.; Snelgrove, J. L.; Fogg, D. E., *J. Am. Chem. Soc.* **2005**, *127*, 11882-11883.
(45) Faucher, A. M.; Bailey, M. D.; Beaulieu, P. L.; Brochu, C.; Duceppe, J. S.; Ferland, J. M.; Ghiro, E.; Gorys, V.; Halmos, T.; Kawai, S. H.; Poirier, M.; Simoneau, B.; Tsantrizos, Y. S.; Llinas-Brunet, M., *Org. Lett.* **2004**, *6*, 2901-2904.
(46) Liverton, N. J.; Holloway, M. K.; McCauley, J. A.; Rudd, M. T.; Butcher, J. W.; Carroll, S. S.; DiMuzio, J.; Fandozzi, C.; Gilbert, K. F.; Mao, S.-S.; McIntyre, C. J.; Nguyen, K. T.; Romano, J. J.; Stahlhut, M.; Wan, B.-L.; Olsen, D. B.; Vacca, J. P., *J. Am. Chem. Soc.* **2008**, *130*, 4607-4609.
(47) McCauley, J. A.; Rudd, M. T.; Nguyen, K. T.; McIntyre, C. J.; Romano, J. J.; Bush, K. J.; Varga, S. L.; Ross, C. W., III; Carroll, S. S.; DiMuzio, J.; Stahlhut, M. W.; Olsen, D. B.; Lyle, T. A.; Vacca, J. P.; Liverton, N. J., *Angew. Chem., Int. Ed.* **2008**, *47*, 9104-9107.

(48) Wilson, L. J.; Malaviya, R.; Yang, C.; Argentieri, R.; Wang, B.; Chen, X.; Murray, W. V.; Cavender, D., *Bioorg. Med. Chem. Lett.* **2009**, *19*, 3333-3338.
(49) Content, S.; Dutton, C. J.; Roberts, L., *Bioorg. Med. Chem. Lett.* **2003**, *13*, 321-325.
(50) Machauer, R.; Veenstra, S.; Rondeau, J.-M.; Tintelnot-Blomley, M.; Betschart, C.; Neumann, U.; Paganetti, P., *Bioorg. Med. Chem. Lett.* **2009**, *19*, 1361-1365.
(51) Jacobson, H.; Stockmayer, W. H., *J. Chem. Phys.* **1950**, *18*, 1600-1606.
(52) Chen, Z.-R.; Claverie, J. P.; Grubbs, R. H.; Kornfield, J. A., *Macromolecules* **1995**, *28*, 2147-2154.
(53) Ivin, K. J.; Mol, J. C., *Olefin Metathesis and Metathesis Polymerization*. Academic Press: New York, 1997.
(54) Rehahn, M.; Mattice, W. L.; Suter, U. W., *Adv. Polym. Sci.* **1997**, *131/132*, 1-19.
(55) Suter, U. W.; Höcker, H., *Makromol. Chem.* **1988**, *189*, 1603-1612.
(56) Höcker, H., *J. Mol. Catal.* **1991**, *65*, 95-99.
(57) Thorn-Csanyi, E.; Ruhland, K., *Macromol. Chem. Phys.* **1999**, *200*, 1662-1671.
(58) Kress, J., *J. Mol. Catal. A* **1995**, *102*, 7-21.
(59) Ercolani, G.; Mandolini, L.; Mencareli, P.; Roelens, S., *J. Am. Chem. Soc.* **1993**, *115*, 3901-3908.
(60) Kirby, A. J., *Adv. Phys. Org. Chem.* **1980**, *17*, 183-278.
(61) Mandolini, L., *Adv. Phys. Org. Chem.* **1986**, *22*, 1-111.
(62) Ercolani, G., *Struct. Bonding* **2006**, *121*, 167-215.
(63) Ercolani, G., *J. Phys. Chem. B* **2003**, *107*, 5052-5057.
(64) Corbett, P. T.; Leclaire, J.; Vial, L.; West, K. R.; Wietor, J.-L.; Sanders, J. K. M.; Otto, S., *Chem. Rev.* **2006**, *106*, 3652-3711.
(65) Cacciapaglia, R.; Di Stefano, S.; Mandolini, L., *J. Am. Chem. Soc.* **2005**, *127*, 13666-13671.
(66) Mulder, A.; Huskens, J.; Reinhoudt, D. N., *Org. Biomol. Chem.* **2004**, *2*, 3409-3424.
(67) Li, X.; Liu, D. R., *Angew. Chem., Int. Ed.* **2004**, *43*, 4848-4870.
(68) Huskens, J.; Mulder, A.; Auletta, T.; Nijhuis, C. A.; Ludden, M. J. W.; Reinhoudt, D. N., *J. Am. Chem. Soc.* **2004**, *126*, 6784-6797.
(69) Cacciapaglia, R.; Di Stefano, S.; Mandolini, L., *Acc. Chem. Res.* **2004**, *37*, 113-122.
(70) Flory, P. J., *Statistical Mechanics of Chain Molecules*. Wiley Interscience: New York, 1969.
(71) Page, M. I.; Jencks, W. P., *Proc. Natl. Acad. Sci. USA* **1971**, *68*, 1678-1683.
(72) Matcha, K.; Maity, S.; Malik, C. K.; Ghosh, S., *Tetrahedron Lett.* **2010**, *51*, 2754-2757.
(73) Malik, C. K.; Yadav, R. N.; Drew, M. G. B.; Ghosh, S., *J. Org. Chem.* **2009**, *74*, 1957-1963.
(74) Aljarilla, A.; Plumet, J., *Heterocycles* **2009**, *77*, 1333-1340.
(75) Bieniek, M.; Michrowska, A.; Usanov, D. L.; Grela, K., *Chem. Eur. J.* **2008**, *14*, 806-818.
(76) Forbes, M. D. E.; Patton, J. T.; Myers, T. L.; Maynard, H. D.; Smith, D. W., Jr.; Schulz, G. R.; Wagener, K. B., *J. Am. Chem. Soc.* **1992**, *114*, 10978-10980.
(77) Ivin, K. J., *J. Polym. Sci., Part A* **2000**, *38*, 2137-2146.
(78) Höcker, H.; Reimann, W.; Reif, L.; Riebel, K., *J. Mol. Catal.* **1980**, *8*, 191-202.
(79) Constable, D. J. C.; Jimenez-Gonzalez, C.; Henderson, R. K., *Org. Process Res. Dev.* **2007**, *11*, 133-137.

(80) Shu, C.; Zeng, X.; Hao, M.-H.; Wei, X.; Yee, N. K.; Busacca, C. A.; Han, Z.; Farina, V.; Senanayake, C. H., *Org. Lett.* **2008**, *10*, 1303-1306.
(81) Monfette, S.; Fogg, D. E., Ring-Closing Metathesis in the Synthesis of Medium and Large Rings: Challenges and Implications for Sustainable Synthesis. In *Green Metathesis Chemistry, NATO Science Series II*, Dragutan, V.; Demonceau, A.; Dragutan, I.; Finkelshtein, E. S., Eds. Springer Verlag: 2009.
(82) Marsella, M. J.; Maynard, H. D.; Grubbs, R. H., *Angew. Chem., Int. Ed. Engl.* **1997**, *36*, 1101-1103.
(83) Fürstner, A., *Eur. J. Org. Chem.* **2004**, 943-958.
(84) Cheung, L. L.; Marumoto, S.; Anderson, C. D.; Rychnovsky, S. D., *Org. Lett.* **2008**, *10*, 3101-3104.
(85) Akine, S.; Kagiyama, S.; Nabeshima, T., *Inorg. Chem.* **2007**, *46*, 9525-9527.
(86) Shima, T.; Hampel, F.; Gladysz, J. A., *Angew. Chem., Int. Ed.* **2004**, *43*, 5537-5540.
(87) Nawara, A. J.; Shima, T.; Hampel, F.; Gladysz, J. A., *J. Am. Chem. Soc.* **2006**, *128*, 4962-4963.
(88) de Quadras, L.; Hampel, F.; Gladysz, J. A., *Dalton Trans.* **2006**, 2929-2933.
(89) Skopek, K.; Barbasiewicz, M.; Hampel, F.; Gladysz, J. A., *Inorg. Chem.* **2008**, *47*, 3474-3476.
(90) Dietrich-Buchecker, C.; Jimenez-Molero, M. C.; Sartor, V.; Sauvage, J.-P., *Pure Appl. Chem.* **2003**, *75*, 1383-1393.
(91) Frey, J.; Kraus, T.; Heitz, V.; Sauvage, J.-P., *Chem. Commun.* **2005**, 5310-5312.
(92) Frey, J.; Kraus, T.; Heitz, V.; Sauvage, J.-P., *Chem. Eur. J.* **2007**, *13*, 7584-7594.
(93) Chuchuryukin, A. V.; Chase, P. A.; Dijkstra, H. P.; Suijkerbuijk, B.; Mills, A. M.; Spek, A. L.; van Klink, G. P. M.; van Koten, G., *Adv. Synth. Catal.* **2005**, *347*, 447-462.
(94) Chuchuryukin, A. V.; Dijkstra, H. P.; Suijkerbuijk, B. M. J. M.; Klein Gebbink, R. J. M.; van Klink, G. P. M.; Mills, A. M.; Spek, A. L.; van Koten, G., *Angew. Chem., Int. Ed.* **2003**, *42*, 228-230.
(95) Song, K. H.; Kang, S. O.; Ko, J., *Chem. Eur. J.* **2007**, *13*, 5129-5134.
(96) Kilbinger, A. F. M.; Cantrill, S. J.; Waltman, A. W.; Day, M. W.; Grubbs, R. H., *Angew. Chem., Int. Ed.* **2003**, *42*, 3281-3285.
(97) Hou, H.; Leung, K. C. F.; Lanari, D.; Nelson, A.; Stoddart, J. F.; Grubbs, R. H., *J. Am. Chem. Soc.* **2006**, *128*, 15358-15359.
(98) Youm, K.-T.; Nguyen, S. B. T.; Hupp, J. T., *Chem. Commun.* **2008**, 3375-3377.
(99) Wakabayashi, R.; Kubo, Y.; Hirata, O.; Takeuchi, M.; Shinkai, S., *Chem. Commun.* **2005**, 5742-5744.
(100) Rudzevich, Y.; Cao, Y.; Rudzevich, V.; Bohmer, V., *Chem. Eur. J.* **2008**, *14*, 3346-3354.
(101) van Gerven, P. C. M.; Elemans, J. A. A. W.; Gerritsen, J. W.; Speller, S.; Nolte, R. J. M.; Rowan, A. E., *Chem. Commun.* **2005**, 3535-3537.
(102) Pentzer, E. B.; Gadzikwa, T.; Nguyen, S. T., *Org. Lett.* **2008**, *10*, 5613-5615.
(103) Lee, L.-S.; Ou, H.-J.; Hsu, H.-L., *Fluid Phase Equilib.* **2005**, *231*, 221-230.
(104) Lysenko, Z.; Maughon, B. R.; Mokhtar-Zadeh, T.; Tulchinsky, M. L., *J. Organomet. Chem.* **2006**, *691*, 5197-5203.
(105) van der Eide, E. F.; Romero, P. E.; Piers, W. E., *J. Am. Chem. Soc.* **2008**, *130*, 4485-4491.
(106) Ulman, M.; Grubbs, R. H., *J. Org. Chem.* **1999**, *64*, 7202-7207.

(107) Sanford, M. S.; Love, J. A.; Grubbs, R. H., *J. Am. Chem. Soc.* **2001**, *123*, 6543-6554.
(108) Monfette, S.; Crane, A. K.; Duarte Silva, J. A.; Facey, G. A.; dos Santos, E. N.; Araujo, M. H.; Fogg, D. E., *Inorg. Chim. Acta* **2010**, *363*, 481-486.
(109) Christoffers, J.; Oertling, H.; Fischer, P.; Frey, W., *Tetrahedron* **2003**, *59*, 3769-3778.
(110) Srikrishna, A.; Dethe, D. H., *Tetrahedron Lett.* **2005**, *46*, 3381-3383.
(111) Lee, C. W.; Grubbs, R. H., *Org. Lett.* **2000**, *2*, 2145-2147.
(112) Fürstner, A.; Thiel, O. R.; Ackermann, L., *Org. Lett.* **2001**, *3*, 449-451.
(113) Alcaide, B.; Almendros, P.; Luna, A., *Chem. Rev.* **2009**, *109*, 3817-3858.
(114) Fürstner, A.; Thiel, O. R.; Ackermann, L.; Schanz, H.-J.; Nolan, S. P., *J. Org. Chem.* **2000**, *65*, 2204-2207.
(115) Bourgeois, D.; Pancrazi, A.; Nolan, S. P.; Prunet, J., *J. Organomet. Chem.* **2002**, *643-644*, 247-252.
(116) Courchay, F. C.; Sworen, J. C.; Ghiviriga, I.; Abboud, K. A.; Wagener, K. B., *Organometallics* **2006**, *25*, 6074-6086.
(117) Petkovska, V. I.; Hopkins, T. E.; Powell, D. H.; Wagener, K. B., *Macromolecules* **2005**, *38*, 5878-5885.
(118) Arisawa, M.; Kato, C.; Kaneko, H.; Nishida, A.; Nakagawa, M., *Perkin 1* **2000**, 1873-1876.
(119) Torisawa, Y.; Hashimoto, A.; Nakagawa, M.; Hino, T., *Tetrahedron Lett.* **1989**, *30*, 6549-6550.
(120) Commercial software programs designed to predict NMR shifts on the basis of Shoolery's rules were found to be limited by their inability to take into account the effects of rigidity and ring strain. Databases that utilize a fragment approach for empirical prediction of peak positions likewise proved unreliable, though they will undoubtedly improve as database volumes increase.
(121) Pregosin, P. S.; Kumar, P. G. A.; Fernandez, I., *Chem. Rev.* **2005**, *105*, 2977-2998.
(122) Schlorer, N. E.; Cabrita, E. J.; Berger, S., *Angew. Chem. Int. Ed.* **2002**, *41*, 107-109.
(123) Pelta, M. D.; Barjat, H.; Morris, G. A.; Davis, A. L.; Hammond, S. J., *Magn. Reson. Chem.* **1998**, *36*, 706-714.
(124) Lee, D.; Sello, J. K.; Schreiber, S. L., *J. Am. Chem. Soc.* **1999**, *121*, 10648-10649.
(125) Blacquiere, J. M.; Jurca, T.; Weiss, J.; Fogg, D. E., *Adv. Synth. Catal.* **2008**, *350*, 2849-2855.
(126) Louie, J.; Grubbs, R. H., *Organometallics* **2002**, *21*, 2153-2164.
(127) P'Pool, S. J.; Schanz, H.-J., *J. Am. Chem. Soc.* **2007**, *129*, 14200-14212.
(128) Stark, A.; Ajam, M.; Green, M.; Raubenheimer, H. G.; Ranwell, A.; Ondruschka, B., *Adv. Synth. Catal.* **2006**, *348*, 1934-1941.
(129) Bieniek, M.; Bujok, R.; Cabaj, M.; Lugan, N.; Lavigne, G.; Arlt, D.; Grela, K., *J. Am. Chem. Soc.* **2006**, *128*, 13652-13653.
(130) Slugovc, C.; Demel, S.; Stelzer, F., *Chem. Commun.* **2002**, 2572-2573.
(131) Hillmyer, M. A.; Laredo, W. R.; Grubbs, R. H., *Macromolecules* **1995**, *28*, 6311-6316.
(132) Liu, W.; Nichols, P. J.; Smith, N., *Tetrahedron Lett.* **2009**, *50*, 6103-6105.
(133) Burdett, K. A.; Harris, L. D.; Margl, P.; Maughon, B. R.; Mokhtar-Zadeh, T.; Saucier, P. C.; Wasserman, E. P., *Organometallics* **2004**, *23*, 2027-2047.
(134) Fürstner, A.; Ackermann, L.; Beck, K.; Hori, H.; Koch, D.; Langemann, K.; Liebl, M.; Six, C.; Leitner, W., *J. Am. Chem. Soc.* **2001**, *123*, 9000-9006.
(135) Goldring, W. P. D.; Hodder, A. S.; Weiler, L., *Tetrahedron Lett.* **1998**, *39*, 4955-4958.

(136) Ritter, T.; Hejl, A.; Wenzel, A. G.; Funk, T. W.; Grubbs, R. H., *Organometallics* **2006**, *25*, 5740-5745.
(137) Love, J. A.; Sanford, M. S.; Day, M. W.; Grubbs, R. H., *J. Am. Chem. Soc.* **2003**, *125*, 10103-10109.
(138) Galli, C.; Illuminati, G.; Mandolini, L.; Tamborra, P., *J. Am. Chem. Soc.* **1977**, *99*, 2591-2597.
(139) Kirkland, T. A.; Grubbs, R. H., *J. Org. Chem.* **1997**, *62*, 7310-7318.
(140) Kamau, S. D.; Hodge, P.; Hall, A. J.; Dad, S.; Ben-Haida, A., *Polymer* **2007**, *48*, 6808-6822.
(141) Bielawski, C. W.; Benitez, D.; Morita, T.; Grubbs, R. H., *Macromolecules* **2001**, *34*, 8610-8618.
(142) Hoye, T. R.; Promo, M. A., *Tetrahedron Lett.* **1999**, *40*, 1429-1432.
(143) Courchay, F. C.; Sworen, J. C.; Wagener, K. B., *Macromolecules* **2003**, *36*, 8231-8239.
(144) Lehman, S. E., Jr.; Wagener, K. B., *Organometallics* **2005**, *24*, 1477-1482.
(145) Petkovska, V. I.; Hopkins, T. E.; Powell, D. H.; Wagener, K. B., *Anal. Chem.* **2006**, *78*, 3624-3631.
(146) Hong, S. H.; Wenzel, A. G.; Salguero, T. T.; Day, M. W.; Grubbs, R. H., *J. Am. Chem. Soc.* **2007**, *129*, 7961-7968.
(147) Smith, A. B., III; Basu, K.; Bosanac, T., *J. Am. Chem. Soc.* **2007**, *129*, 14872-14874.
(148) Fürstner, A.; Schlede, M., *Adv. Synth. Catal.* **2002**, *344*, 657-665.
(149) Fürstner, A.; Thiel, O. R.; Lehmann, C. W., *Organometallics* **2002**, *21*, 331-335.
(150) Fürstner, A.; Langemann, K., *J. Am. Chem. Soc.* **1997**, *119*, 9130-9136.
(151) Yang, Q.; Xiao, W.-J.; Yu, Z., *Org. Lett.* **2005**, *7*, 871-874.
(152) Li, Y.; Zhang, T.; Li, Y.-L., *Tetrahedron Lett.* **2007**, *48*, 1503-1505.
(153) Selvakumar, N.; Kumar, P. K.; Reddy, K. C. S.; Chary, B. C., *Tetrahedron Lett.* **2007**, *48*, 2021-2024.
(154) Xu, Z.; Johannes, C. W.; Houri, A. F.; La, D. S.; Cogan, D. A.; Hofilena, G. E.; Hoveyda, A. H., *J. Am. Chem. Soc.* **1997**, *119*, 10302-10316.
(155) Gessler, S.; Randl, S.; Blechert, S., *Tetrahedron Lett.* **2000**, *41*, 9973-9976.
(156) Lemarchand, A.; Bach, T., *Tetrahedron* **2004**, *60*, 9659-9673.
(157) Rivkin, A.; Biswas, K.; Chou, T.-C.; Danishefsky, S. J., *Org. Lett.* **2002**, *4*, 4081-4084.
(158) Yamamoto, K.; Biswas, K.; Gaul, C.; Danishefsky, S. J., *Tetrahedron Lett.* **2003**, *44*, 3297-3299.
(159) Crimmins, M. T.; Brown, B. H., *J. Am. Chem. Soc.* **2004**, *126*, 10264-10266.

4. Understanding the role of the anionic ligands on Ru metathesis catalysts: synthesis, characterization and reactivity of catecholate catalysts*

4.1 Introduction

Ruthenium-catalyzed olefin metathesis is one of the most powerful methods for constructing C=C bonds. The groundbreaking advances achieved with the Grubbs catalysts in organic synthesis[1-10] have tended to obscure some of their important limitations, however. These include: (1) the control over the olefin geometry (E vs. Z), (2) the enantioselectivity of the products during asymmetric metathesis and (3) the typically low turnover number of these catalysts. Mixtures of isomeric products require separation in a slow and unattractive process while the development of highly active yet robust catalysts would also aid in reducing the typical catalyst loadings (>5 mol%)[11-14] employed in organic synthesis. While such loadings are not always necessary, and are employed to ensure complete reaction, they nevertheless complicate purification of organic products (see Chapter 6), and contribute to the high costs on production scale.

Improving the selectivity and lifetime of the Grubbs catalysts has been sought chiefly through catalyst design. The catalytically active species characteristic of the Grubbs catalysts is the four-coordinate complex $RuCl_2(L)(=CHR)$. Improvements in catalyst lifetime or selectivity thus require redesign of one or more of these four ligands. By far, most studies have focused on the neutral ligands.[15,16] As Chapter 1 described the current progress made in this area, only the key aspects will be recapitulated here. Barring issues of catalyst initiation, modification of the alkylidene ligand will have limited impact on lifetime or selectivity since this ligand is lost after one turnover. Modification of the neutral L ligand, which remains bound to the metal throughout the catalytic cycle, is more useful, and has thus received much attention.[15,16] The introduction of *N*-heterocyclic carbenes (NHC) as ligands in second-generation Grubbs catalysts, in 1998, was groundbreaking.[17-19] The resulting catalysts (e.g. **Ru-4b**) are almost all characterized by dramatically higher metathesis activity, and

* Much of the work described in this Chapter has been published: (a) Monfette, S.; Fogg, D. E., *Organometallics* **2006,** *25*, 1940-1944. (b) Monfette, S.; Duarte Silva, J. A.; Gorelsky, S. I.; Dalgarno, S. J.; dos Santos, E. N.; Araujo, M. H.; Fogg, D. E., *Can. J. Chem.* **2009,** *87*, 361-367. (c) Monfette, S.; Camm, K. D.; Gorelsky, S. I.; Fogg, D. E., *Organometallics* **2009,** *28*, 944-946.

heightened lifetime relative to their first-generation counterpart. Subsequent modifications of the NHC ligands have led to hundreds of different Ru-NHC catalysts,[15,16] of which a few exhibit improved reactivity[20-24] or selectivity[25-34] relative to the benchmark system **Ru-4b**. Unsurprisingly, NHC ligands remain the neutral ligand of choice in current Ru metathesis catalysts.

As exemplified within Schrock molybdenum catalysts,[35,36] derivatization of the anionic ligands offers a powerful means to modulate both catalyst activity and selectivity. As the ubiquitous chloride ligands of the Grubbs catalysts are implicated in catalyst decomposition,[37-40] introduction of pseudohalide ligands could provide a powerful means of improving both catalyst lifetime as well as selectivity. Given these prospects, and the limited improvements gained by modification of the NHC ligand over the last 12 years, it is perhaps surprising that the anionic ligands have been relatively little examined for their potential in ruthenium-catalyzed olefin metathesis. The early finding that pseudohalide catalysts exhibited lower rates of metathesis relative to their dichloride parents may have contributed to the limited developments in this area.[1] The pseudohalide ligands are not necessarily the cause of the modest catalytic results, however. These are traced back to three different design flaws: (1) excessive crowding of the metal center, (2) the presence of four non-labile ligands in the basal plane and (3) an active species with neutral donor of lower basicity relative to (e.g.) PCy_3 or NHC ligands.[1] While the first two prevent interaction of the metal complex with an olefin substrate, the third presumably disfavors formation of the metallacyclobutane intermediate. The presence of one or a combination of any of these three factors leads to poor catalytic results, irrespective of the nature of the anionic ligands.

Attesting to the benefits gained by understanding the role of the ligands on the active catalyst, recent examples of pseudohalide metathesis catalysts, constructed based on the above three parameters, show promising results. A significant contribution in this area comes from the work of the Fogg group, which focused chiefly on the incorporation of aryloxide ligands onto the Grubbs catalysts (e.g. **Ru-7**, Chart 1a).[41-44] The resulting bis-pentafluorophenoxide (**Ru-7a**) or pentabromophenoxide (**Ru-7b**) catalysts showed, respectively, improved lifetime[44] or activity[43] relative to parent **Ru-6a**. Thus, **Ru-7a** effected 40,000 turnovers in the RCM of diethyl diallyl malonate (0.5 M diene, refluxing $CDCl_3$, 24 h, 5×10^{-4} mol% [Ru]) while **Ru-7b** outperforms its dichloride analog in RCM

macrocyclization of flexible dienes (see Chapter 3) as well as enyne metathesis.[43] Additional benefits come from the ease of removal of these aryloxide catalysts following reaction, a function of the greater polarity of the Ru-OAr bond. A single cycle of silica gel chromatography is sufficient to bring the ruthenium content of organic products below 100 ppm,[43] where much lengthier efforts are required to remove first-generation **Ru-3** to comparable levels.[45-48]

Additional work by other groups was directed at the synthesis of carboxylate[49-54], sulfonate,[55] alkoxide[56,57] and Schiff base[58-61] complexes (Chart 1b-g). The carboxylate and sulfonate catalysts show comparable performance to the benchmark **Ru-4b/5b** systems in RCM of common rings.[52,55] Interestingly, the lifetime of these catalysts is closely similar to that of the dichloride parents, despite substitution of both chloride atoms. As expected from the chelating nature of the bidentate *O,N*-alkoxide or Schiff base ligands (Chart 1d-e), decoordination of the nitrogen donor is slow at room temperature, which retards creation of the vacant site required for metathesis.[53,56,59,61,62] Upon heating or use of additives (e.g. Brönsted or Lewis acids), these catalysts show comparable, or lower performances with respect to the benchmark systems. Other types of chelating, mono-anionic ligands (*O,O* and *O,P*; Chart 1f-g) have been recently investigated by the Grubbs group.[53] In line with the *O,N* ligands, poor initiation was found for both *O,O* and *O,P* catalysts at room temperature. Although addition of CuCl significantly improved conversion profiles by sequestration of the neutral phosphine ligands in the case of the *O,P* catalyst, no beneficial effect was noted for the *O,O* catalyst. Grubbs attributed this to the lower affinity of the CuCl towards the "hard" oxygen atom.[53]

References page 158

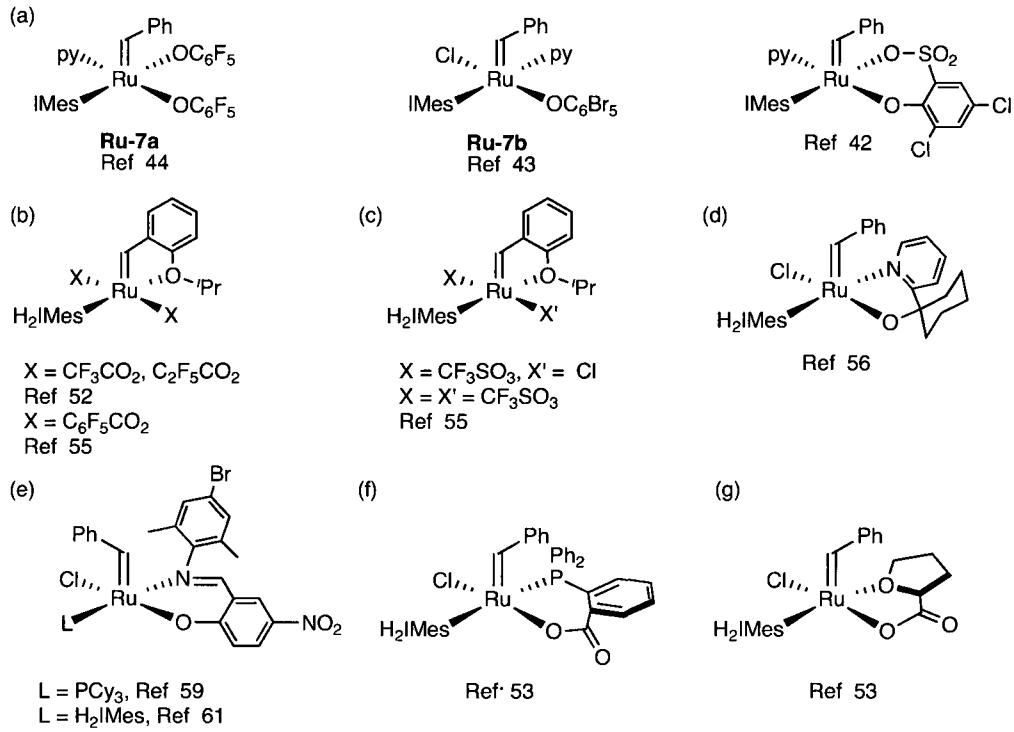

Chart 1. Selected examples of Ru metathesis catalysts bearing (a) aryloxide, (b) carboxylate, (c) sulfonate, (d) alkoxide, (e) Schiff base, (f) *O,P* and (g) *O,O* ligands. py = pyridine.

Clearly, the nature of the anionic ligands strongly affects the activity of the resulting metathesis catalyst. In general, however, specific design criteria required for maximum metathesis activity remain poorly understood. To date, only a handful of experimental studies have examined the electronic effect of the anionic ligands on metathesis activity within the ruthenium family of catalysts.[63-65] While Schrock demonstrated in early work that the activity of his group 6 catalysts can be increased by orders of magnitude by reducing the pK_a of the alkoxide ligand (this serving to enhance the rate of olefin binding),[66,67] no such unequivocal relationship has been established for the ruthenium system. Grubbs has suggested, however, that the same behavior should hold true for the ruthenium catalysts. Likewise, in a quantitative structure-activity relationship study, Jensen and co-workers proposed that catalyst activity may be maximized where electron-withdrawing anionic ligands can lower the barrier to formation of the Ru^{IV} intermediate.[68] Consistent with this suggestion is the trend in RCM rates reported by the Grubbs group for $RuX_2(=CHCH=CPh_2)(PCy_3)_2$: Cl > Br > I.[63] However, the increase in steric effects along this series, which runs counter to the inductive effect of the halide ligands, cannot be discounted.

Moreover, a contrary trend (Cl < Br ~ I) was reported for derivatives of second-generation **Ru-4b**,[64] while the Mol group found no correlation between activity and proligand pK_a within a series of carboxylate derivatives of first-generation **Ru-3**.[65]

For the rational development of new pseudohalide metathesis catalysts, an unambiguous understanding of how the anionic ligands exert an electronic influence on catalytic activity is essential. At the most fundamental level, a deeper analysis of the electronic bonding between the aryloxide ligand(s) and the ruthenium center is required. Thus, the first part of this Chapter examines the changes in electronic structure that result from replacing the chloride ligands by an aryloxide group, within a model Ru(*o*-cat)$(PPh_3)_3$ complex. Key to the isolation of the electronic influence of the OAr ligand in these systems is our choice of a catecholate ligand platform, which enables examination of electronic parameters while excluding any potential steric effects (e.g. coordination of an *o*-halogen group as in perbromoaryloxide **Ru-7b**).[69] The second half of this chapter exploits this deconvolution of steric and electronic effects to isolate, for the first time, the electronic influence of the anionic ligands on metathesis activity within a family of Ru-benzylidene catalysts of general formula Ru(*o*-cat)(CHPh)(IMes)(py).

4.2 Analysis of Ru-OAr bonding within a five-coordinate Ru^{II} complex

Initial studies focused on the evaluation of the electronic interactions specific to the basal Ru-aryloxide moiety within the square pyramidal coordination geometry. To limit unnecessary complications, the variety of additional bonding interactions present in the aryloxide catalysts **Ru-7** (e.g. Ru=CHPh, Ru-NHC) was excluded. To accomplish this goal, a simple five coordinate Ru^{II} complex bearing aryloxide ligand(s) was sought. While five-coordinate ruthenium complexes containing monodentate phosphine and a phenoxide ligand (e.g. RuX(OPh)$(PPh_3)_3$) would be suitable candidates, these are unstable with respect to isomerization to catalytically inactive piano-stool structures (Scheme 1).[70,71] In earlier work, $\sigma-\pi$ isomerization was curbed by use of an electron-deficient aryloxide ligand such as perhaloaryloxide; (see Chart 1). However, the halogen atoms can obscure the steric and electronic influence of the aryloxide ligand itself. This study therefore focused on the

catecholate ligand, which resists σ–π isomerization, owing to its chelate ring size (Section 4.2.2). Specifically, the complex Ru(*o*-cat)$(PPh_3)_3$ was targeted as a model for this study.

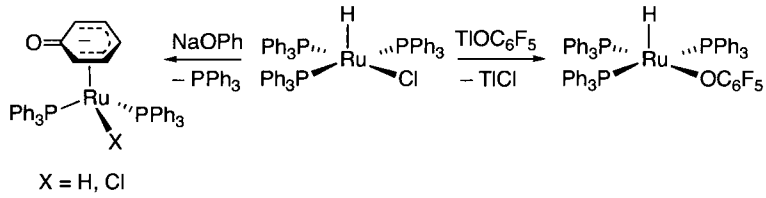

Scheme 1. Electron-rich phenoxides undergo σ–π isomerization while electron-deficient phenoxides form stable σ complexes.[44,70,71]

4.2.1 Synthesis and characterization of Ru(κ²-$O_2C_6H_4$)$(PPh_3)_3$

Addition of solid thallium catecholate (**38a**) to a homogeneous solution of $RuCl_2(PPh_3)_3$ (**Ru-1**) in THF causes a color change from brown to deep blue within 1 h at room temperature, accompanied by precipitation of TlCl (Scheme 2). $^{31}P\{^1H\}$ NMR analysis of the crude reaction mixture indicated clean formation of a single ruthenium product, without liberation of PPh_3. The suspension was filtered through Celite, and the ruthenium product was isolated in 94% yield following precipitation from THF-hexanes. In some cases, a small proportion of an unidentified impurity was observed by ^1H and ^{31}P NMR spectroscopy even after reprecipitation (^1H NMR: poorly resolved multiplet, 7.90–7.84 ppm; $^{31}P\{^1H\}$ NMR: s, 26.1 ppm; C_6D_6). It is easily removed by passing a THF solution of the crude product through a short plug of neutral alumina. The major product of the reaction was identified as Ru(κ²-$O_2C_6H_4$)$(PPh_3)_3$ (**Ru-2a**) on the basis of spectroscopic, crystallographic (Figure 2) and combustion analysis. Several trials were necessary in order to obtain satisfactory elemental analysis, owing to the acute air-sensitivity of **Ru-2a** even in the solid state.

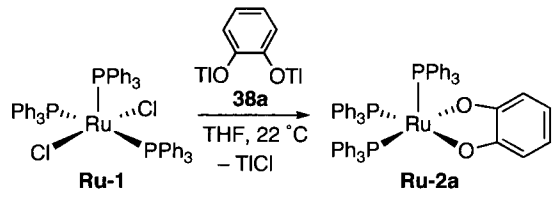

Scheme 2. Synthesis of **Ru-2a**.[72]

The anaerobic charge-transfer (CT) MALDI-TOF[73] mass spectrum of **Ru-2a** revealed a well-defined isotope pattern for $[M–PPh_3]^{+\bullet}$ at *m/z* 734.4 Da. The facile elimination of one triphenylphosphine group in the gas phase probably reflects the steric pressure within the

three approximately facial PPh_3 ligands. Retention of all three of these ligands in the solid state is confirmed by X-ray analysis (Figure 2). Their retention in solution is inferred from the ^1H NMR integration values, as well as the absence of a signal for free PPh_3 in the $^{31}P\{^1H\}$ NMR spectrum of the crude reaction mixture. Surprisingly, however, a sharp $^{31}P\{^1H\}$ NMR *singlet* was observed at 55.1 ppm, rather than the A_2X pattern for the expected square pyramidal geometry shown in Scheme 2, which is confirmed as the energetic minimum by DFT analysis. Notably, this singlet undergoes no change in multiplicity even on cooling to –90 °C (C_7D_8). The steric constraints in **Ru-2a** may favor a greater degree of distortion in solution, possibly through a Berry pseudorotation of the square pyramidal coordination geometry (Figure 1).

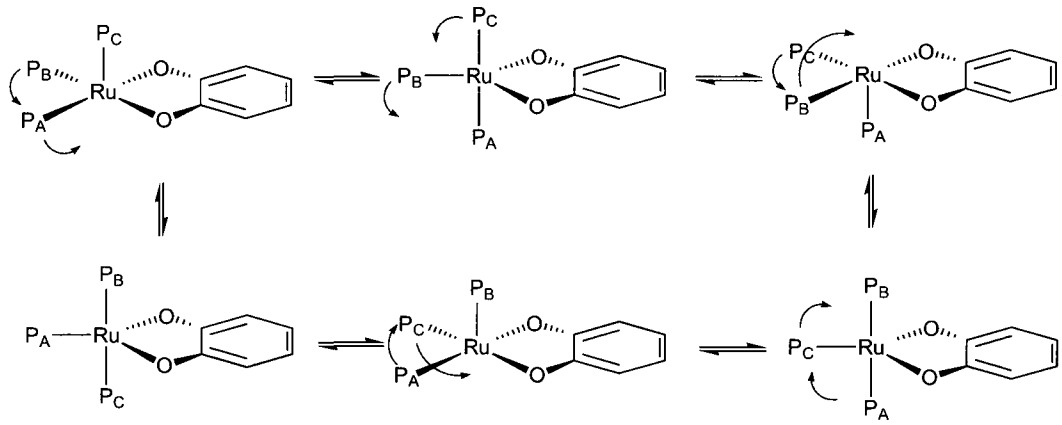

Figure 1. A Berry pseudorotation may average the phosphine environments within **Ru-2a**.

Blocky blue crystals of **Ru-2a** suitable for X-ray analysis were obtained by slow evaporation of a benzene solution. Only one five-coordinate Ru-catecholate complex, Ru(*o*-cat)$_2$(≡N), has previously been structurally characterized.[74] In contrast with the slightly distorted square pyramidal geometry of Ru(*o*-cat)$_2$(≡N), the structure of **Ru-2a** exhibits significant deviations, though it remains closer to square pyramidal than trigonal bipyramid at the metal center, as judged by the tau (τ)* parameter[75] value of 0.22 for **Ru-2a**. The distorted geometry of **Ru-2a** is unsurprising, given the rigidity and small bite angle of the catecholate ligand, and the steric interaction between the three cis-PPh_3 ligands. In

* The τ parameter assesses whether a given five-coordinate complex is closer to the square-pyramidal or trigonal bipyramidal geometry. The τ parameter is calculated by substracting the two largest interligand angles within the complex and dividing the result by 60. A τ values approaching 0 is indicative of a square pyramid; a value approaching 1 indicates a trigonal bipyramidal complex.

comparison, the crystal structure of dichloride **Ru-1**, containing a meridional arrangement of these ligands, shows little distortion in the bond angles about ruthenium.[76] Similarly, six-coordinate Ru^{II} catecholate complexes containing smaller neutral ligands such as PMe_3[77] or pyridine[78] form reasonably regular octahedral complexes, as indicated by small deviations from the expected bond angles.

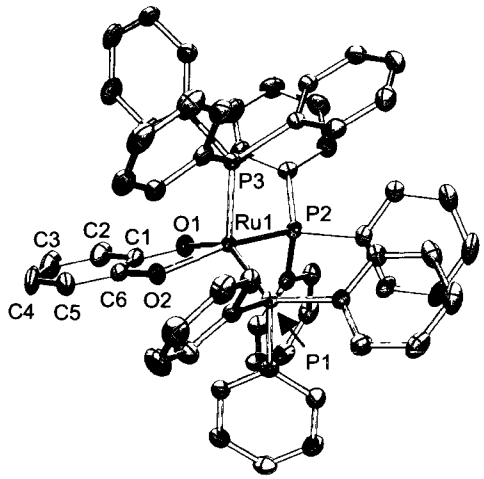

Figure 2. ORTEP representation of **Ru-2a** (the crystals were grown in collaboration with Joao Duarte Silva, a visiting Ph.D. student in the Fogg group). Thermal ellipsoids are shown at 50% probability. Hydrogen atoms and benzene solvate are omitted for clarity. Only relevant atoms are labeled here. See Figure A-1 in the Appendix B for full structural detail.

Two "basal" PPh_3 ligands lie trans to the catecholate oxygen donors (P(1)-Ru(1)-O(1) = 144.61(4)°; P(2)-Ru(1)-O(2) = 158.53(4)°), with the third phosphine approximately apical (P(3)-Ru(1)-P(1) = 97.766(17)°; P(3)-Ru(1)-P(2) = 99.561(17)°; P(3)-Ru(1)-O(1) = 116.13(4)°; P(3)-Ru(1)-O(2) = 98.45(4)°), trans to the vacant site. The extent of distortion is also evident from the 0.05 Å difference in length between the two Ru-P bonds in the basal plane (Ru(1)-P(1) 2.2954(5) Å; Ru(1)-P(2) 2.3496(5) Å). The apical Ru-P bond (Ru(1)-P(3) 2.2527(5) Å) is shorter by 0.04 Å-0.09 Å. This is *not* due to population of the Ru-P(3) σ* orbital (LUFO+1 of $[Ru(PPh_3)_3]^{2+}$; see below): while there is indeed a 19% population of this orbital, the basal Ru-P bonds are likewise populated, and to a greater extent (22% for LUFO; 11% for LUFO+2). Instead, the decreased bond length is due to the apical position of the phosphine ligand involved, and the consequent absence of a trans ligand that would give rise to a competing donor-acceptor interaction. A similar effect was found for the apical Ru-P bond in the dichloride analogue **Ru-1**.[76]

The C-O bond lengths within **Ru-2a** (1.350(2) Å and 1.345(2) Å for C(1)-O(1) and C(6)-O(2) respectively) are within the range of 1.34-1.47 Å reported for Ru-catecholate complexes; benzoquinone complexes exhibit shorter C-O bond lengths (1.27-1.31 Å).[79,80] The magnitude and uniformity of C-C bond lengths within the $(O_2C_6H_4)^{2-}$ ligand (1.372(4)-1.407(4) Å) likewise support formulation of **Ru-2a** as a Ru-catecholate complex. Infrared analysis revealed a band for ν_{CO} at 1270 cm^{-1} (Nujol), which is not observed for starting **Ru-1**, but present in the IR spectra of the catecholate salts.

4.2.2 Probing the electronic structure of Ru-2a by UV-Vis spectroscopy and TD-DFT calculations

To establish the key metal-ligand bonding contributions, the electronic structure of **Ru-2a** was analyzed experimentally by UV-vis spectroscopy, and theoretically by use of time-dependent DFT[81-83] calculations (TD-DFT) at the B3LYP/DZVP level of theory. Further motivation for this analysis stems from the unusual blue color of **Ru-2a**, rare in Ru^{II} complexes,[84-91] which could provide added insight into its electronic structure. A fragment molecular orbital (FMO) analysis enabled quantification of charge donation. Orbital interactions were considered in terms of dative bonds between the highest occupied fragment orbitals (HOFOs) of the $(O_2C_6H_4)^{2-}$ ligand, and the lowest unoccupied fragment orbitals (LUFOs) of the metal fragment $[Ru(PPh_3)_3]^{2+}$.

The calculated electronic spectrum of **Ru-2a** is in very good agreement with the experimental spectrum (Figure 3). The latter, measured in THF, is comprised of three absorption maxima of near-identical intensity (16,000, 18,400 and 23,500 cm^{-1}), whereas TD-DFT predicts three principal bands (16,500, 19,700, 23,200 cm^{-1}), of which the latter two overlap with weaker bands at 18,000 and 23,600 cm^{-1}. The agreement between experimental and calculated frequencies is thus much better than the more typical agreement of 2,000 cm^{-1}.[81-83,92] A minor difference in intensity is also evident. The level of theory was therefore deemed appropriate for analysis of the electronic transitions. Electronic excitations contributing to each band are summarized in Table 1.

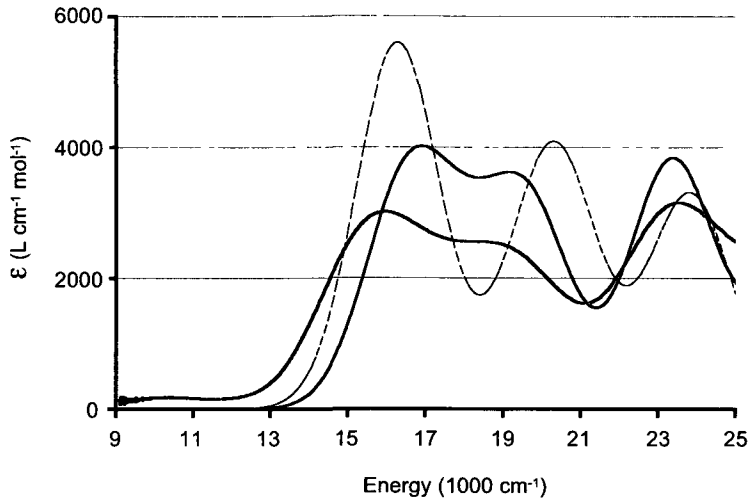

Figure 3. Experimental and calculated electronic spectra for **Ru-2a** (solid black and red lines, respectively), and calculated spectrum for **Ru-2b** (dashed red line).

Table 1. Electron excitation for each band in the visible region.

Experimental[a]	Calculated by TD-DFT (B3LYP/DZVP)		
	Energy[a]	F[b]	Assignment[c]
16.0	16.5	0.0370	H→L (44%), H-2→L (29%), H-1→L (10%)
18.4	18.0	0.0190	H-1→L (57%). H→L (17%)
	19.7	0.0338	H-2→L (45%), H-3→L (24%)
			H→L (15%)
23.5	23.2	0.0272	H-3→L (31%), H-4→L (20%)
			H→L+1 (15%)
	23.6	0.0166	H→L+1 (47%)

[a] Band location in 10^3 cm^{-1}. [b] Oscillator strength. [c] H = HOMO; L = LUMO. Only the major (>10%) parent one-electron excitations are reported. The percentage contributions to wavefunctions of excited states are given in parentheses.

The FMO analysis indicates that formation of **Ru-2a** involves a significant (>2%) change in the electronic population for only three orbitals on the Ru fragment. The following discussion is therefore confined to the metal-based orbital donations that contribute to these three acceptor orbitals. Contributions from ruthenium are cited as the composite of s, p, and d contributions; those from PPh_3 are largely p in character (for individual constituents, see Figure 4). The LUFO is 62% Ru and 38% PPh_3 in character (of the latter, 21% is contributed from the phosphorus atoms); cf. relative contributions of 58% Ru + 42% PPh_3 for LUFO+1, and 59% Ru + 41% PPh_3 for LUFO+2. The population of each of these orbitals increases

from its null value in the non-interacting fragment to 22%, 19% and 11%, respectively, in **Ru-2a**. The LUFO and LUFO+2 orbitals participate in forming the two σ bonds with the ligand, while LUFO+1 forms a π bond (19% × 2 = 0.38 e-). For the catecholate FMOs, turning on the bonding interaction with the ruthenium complex results in a significant change in population for six occupied and one unoccupied orbital. These are the HOFO (–21%; i.e. 21% depopulation), HOFO-1 (–14%), HOFO-2 (–7%), HOFO-3 (–3%), HOFO-6 (–5%), HOFO-7 (–4%), and LUFO (+5% population). Thus, in addition to strong ligand-to-metal charge donation (0.94 e-), formation of the complex involves significant polarization of the electron density on the catecholate ligand, through 5% population of the LUFO. (This point will become highly important in the reactivity studies discussed in Section 4.3.4). This charge distribution description is consistent with the Mulliken population analysis[93-96] and the NPA-derived charges assessed for the catecholate ligand in the complex (-1.06 a.u. and -1.17 a.u., respectively; NPA = natural population analysis, a.u. = atomic units).

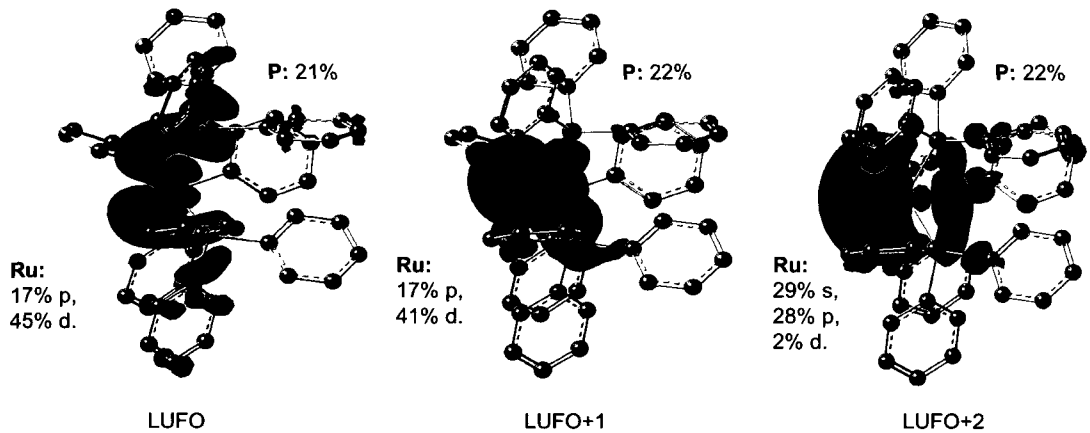

Figure 4. Lowest unoccupied fragment orbitals (LUFOs) of $[Ru(PPh_3)_3]^{2+}$ and their compositions. Individual contributions from PPh_3 phenyl groups are not shown. Isosurface contour value for orbital images = 0.03 au.

The molecular orbitals that contribute to the visible spectrum of **Ru-2a** are summarized in Table 2; visual depictions of the HOMO and LUMO of **Ru-1** and **Ru-2a** are shown in Figure 5. The LUMO is a σ* orbital for the apical Ru-PPh_3 bond, while LUMO+1 consists principally of the aromatic π* orbitals of all three PPh_3 ligands, with a 7% contribution from the Ru 4d orbitals. The low energy of the LUMO of **Ru-2a** derives from the fact that a single (apical) phosphine ligand contributes to this σ* orbital (p_z(P)–d_{z^2}(Ru)), while the other σ*

orbital involves both basal PPh_3 ligands. The HOMO is a π bonding orbital between the catecholate and ruthenium. The HOMO-1, HOMO-2, and HOMO-3 are also dominated by contributions from the catecholate and Ru: these are a largely non-bonding π orbital, a largely σ non-bonding orbital, and a σ–π hybrid, respectively. Finally, HOMO-4 is non-bonding composed of a ruthenium d orbital and the catecholate π orbital.

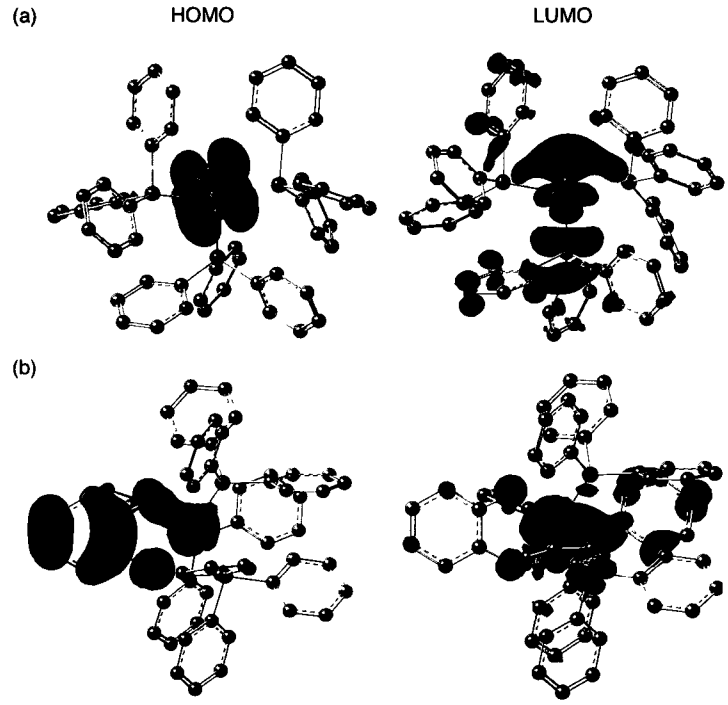

Figure 5. Frontier orbitals for (a) **Ru-1** and (b) **Ru-2a**. Isosurface contour value for orbital images = 0.03 au.

Table 2. Molecular orbital energies (E) and atomic contribution[a] for **Ru-1** and **Ru-2a**.

Orbital	-E (eV)	Ru (%)	PPh_3 (%)	X-ligand (%)
		Ru-1		
LUMO	2.03	47.3	47.6	5.1
HOMO	5.10	55.6	5.9	38.5
		Ru-2a		
LUMO + 1	1.07	7.0	91.5	1.5
LUMO	1.81	38.5	49.1	12.4
HOMO	4.62	12.8	8.5	78.7
HOMO – 1	5.26	34.3	7.9	57.8
HOMO – 2	5.43	46.5	11.8	41.7
HOMO – 3	5.80	53.3	16.9	29.8
HOMO – 4	6.13	59.3	12.9	27.8

[a] Evaluated by Mulliken population analysis.

For four of the five visible bands calculated for **Ru-2a**, the LUMO (σ* orbital of the apical Ru-PPh_3 bond) participates in the electronic excitations. However, the LUMO+1, composed of the π* orbitals of the aromatic rings of the PPh_3 ligands (Table 2), is also implicated in the absorption bands at 23,200 and 23,600 cm^{-1}. To assess whether this orbital plays a significant role in the electronic excitations, the electronic spectrum was calculated for Ru(*o*-cat)$(PMe_3)_3$ **Ru-2b**, in which any potential involvement of the phosphine phenyl groups is eliminated. The calculated spectra for **Ru-2a** and **Ru-2b** are very similar, as shown in Figure 3 (**Ru-2b**: three absorption maxima at 16,300, 20,400 and 23,800 cm^{-1}; cf. the values for **Ru-2a** noted above). This means that the LUMO is more critical to the spectroscopic features in the visible region than is LUMO+1. The intense blue color of **Ru-2a** (ε 3,000 L mol^{-1} cm^{-1}) is thus due to charge transfer from the Ru-catecholate π bond (localized chiefly on catecholate) to the low-lying σ* orbital on the apical Ru-PPh_3 bond. Replacing the two chloride ligands in **Ru-1** by a catecholate reduces the magnitude of the HOMO-LUMO gap, as evidenced by the change in color from brown to blue. Consistent with this, the calculated values drop from -3.06 eV for **Ru-1** to -2.81 eV for **Ru-2a**. The coordination number also affects the energy of the relevant electronic transitions, as noted above; Ru(*o*-cat)$(PMe_3)_4$[77] and Ru(*o*-cat)$(py)_4$,[78] for example, are yellow in color. While crystallographic analysis has demonstrated that a phenyl ring blocks the sixth coordination site in **Ru-1**, the long Ru-H distance of 2.82 Å, which translates into a bond order of 0.03, precludes the presence of an agostic interaction.[97] The explanation of the higher-energy visible transition for **Ru-1** originating from the octahedral coordination was thus excluded. The smaller HOMO-LUMO gap in **Ru-2a** is thus due principally to the higher energy of the HOMO, the Ru-P_{apical} σ* LUMO interaction being conserved, as shown in Figure 5.

4.2.3 Reactivity of Ru-2a towards alkynes

The higher energy of the HOMO in **Ru-2a** might be expected to render this complex a better electron donor, hence increasing its reactivity. Qualitative evidence of this reactivity is readily apparent from the excruciating sensitivity of **Ru-2a** towards oxygen. Exploration of the metathesis activity of complexes bearing the catecholate moiety, under anaerobic conditions, was thus of keen interest. The metal alkylidene ($M=CR_2$) is the key structural feature that allows the well-defined Mo and Ru metathesis catalysts to participate in olefin

metathesis. Thus, an easy, quick and ideally high-yielding route to alkylidene complexes was sought using **Ru-2a** as precursor.

The reported procedure for installation of the alkylidene functionality within **Ru-3** consists in the carbene transfer from phenyldiazomethane (**26**) to **Ru-1** (Scheme 3a).[98] Although the reported yield of this reaction (>99%) seems ideal,[98] in our hands, this synthetic method proceeds in an average yield of 50-70%. This presumably originates from the rapid decomposition, and hence low purity, of the diazo reagent. (Noteworthy, a recent report from the Chirik group suggests that phenyldiazomethane of high purity can be obtained by vacuum pyrolysis of the tosylhydrazone precursor).[99] Additionally, the phenyldiazomethane route demands meticulous manipulation at low temperatures and carries the hazards of working with an unstable and potentially explosive material. This obviously precludes the stocking of a large quantity of the diazo compound, a necessary requirement for reactivity studies.

Alternative methods for installation of the alkylidene moiety[100] include reaction with Ph_2S=CHPh[101] or 2,2-diphenylcyclopropene[102] (Scheme 3b/c), the latter suffering from similar synthetic inconveniences as phenyldiazomethane. The tautomerization of 1-alkynes is another viable route to ruthenacumulenylidenes (Scheme 3d).[38,103] This method is particularly advantageous as 1-alkynes are stable, commercially available and undergo rapid attachment to the metal center.[104] Although cumulenylidenes are well-established as being much less reactive than their benzylidene counterparts,[1,64] their ease of formation can be a key asset in establishing quick routes to alkylidene complexes.[105]

References page 158

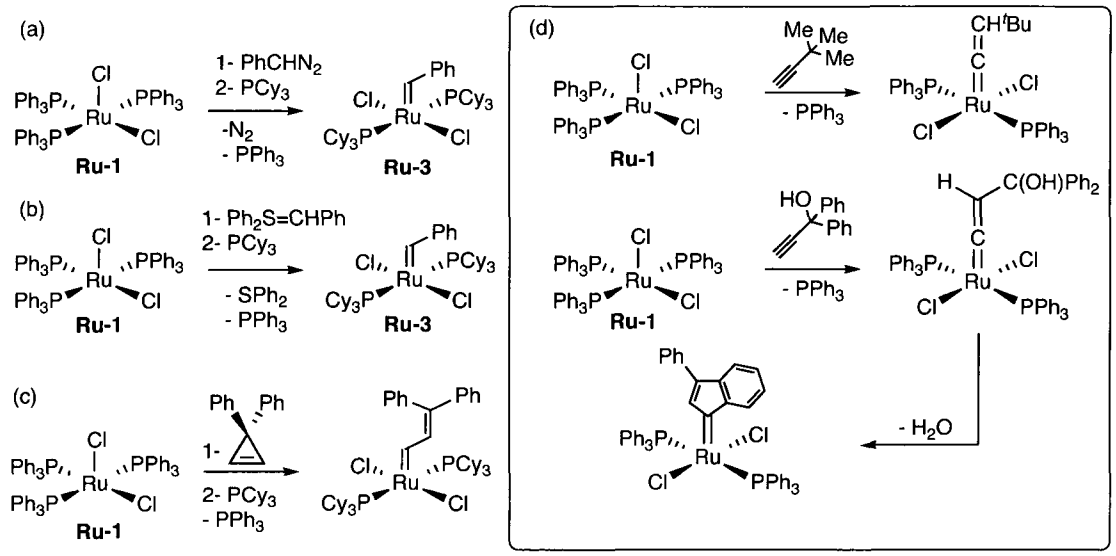

Scheme 3. Synthetic routes to ruthenium alkylidenes by (a) carbene transfer (b) ring-opening of a strained olefin and (c) alkyne tautomerization.[100]

The reactivity of catecholate **Ru-2a** towards 3,3-dimethylbutyne and 1,1-diphenylpropargyl alcohol was studied under various conditions. Experiments were carried out as NMR-scale reactions, and assessed by both ^{1}H and $^{31}P\{^{1}H\}$ NMR analysis (Table 3). Surprisingly, very low reactivity was found between **Ru-2a** and both alkynes. Even under forcing conditions (6 equiv. 3,3-dimethylbutyne, C_6D_6, 60 °C, 72 h; Table 3, Entries 1/2), only unreacted starting **Ru-2a** was observed in the NMR spectra. Similarly, no reaction could be observed between **Ru-2a** and 1,1-diphenyl-2-propyn-1-ol (5 equiv. in C_6D_6, 23 °C, 24 h; Table 3, Entry 3). Upon heating an identical solution to 70 °C, species **Ru-2a** was the sole species observed after 1 h. However, multiple (>10) species were observed by ^{31}P NMR after a total of 17 h (C_6D_6, δ 52.4 –21.9 ppm; Table 3 entries 4/5). No attempts to identify these species were made. These results contrast with prior work showing facile, clean incorporation of 3,3-dimethylbutyne to RuCl(dcypb)(μ-Cl)$_3$Ru(dcypb)(N_2) (dcypb = 1,4-bis(dicyclohexylphosphino) butane) in less than 12 h at room temperature.[38]

Table 3. Reactivity of **Ru-2a** towards alkynes and neutral ligands.[a]

Entry	Reactant	Equiv.	Time (h)	T (°C)	Conv.[b] (%)
1	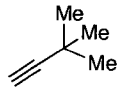	6	18	22	<2
2		6	72	60	<2
3	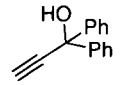	5	24	22	<2
4		5	1	70	<2
5		5	17	70	83
6	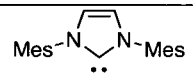	20	24	70	14
7		300	24	22	<2

[a] C_6D_6 was used as solvent in all cases. [b] Determined by $^{31}P\{^1H\}$ NMR analysis by integration against PPh_3=O as internal standard. The $^{31}P\{^1H\}$ NMR singlet for starting **Ru-2a** appears at 55.1 ppm.

The low reactivity of **Ru-2a** towards terminal alkynes may be due to the low lability of the PPh_3 ligands noted above. This is also consistent with the minimal replacement (14%) of the PPh_3 by the more basic IMes ligand even under forcing conditions (20 equiv. in C_6D_6, 70 °C, 24 h; Table 3, Entry 6). Despite low conversions, a single product is obtained, which is characterized by a $^{31}P\{^1H\}$ singlet at 61.5 ppm. The 2:1 integration relative to free PPh_3 (–5.06 ppm; in situ analysis) indicates that only one PPh_3 ligand is replaced by IMes. This new complex is presumed to be $Ru(\kappa^2\text{-}O_2C_6H_4)(PPh_3)_2(IMes)$, however, due to the low conversions to this new product, no attempts to isolate this species were undertaken. While the significant steric demand of IMes could hamper its incorporation onto **Ru-2a**, this complex also resists reaction with pyridine (Table 3, Entry 7). As pyridine readily displaces one PPh_3 ligand within **Ru-1**,[106] failure to do so in the case of **Ru-2a** is indicative of the thermodynamic stability of this complex. Indeed, the stronger donation and back-donation involving the basal PPh_3 ligands in **Ru-2a** increase the binding energy for this ligand (–16.0 kcal mol^{-1} in **Ru-2a** vs. –10.6 kcal mol^{-1} in **Ru-1**). The weaker donation from the catechol ligand relative to chloride, anticipated on the basis of their relative electronegativities, is reinforced by the capacity of the catecholate phenyl ring to delocalize the negative charge. Consistent with this view, the NPA-derived charge for the catecholate ligand is –1.20 a.u., while the corresponding sum for the chloride ligands is –1.11 a.u. Thus, in contrast to **Ru-1**,

for which phosphine dissociation is the stepping stone to a rich coordination chemistry,[107] the strong Ru-PPh_3 bonds within **Ru-2a** significantly reduce the lability of these ligands.

4.2.4 Key findings

The above experimental and theoretical studies reveal interesting properties for Ru-catecholate complexes. Incorporation of catechol as an anionic ligand raises the energy of the HOMO within **Ru-2a**, relative to the dichloride parent **Ru-1**. Consequently, Ru-benzylidene complexes bearing the catecholate ligand may be more susceptible to interact with electron-deficient olefins, which are characterized by a higher energy LUMO. Although the second-generation Grubbs catalysts can carry out metathesis of electron-deficient olefins,[108] the catechol catalysts may show higher reactivity towards these substrates relative to their dichloride parent. While the energy of the LUMO within **Ru-2a** is also raised, the magnitude of the change is much smaller. Consequently, the ability of the catechol complex to accept σ-donation from the HOMO of a potential olefinic substrate should be less affected. Potentially problematic, however, is the low lability of the PPh_3 ligands within **Ru-2a**, which could lead to low metathesis activity of alkylidene complexes bearing the catecholate ligand.

Issues of reactivity notwithstanding, the electronic bonding between the metal center and the catechol ligand was found to be highly dependent on the nature of the donor atom, in this case oxygen, and the presence of an aromatic ring, which acts as an electron acceptor. This implies that the perturbation of the molecular orbitals induced by introduction of the catecholate ligand can be extended to all aryloxide catalysts.

4.3 Catecholate catalysts

In contrast to the tendency of electron-rich aryloxide ligands towards $\sigma - \pi$ isomerization,[70,71] a very important aspect of the catecholate ligand is the σ bonding mode, even in the absence of electron-withdrawing groups on the aromatic ring. Clearly, the combination of the chelate effect and small bite angle of the catechol stabilizes the O-binding mode. The stability of this binding mode indicates that, in contrast to the phenoxide ligands, catecholate bearing electron-donating groups should also be suitable ligands for metathesis catalysts. Furthermore, X-ray analysis (see below) indicates that a long distance (>4 Å) separates the catechol substituents from the pyridine "placeholder" ligand. Thus, varying the

size of these substituents should have a negligible effect on the steric environment of the catalytic site generated upon loss of pyridine. Consequently, and for the first time, exploring the electronic effects of the anionic ligands on metathesis activity without the complicating interference of the varying steric demand can be performed.

The following discussion of the catecholate catalysts will be presented in four sections. First, the synthesis of catechols and catecholate salts will be presented. Second, the complexation of the catecholates with Ru-benzylidene precursors will be discussed. Third, the characterization of the catecholate catalysts, in both solution and solid state, will be given. Fourth, the catalytic activity of the family of catecholate catalysts will be examined for both RCM and ROMP reactions.

4.3.1 Synthesis of catechols and catecholates

A series of catecholate derivatives was prepared from catechols spanning a pK_a range of 4.5 units. The metathesis activity of the resulting complexes was then correlated with the electronic donating ability of the catechol ligand (using the pK_a as indicator, see Section 4.3.4). Nine catecholate derivatives bearing electron-donating and electron-withdrawing substituents were selected (Chart 2). With the exception of **37a/b**, all thallium salts shown in Chart 2 were prepared from commercially available catechols. Syntheses of catechol precursors to **37a/b** (**34** and **36**) were performed according to Schemes 4 and 5.

	X =	Cmpd #	pK_a
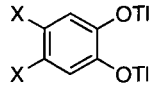	NMe_2	**37a**	N R
	Me	**37b**	9 92
	Cl	**37c**	8 10
	Br	**37c**	7 98
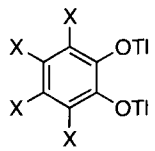	H	**38a**	9 36 (9 32)
	F	**38b**	6 26
	Cl	**38c**	5 83 (4 95)
	Br	**38c**	5 49
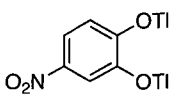		**39**	6 84 (6 60)

Chart 2. Various catecholate salts used in this study with the respective, predicted[109] pK_a of the parent diol. The experimentally determined pK_a (H_2O) is shown in brackets, where available: **38a**,[110] **38c**[112] and **39**.[111] The pK_a of the parent diol of **38c** was measured in DMF. The conversion for the solvent was performed using the reported method.[113] N. R. = not reported.

Electron-rich 4,5-dimethylaminocatechol **34** was prepared in four steps in an overall yield of 10% (Scheme 4). Treatment of commercially-available veratrole (1,2-dimethoxybenzene) with nitric acid afforded the doubly nitrated **31** as yellow plates in 53% yield, following recrystallization from hot ethanol. Subsequent reduction to the bis-amine using hydrazine and Pd/C in refluxing ethanol afforded diamine **32** in 73% yield after recrystallization from hot THF. Initially obtained as off-white needles, compound **32** is highly hygroscopic and turns brown (while conserving its crystalline aspect) over a few days at room temperature. No change was evident by GC-FID and ^{1}H NMR analysis, suggesting that the brown color is not due to decomposition. Alkylation of **32** with dimethyl sulfate (DMS) proved unsuccessful, and starting **32** was recovered. However, reductive methylation with aqueous formaldehyde and zinc-modified sodium cyanoborohydride[114] proceeded smoothly, as judged by TLC, to afford **33** as a brown oil. The crude product appears sensitive to decomposition, as ^{1}H NMR analysis ($CDCl_3$) revealed many unidentified signals. Column chromatography purification was unsuccessful, but distillation afforded clean **33** as a colorless oil in 48% yield. Deprotection of the methoxy substituents using BBr_3 afforded **34** in 56% yield. The high solubility of this catechol in water complicated its separation from the $B(OH)_3$ by-product, lowering the isolated yield of **34**.

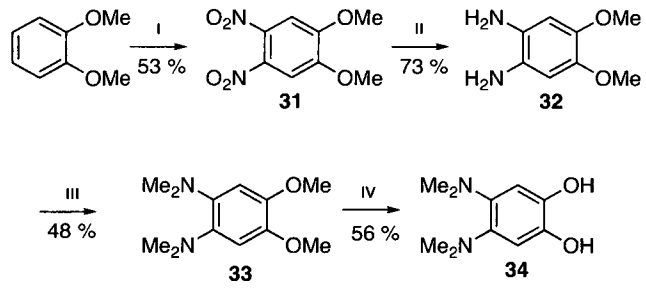

Scheme 4. Synthesis of **34**. (i) 10:1 (v/v) HNO_3: H_2O, 22 °C for 1 h then 60 °C for 3h; (ii) N_2H_4, Pd/C; EtOH, Δ, 1.5 h; (iii) HCHO, $NaBH_3CN$, $ZnCl_2$, MeOH, 22 °C, 24 h; (iv) BBr_3, CH_2Cl_2, 0 °C, <5 min.

The synthesis of 4,5-dimethylcatechol **36** (Scheme 5) was initiated by oxidation of commercially available 3,4-dimethylphenol using Fremy's salt ($K_2[NO(SO_3)_2]$) in water.[115] Although the desired quinone **35** can be isolated, this product rapidly undergoes a Diels-Alder dimerization at room temperature.[116] Therefore, unlike the reported procedure,[116] subsequent reduction of the quinone was performed without isolation of **35**, in order to

maximize yields. Extraction of **35** with chloroform was immediately followed by addition of a saturated aqueous solution of sodium dithionite ($Na_2S_2O_4$), which effected a quick color change from red to yellow. Stirring for 20 minutes and subsequent evaporation of the solvent yielded **36** in 53% overall yield.

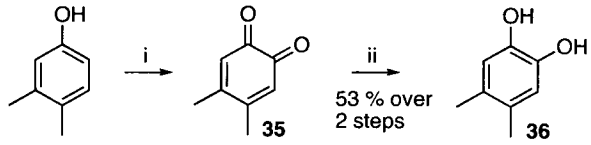

Scheme 5. Synthesis of **36**. (i) $K_2[NO(SO_3)_2]$, H_2O, 22 °C, 20 min ; (ii) $Na_2S_2O_4$, $CHCl_3$, 22 °C, 20 min.

Preparation of the thallium catecholates is straightforward. On mixing ether solutions of commercially-available thallium ethoxide with the desired catechol, the salts precipitate instantly and were isolated by filtration. The calculated pK_a values, assessed using Advanced Chemistry Development (ACD/Labs) Software V8.14 for Solaris, for the parent catechols are shown in Chart 2, with experimental values (where reported) in brackets. The experimental and predicted and pK_a agree reasonably well with each other, validating the computed values. The pK_a of the parent catechol is used as an indicator of the electronic density at the catecholate oxygens for correlation with catalytic activity (Section 4.3.4).

To study the uptake of catecholate as sodium salts on the metal center, $Na_2O_2C_6H_4$ (**40**) was prepared. Compound **40** was obtained by treating a diethyl ether solution of catechol with solid NaH. A gray precipitate formed instantly and was collected by filtration. To avoid contamination of **40** with NaH, a slight excess (0.1 equiv) of catechol was used, which can be easily removed by washing **40** with diethyl ether.

4.3.2 Synthesis of catecholate catalysts

With nine different catecholates in hand, the incorporation of these salts on a Ru-benzylidene precursor was studied. As the unsubstituted catecholate is by far the most inexpensive of the series, initial studies focused on the incorporation of the thallium salt **38a** on the metal center. Prior work within the Fogg group revealed that incorporation of perhaloaryloxide(s) on the Grubbs catalyst requires use of sterically unencumbered precursors such as **Ru-6a**.[44] Use of the first-generation Grubbs catalyst **Ru-3**, bearing two bulky PCy_3 groups, resulted in deprotonation of the alkylidene to give a well-defined Ru-

alkylidyne product (Scheme 6). The role of sterically demanding ancillary ligands in driving such α-elimination reactions is well established.[66] Given the lower steric demand of catecholates vs. (bis)perhaloaryloxides, the scope of the Ru-benzylidene precursors was re-evaluated. Of interest is the potential accessibility of phosphine-ligated precatalysts (e.g. **Ru-3**, **Ru-4**), which exhibit longer lifetime than their pyridine analogues such as **Ru-6**, a function of the stronger coordination and hence stabilizing effect of the phosphine vs. pyridine. As the chelate effect is expected to accelerate coordination of the catecholate ligand to the metal center, the possibility of introducing the catechol moiety as a sodium salt over highly toxic thallium salt required for monodentate aryloxide was also investigated.

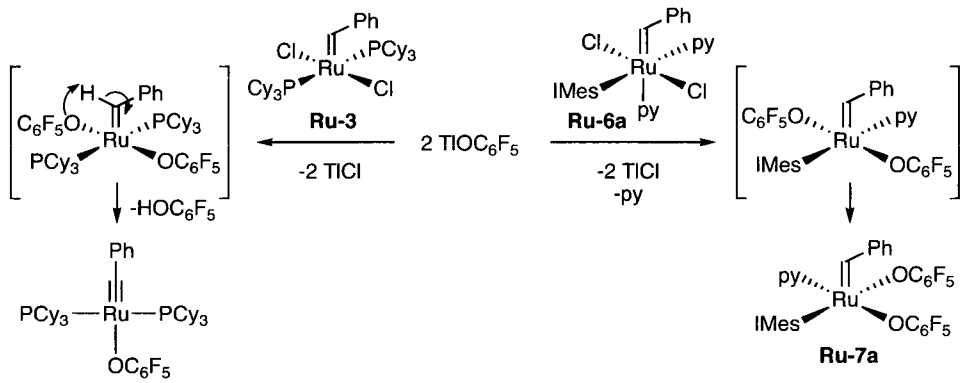

Scheme 6. $TlOC_6F_5$ reacts with **Ru-3** to form an alkylidyne complex, but reacts with **Ru-6a** to form an alkylidene complex.[44]

Probe experiments were conducted on NMR scale, wherein C_6D_6 solutions of **Ru-3**, **Ru-4a** and **Ru-6a** were reacted with 1.1 equiv of **38a** at room temperature (Scheme 7). The progress of these reactions was assessed by ^1H NMR monitoring of the alkylidene region (15-20 ppm), supplemented by ^{31}P NMR analysis in the case of **Ru-3** and **Ru-4a**. As expected from the aryloxide precedents,[43,44] reaction of dithallium catecholate **38a** with **Ru-6a** proceeds smoothly to afford a sole new complex in less than 2 h at room temperature. Diagnostic NMR evidence includes a new benzylidene NMR singlet at 17.1 ppm and the complete disappearance of that due to **Ru-6a** at ca. 20.0 ppm.

In contrast, identical reactions using the PCy_3 complexes **Ru-3** and **Ru-4a** exhibit no new NMR signals after six hours at room temperature. For first-generation **Ru-3**, a new benzylidene triplet (δ 17.1 ppm, $^3J_{HP}$ = 16.9 Hz; C_6D_6) was observed after 24 h. At the same time, $^{31}P\{^1H\}$ NMR analysis revealed a new singlet at 43.1 ppm (cf. 37.6 ppm for **Ru-3**).

Both of these new peaks correlate via ^{1}H-^{31}P HMBC analysis, confirming their presence on the same ruthenium center. Integration of the new signals against those of **Ru-3**, in both ^{1}H and ^{31}P NMR spectra, revealed only 25% conversion to the new complex. Longer reaction time did not improve conversions and only degradation of the signal-to-noise ratio was observed, presumably reflecting decomposition into paramagnetic products. Reaction of **38a** with second-generation **Ru-4a** is even slower than for **Ru-3**. After stirring for 24 hours at room temperature, a very weak doublet was observed at 16.5 ppm in the ^{1}H NMR spectrum ($^{3}J_{HP}$ = 17.6 Hz; C_6D_6); a singlet at 47.2 ppm was also detected by $^{31}P\{^{1}H\}$ NMR analysis. Integration against **Ru-4a** revealed that the new species is present in <5%. The expected ^{1}H-^{31}P HMBC correlation between the new signals could not be observed, presumably due to the very weak intensity of the new peaks. The resistance to incorporation of the catecholate ligand on **Ru-3** and **Ru-4a** is unsurprising, given the prohibitive steric encumbrance resulting from the cis arrangement of two PCy_3 ligands (for **Ru-3**), or IMes and PCy_3 (for **Ru-4a**). As a result, **Ru-6a** was retained as the benzylidene precursor for the installation of the catecholate ligands.

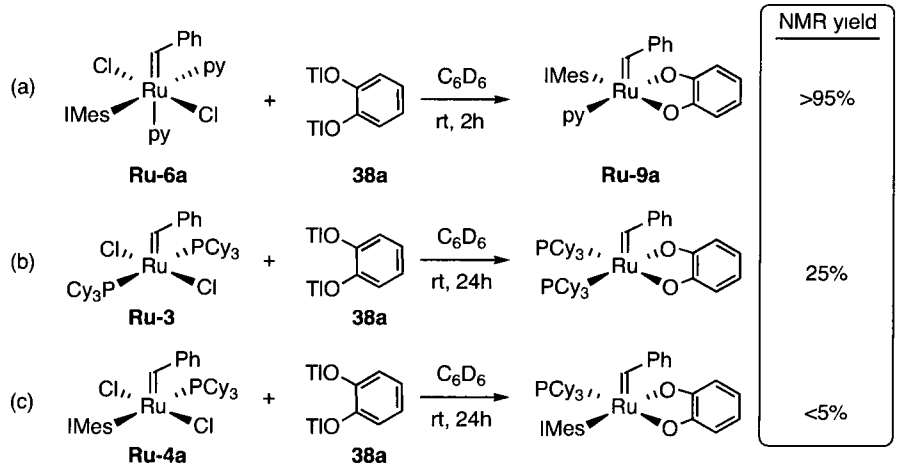

Scheme 7. Efficiency of the reaction between the catecholate proligand **38a** and (a) **Ru-6a**, (b) **Ru-3** and (c) **Ru-4a**.

Next, the possibility of introducing the catechol moiety using a more benign sodium salt was investigated. Due to the sensitivity of pyridine-ligated **Ru-6a** towards thermal decomposition, all salt metathesis reactions using sodium catecholate **40** were conducted at room temperature. The uptake of **40** on **Ru-6a** over time is shown in Figure 6. Consistent with the earlier aryloxide experiments, incorporation of **40** on **Ru-6a** proved much slower

than the corresponding reaction using the thallium salt. Thus, addition of 1.1 equiv. of **40** to a C_6D_6 solution **Ru-6a** resulted in no detectable reaction after the two-hour period required for complete uptake of the thallium salt **38a**. Conversions of **Ru-6a** reach only 54% after 24 h, and although some of the desired catecholate **Ru-9a** is present (21%), decomposition to non-alkylidene species competes (25%). Reaction was faster in THF (Figure 6b), but 28% unreacted **Ru-6a** still remained after 24 h. While a higher proportion of **Ru-9a** was present (43%), the extent of decomposition was still unacceptably high, at ca. 30%. In related Na_2-binaphtholate chemistry, use of pyridine as reaction medium proved highly successful in preventing such catalyst decomposition.[117] This strategy was unsuccessful in the catecholate chemistry (**Ru-6a** + **40**) owing to the insolubility of the catechol salt. Thus, as low conversions and competing decomposition impede the synthesis of **Ru-9a** using **40**, all subsequent experiments using catechol or other catechol derivatives were carried out using thallium salts.

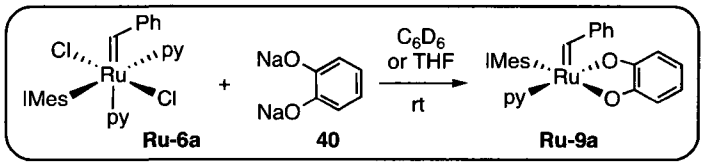

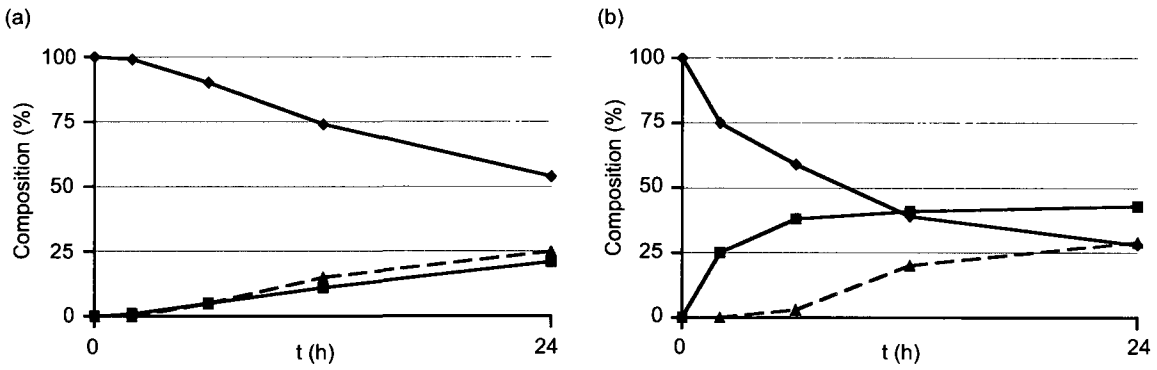

Figure 6. Conversion of **Ru-6a** (♦) to **Ru-9a** (■) using **40** at room temperature in (a) C_6D_6 and (b) THF. Conversions determined by ^1H NMR spectroscopy (300 MHz) using 1,3,5-trimethoxybenzene as internal, integration standard. The amount of decomposition (dashed ▲) was determined by difference.

For most of the remaining thallium catecholates, reaction with **Ru-6a** proceeded without incident (Scheme 8). Consistent with the synthesis of **Ru-9a** described above (Scheme 7a), a reaction time of 2 h at room temperature proved sufficient for complete salt metathesis. The catecholate complexes were isolated as brown-green solids in generally good to excellent

yields (77-91%). Lower yields (52 and 66%) were obtained for tetrachloro **Ru-9c** and tetrabromo **Ru-9d** respectively, owing to their low solubility in common organic solvent (C_6H_6, C_7H_8, C_6H_5Cl, THF, CH_2Cl_2, hexanes and diethyl ether), which impedes their separation from the TlCl co-product by filtration through Celite. Loss of material during filtration is evidenced by the green coloration of the Celite bed, which does not diminish on repeated washing.

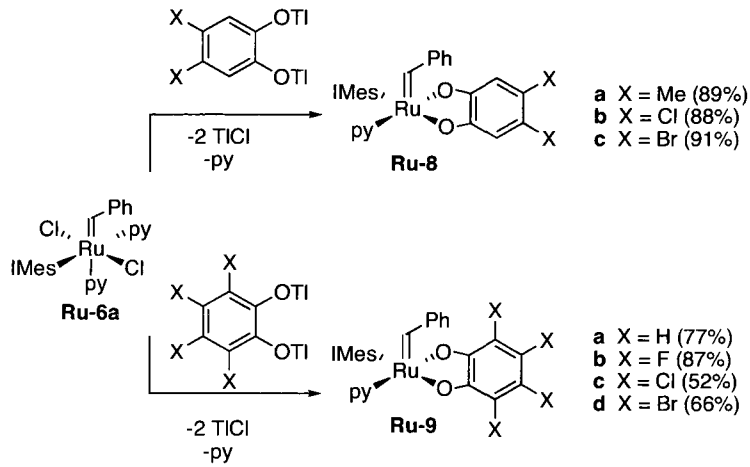

Scheme 8. Synthesis of **Ru-8/9**. Isolated yields in parentheses. Reactions at room temperature in C_6H_6 or THF for 2 h.

Greater difficulty was encountered during synthesis of dimethylamino catecholate **Ru-10**. Addition of 1.1 equiv of **37a** to a C_6D_6 solution of **Ru-6a** affords a new benzylidene species, characterized by a ^1H NMR singlet at 17.1 ppm, after 2.5 h (Scheme 9a), albeit in small proportion (10%). The mass balance corresponds to starting **Ru-6a**. Charge-transfer[73] MALDI MS analysis of the crude reaction mixture revealed a peak cluster at *m/z* 768.6 Da, consistent with the proposed structure of **Ru-10**, suggesting that the new alkylidene observed may be due to the expected catecholate complex. Use of THF in place of C_6D_6, or excess **37a**, did not improve in situ yields of **Ru-10**, which were limited to ca. 14%. Warming the reaction to 50 °C (C_6D_6 or THF) led to formation of a black solution with no evident benzylidene signals. Given these poor conversions, and the successful synthesis of seven other members of this family of catecholate catalysts, synthesis of **Ru-10** was abandoned.

Reaction of 1.1 equiv. of 4-nitro catecholate **39** with **Ru-6a** in both C_6D_6 and THF for 2.5 h led to formation of two new alkylidene singlets at 17.40 and 17.26 ppm respectively (C_6D_6; 2:1 ratio respectively, Scheme 9b). These signals stem from the formation of both possible

isomers of **Ru-11**. However, conversion to **Ru-11** only reached 22%, as judged by ^{1}H NMR analysis. As broad hydride signals are also observed at –1.45 and –5.87 ppm by ^{1}H NMR analysis (C_6D_6), synthesis of **Ru-11** was also abandoned.

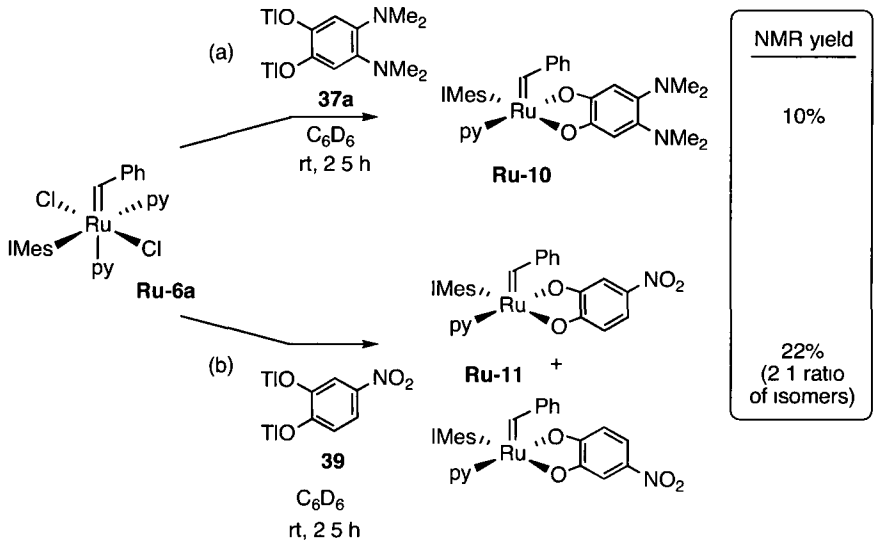

Scheme 9. Unsuccessful reactions between **Ru-6a** and (a) **37a** and (b) **39**.

4.3.3 Characterization of catecholate catalysts

The structures of all isolated catecholate complexes were assessed by NMR analysis, MALDI-MS, elemental analysis and, in the case of 4,5-dibromo **Ru-8c**, unsubstituted catechol **Ru-9a** and tetrafluoro **Ru-9b**, X-ray analysis (see Figure 9). The C_1 symmetry of catecholates **Ru-8/9** is clearly apparent from $^{13}C\{^1H\}$ NMR analysis, which revealed six distinct carbons resonances for the catechol ring. This is further supported by the observation of two independent signals for the methyl substituents on the catechol ring in **Ru-8a**, and four distinct ^{1}H or ^{19}F resonances for **Ru-9a** and **Ru-9b**, respectively (Figure 7a). The consistent observation of three different methyl signals (relative integration 1:1:1) for the mesityl "arms" of the IMes ligand suggests restricted rotation around the N-C_{Mes} bond (Figure 7b). NOESY experiments permitted assignment of the two signals due to the ortho methyl groups on the mesityl ring.[69] The implied chemical inequivalence of the two sp^2 protons on the mesityl ring is confirmed by the observation of two distinct resonances, although the expected coupling between these protons was not observable. Such $^4J_{HH}$ coupling constants between meta protons are characteristically small (often ca. 2-3 Hz).[118] Rapid rotation around the Ru-C_{NHC} bond on the NMR timescale is suggested by the

observation of one olefinic signal, rather than two, for the imidazole ring protons. While rotation around M-C_{NHC} bond is not uncommon,[119-121] this rotation within Ru alkylidenes is often presumed to be higher in energy compared to spinning about the N-C_{Mes} bond.[122-124] These issues were examined in recent work from the Fogg group in a detailed NMR analysis of dichloride **Ru-6a**, perbromoaryloxide **Ru-7b** and catecholate **Ru-9a**.[69]

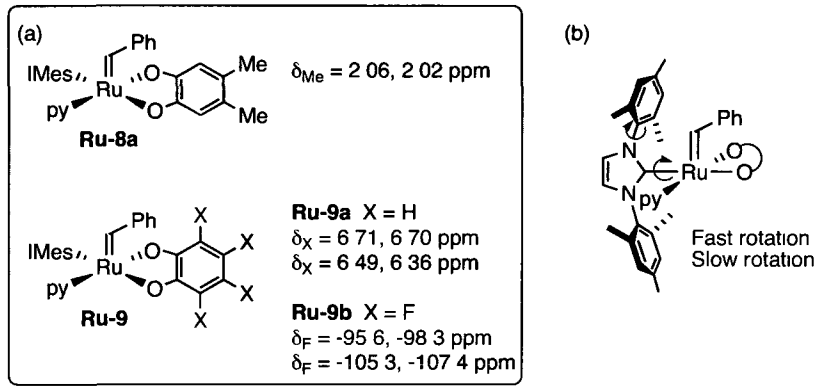

Figure 7. (a) NMR evidence for C_1 symmetry in **Ru-8a** and **Ru-9a/b** ($CDCl_3$ solvent). (b) Relative rates of rotation about the Ru-C_{NHC} and the N-C_{Mes} bonds in catecholate catalysts.

CT-MALDI analysis of **Ru-8/9** confirmed replacement of the chlorides by the catecholate ligand. Near-perfect matches are found between the predicted and observed isotope patterns for all catecholate catalysts; selected examples are shown in Figure 8. Generally, analysis of metathesis catalysts bearing pyridine as ancillary ligand (e.g. **Ru-6a**, **Ru-7a**), reveals an isotope pattern with a *m/z* ratio consistent with the loss of the labile pyridine ligand(s) in the gas phase ($[M\text{-}py]^+$). When the catecholate complexes were analyzed in a similar manner, however, observation of a weak molecular ion was sometimes possible. While this observation is in line with the low lability of the pyridine in the catecholate system, as discussed in more detail in Section 4.3.4, no correlation was found between the initiation efficiency of the catalyst and observation of the molecular ion. As empirical observations by Johanna Blacquiere of this group suggest that fragmentation of the Grubbs catalysts seems to be independent of laser power, the observation of the molecular ion for some catecholate complexes may be simply due to better signal to noise ratio in these particular cases.

References page 158

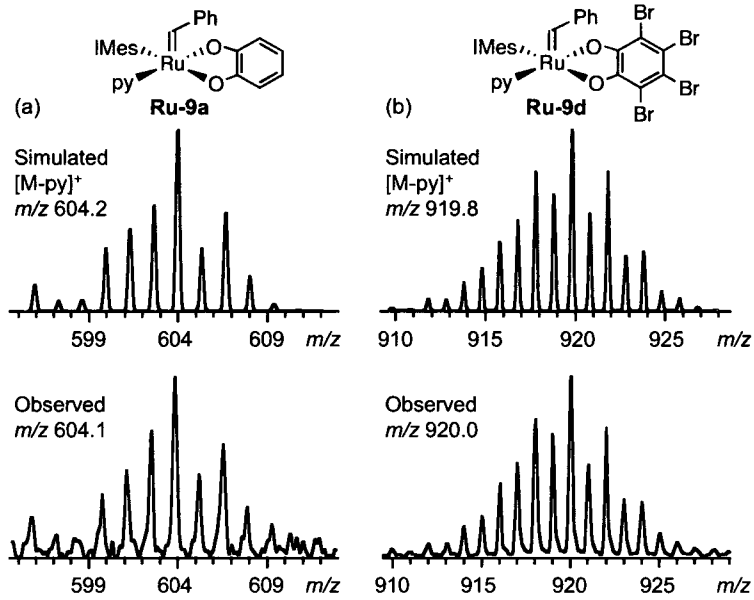

Figure 8. Selected CT-MALDI MS spectra of (a) unsubstituted catecholate **Ru-9a** and (b) tetrabromo catecholate **Ru-9d**. Pyrene was used as matrix in both cases.

Green prisms of the unsubstituted catechol **Ru-9a**, dibromo **Ru-8c** and tetrafluoro **Ru-9b** suitable for X-ray analysis were grown by vapor diffusion of hexanes into a saturated THF solution of the corresponding complex. The geometry of these catecholate complexes is best represented as a distorted square pyramid wherein the alkylidene ligand occupies the apical coordination site (Figure 9). The τ parameter[75] values for the unsubstituted catechol **Ru-9a**, dibromo **Ru-8c** and tetrafluoro **Ru-9b** are 0.16, 0.06 and 0.20 respectively.

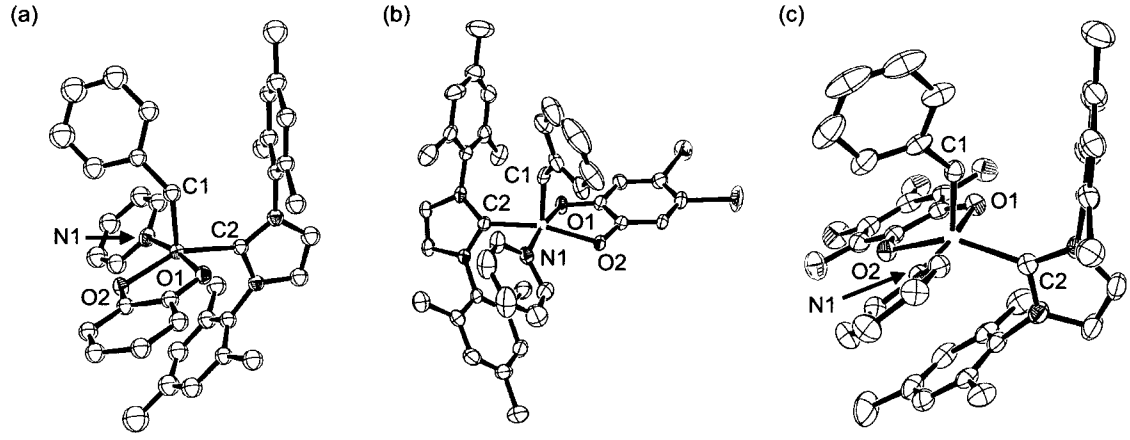

Figure 9. ORTEP representations of (a) **Ru-9a**, (b) **Ru-8c** and (c) **Ru-9b**. Hydrogens atoms are omitted for clarity. Thermal ellipsoids are drawn at 50% probability. Only relevant atoms are labeled here. See Figures A-2-4 in Appendix B for full structural detail.

A summary of relevant bond lengths and angles is provided in Table 4. The Ru=C and Ru-C_{NHC} bond lengths compare well with those of closely related **Ru-6b**.[125] Differences in the two Ru-O bond lengths are observed for all three catecholate complexes, consistent with the different ligands trans to these bonds (IMes or pyridine). Unexpectedly, the Ru-O(2) bond (trans to IMes) is always shorter relative to Ru-O(1) (trans to pyridine), particularly in the case of **Ru-9b**. In all three catecholate complexes, the Ru-O(2) bond, like the Ru-C_{NHC} bond, is tilted away from the basal plane, as evidenced from the O(2)-Ru-C(2) angles ranging between 145-160°. In contrast, the O(1)-Ru-N(1) angles approach linearity, ranging between 172-174°. The longer Ru-O(1) bond may result from a stronger push-pull interaction between the pyridine ligand and the catecholate O(1), due to the more linear arrangement of these ligands. It is worth noting that the Ru-N(1) bond length in these catecholate complexes, while uniform within the catecholate family, is much shorter than in dichloride **Ru-6b**.[125] While this is consistent with the low lability of this ligand (see next Section), comparison to **Ru-6b** is complicated by the presence of two pyridines in the latter complex, which will affect the stereoelectronic properties and, potentially, ruthenium-ligand bond distances.

Table 4. Summary of relevant bond lengths and angles for **Ru-9a**, **Ru-8c** and **Ru-9b**.

Bond length (Å) Angles (°)	**Ru-9a**	**Ru-8c**	**Ru-9b**	**Ru-6b**
Ru=C(1)	1.843(4)	1.819(7)	1.831(2)	1.873(4)
Ru-C(2)	2.056(4)	2.045(5)	2.031(2)	2.033(4)
Ru-N(1)	2.082(4)	2.081(5)	2.0752(17)	2.203(3)[a]
Ru-O(1)	2.053(3)	2.038(4)	2.0742(15)	-
Ru-O(2)	2.014(3)	2.033(4)	2.0145(14)	-
O(1)-Ru-O(2)	82.57(13)	81.32(16)	82.28(6)	-
C(1)-Ru-C(2)	98.33(17)	97.2(2)	100.92(9)	93.61(17)

[a] pyridine ligand trans to the H_2IMes ligand.

For **Ru-8c**, **Ru-9a** and **Ru-9b**, the C(1)-Ru-C(2) angles are larger than 90°, and range from 97° to 101°. This allows one of the mesityl "arms" of the IMes ligand to reside in the empty coordination site trans to the alkylidene ligand. The large distance (>4 Å) between the Ru center and the mesityl aromatic ring suggests that no interaction is present. The relevance of this "tilting away" of the NHC ligand from the benzylidene axis has been highlighted by Cavallo[126] and Jensen,[68] who note a positive correlation between the C(1)-Ru-C(2) angle and metathesis activity. These workers propose that the steric repulsion between cis-disposed L

(e.g. IMes) and methylidene ligands, as indicated by the C(1)-Ru-C(2) angle, is partly relieved upon formation of the metallacyclobutane intermediate: that is, the reduced repulsion between ligands within the metallacyclobutane complex creates a driving force for formation of this key intermediate (Figure 10a). Although the C(1)-Ru-C(2) angles within the catecholate complexes (97-101°) are similar to that found in highly active second-generation **Ru-4a** (99.2 (1)°),[18] extension of the relationship between the C(1)-Ru-C(2) angles and metathesis activity to the catecholate catalysts is not straightforward. A major difference between the catecholate and the dichloride catalysts is the disposition of their respective anionic ligands. For the Grubbs catalysts, the trans-disposition of the chlorides leads to the formation of a metallacyclobutane pointing away from the NHC ligand (Figure 10a). In contrast, given the required cis arrangement of both anions, the metallacyclobutane formed for the catecholate catalysts remains in the same plane as the mesityl groups on the NHC ligand. Thus, it is unclear whether formation of this intermediate for the catechol catalysts will lead to a decrease in repulsion between the IMes and the metallacycle.

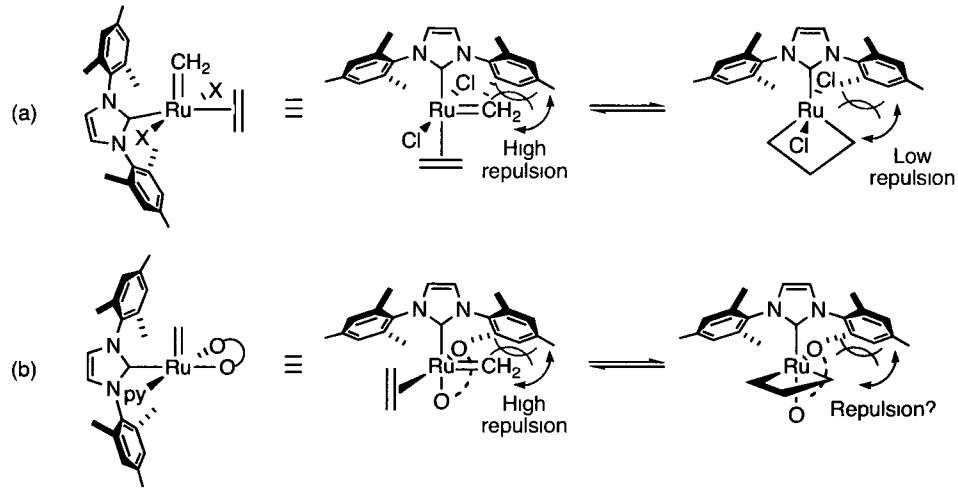

Figure 10. Metallacyclobutane formation for complexes bearing (a) trans-disposed chloride ligands and (b) cis-disposed catecholate ligand.

4.3.4 Establishing the influence of the anionic ligands on metathesis activity

Preliminary investigation into the catalytic activity of the family of catechol catalysts was sought using RCM of a series of high-EM dienes featuring various functional groups such as amine, ester, alcohol, silane, ether and sulfide (Figure 11b). These substrates were also chosen from the various level of difficulty they pose to the ruthenium catalysts. While tosyl

amine **9a** and diethyl diallyl malonate **11a** are considered to be "easy" substrates, silane **15** and sulfide **19** are more problematic while the strained 8-membered ring formed upon ring-closure of **7** also renders this substrate challenging for RCM. To elicit distinctions in catalyst performance across these substrates, RCM was performed at a low catalyst loading of 0.5 mol% [Ru]. Screening was conducted as single data point experiments under arbitrary conditions (50 mM diene in CH_2Cl_2, Δ, 3 h, 0.5 mol% [Ru]); conversions to the RCM products were assessed by both ^{1}H NMR and GC-FID analyses.

Higher activity correlates with higher catechol pK_a (Figure 11c: catalysts in order of pK_a), with the electron-rich dimethylcatecholate catalyst **Ru-8a** effecting complete RCM of **9-17** within 3 h. The histograms for **9-17** establish a clear demarcation between the tetrahalocatecholates **Ru-9b-d** and the more active catalysts **Ru-8** and **Ru-9a**. Maximum discrimination within tetrahalo catecholate catalysts **Ru-9b-d** emerges for diethyl diallyl malonate **11a** and diphenyl silane **15**, which reveal a systematic decrease in conversions as the pK_a of the catecholate decreases. Ethers **17** and **7** enable discrimination between the more active catalysts. For **17**, catalysts **Ru-8a/b** and **Ru-9a** effect quantitative RCM compared to 80% for dibromo catalyst **Ru-8c** (and 15-20% for **Ru-9b-d**). None of these catalysts effect complete RCM of catechol ether **7** under the conditions used. Nevertheless, the trend in activity is conserved; the activity of dimethyl **Ru-8a** is double that of the next most active catalyst **Ru-9a**. All catalysts show low activity for diallylsulfide **19**, an established poison for ruthenium metathesis catalysts.[127]

References page 158

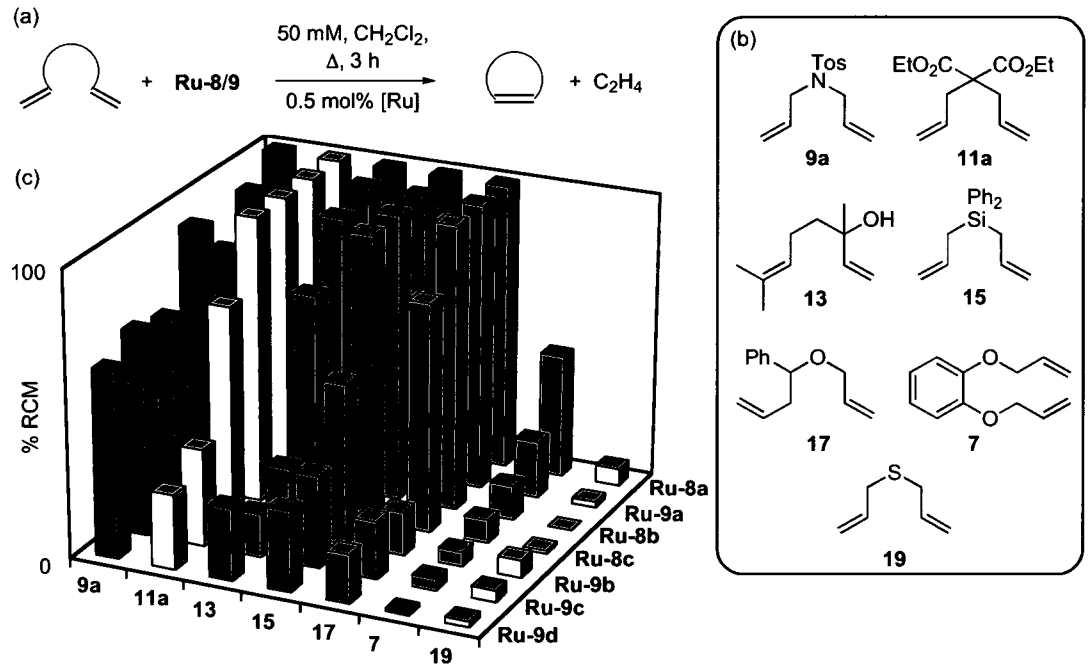

Figure 11. (a) General RCM scheme. (b) Substrates **7-19**. (c) % Conversion to the RCM products. Conditions: 50 mM diene in CH_2Cl_2, Δ, 3 h, 0.5 mol% [Ru]. Calibrated GC-FID analysis (±3% in replicate runs).

In a more detailed examination, the rate curves were measured for RCM of tosyl amine **9a** and diethyl diallyl malonate **11a** and ROMP of norbornene monomer **21** using all seven catalysts (Figure 12). These substantiate the trend in catalyst activity qualitatively evident from Figure 11c. The corresponding TOF values (Table 5) reveal that dimethylcatecholate **Ru-8a** is almost twice as active as **Ru-9a**, its nearest competitor, in RCM of **9a** or **11a** and 50× faster than the least active catalyst, tetrabromo catecholate **Ru-9d**, in RCM of **9a**. In ROMP of **21**, this trend is even more pronounced: **Ru-8a** is nearly 3× more reactive than **Ru-9a**, and nearly 90× more than **Ru-9d**. These data unequivocally confirm a dramatic drop in catalyst activity as the catecholate becomes more electron-deficient.

References page 158

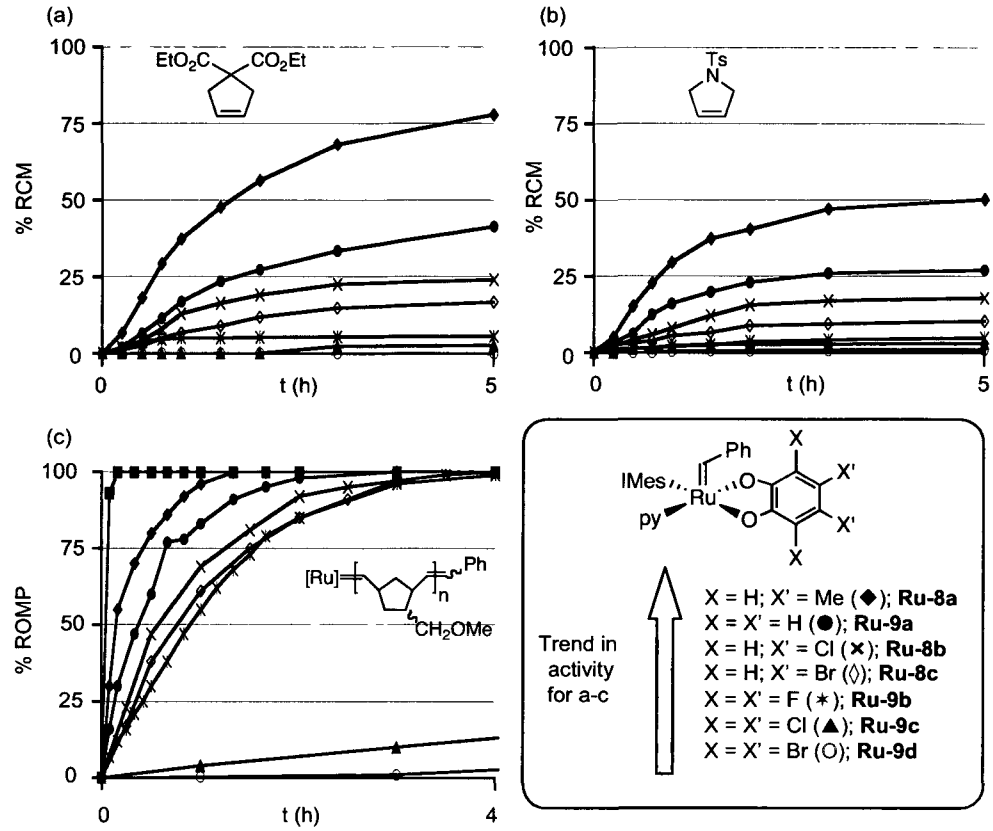

Figure 12. Conversion profiles for the RCM of (a) **11a** and (b) **9a**. Conditions: 5 mM diene in C_7H_8, 60 °C, 0.5 mol% [Ru]. Calibrated GC-FID analysis (±2% in replicate runs). (c) ROMP of **21**. Conditions: 100 mM in $CDCl_3$, 23 °C, 1 mol % [Ru]. ^{1}H NMR analysis (±3% in replicate runs). **Ru-6a** (■; shown for the ROMP reaction only).

As a composite of initiation and propagation, TOF values do not distinguish between a highly-active, poorly-initiating catalyst and a less active but efficiently-initiating catalyst. Several other lines of evidence, however, indicate that initiation and propagation follow the same qualitative trend for **Ru-8/9**. The DFT-calculated Ru-pyridine bond strengths increase in the expected order (dimethyl **Ru-8a**, 22.5; unsubstituted **Ru-9a**, 22.6; tetrafluoro **Ru-9b**, 24.9 kcal mol^{-1}; cf. 18.3 kcal mol^{-1} for dichloride **Ru-6a**). This suggests greater resistance to initiation via loss of pyridine as the catalyst becomes more electron deficient.[64] Very slow initiation, even for dimethyl catecholate **Ru-8a**, precludes use of standard NMR methods[128-130] to measure the rates of initiation k_i: no signal for the propagating alkylidene is observed even at 10:1 **21**:[Ru]. Where NMR methods are not feasible, initiation efficiencies can nevertheless be inferred from comparisons of ROMP polymer chain lengths with theoretical values (Table 6).[131-133] This requires that ring-opening be irreversible and intramolecular

chain-transfer (backbiting) be slow. In the case of substituted polynorbornenes, backbiting of the polymer is inhibited by both steric encumbrance and the high rigidity of the polymeric chain, and thus does not normally compete with ROMP itself.[134] The initiation efficiencies of the catecholate complexes determined from polymer molecular weights are low, with absolute values of 0.16-1.1%, but tend to support the reactivity trend described above, the fastest initiation being found for electron-rich dimethyl **Ru-8a**.

Table 5. Relative activity and initiation efficiency for catalysts **Ru-8/9**.[a]

	TOF (h^{-1})			TOF_{rel}[b]			
Cat.	**11a**	**9a**	**21**	**11a**	**9a**	**21**	IE (IE_{rel}; %)
Ru-8a	100	156	350	50	31	87	1.06 (6.6)
Ru-9a	54	83	135	27	16	34	0.92 (5.8)
Ru-8b	36	48	83	18	9	21	0.58 (3.6)
Ru-8c	21	34	64	10	7	16	0.48 (3.0)
Ru-9b	10	11	56	5	2	14	0.43 (2.7)
Ru-9c	6	5	5	3	1	1.2	0.20 (1.3)
Ru-9d	2	0	4	1	-	1	0.16 (1)

[a] Conditions: for RCM, 5 mM diene in toluene, 60 °C, 0.5 mol % [Ru]; for ROMP, 100 mM **21** in $CDCl_3$, 23 °C, 1 mol % [Ru]. RCM TOF values at 5 h (identical trends found in TOF at 10% conversion for **Ru-8** and **Ru-9a** (**Ru-9b-d**, conversion <6%). ROMP TOF values at 50% conversion. [b] Normalized to values for the slowest reacting catalyst. IE values extracted from M_n data at 100% conversion; IE_{rel} = [M_n(calcd.)/M_n(exptl.)]/[M_n(calcd. for **Ru-9d**)/M_n(exptl. for **Ru-9d**)]. M_n for poly-**21** determined by light-scattering GPC.

Two further points indicate that the trend in overall activity is dominated by propagation. First, the high polymer molecular weights (Table 6), as well as the in situ NMR data, show that propagation is very fast relative to initiation. Second, the range in initiation efficiency values from **Ru-8a** to **Ru-9d** (<1%) is far too small to account for a TOF difference approaching two orders of magnitude. This implies that while both initiation *and* propagation are retarded as the anionic ligands become more electron-withdrawing, the effect on propagation is significantly greater. Increased electron-deficiency in related ligands has been shown[135] to increase the positive charge on ruthenium.[135] In the present context, this appears to disfavor not only pyridine loss, but also formation of the Ru^{IV} intermediate.

Table 6. Data for poly-**21** obtained using different catalysts.[a]

Cat.	Time (h)	M_n ($\times 10^{-3}$)	% Conv.	% Yield	PDI	IE (%)[b]
Ru-6a	10 min	15	100	75[c]	1.10	92
Ru-8a	1.5	1300	100	92	1.12	1.06
Ru-9a	2.5	1500	100	90	1.13	0.92
Ru-8b	4	2400	100	91	1.23	0.58
Ru-8c	4	2900	100	88	1.27	0.48
Ru-9b	4	3200	100	88	1.20	0.43
Ru-9c	17	6800	100	83	1.7	0.20
Ru-9d	20	8800	100	89	1.7	0.16

[a] % Conv. = % conversion to polymer at stated time (^{1}H NMR analysis). [b] % IE = M_n (calcd.)/M_n (exptl.) × 100 (M_n (calcd.) = 13.8 × 10^3 Da). M_n(exptl.) is the average of two separate ROMP experiments; M_n data measured in duplicate for each; errors range from ±2-6%. [c] The isolated yield of polymer obtained using **Ru-6a** was limited by incomplete precipitation.

4.4 Conclusions

Theoretical and experimental investigations revealed that replacement of the ubiquitous chloride ligands of the Grubbs catalysts by aryloxide donors significantly perturbs the electronic properties of the resulting complex. Within a model Ru^{II} complex, introduction of a catecholate ligand raises the energy of the HOMO and, to a lesser extent, the energy of the LUMO. Significant polarization of electronic density towards the catecholate moiety is also observed, which promotes strong metal-ligand bond (e.g. Ru-PPh_3) and discourages ligand loss. This effect is evident from the low reactivity of model **Ru-2a** towards a variety of neutral ligands and the low initiation efficiency of catecholate catalysts **Ru-8/9**. As a result, both ROMP and RCM studies showed a consistently lower activity for the catecholate catalysts, relative to the parent dichloride complex **Ru-6a**.

The study on the effect of the anionic ligands on metathesis activity described herein is without a doubt the most important contribution of this Chapter. Key to this success was the remote location of the catechol substituents relative to the pyridine ligand, which removes any complication arising from varying steric demand from the equation. Of fundamental importance, the trend in activity observed is the opposite of that found in the Schrock group 6 system. That is, the activity of the Ru catalysts declines as the anionic ligands become more electron-deficient. While both initiation and propagation rates are affected, the effect in propagation is significantly greater. Thus, synthesis of catecholate catalysts bearing alternative, more labile placeholder ligands may show dramatically improved metathesis

activity. Alternatively, pseudohalide ligands with donor atoms of lower electronegativity may facilitate catalyst initiation. To this end, the next Chapter describes the synthesis and catalytic activity of nitrogen-bound pseudohalide catalysts. The lower electronegativity of this element is envisioned to limit the build-up of positive charge on the ruthenium, which could promote pyridine loss as well as favor metathesis by facilitating formation of the metallacyclobutane intermediate.

4.5 References

(1) Conrad, J. C.; Fogg, D. E., *Curr. Org. Chem.* **2006**, *10*, 185-202.
(2) Trnka, T. M.; Grubbs, R. H., *Acc. Chem. Res.* **2001**, *34*, 18-29.
(3) Jafarpour, L.; Nolan, S. P., *Adv. Organomet. Chem.* **2001**, *46*, 181-222.
(4) Jafarpour, L.; Nolan, S. P., *J. Organomet. Chem.* **2001**, *617*, 17-27.
(5) Buchmeiser, M. R., *Chem. Rev.* **2000**, *100*, 1565-1604.
(6) Katayama, H.; Ozawa, F., *Coord. Chem. Rev.* **2004**, *248*, 1703-1715.
(7) Grubbs, R. H., *Handbook of Metathesis*. Wiley-VCH: Weinheim, 2003.
(8) Fürstner, A., *Eur. J. Org. Chem.* **2004**, 943-958.
(9) Nicolaou, K. C.; Bulger, P. G.; Sarlah, D., *Angew. Chem., Int. Ed.* **2005**, *44*, 4490-4527.
(10) Fürstner, A., *Angew. Chem., Int. Ed.* **2000**, *39*, 3012-3043.
(11) van Otterlo, W. A. L.; de Koning, C. B., *Chem. Rev.* **2009**, *109*, 3743-3782.
(12) Kotha, S.; Lahiri, K., *Synlett* **2007**, 2767-2784.
(13) Gradillas, A.; Perez-Castells, J., *Angew. Chem., Int. Ed.* **2006**, *45*, 6086-6101.
(14) Martin, W. H. C.; Blechert, S., *Curr. Top. Med. Chem.* **2005**, *5*, 1521-1540.
(15) Samojlowicz, C.; Bieniek, M.; Grela, K., *Chem. Rev.* **2009**, *109*, 3708-3742.
(16) Vougioukalakis, G. C.; Grubbs, R. H., *Chem. Rev.* **2010**, *110*, 1746-1787.
(17) Weskamp, T.; Schattenmann, W. C.; Spiegler, M.; Herrmann, W. A., *Angew. Chem., Int. Ed.* **1998**, *37*, 2490-2493.
(18) Huang, J.; Stevens, E. D.; Nolan, S. P.; Petersen, J. L., *J. Am. Chem. Soc.* **1999**, *121*, 2674-2678.
(19) Scholl, M.; Ding, S.; Lee, C. W.; Grubbs, R. H., *Org. Lett.* **1999**, *1*, 953-956.
(20) Stewart, I. C.; Douglas, C. J.; Grubbs, R. H., *Org. Lett.* **2008**, *10*, 441-444.
(21) White, D. E.; Stewart, I. C.; Grubbs, R. H.; Stoltz, B. M., *J. Am. Chem. Soc.* **2008**, *130*, 810-811.
(22) Stewart, I. C.; Ung, T.; Pletnev, A. A.; Berlin, J. M.; Grubbs, R. H.; Schrodi, Y., *Org. Lett.* **2007**, *9*, 1589-1592.
(23) Berlin, J. M.; Campbell, K.; Ritter, T.; Funk, T. W.; Chlenov, A.; Grubbs, R. H., *Org. Lett.* **2007**, *9*, 1339-1342.
(24) Chung, C. K.; Grubbs, R. H., *Org. Lett.* **2008**, *10*, 2693-2696.
(25) Seiders, T. J.; Ward, D. W.; Grubbs, R. H., *Org. Lett.* **2001**, *3*, 3225-3228.
(26) Funk, T. W.; Berlin, J. M.; Grubbs, R. H., *J. Am. Chem. Soc.* **2006**, *128*, 1840-1846.
(27) Berlin, J. M.; Goldberg, S. D.; Grubbs, R. H., *Angew. Chem., Int. Ed.* **2006**, *45*, 7591-7595.
(28) Fournier, P.-A.; Collins, S. K., *Organometallics* **2007**, *26*, 2945-2949.

(29) Fournier, P.-A.; Savoie, J.; Stenne, B.; Bedard, M.; Grandbois, A.; Collins, S. K., *Chem. Eur. J.* **2008**, *14*, 8690-8695.
(30) Grisi, F.; Costabile, C.; Gallo, E.; Mariconda, A.; Tedesco, C.; Longo, P., *Organometallics* **2008**, *27*, 4649-4656.
(31) Van Veldhuizen, J. J.; Garber, S. B.; Kingsbury, J. S.; Hoveyda, A. H., *J. Am. Chem. Soc.* **2002**, *124*, 4954-4955.
(32) Van Veldhuizen, J. J.; Gillingham, D. G.; Garber, S. B.; Kataoka, O.; Hoveyda, A. H., *J. Am. Chem. Soc.* **2003**, *125*, 12502-12508.
(33) Gillingham, D. G.; Kataoka, O.; Garber, S. B.; Hoveyda, A. H., *J. Am. Chem. Soc.* **2004**, *126*, 12288-12290.
(34) Stenne, B.; Timperio, J.; Savoie, J.; Dudding, T.; Collins, S. K., *Org. Lett.* **2010**, *12*, 2032-2035.
(35) Schrock, R. R., *Chem. Rev.* **2009**, *109*, 3211-3226.
(36) Malcolmson, S. J.; Meek, S. J.; Sattely, E. S.; Schrock, R. R.; Hoveyda, A. H., *Nature* **2008**, *456*, 933-937.
(37) Amoroso, D.; Snelgrove, J. L.; Conrad, J. C.; Drouin, S. D.; Yap, G. P. A.; Fogg, D. E., *Adv. Synth. Catal.* **2002**, *344*, 757-763.
(38) Amoroso, D.; Yap, G. P. A.; Fogg, D. E., *Organometallics* **2002**, *21*, 3335-3343.
(39) Leitao, E. M.; Dubberley, S. R.; Piers, W. E.; Wu, Q.; McDonald, R., *Chem. Eur. J.* **2008**, *14*, 11565-11572.
(40) Hong, S. H.; Wenzel, A. G.; Salguero, T. T.; Day, M. W.; Grubbs, R. H., *J. Am. Chem. Soc.* **2007**, *129*, 7961-7968.
(41) Monfette, S.; Camm, K. D.; Gorelsky, S. I.; Fogg, D. E., *Organometallics* **2009**, *28*, 944-946.
(42) Monfette, S.; Fogg, D. E., *Organometallics* **2006**, *25*, 1940-1944.
(43) Conrad, J. C.; Parnas, H. H.; Snelgrove, J. L.; Fogg, D. E., *J. Am. Chem. Soc.* **2005**, *127*, 11882-11883.
(44) Conrad, J. C.; Amoroso, D.; Czechura, P.; Yap, G. P. A.; Fogg, D. E., *Organometallics* **2003**, *22*, 3634-3636.
(45) Paquette, L. A.; Schloss, J. D.; Efremov, I.; Fabris, F.; Gallou, F.; Mendez-Andino, J.; Yang, J., *Org. Lett.* **2000**, *2*, 1259-1261.
(46) Ahn, Y. M.; Yang, K.; Georg, G. I., *Org. Lett.* **2001**, *3*, 1411-1413.
(47) Maynard, H. D.; Grubbs, R. H., *Tetrahedron Lett.* **1999**, *40*, 4137-4140.
(48) Cho, J. H.; Kim, B. M., *Org. Lett.* **2003**, *5*, 531-533.
(49) Braddock, D. C.; Tanaka, K.; Chadwick, D.; Boehm, V. P. W.; Roeper, M., *Tetrahedron Lett.* **2007**, *48*, 5301-5303.
(50) Zhang, W.; Liu, P.; Jin, K.; He, R., *J. Mol. Catal. A* **2007**, *275*, 194-199.
(51) Gawin, R.; Makal, A.; Wozniak, K.; Mauduit, M.; Grela, K., *Angew. Chem., Int. Ed.* **2007**, *46*, 7206-7209.
(52) Halbach, T. S.; Mix, S.; Fischer, D.; Maechling, S.; Krause, J. O.; Sievers, C.; Blechert, S.; Nuyken, O.; Buchmeiser, M. R., *J. Org. Chem.* **2005**, *70*, 4687-4694.
(53) Samee, J. S. M.; Grubbs, R. H., *Chem. Eur. J.* **2008**, *14*, 2686-2692.
(54) Gawin, R.; Czarnecka, P.; Grela, K., *Tetrahedron* **2010**, *66*, 1051-1056.
(55) Krause, J. O.; Nuyken, O.; Wurst, K.; Buchmeiser, M. R., *Chem. Eur. J.* **2004**, *10*, 777-784.
(56) Jordaan, M.; Vosloo, H. C. M., *Adv. Synth. Catal.* **2007**, *349*, 184-192.

(57) Denk, K.; Fridgen, J.; Herrmann, W. A., *Adv. Synth. Catal.* **2002**, *344*, 666-670.
(58) Ledoux, N.; Drozdzak, R.; Allaert, B.; Linden, A.; Van Der Voort, P.; Verpoort, F., *Dalton Trans.* **2007**, 5201-5210.
(59) Monsaert, S.; Ledoux, N.; Drozdzak, R.; Verpoort, F., *J. Polym. Sci., Part A: Polym. Chem.* **2010**, *48*, 302-310.
(60) Vila, A. M. L.; Monsaert, S.; Drozdzak, R.; Wolowiec, S.; Verpoort, F., *Adv. Synth. Catal.* **2009**, *351*, 2689-2701.
(61) Occhipinti, G.; Jensen, V. R.; Bjorsvik, H.-R., *J. Org. Chem.* **2007**, *72*, 3561-3564.
(62) Hahn, F. E.; Paas, M.; Froehlich, R., *J. Organomet. Chem.* **2005**, *690*, 5816-5821.
(63) Dias, E. L.; Nguyen, S. T.; Grubbs, R. H., *J. Am. Chem. Soc.* **1997**, *119*, 3887-3897.
(64) Sanford, M. S.; Love, J. A.; Grubbs, R. H., *J. Am. Chem. Soc.* **2001**, *123*, 6543-6554.
(65) Buchowicz, W.; Ingold, F.; Mol, J. C.; Lutz, M.; Spek, A. L., *Chem. Eur. J.* **2001**, *7*, 2842-2847.
(66) Schrock, R. R., *Angew. Chem., Int. Ed.* **2006**, *45*, 3748-3759.
(67) Schrock, R. R.; Murdzek, J. S.; Bazan, G. C.; Robbins, J.; DiMare, M.; O'Regan, M., *J. Am. Chem. Soc.* **1990**, *112*, 3875-3886.
(68) Occhipinti, G.; Bjorsvik, H.-R.; Jensen, V. R., *J. Am. Chem. Soc.* **2006**, *128*, 6952-6964.
(69) Kotyk, M. W.; Gorelsky, S. I.; Conrad, J. C.; Carra, C.; Fogg, D. E., *Organometallics* **2009**, 5424–5431.
(70) Snelgrove, J. L.; Conrad, J. C.; Moriarty, M. M.; Yap, G. P. A.; Fogg, D. E., *Organometallics* **2005**, *24*, 103-109.
(71) Snelgrove, J. L.; Conrad, J. C.; Yap, G. P. A.; Fogg, D. E., *Inorg. Chim. Acta* **2003**, *345*, 268-278.
(72) Monfette, S.; Duarte Silva, J. A.; Gorelsky, S. I.; Dalgarno, S. J.; dos Santos, E. N.; Araujo, M. H.; Fogg, D. E., *Can. J. Chem.* **2009**, *87*, 361-367.
(73) Eelman, M. D.; Blacquiere, J. M.; Moriarty, M. M.; Fogg, D. E., *Angew. Chem., Int. Ed.* **2008**, *47*, 303-306.
(74) Fang, G.-S.; Huang, J.-S.; Zhu, N.; Che, C.-M., *Eur. J. Inorg. Chem.* **2004**, 1341-1348.
(75) Addison, A. W.; Rao, T. N.; Reedijk, J.; Van Rijn, J.; Verschoor, G. C., *J. Chem. Soc., Dalton Trans.* **1984**, 1349-1356.
(76) Hoffman, P. R.; Caulton, K. G., *J. Am. Chem. Soc.* **1975**, *97*, 4221-4228.
(77) Hirano, M.; Sato, H.; Kurata, N.; Komine, N.; Komiya, S., *Organometallics* **2007**, *26*, 2005-2016.
(78) Masui, H.; Lever, A. B. P.; Auburn, P. R., *Inorg. Chem.* **1991**, *30*, 2402-2410.
(79) Carugo, O.; Castellani, C. B.; Djinovic, K.; Rizzi, M., *J. Chem. Soc., Dalton Trans.* **1992**, 837-841.
(80) Boyer, J. L.; Rochford, J.; Tsai, M.-K.; Muckerman, J. T.; Fujita, E., *Coord. Chem. Rev.* **2010**, *254*, 309-330.
(81) Casida, M. E., *Recent Adv. Comput. Chem.* **1995**, *1*, 155-192.
(82) Casida, M. E., *Theor. Comput. Chem.* **1996**, *4*, 391-439.
(83) Stratmann, R. E.; Scuseria, G. E.; Frisch, M. J., *J. Chem. Phys.* **1998**, *109*, 8218-8224.
(84) Derrah, E. J.; Pantazis, D. A.; McDonald, R.; Rosenberg, L., *Organometallics* **2007**, *26*, 1473-1482.
(85) Banerjee, P.; Das, S.; Fanwick, P. E.; Goswami, S., *J. Organomet. Chem.* **2006**, *691*, 2915-2923.

(86) Jasimuddin, S.; Byabartta, P.; Sinha, C.; Mostafa, G.; Lu, T.-H., *Inorg. Chim. Acta* **2004**, *357*, 2015-2026.
(87) Das, C.; Saha, A.; Hung, C.-H.; Lee, G.-H.; Peng, S.-M.; Goswami, S., *Inorg. Chem.* **2003**, *42*, 198-204.
(88) Byabartta, P.; Jasimuddin, S.; Ghosh, B. K.; Sinha, C.; Slawin, A. M. Z.; Woollins, J. D., *New J. Chem.* **2002**, *26*, 1415-1424.
(89) Fallahpour, R.-A.; Neuburger, M., *Helv. Chim. Acta* **2001**, *84*, 715-721.
(90) Mashima, K.; Kaneyoshi, H.; Kaneko, S.-i.; Mikami, A.; Tani, K.; Nakamura, A., *Organometallics* **1997**, *16*, 1016-1025.
(91) tom Dieck, H.; Kollvitz, W.; Kleinwaechter, I., *Inorg. Chem.* **1984**, *23*, 2685-2691.
(92) Gorelsky, S. I.; Lever, A. B. P., *J. Organomet. Chem.* **2001**, *635*, 187-196.
(93) Mulliken, R. S., *J. Chem. Phys.* **1955**, *23*, 2343-2346.
(94) Mulliken, R. S., *J. Chem. Phys.* **1955**, *23*, 2338-2342.
(95) Mulliken, R. S., *J. Chem. Phys.* **1955**, *23*, 1841-1846.
(96) Mulliken, R. S., *J. Chem. Phys.* **1955**, *23*, 1833-1840.
(97) La Placa, S. J.; Ibers, J. A., *Inorg. Chem.* **1965**, *4*, 778-783.
(98) Schwab, P.; Grubbs, R. H.; Ziller, J. W., *J. Am. Chem. Soc.* **1996**, *118*, 100-110.
(99) Russell, S. K.; Lobkovsky, E.; Chirik, P. J., *J. Am. Chem. Soc.* **2009**, *131*, 36-37.
(100) Fogg, D. E.; Foucault, H. M., Ring-Opening Metathesis Polymerization. In *Comprehensive Organometallic Chemistry III*, Crabtree, R. H.; Mingos, D. M. P., Eds. Elsevier: Oxford, 2007; Vol. 11, pp 623-652.
(101) Gandelman, M.; Rybtchinski, B.; Ashkenazi, N.; Gauvin, R. M.; Milstein, D., *J. Am. Chem. Soc.* **2001**, *123*, 5372-5373.
(102) Nguyen, S. T.; Johnson, L. K.; Grubbs, R. H.; Ziller, J. W., *J. Am. Chem. Soc.* **1992**, *114*, 3974-3975.
(103) Harlow, K. J.; Hill, A. F.; Wilton-Ely, J. D. E. T., *J. Chem. Soc., Dalton Trans.* **1999**, 285-292.
(104) Cadierno, V.; Gimeno, J., *Chem. Rev.* **2009**, *109*, 3512-3560.
(105) Lozano-Vila, A. M.; Monsaert, S.; Bajek, A.; Verpoort, F., *Chem. Rev.* **2010**, *110*, 4865-4909.
(106) Batista, A. A.; Santiago, M. O.; Donnici, C. L.; Moreira, I. S.; Healy, P. C.; Berners-Price, S. J.; Queiroz, S. L., *Polyhedron* **2001**, *20*, 2123-2128.
(107) Seddon, E. A.; Seddon, K. R., *The Chemistry of Ruthenium*. Elsevier: Amsterdam, 1984.
(108) Love, J. A.; Morgan, J. P.; Trnka, T. M.; Grubbs, R. H., *Angew. Chem., Int. Ed.* **2002**, *41*, 4035-4037.
(109) The pK_a of the parent catechol was calculated using Advanced Chemistry Development (ACD/Labs) Software V8.14 for Solaris (1994-2005 ACD/Labs).
(110) Herrero-Martinez, J. M.; Sanmartin, M.; Roses, M.; Bosch, E.; Rafols, C., *Electrophoresis* **2005**, *26*, 1886-1895.
(111) Nurchi, V. M.; Pivetta, T.; Lachowicz, J. I.; Crisponi, G., *J. Inorg. Biochem.* **2009**, *103*, 227-236.
(112) Kurek, S. S.; Laskowska, B. J.; Stoklosa, A., *Electrochim. Acta* **2006**, *51*, 2306-2314.
(113) Chmurzynski, L., *Anal. Chim. Acta* **1996**, *321*, 237-244.
(114) Kim, S.; Oh, C. H.; Ko, J. S.; Ahn, K. H.; Kim, Y. J., *J. Org. Chem.* **1985**, *50*, 1927-1932.

(115) Zimmer, H.; Lankin, D. C.; Horgan, S. W., *Chem. Rev.* **1971**, *71*, 229-246.
(116) Teuber, H. J.; Staiger, G., *Chem. Ber.* **1955**, *88*, 802-827.
(117) Blacquiere, J. M.; McDonald, R.; Fogg, D. E., *Angew. Chem., Int. Ed.* **2010**, *49*, 3807-3810.
(118) Silverstein, R. M.; Webster, F. X., *Spectroscopic Identification of Organic Compounds*. 6th Ed. ed.; John Wiley & Sons: New York, 1998; p 482.
(119) Lee, J. P.; Ke, Z.; Ramirez, M. A.; Gunnoe, T. B.; Cundari, T. R.; Boyle, P. D.; Petersen, J. L., *Organometallics* **2009**, *28*, 1758-1775.
(120) Ritleng, V.; Barth, C.; Brenner, E.; Milosevic, S.; Chetcuti, M. J., *Organometallics* **2008**, *27*, 4223-4228.
(121) Dible, B. R.; Sigman, M. S., *Inorg. Chem.* **2006**, *45*, 8430-8441.
(122) Ben-Asuly, A.; Tzur, E.; Diesendruck, C. E.; Sigalov, M.; Goldberg, I.; Lemcoff, N. G., *Organometallics* **2008**, *27*, 811-813.
(123) Leuthaeusser, S.; Schmidts, V.; Thiele, C. M.; Plenio, H., *Chem. Eur. J.* **2008**, *14*, 5465-5481.
(124) Gallagher, M. M.; Rooney, A. D.; Rooney, J. J., *J. Organomet. Chem.* **2008**, *693*, 1252-1260.
(125) Sanford, M. S.; Love, J. A.; Grubbs, R. H., *Organometallics* **2001**, *20*, 5314-5318.
(126) Cavallo, L., *J. Am. Chem. Soc.* **2002**, *124*, 8965-8973.
(127) Armstrong, S. K., *J. Chem. Soc., Perkin Trans.* **1998**, 371-388.
(128) Bazan, G. C.; Khosravi, E.; Schrock, R. R.; Feast, W. J.; Gibson, V. C.; O'Regan, M. B.; Thomas, J. K.; Davis, W. M., *J. Am. Chem. Soc.* **1990**, *112*, 8378-8387.
(129) Benedicto, A. D.; Claverie, J. P.; Grubbs, R. H., *Macromolecules* **1995**, *28*, 500-511.
(130) Ivin, K. J.; Mol, J. C., *Olefin Metathesis and Metathesis Polymerization*. Academic Press: New York, 1997.
(131) Six, C.; Beck, K.; Wegner, A.; Leitner, W., *Organometallics* **2000**, *19*, 4639-4642.
(132) Gstrein, X.; Burtscher, D.; Szadkowska, A.; Barbasiewicz, M.; Stelzer, F.; Grela, K.; Slugovc, C., *J. Polym. Sci., Part A* **2007**, *45*, 3494-3500.
(133) Nomura, K.; Sakai, I.; Imanishi, Y.; Fujiki, M.; Miyamoto, Y., *Macromol. Rapid Commun.* **2004**, *25*, 571-576.
(134) Breslow, D. S., *Prog. Polym. Sci.* **1993**, *18*, 1141-1195.
(135) Wada, T.; Yamanaka, M.; Fujihara, T.; Miyazato, Y.; Tanaka, K., *Inorg. Chem.* **2006**, *45*, 8887-8894.

5. Second-generation, *N*-bound pseudohalide catalysts

5.1 Introduction

Understanding how ligand steric and electronic properties affect reactivity is central to catalyst design. In Ru-catalyzed olefin metathesis, much research effort has been directed at establishing the effect of the neutral phosphine and *N*-heterocyclic carbene (NHC) ligands on catalyst lifetime, activity and selectivity (see Chapter 1).[1,2] In comparison, the influence of the anionic ligands on these parameters remains little examined. The catecholate study described in Chapter 4 established the first unequivocal, positive correlation between metathesis activity and the electron-donating capacity of the anionic ligands.[3] Importantly, this trend is opposite to that originally proposed by the groups of Grubbs[4] and Jensen.[5]

Even for catalysts containing electron-rich catecholates, however, metathesis rates were slower than those for the parent dichloride complexes. Likewise, many of the aryloxide catalysts developed in the Fogg group[3,6-9] as well as carboxylate,[10-15] sulfonate[16] and alkoxide[17,18] catalysts developed by others, suffer from low activity at ambient temperature. Within the aryloxide system, this behavior reflects the stronger Ru-pyridine bond, which stems from the higher electronegativity of the oxygen atom relative to chloride. Charge polarization toward the aryloxide ligand starves the metal center of electronic density, and this is exacerbated when electron-withdrawing substituents are introduced to stabilize monodentate aryloxides against $\sigma-\pi$ isomerization.[19,20] Stronger binding of the other ancillary ligands compensates for the reduced electron density at the metal center, rendering them less labile. For the bis-perfluorophenoxide,[8] catecholate[3,6] and binaphtholate[7] catalysts, the cis arrangement of the anionic ligands also limits initiation, as also reported for cis-dichloride catalysts.[21-23]

For RCM reactions, strong pyridine binding to the metal center is partly mitigated by the elevated temperatures commonly employed[24,25] (which are now recognized as a key *entropic* contributor to the successful synthesis of medium and macrocyclic rings; Chapter 3). However, such conditions promote catalyst decomposition, particularly for the methylidene propagating species.[26-28] In ROMP applications, poor initiation rates limit control over polymer chain lengths and polydispersities, and use of elevated temperature does not offer a practical solution, as this also affects the rates of propagation. (Moreover, polymerization of

strained norbornenes still takes place at room temperature, preventing use of the aryloxide complexes as latent initiators).[29]

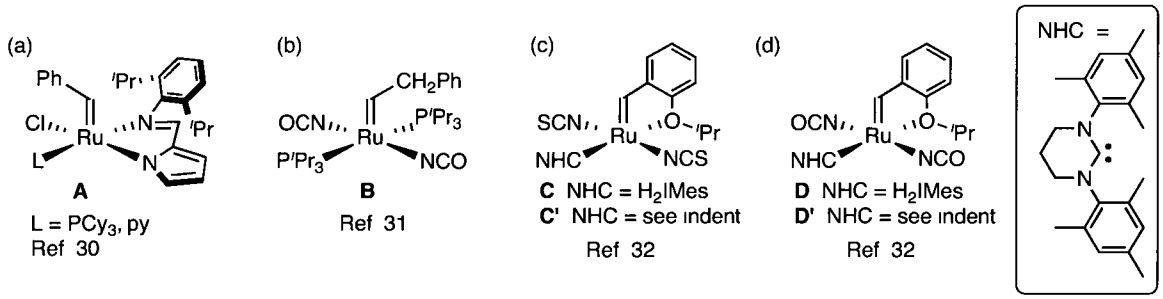

Chart 1. Ru-alkylidene complexes bearing *N*-anionic pseudohalide ligands.

Incorporation of nitrogen-bound anionic ligands was therefore considered. The lower electronegativity of nitrogen, vs. oxygen and chloride (N = 3.0, O = 3.4, Cl = 3.2) could limit the buildup of positive charge on the metal, resulting in faster initiation and propagation (Chapter 4). However, only four examples of Ru-alkylidene complexes bearing anionic nitrogen donors have so far been reported (Chart 1).[30-32] The imino-pyrrolato complexes **A** reported by our group[30] are essentially inactive for RCM at room-temperature even using the high-EM diethyl diallyl malonate (DeDAM, **11a**), although they are active at 70 °C in air. The low reactivity reflects the following factors: (1) the presence of four basal ligands of low lability, (2) the stability of the five-membered chelate ring, owing to which loss of the PCy_3 or py ligand is favored over loss of the imine donor, and (3), following loss of PCy_3 (to form PCy_3=O in air), weak electronic donation from the remaining ligands.

Two groups have pursued incorporation of the monodentate (NCE) ligand set (E = S, O). Attractive features of these ligands, in our view, are their low steric demand, their imperviousness to σ–π isomerization,[33] and their trans-disposition in **B**-**D** (Chart 1). Surprisingly, Werner and co-workers did not examine the metathesis activity of complex **B**.[31] The Buchmeiser group did assess the metathesis activity of their styrenyl ether derivatives **C**-**D**,[32] but puzzling inconsistencies emerged in catalyst performance.[34] In particular, the isocyanate complex **D** exhibited higher activity than isothiocyanate catalyst **C** in ROMP and CM, but this trend is reversed for RCM and cyclopolymerization (Scheme 1).[32] Likewise, the tetrahydropyrimidine catalysts showed faster ROMP and CM for **D'**, but faster RCM for **C'**.

Cyclopolymerization, however, was fastest for **D'**, rather than **C'**. No explanation for these behavior patterns was advanced.

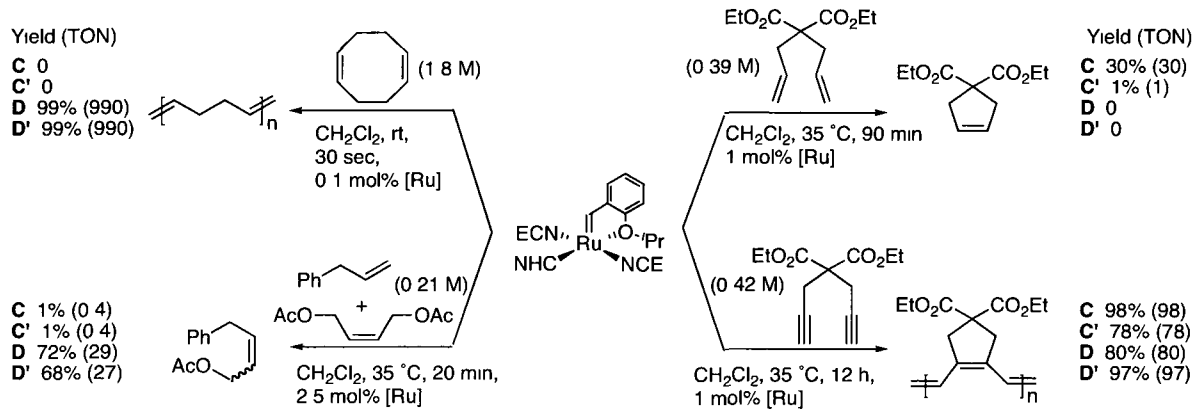

Scheme 1. Conflicting reactivity trends in Buchmeiser isothiocyanate and isocyanate complexes.[32]

At the outset of this work, the Werner complex was the only reported example of a ruthenium alkylidene complex bearing these linear pseudohalide ligands. In the hope of improving initiation efficiency relative to the aryloxide catalysts, high-yield routes to Ru(NCE-κ*N*)$_2$(CHPh)(IMes)(py)$_2$ were sought (**Ru-12a**: E = S, **Ru-12b**: E = O). This chapter describes their synthesis, characterization, and activity for metathesis under mild conditions. Remarkable differences in reactivity between the superficially very similar complexes **Ru-12a** and **Ru-12b** were revealed, which – in contrast with the styrenyl ether complexes – showed a consistent pattern in the RCM and ROMP manifolds. Thus, while the isocyanate complex **Ru-12b** proved highly active, the isothiocyanate **Ru-12a** was barely reactive under the same conditions. Importantly, the isocyanate catalyst **Ru-12b** also allowed controlled polymerization of a norbornene monomer, a goal that had proved elusive for the aryloxide catalysts.[3,35] The last part of this chapter presents an experimental and computational study aimed at understanding the origin of this reactivity difference.

5.2. Synthesis and characterization of Ru-12a/b

Commercially available Ag(NCE) salts were used to introduce the cyanate (NCO) and thiocyanate (NCS)$^-$ anions onto **Ru-6a**, in preference to the alkali metal salts, for the reasons given in Chapter 4.[38] Briefly, the rate of ligand exchange, vs. decomposition, is improved by using the Ag(I) salt to accelerate halide substitution.[36] Preliminary studies involved NMR-

scale reactions, in which integration of the benzylidene ^{1}H NMR signals against 1,3,5-trimethoxybenzene (TMB) as internal standard was employed to reveal any decomposition to non-alkylidene products. The thiocyanate reaction proceeded rapidly and cleanly at ambient temperature (Scheme 2). Thus, within 1 h of adding two equivalents of Ag(NCS) to a rapidly-stirred solution of **Ru-6a** in C_6D_6, the benzylidene singlet due to **Ru-6a** was completely replaced by a new singlet (20.02 and 18.48 ppm, respectively). Integration against TMB accounted for >95% of the starting **Ru-6a**, indicating essentially quantitative conservation of the benzylidene group. Reaction on 200 mg scale afforded analytically clean **Ru-12a** as a fine green powder in 97% yield following purification. NMR, MALDI-MS, XRD and combustion analyses support the structure depicted. Consistent with the small steric demand of the (NCS) ligand, and in contrast to prior work using bulkier perhaloaryloxide[8,9] or catecholate ligands,[3 6] both pyridine groups are retained in **Ru-12a**, as deduced from ^{1}H integration values. Infrared analysis revealed a band at 2095 cm ^{1}, which was attributed to the ν_{CN} stretch. This values compares well with that of 2083 cm^{-1} in the Buchmeiser isothiocyanate complex **D** (Chart 1).

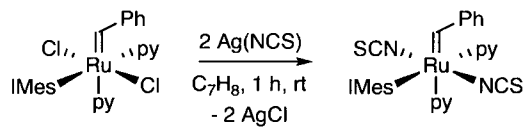

Ru-6a **Ru-12a**

Scheme 2. Synthesis of isothiocyanate catalyst **Ru-12a**.

Incorporation of the $(NCO)^-$ ligand presented some minor complications, in comparison. Preliminary ^{1}H NMR experiments using 2 equiv. Ag(NCO) afforded two Ru-benzylidene ^{1}H NMR singlets (19.54 and 19.11 ppm, respectively; 1:10) after 45 min at room temperature. No change was observed over a further 2 h reaction time, suggesting that salt metathesis was complete after the initial 45 min period. Integration versus TMB indicated quantitative conversion of **Ru-6a**, as before. The major product was assigned as the desired **Ru-12b**, and the minor product as mono-NCO derivative **Ru-12c** (Scheme 3), following observation of solely the benzylidene ^{1}H NMR singlet at 19.11 ppm on use of excess Ag(NCO).

On scaling up to 300 mg of **Ru-6a**, and using 3 equiv Ag(NCO) to effect complete chloride exchange, a yellow-green precipitate was obtained in 95% crude yield. Again, however, some minor complications were encountered. While the major constituent was **Ru-**

12b, two unexpected methyl singlets (2.17, 2.07 ppm; ratio 2:1; $CDCl_3$) were observed. These were traced to $[Ag(IMes)_2][NCO]$ **Ag-1**, a by-product arising from the use of excess Ag(NCO), present in ca. 12% yield. On limiting the proportion of Ag(NCO) to 2.2 equivalents, emerald-green **Ru-12b** could be isolated in 92% yield, accompanied by only trace **Ag-1** (3%). Attempts to remove **Ag-1** by extracting with common organic solvents were thwarted by the similar solubility of **Ag-1** and **Ru-12b**. Efforts at reprecipitation likewise proved unsuccessful, but small amounts of analytically clean **Ru-12b** could be reproducibly obtained by vapor diffusion of hexanes into a saturated THF solution at –35 °C. These crystals were utilized for catalysis and microanalysis, and also proved suitable for X-ray analysis. The structure depicted in Scheme 3 is thus supported by ^1H and ^{13}C NMR, MALDI-MS, combustion, and X-ray analysis. The ν_{CN} stretch was observed at 2230 cm^{-1},[37] a location identical to that reported for **B**[31] and close to the value of 2216 cm^{-1} reported for **D** (Chart 1b/d).[32]

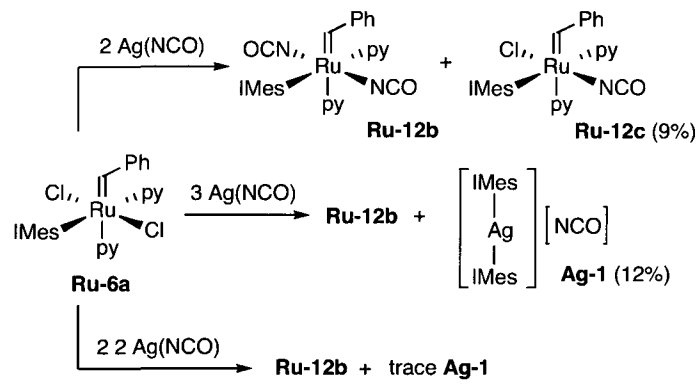

Scheme 3. Optimizing the synthesis of isocyanate catalyst **Ru-12b** (reactions at room temperature in C_6D_6 or toluene).

The identity of **Ag-1** was confirmed by its independent synthesis from Ag(NCO) and IMes (2.1 equiv) in acetone (Figure 1a). The complex was obtained as a white, analytically clean powder in 63% yield following reaction for 2 h at room temperature, workup (filtering through Celite, stripping to a red oil, and treating with diethyl ether to precipitate an off-white solid and leaving a red supernatant), and reprecipitation from CH_2Cl_2-hexanes. ^1H NMR values show excellent agreement with those assigned to **Ag-1** during synthesis of **Ru-12b**, as well as those reported for the cation $[Ag(IMes)_2]^+$ by the Arduengo group and others.[38-41] Of particular note is the doublet multiplicity of the imidazole ring protons, which

reveals long-range coupling to silver (7.15 ppm, $^{4}J_{Ag\text{-}H}$ = 1.5 Hz; $CDCl_3$). Closely similar values of 2.0 Hz were reported by the groups of Hedrick[42] and James.[41] The carbene carbon appears as a pair of $^{13}C\{^{1}H\}$ NMR doublets (182.4 ppm; $^{1}J_{Ag\text{-}C}$ = 208, 180 Hz; Figure 1b), owing to splitting by the ^{109}Ag and ^{107}Ag isotopomers, respectively. The location and coupling constants agree precisely with values reported for $[Ag(IMes)_2]X$ (X = PF_6^- or $[Ag(closo\text{-}CB_{11}H_{12})_2]^-$).[39,41] Finally, charge-transfer MALDI-TOF MS reveals a peak cluster at *m/z* 715.1 Da for $[Ag(IMes)_2]^+$ (theoretical value 715.3), with an isotope pattern corresponding exactly to that predicted (Figure 1c). The presence of the $(NCO)^-$ counteranion in **Ag-1** is indicated by the presence of a $^{13}C\{^{1}H\}$ NMR singlet at 136.6 ppm that correlates with no ^{1}H NMR signals (HMQC, HMBC), and an IR band at 2205 cm^{-1} assigned to the ν_{CN} stretch.

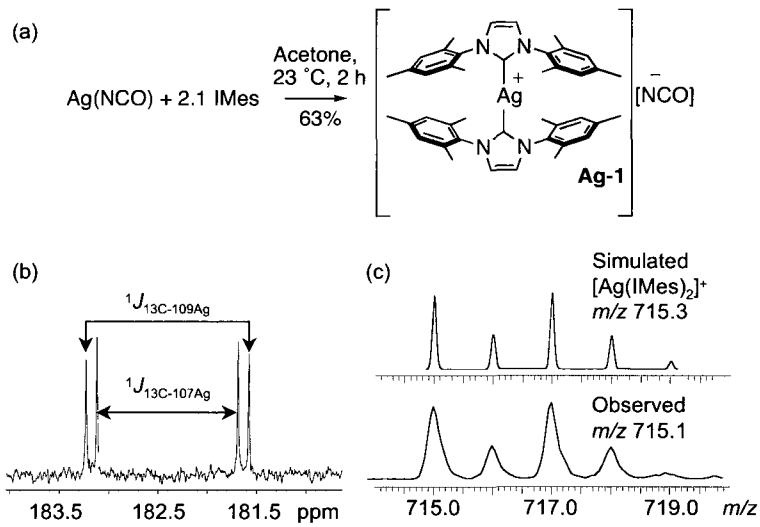

Figure 1. (a) Synthesis of **Ag-1**. (b) $^{13}C\{^{1}H\}$ NMR spectrum of the carbene region for **Ag-1** ($CDCl_3$; 125 MHz). (c) CT-MALDI MS spectra of **Ag-1** showing the simulated and observed isotope patterns for the $[Ag(IMes)_2]^+$ cation.

Formation of **Ag-1** during synthesis of **Ru-12b** implies formation of an additional, unidentified ruthenium complex. The observation of a single benzylidene signal suggests that this species is either not a benzylidene complex, or that it is paramagnetic. The latter is deemed unlikely given the excellent signal-to-noise ratio obtained for in situ NMR spectra. Given that ^{1}H and ^{13}C NMR analysis of the isolated product does not reveal extra signals (besides those of **Ag-1**), this side-product appears to be readily extracted. As NMR analysis

of the washings revealed only **Ru-12b** and **Ag-1**, no further attempts were made to identify the side-product.

5.3 X-ray analysis of Ru-12a/b

Blocky green crystals suitable for X-ray analysis were obtained by vapor diffusion of hexanes into a saturated THF solution of each complex at –35 °C. ORTEP representations are given in Figure 2, with relevant bond lengths and angles in Table 1. Both complexes adopt a slightly distorted octahedral geometry containing the usual iso(thio)cyanate linkage isomer (for detail, see Section 5.4). The Ru=C (**Ru-12a**: 1.901(6) Å; **Ru-12b**: 1.873(10) Å) and Ru-C_{NHC} (**Ru-12a**: 2.068(4) Å; **Ru-12b**: 2.050(6) Å) bond lengths agree well with those reported for dichloride **Ru-6b** (Ru=C: 1.873(4) Å; Ru-C_{NHC} 2.033(4) Å).[43] Comparison with the Buchmeiser isocyanate complex **D**[32] (Chart 1) is complicated by the presence of a styrenyl ether ligand and its square pyramidal geometry. Thus, both the Ru=C and Ru-C_{NHC} bonds are shorter (1.808(4) and 1.967(3) Å respectively) in **D** relative to **Ru-12a** and **Ru-12b** and **Ru-6b**. In contrast, the Ru-N_{NCE}(1) and Ru-N_{NCE}(2) bond distances for **Ru-12a** and **Ru-12b**, which range between 2.03-2.05 Å, are in good agreement with the corresponding values of 2.024(4) and 2.008(4) for **D**.[32] The Ru-N_{py}(3) bond lengths for **Ru-12a** and **Ru-12b** (2.191(4) and 2.195(5) Å respectively) are within experimental error of the 2.203(3) Å distance observed in **Ru-6b**,[43] but more than 0.1 Å longer than the corresponding values for the aryloxide and catecholate catalysts **Ru-7a**,[8] **Ru-8c**, **Ru-9a** and **Ru-9c** (Chapter 4).

Consistent with the majority of M-NCE complexes,[44] the N=C=E angles within **Ru-12a** and **Ru-12b** are essentially linear (178-179°). Although Burmeister has documented a greater variation for the M-N-C angle (126-179°),[44] the Ru-(N1,2)-C(3,4) angles are also near-linear (170°-174°). The steric pressure engendered by the proximity of the cis-disposed pyridine and mesityl group of IMes most likely accounts for the C(1)-Ru-N(4) angles of 161.54(18)° and 157.44(4)° observed in **Ru-12a** and **Ru-12b** respectively. That these angles are not influenced by the anionic ligands is evidenced by the very similar angle of 161.18(14)° found in the dichloride analog **Ru-6b**.[43] Stacking of the aromatic rings of the cis-disposed pyridine and mesityl arm of IMes is evidenced by a near-parallel arrangement of these rings; a deviation from co-planarity of 12.9° and 10.5° is observed in **Ru-12a** and **Ru-12b** respectively. The shortest distance between these rings is 3.4 Å in both **Ru-12a and Ru-12b**,

well within the range observed for two interacting aromatic rings (3-4 Å).[45] This distance is also in good agreement with the 3.0-3.6 Å separation found for the structurally reminiscent stacking of the benzylidene and mesityl rings of (e.g.) IMes in a range of related complexes.[46-51]

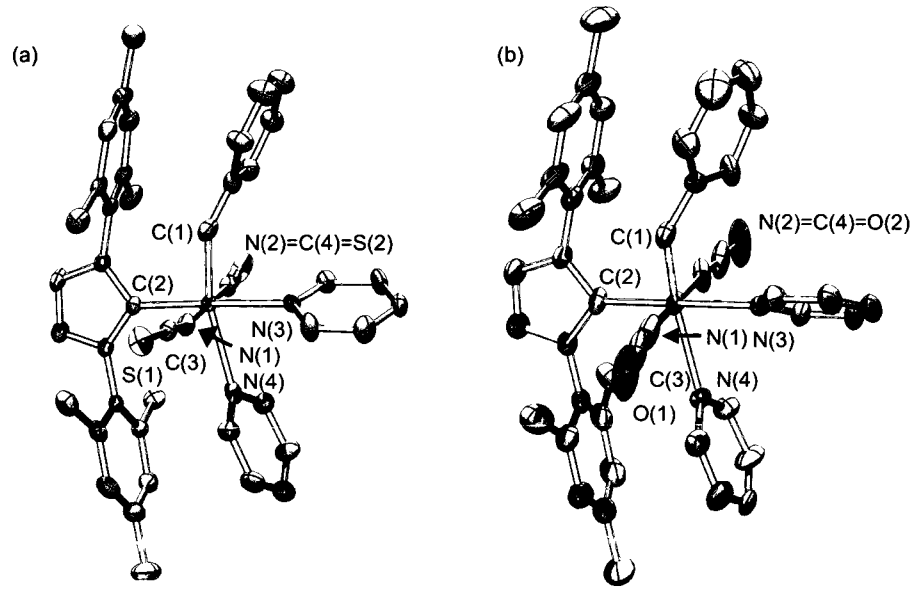

Figure 2. ORTEP representations of (a) **Ru-12a** and (b) **Ru-12b**. Hydrogens atoms and the THF solvate present in **Ru-12a**•THF are omitted for clarity. Thermal ellipsoids are drawn at 30% probability. Only relevant atoms are labeled here. See Figures A-5/6 in Appendix B for full structural detail.

Table 1. Selected bond lengths and angles for **Ru-12a** and **Ru-12b**.

Bond lengths (Å), angles (°)	**Ru-12a**	**Ru-12b**
Ru-C(1)	1.901(6)	1.873(10)
Ru-C(2)	2.068(4)	2.050(6)
Ru-N(1)	2.042(4)	2.034(5)
Ru-N(2)	2.050(4)	2.034(5)
Ru-N(3)	2.191(4)	2.195(5)
Ru-N(4)	2.331(4)	2.375(12)
C(1)-Ru-C(2)	96.3(2)	92.1(3)
C(2)-Ru-N(3)	176.67(16)	180.0
C(1)-Ru-N(4)	161.54(18)	157.4(4)
N(1)-Ru-N(2)	176.55(16)	178.8(3)
Ru-N(1)-C(3)	173.2(4)	174.0(5)
Ru-N(2)-C(4)	170.2(4)	174.0(5)
N(1)-C(2)-S(1)	178.1(5)	178.8(9)
N(3)-C(4)-O(2)	178.4(5)	178.8(9)

References page 188

5.4 Distinguishing between the $(NCE)^-$ ligand linkage isomers

Ever since the pioneering work of Werner and Jorgensen on the linkage isomer of the $(NO_2)^-$ anion over 100 years ago,[52] ambidentate ligands have been much studied in coordination chemistry.[44] Identification of the binding mode can be more challenging than commonly assumed. In the work described above, the more common pnictogen-bound isomer was attributed to **Ru-12a** and **Ru-12b**, based largely on the X-ray structural analysis. While this enables unequivocal assignment of the donor atom in the case of the $(NCS)^-$ ligand, it is less reliable for the $(NCO)^-$ anion, owing to the similar scattering factors for oxygen and nitrogen.[53] Examination of the refinement statistics can permit differentiation for high-quality crystals, however. In isocyanate **Ru-12b**, an improved fit is found for the isocyanate, vs. cyanate isomer ($R_1(F) = 0.0452$, $wR_2(F^2) = 0.1097$; $R_1(F) = 0.0467$, $wR_2(F^2) = 0.1153$, respectively). More convincing evidence comes from the displacement parameters (U_{eq}), which provide a measure of the positional uncertainty of the atoms in question. Since the only difference lies in the nature of the donor and terminal $(NCO)^-$ atoms, the U_{eq} parameters of interest are those for the nitrogen and oxygen atoms. As the position of the atom bound to the metal should be determined with greater accuracy, given the greater electron density at this location, the U_{eq} value is expected to be smaller for the Ru-ligated atom vs. the terminal atom. For the cyanate isomer, the U_{eq} values for oxygen and nitrogen are almost equal (0.1018(16) Å^2 and 0.103(2) Å^2 respectively), inconsistent with the expected trend. In contrast, the corresponding U_{eq} values for the isocyanate isomer (U_{eq}(N1) = 0.0777(15) Å^2, U_{eq}(O1) = 0.130(2) Å^2) follow the expected trend, supporting assignment as the isocyanate isomer.

Other characterization tools can aid in assigning the bonding mode. ^{13}C NMR analysis is particularly useful for the $(NCS)^-$ anion. As illustrated in Chart 2a for representative M-(NCE) complexes, the >15 ppm downfield shift for the $(NCS)^-$ carbon in the *N*-bound isothiocyanate isomer facilitates its identification, where both isomers are accessible. Establishing such trends for the $(NCO)^-$ ligand is more complicated, since no ruthenium cyanate complexes, and only a handful of M-OCN complexes[44] have been structurally characterized. As shown in Chart 2b, however, very similar chemical shifts are found for the $(NCO)^-$ carbon in selected ruthenium isocyanate complexes, and the recently characterized

tungsten cyanate complex reported by the Cummins group.[54] The utility of ^{13}C NMR analysis in differentiating between linkage isomers may thus be limited to the $(NCS)^-$ ligand.

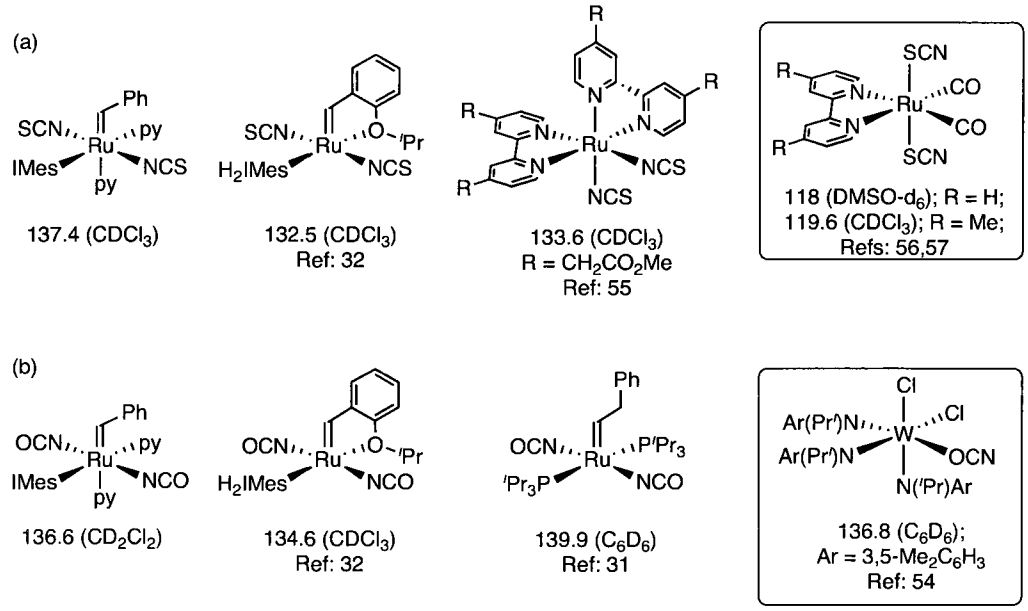

Chart 2. Selected examples of (a) $(NCS)^-$ and (b) $(NCO)^-$ complexes where the ^{13}C chemical shift of the $(NCE)^-$ ligand has been assigned.

Infrared analysis is commonly used to differentiate between M=N=C=E and M-E-C≡N moieties. In practice, however, this can be risky as band assignments are complicated by the dependence of stretching frequencies on the spin state and ligand environment around the metal.[58,59] For the $(NCE)^-$ ligands, three IR bands are expected: ν_{CN}, ν_{CE} stretch and δ_{NCE} in-plane bending.[60] Although the ν_{CE} band has been proposed to offer the most reliable IR handle for differentiating between linkage isomers for both $(NCS)^-$ and $(NCO)^-$,[60] its use is hampered by low intensity and its location in the fingerprint region (ν_{CO}: 1380-1140 cm^{-1}, ν_{CS}: 800 cm^{-1}). Reliance on the ν_{CN} stretch is thus more common.[60] For thiocyanate complexes, a 2075-2135 cm^{-1} range has been cited,[61] vs. a lower-energy location of ca. 2050 cm^{-1} for the isothiocyanate ligand.[61-64] A larger difference is found for the ν_{CN} stretch of the two linkage isomers of the $(NCO)^-$ anion: 2210–2235 cm^{-1} for the isocyanate isomer, 2005-2190 cm^{-1} for the cyanate isomer.[61] For **Ru-12b**, observation of the ν_{CN} band at 2230 cm^{-1} supports assignment as an isocyanate complex, consistent with the X-ray evidence. In contrast, however – and illustrative of the limitations of these IR assignments – the 2095

cm^{-1} location of the ν_{CN} stretch for **Ru-12a** would lead to assignment as the thiocyanate isomer (despite the conclusive X-ray evidence for the isothiocyanate bonding mode).

5.5 Catalytic activity of Ru-12a/b

5.5.1 Preliminary screening

As described in the introduction to this Chapter, no clear trend in reactivity for **C** and **D** emerged in the Buchmeiser study.[32] A systematic investigation of the catalytic reactivity of **Ru-12a** and **Ru-12b** was undertaken in order to uncover differences in activity between these two catalysts, and to assess their metathesis activity relative to the parent dichloride catalyst **Ru-6a** (Figure 3). The presence in the latter of a strongly activating IMes ligand with labile pyridine donors results in high metathesis activity,[65] and outstanding initiation efficiency, in contrast with the "second-generation" PCy_3-ligated catalysts **Ru-4**.[66] Probe reactions involved ROMP of norbornene monomer **21** (for which a large body of data was accumulated with the catecholate catalysts; Chapter 4) and RCM of high-EM dienes **9a** and **11a**. The results of the primary screen are shown in Figure 3c.

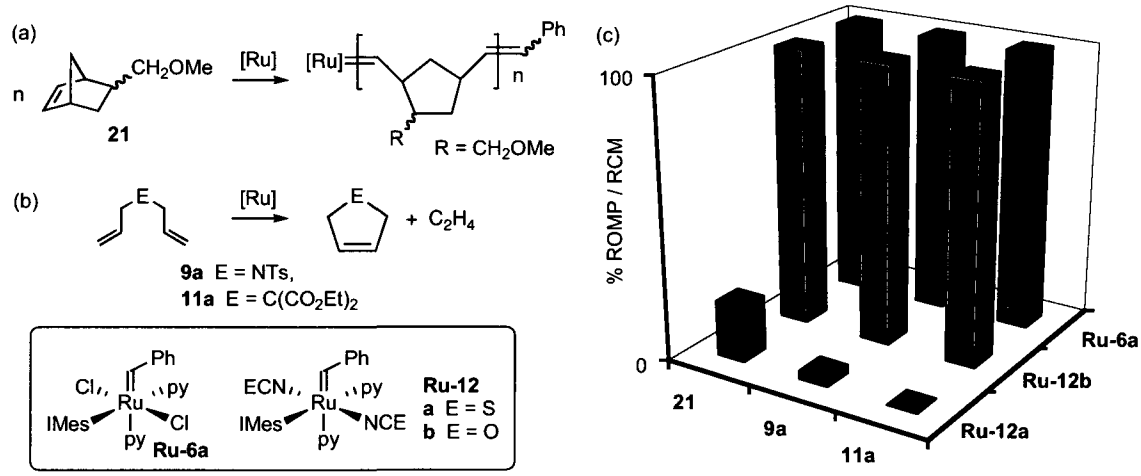

Figure 3. Initial reactions used to benchmark the metathesis activity of **Ru-12a** and **Ru-12b** relative to **Ru-6a**. (a) ROMP of **21**. (b) RCM of **9a** and **11a**. (c) Catalytic results. Conditions: **21**: 100 mM in CH_2Cl_2, 24 °C, 1 mol% [Ru]; conversion to product at 5 min for **Ru-6a** and **Ru-12b**; at 24 h for **Ru-12a**. **9a, 11a**: 100 mM in CH_2Cl_2, Δ, 0.5 mol% [Ru]; conversion to the RCM product at 15 min. ^1H NMR or calibrated GC-FID analysis (±1% in replicate runs).

ROMP of **21** is easily monitored by ^{1}H NMR analysis, from the upfield shift of the olefinic signals following ring-opening (ca. 6.1 ppm for **21**, vs. 5.3 ppm for the ROMP polymer; values in $CDCl_3$). Polymerization by **Ru-12b** was complete within 5 min under the same conditions of Chapter 4 (100 mM **21** in CH_2Cl_2, 24 °C, 1 mol% [Ru]). The reactivity of this catalyst is thus to completely polymerize **21** under identical conditions. Similar results were found for **Ru-6a**, but isothiocyanate **Ru-12a** was very unreactive (ca. 20% ROMP after 24 h). Thus, this catalyst is even less reactive than the slowest of the catecholate series, tetrabromo catecholate **Ru-9d**. The trend in reactivity, **Ru-12b** >> **Ru-12a**, is maintained in RCM reactions (conditions as in ROMP, but at reflux using 0.5 mol% [Ru]). While both isocyanate **Ru-12b** and dichloride **Ru-6a** effect quantitative cyclization of tosylamine **9a** and DeDAM **11a** in less than 15 min, **Ru-12a** was barely active (3% and <1% RCM for **9a** and **11a**). No increase in conversion was found over a further 5 h reaction, implying either fast decomposition or extremely low RCM rates for **Ru-12a**.

5.5.2 RCM of high-EM substrates

While Figure 3 demonstrates the remarkable difference in reactivity between the isothiocyanate and isocyanate catalysts, it tends to compress the activity difference between the more active isocyanate and dichloride catalysts **Ru-12b** and **Ru-6a**. Turnover frequency values measured at 50% conversion (TOF_{50}) offer a more useful comparison. These were extracted from the rate profile for RCM of DeDAM **11a** (Figure 4). Given the low reactivity of **Ru-12a**, this catalyst was not included in the RCM study, though it was further assessed in ROMP (Section 5.5.4).

RCM experiments were carried out at ambient temperature and low diene concentration (24 °C, 5 mM), in order to retard reaction sufficiently to obtain reproducible conversion curves (Figure 4). This deliberately restrained activity means that *no* catalyst achieved quantitative conversion of DeDAM **11a** into **12a**. Interestingly, despite the much higher initial TOF of **Ru-6a** and **Ru-12b**, the conversions observed after 6 h differed by <15% for these catalysts, vs. **Ru-4b** (pyridine-ligated **Ru-6a**: 86%; isocyanate **Ru-12b**: 75%; PCy_3-ligated **Ru-4b**: 71%). This, in conjunction with the plateau in their RCM curves, indicates that deactivation offsets the initially higher activity of **Ru-6a** and **Ru-12b**.

References page 188

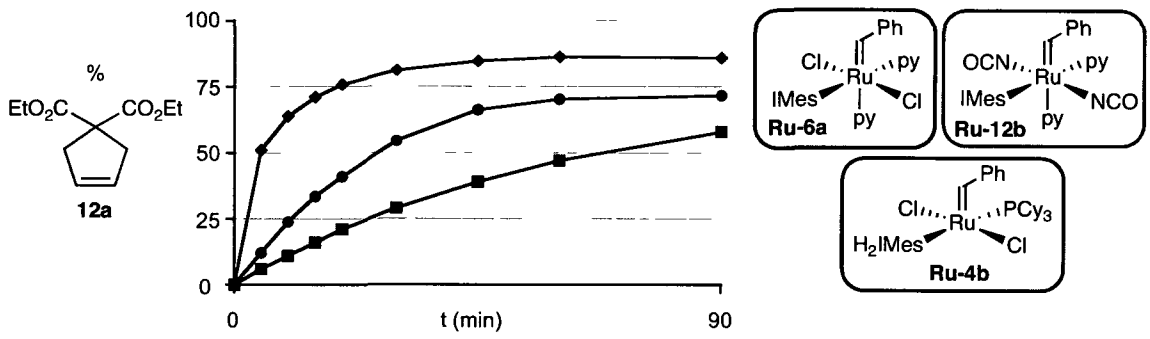

Figure 4. RCM formation of **12a** catalyzed by **Ru-4b** (■), **Ru-6a** (◆) and **Ru-12b** (●). Conditions: 5 mM **12a** in CH_2Cl_2, 24 °C, 1 mol% [Ru]. Calibrated GC-FID analysis (±1% in replicate runs). TOF_{50} values for **Ru-6a**, **Ru-12b**, **Ru-4b**: 600, 113, 44 h^{-1}.

Catalyst lifetime was assessed for **Ru-12b** vs. **Ru-6a** in RCM of DeDAM **11a** at low catalyst loadings (10,000 equiv. **11a**; 0.01 mol%) over 18 h at 40 °C, at a diene concentration of 100 mM. In CH_2Cl_2, a maximum TON of 2,720 was found for **Ru-12b**, vs. 4,600 for dichloride **Ru-6a**. TON values drop in THF, to 2,380 and 3,245 for **Ru-12b** and **Ru-6a** respectively. Interestingly, dichloride **Ru-6a** shows a greater sensitivity to this solvent switch, with a drop in TON of 1355, vs. 340 for **Ru-12b**. This may indicate that **Ru-12b** binds THF less strongly.

5.5.3 RCM macrocyclization

As discussed in Chapter 3, RCM of conformationally flexible α,ω–dienes proceeds via an oligomerization-backbiting pathway for any second- or third-generation Grubbs catalyst. Further, perbromoaryloxide **Ru-7b** exhibits a strong kinetic bias toward macrocyclization, over oligomerization.[9] The pentabromophenoxide ligand is clearly implicated in this selectivity. It was unclear, however, whether this effect originated in steric or electronic differences between the chloride and perbromophenoxide ligands. Chapter 3 concluded with a call for investigation of other pseudohalide catalysts for RCM macrocyclization, to gain insight into the origin of this selectivity difference. Where use of the catecholate catalysts of Chapter 4 was impeded by their low reactivity and thermal instability, the higher reactivity of isocyanate **Ru-12b** opens the door for such a study. Of particular interest is the question of whether this catalyst behaves like the Grubbs second-generation catalysts, or if it shares the kinetic bias of **Ru-7b** toward RCM.[9]

References page 188

Macrolactonization of **1b** was carried out as in Chapter 3, in CH_2Cl_2 at 20 °C and 40 °C. Dichloride **Ru-6a** exhibited higher RCM activity than **Ru-12b** at either temperature (Figure 5b/c). At 20 °C, 24% conversion to **2b** was evident after 30 min, with conversions reaching a plateau at 39% after 5 h. In comparison, <2% **2b** was detected at 30 min for **Ru-12b**, 13% at 5 h, with a plateau at 18% after 7 h. The proportion of oligomers using either catalyst reached 7% at 15 min, and then remained constant. Elevated temperatures may be required to accelerate backbiting of oligomers.[67 68]

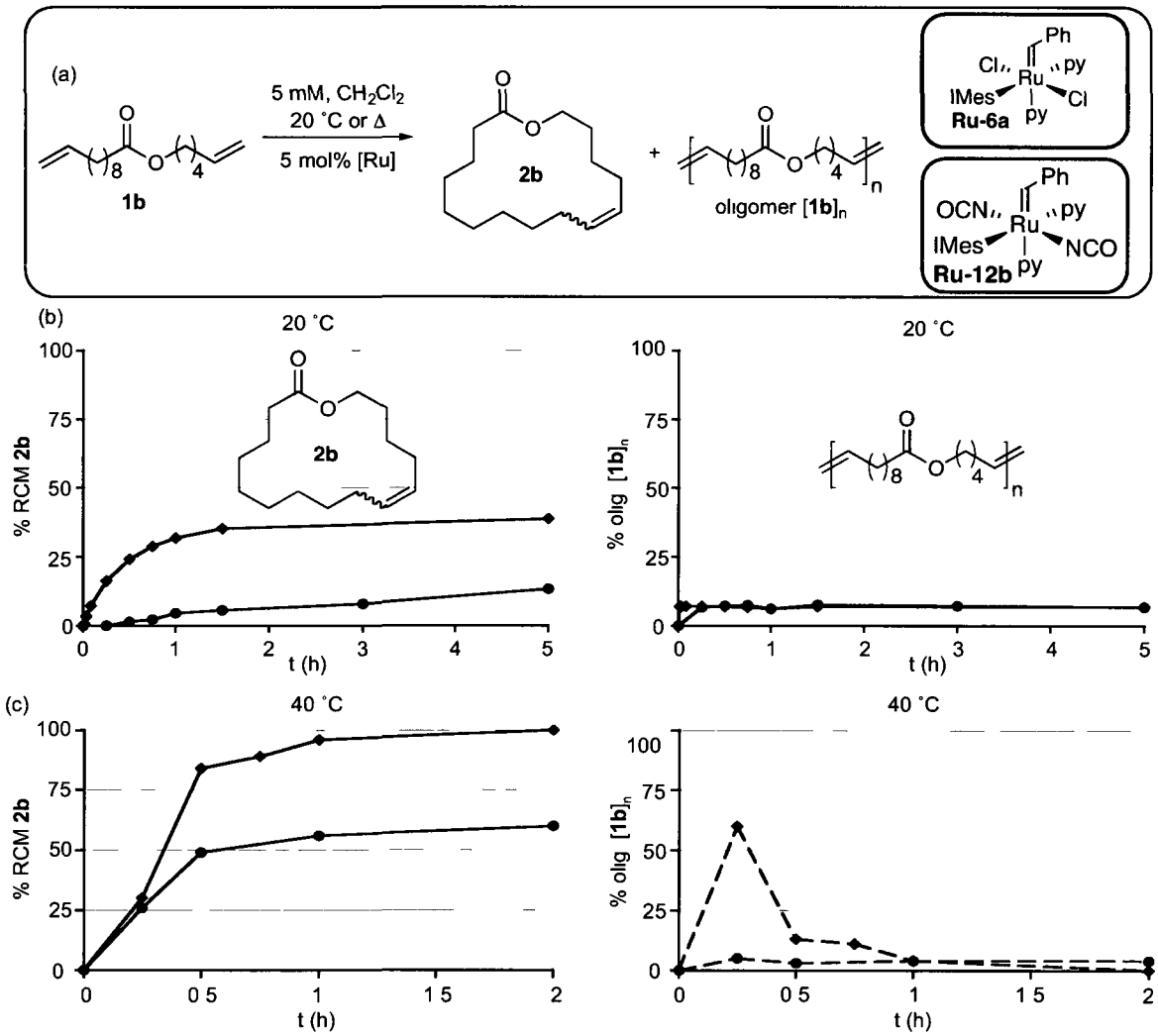

Figure 5. (a) RCM macrocyclization reaction investigated. (b) Proportion of macrolactone **2b** (left) and oligomeric species (right) formed during RCM of **1b** as a function of time at 20 °C. (c) Proportion of **2b** (left) and oligomers (right) over time at 40 °C. Conditions: (b) 5 mM **1b** in CH_2Cl_2, 20 °C, 5 mol% [Ru]; (c) 5 mM **1b** in CH_2Cl_2, Δ, 5 mol% [Ru]. Calibrated GC-FID analysis (±1% in replicate runs). **Ru-6a** (◆) and **Ru-12b** (●).

In refluxing CH_2Cl_2 (Figure 5c), **Ru-12b** showed a kinetic selectivity for cyclic **2b**. At 15 min, 26% **2b** and 5% oligomers were observed, this increasing to 60% and 5% at 2 h (after which reaction ceased). In comparison, **Ru-6a** achieved 90% conversion of starting **1b** at just 15 min, but the product contained only 30% **2b**. RCM was quantitative at 2 h, indicating complete backbiting of initially-formed oligomers.

Earlier work from our group described macrocyclization of **1b** via pentabromoaryloxide **Ru-7b**.[9] RCM was complete at 15 min, without formation of oligomers, on dropwise addition of catalyst and substrate solutions to refluxing CH_2Cl_2. While this protocol was designed to curb thermal decomposition of **Ru-7b**, it may artificially limit oligomerization. The "single-dose" addition protocol used here permits a more unambiguous assessment of the bias toward RCM. The low proportion of oligomers formed by **Ru-12b** confirms that macrocyclization is preferred. Both **Ru-7b** and **Ru-12b** effect minimal oligomerization of **1b**, despite a significant difference in size between the pentabromophenoxide and the isocyanate ligands. The bias of these catalysts toward RCM of flexible substrates may therefore be electronic in nature.

5.5.4 ROMP study

The dramatically lower metathesis activity of **Ru-12a**, vs. **Ru-12b** (Section 5.5.1), was initially unexpected given the lower electronegativity of sulfur vs. oxygen (2.6 vs. 3.4). The structural similarity between the two catalysts suggests that this activity difference is electronic in origin. As a difference in pyridine lability was suspected as the immediate cause, the initiation efficiency of **Ru-12a** and **Ru-12b** was assessed in ROMP of **21**. The Ru-py bond energy was also evaluated by DFT methods, as discussed in Section 5.6.2.

ROMP using third-generation Grubbs catalysts such as **Ru-6a** is typically accompanied by an instantaneous color change from green to yellow-brown on initiation. No such immediate color change was evident for the aryloxide and catecholate catalysts, consistent with their low turnon efficiency.[3,35] Likewise, no rapid color change was observed for isothiocyanate **Ru-12a** on addition of norbornene monomer **21**. For the aryloxide and isothiocyanate catalysts, the expected color change took place over several hours. In contrast, ROMP of **21** by isocyanate **Ru-12b** is accompanied by a time-of-mixing color change from emerald green to yellow-brown. This qualitative indicator suggests very fast initiation for **Ru-12b**.

Established NMR methods[69-71] were used to determine the rates of propagation vs. initiation (k_p/k_i) for **Ru-12b**. Thus, a $CDCl_3$ solution of monomer **21** and catalyst **Ru-12b** (100 mM **21**, 10 mol% **Ru-12b**) was analyzed after 5 min at room temperature, vs. identical solutions containing **Ru-6a** as catalyst. Complete polymerization was evident for both **Ru-6a** and **Ru-12b**, as expected from Figure 3. Figure 6 shows the ^1H NMR spectra (alkylidene region) for these catalysts after 5 min. In both cases, the propagating alkylidene gives rise to a broad multiplet ca. 0.4 ppm upfield of the parent benzylidene singlet, in 6:1 ratio for **Ru-6a** and 1.3:1 for **Ru-12b**. Use of equation (1)[35,69] indicates a k_p/k_i ratio of 5.1 and 11.9 for **Ru-6a** and **Ru-12b** respectively (N.B. Given the low rate of metathesis via **Ru-12a**, the k_p/k_i ratio for this catalyst could not be measured). The k_p/k_i ratio for **Ru-12b** is >20× smaller than the value of 266 measured for **Ru-7b** with (±)-5-norbornene-2-methylacetate as monomer,[35] implying a significantly faster initiation for **Ru-12b**. Minimal change in k_p/k_i is found for this monomer vs. **21** using **Ru-6a** (5.1 vs. 4.7),[35] suggesting that the difference between **Ru-12b** and **Ru-7b** is not due to the different monomer employed. **Ru-12b** thus appears to be the first Ru-pseudohalide catalyst that can afford ROMP polymers with well-defined chain lengths. The polymers were therefore isolated and characterized.

$$\frac{k_p}{k_i} = \frac{-M_0 / I_0}{\ln\left(\frac{I_t}{I_0}\right) + (I_t)\left(\frac{I_t}{I_0} - 1\right)} \qquad (1)$$

M_0 = Initial monomer concentration
I_0 = Initial initiator concentration
I_t = Initiator concentration at time t

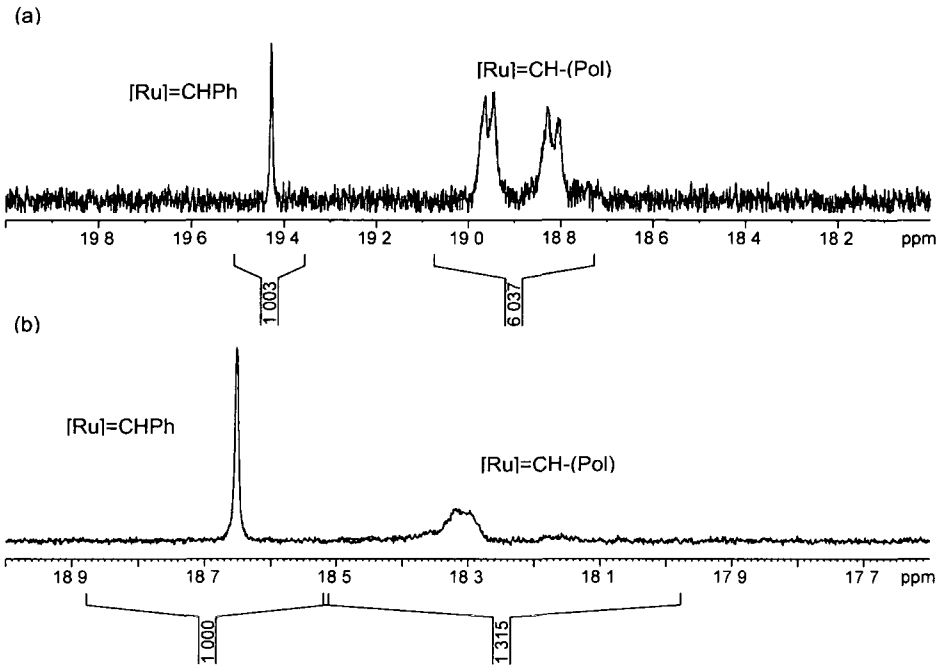

Figure 6. ^{1}H NMR spectra of the alkylidene region for (a) **Ru-6a** and (b) **Ru-12b** after complete ROMP of **21**. Conditions: 100 mM **21** in $CDCl_3$, 24 °C, 5 min, 10 mol% [Ru].

Polymerization of **21** was carried out on 100 mg scale with catalysts **Ru-6a**, **Ru-12a** and **Ru-12b**, as in Section 5.5.1. Polymer molecular weights and polydispersities were assessed by light-scattering GPC (Table 2). Initiation efficiencies can be inferred by comparing polymer chain lengths with theoretical values (Eq 2), as explained in Section 4.3.4.[72-74]

$$\text{IE} = M_n(\text{calcd.}) / M_n(\text{exptl.}) \quad (2)$$

Owing to their fast initiation, **Ru-6a** and its H_2IMes analog **Ru-6b** are regarded as ideal for synthesis of well-defined ROMP polymers.[75-78] The results obtained with **Ru-6a** and **Ru-12b** are thus striking. Respectable polydispersities were found (1.1 and 1.13, respectively), and average chain lengths (108 and 167 repeating units) close to the theoretical value of 100, based on 1 mol% [Ru]. In comparison, dimethyl catecholate **Ru-8a** and catechol **Ru-9a**, the two most reactive catecholate catalysts, afforded polymers 100× longer than predicted. Likewise, perbromoaryloxide **Ru-7b** affords a polymer ca. 10× longer than predicted, with a PDI of 1.48. For the isothiocyanate catalyst **Ru-12a**, polymer chains >150× longer than theoretical values were obtained. Relative initiation efficiencies calculated from the polymer molecular weights are two orders of magnitude higher for **Ru-12b** vs. **Ru-12a**. Indeed, **Ru-12b** is the highest-performing Ru-pseudohalide initiator so far reported for the synthesis of

well-defined polymers and opens the door to tandem ROMP-hydrogenation.[76,79] Also of interest given the polarity of the isocyanate ligand of **Ru-12b** (see Section 5.6.2) is the potential of this catalyst to be easily removed from the organic products by column chromatography, as was previously shown for aryloxide catalysts.[9]

Table 2. Data for poly-**21** obtained using different catalysts.

Catalyst	Time	M_n ($\times 10^{-3}$)	% Conv.[a]	% Yield[b]	PDI	Rel. IE (%)[c]
Ru-6a	10 min	15	100	91	1.10	1
Ru-7b	30 min	140	100	87	1.48	0.1
Ru-12a	24 h	354[d]	15	13	1.45	0.007
Ru-12b	10 min	23	100	90	1.13	0.7

[a] % Conv. = % conversion to polymer at time stated (^{1}H NMR analysis). [b] % Yield = isolated yield. [c] % IE (initiation efficiency) = M_n (calcd.)/M_n (exptl.) × 100 (M_n (calcd.) = 13.8 × 10^3 Da). M_n (exptl.) is the average of two separate ROMP experiments; M_n data measured in duplicate for each; errors range from ±2-6%. [d] At 15% conversion, M_n (calcd.) = 2.1 × 10^3 Da.

5.6 Computational studies

The origin of the preference for the *N*-bound $(NCE)^-$ isomers, and the reactivity difference between **Ru-12a** and **Ru-12b**, were explored in a DFT study of the non-truncated complexes at the B3LYP/DZVP level of theory.

5.6.1 Energy difference between the binding modes of the $(NCE)^-$ ligands

Testimony to the long-standing interest in $(NCE)^-$ ligands, Tuan and Hoffmann explored the binding mode of these anions in two computational studies dating back 20 years.[80,81] A fragment orbital analysis was undertaken using the extended Hückel method to evaluate the energy difference between the linkage isomers of $[Ru(NH_3)_5(NCO)]^+$. The consistently higher stability of the isocyanate isomer was attributed to the larger spatial extension of the nitrogen atomic orbitals, relative to oxygen, which enables better overlap with the metal center, stabilizing the isocyanate complex.[80] In a subsequent study, these authors suggested a small energy difference between linkage isomers for $[Ru(NH_3)_5(NCS)]^+$,[81] and indeed both isomers are evident (IR, UV-Vis) for the Ru^{III} analog $[Ru(NH_3)_5(NCS)]^{2+}$.[82]

Quantitative assessment of the metal-ligand interactions in **Ru-12a/b** was undertaken in the present work by energy decomposition analysis (EDA) of the overall electronic bond energy (ΔE_E; Eq 3).

$$\Delta E_E = \Delta E_{Pauli} + \Delta E_{elec} + \Delta E_{orb} = \Delta E_{st} + \Delta E_{orb} \quad (3)$$

Since its development by Morokuma[83] and by Ziegler,[84] EDA has been used to evaluate the electronic interactions in many different types of chemical bonds between atoms across the periodic table,[85-89] including in a study of donor-acceptor interactions in the Grubbs catalysts.[90] The method begins by dividing the bond of interest into fragments that are analyzed independently, then brought together from an infinite distance with appropriate alignment for reaction (Figure 7). As the inter-fragment distance decreases, an attractive electrostatic energy (ΔE_{elec}) between nuclear charges develops. A compensating electronic repulsion (termed ΔE_{Pauli} after the Pauli exclusion principle) is generated between the filled orbitals of the two fragments. The sum of these opposing energies gives the total steric interaction (ΔE_{st}), the first of two terms contributing to the total electronic bond energy (ΔE_E). The second is the orbital interaction term (ΔE_{orb}): that is, the energy change incurred when the orbitals of fragments A and B mix and relax to the optimal geometry of molecule AB. The ΔE_{orb} term accounts for charge-transfer as well as polarization effects within the A-B bond.[91] The total electronic bond energy (ΔE_E; Eq 3) is the sum of the ΔE_{Pauli}, ΔE_{elec} and ΔE_{orb} terms. To put these parameters in relation to one another, the electrostatic attraction (ΔE_{elec}) and orbital interaction (ΔE_{orb}) strengthen the A-B bond, while the electronic repulsion (ΔE_{Pauli}) weakens it. It may be noted that ΔE_E does not correspond precisely to the A-B bond dissociation energy, but is closely related to the enthalpy term for formation of the A-B bond.[91]

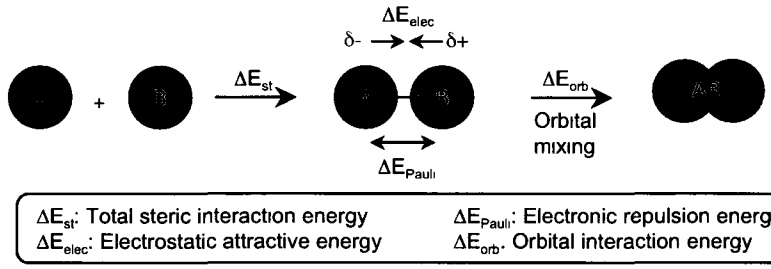

Figure 7. Cartoon representation of the different energies contributing to the total electronic bond energy. Adapted from reference 91.

Evaluation of the energy difference between linkage isomers for **Ru-12** necessitates fragmentation at the [Ru]-(NCE) bonds. Fragment 1 (F1) is thus $[Ru(CHPh)(IMes)(py)_2]^{2+}$; Fragment 2, $(NCS)^-$; Fragment 3, $(NCO)^-$. An energy diagram of the frontier orbitals of F2 and F3 appears in Figure 8. In accordance with Eq 3, ΔE_{orb} and ΔE_{st} were calculated for both linkage isomers to evaluate their energy differences.

ΔE_{orb} of pnictogen binding mode. σ-Donation from F2 to the Ru-based F1 LUFO dominates the Ru-NCS orbital interactions in $Ru(NCS\text{-}\kappa N)_2(CHPh)(IMes)(py)_2$. Thus, the net population of HOFO-2 and HOFO-5 in F2 drops by 35.6% on turning on the F1-F2 interaction, corresponding to a transfer of 0.71 electrons (e^-). This is augmented by a weak ligand-to-metal π donation (0.13 e^-) from the HOFO-0,1 and HOMO-3,4 of F2. A small compensating metal-to-ligand back-donation contributes an 0.18 e^- increase in the F2 π* population (LUFO+0,1).

The Ru-NCO orbital interactions in $Ru(NCO\text{-}\kappa N)_2(CHPh)(IMes)(py)_2$ are likewise dominated by σ-donation from F3 to F1. However, only the HOFO-2 levels contribute to σ-donation. Contributions from HOFO-5 are limited by its low energy and low nitrogen-character (4% N; cf. 15% for F2; Figure 8). The population of HOFO-2 drops by 32.6% on turning on the F1-F3 interaction, corresponding to a transfer of 0.65 e^-, reinforced by π-donation of 0.15 e^- from HOFO-0,1 of $(NCO)^-$ to F1. This interaction is slightly stronger than in the $(NCS)^-$ complex, owing to the higher energy of the HOMO-0,1 π levels of F3. The higher energy of the π* levels in F3, however, results in weaker Ru-to-NCO π* back-donation (0.11 e^-). The total ligand-to-metal charge transfer is thus similar for both $(NCE)^-$ ligands, with transfer of 0.66 e^- from F2 and 0.69 e^- from F3 to the Ru fragment. The ΔE_{orb} extracted from the fragment analysis is -128.0 kcal mol^{-1} for **Ru-12a** and -134.0 kcal mol^{-1} for **Ru-12b**.

References page 188

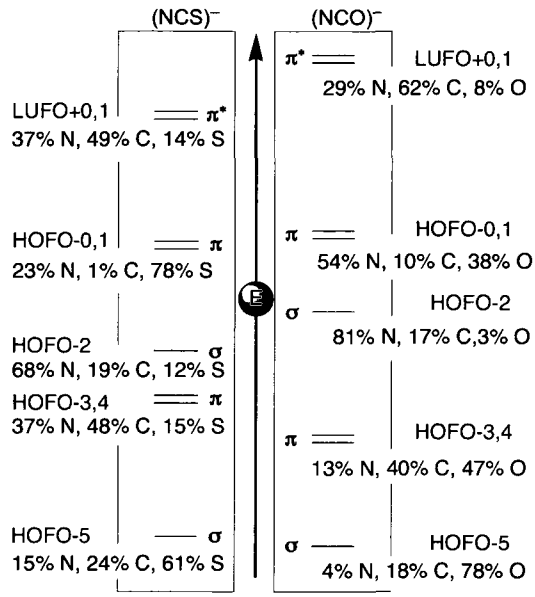

Figure 8. Relative energy levels and atomic contributions to the frontier orbitals of the $(NCE)^-$ ligands.

ΔE_{orb} of chalcogen binding mode. Unlike the FMO interactions that affect pnictogen binding, the interactions in Ru(ECN-κ*E*)$_2$(CHPh)(IMes)(py)$_2$ are driven solely by ligand-to-metal σ-donation. In Ru(SCN-κ*S*)$_2$(CHPh)(IMes)(py)$_2$ this donation involves chiefly the HOFO-0, HOFO-1 and HOMO-5 of $(NCS)^-$. The six HOFOs (HOFO-0 to HOFO-5) of the $(NCS)^-$ ligands decrease by 56.9% in population, corresponding to transfer of 1.14 e^- from these MOs. In Ru(OCN-κ*O*)$_2$(CHPh)(IMes)(py)$_2$, σ-donation is weaker by nearly 50%, the same six HOFOs decreasing in population by only 32.4%, for a transfer of 0.65 e^-. This reflects the lower chalcogen character of HOFO-0,1: 38% for the $(NCO)^-$ ligand, vs. 78% for the $(NCS)^-$ ligand. The EDA-calculated ΔE_{orb} for the Ru-ECN interaction is -122.6 kcal mol^{-1} in Ru(SCN-κ*S*)$_2$(CHPh)(IMes)(py)$_2$, and -105.8 kcal mol^{-1} for Ru(OCN-κ*O*)$_2$(CHPh)(IMes)(py)$_2$, energies 11.4 and 22.2 kcal mol^{-1} (respectively) higher than their *N*-bound linkage isomers.

ΔE_{st} between chalcogen and pnictogen binding mode. The steric interaction energies calculated for isothiocyanate **Ru-12a** and isocyanate **Ru-12b** are 11.9 and 1.3 kcal mol^{-1}, respectively, lower than their chalcogen-bound linkage isomer. Destabilization of the latter can arise from filled-filled orbital repulsion (higher ΔE_{Pauli}) for M-ECN complexes that are bent at E.[44] The near-linear M-N-C angles in **Ru-12a/b** (Figure 2, Table 1) minimize such

effects, however. The smaller difference in ΔE_{st} for the $(NCO)^-$ linkage isomers presumably originates in the stronger electrostatic interaction between F1 and F3, a function of the higher Pauling electronegativity of oxygen vs. sulfur (3.4 vs. 2.6 respectively).

The combined ΔE_{orb} and ΔE_{st} (Table 3) energies calculated for the linkage isomers of **Ru-12a/b** predict greater stability for the pnictogen binding mode, consistent with the X-ray results. The extent of the thermodynamic preference is rather similar. Thus, within the $(NCS)^-$ complexes, the isothiocyanate isomer **Ru-12a** is favored by 27.2 kcal mol^{-1}; within the $(NCO)^-$ complexes, the isocyanate isomer **Ru-12b** is favored by 29.2 kcal mol^{-1}.

Table 3. Energy decomposition analysis (kcal mol^{-1}) of the Ru-(NCE-κ*N*) and Ru-(ECN-κ*E*) interactions at the B3LYP/DZVP level of theory.

	Complex	ΔE_E	E_{st}	E_{orb}	-LUFO eV	q(Ru)[a] fragment	q(Ru)[a] complex
1	Ru(NCS-κ*N*)$_2$(CHPh)(IMes)(py)$_2$	0.0	-171.6	-128.0	-10.40	+0.95	+0.61
2	Ru(SCN-κ*S*)$_2$(CHPh)(IMes)(py)$_2$	27.2	-156.7	-122.6	-10.47	+0.95	+0.42
3	Ru(NCO-κ*N*)$_2$(CHPh)(IMes)(py)$_2$	0.0	-185.7	-134.0	-10.43	+0.95	+0.64
4	Ru(OCN-κ*O*)$_2$(CHPh)(IMes)(py)$_2$	29.2	-184.4	-105.8	-10.38	+0.95	+0.77
5	Ru(NCS-κ*N*)$_2$(CHPh)(IMes)		-176.4	-166.6	-11.62	+0.77	+0.70
6	Ru(NCO-κ*N*)$_2$(CHPh)(IMes)		-192.9	-174.9	-11.51	+0.77	+0.75

[a] Calculated using Mulliken natural population analysis.

5.6.2 Origin of the reactivity difference between Ru-12a/b

In the second part of this computational study, the origin of the reactivity difference between **Ru-12a** and **Ru-12b** was investigated. The very low lability of the pyridine ligand within **Ru-12a** was demonstrated in the ROMP study described above (Section 5.5.4). DFT calculations support this finding. The calculated bond dissociation energy for the second pyridine ligand, which must be lost to generate the four-coordinate, catalytically-active species, is 22.6 kcal mol^{-1} in **Ru-12a**, as compared to 19 and 18.3 kcal mol^{-1} for isocyanate catalyst **Ru-12b** and dichloride **Ru-6a**. (The energy required for the loss of the first, "solvating" pyridine ligand in **Ru-12a** is 6.6 kcal mol^{-1} vs. 5.0 kcal mol^{-1} for **Ru-12b**). This energetic difference in Ru-py bond energy cannot be rationalized on the basis of the EDA analysis described above, however. The similarity in ligand-to-metal charge transfer in **Ru-**

12a and **Ru-12b** (0.66 vs. 0.69 e^-) results in a similar charge at Ru (+0.61 and +0.64, respectively). Thus, no significant changes in electrostatic interaction between the metal and the nitrogen atom of the pyridine ligand are found. Likewise, assessment of ΔE_{orb} for the Ru(NCE-κ*N*)$_2$ (CH_2)(IMes) and pyridine fragments indicated minimal difference (E = S: -33.1 kcal mol^{-1}; E = O: -32.5 kcal mol^{-1}), indicating very similar electronic stabilization on binding of pyridine. Clearly, the electrostatic and electronic interactions between the Ru and pyridine fragments do not account for the much lower pyridine lability characteristic of the isothiocyanate catalyst **Ru-12a**. We thus considered the possibility that stronger inter-ligand electrostatic attractions could be present. The charge distribution in both Ru(NCE-κ*N*)$_2$(py) fragments (E = S, O) was therefore evaluated using a point charge model for all atoms present. Because only the anionic ligands change between **Ru-12a** and **Ru-12b**, the IMes and alkylidene ligands can be excluded, eliminating unnecessary complications.

As expected from the similar charge-transfer between the Ru and pyridine fragments in the Ru(NCE-κ*N*)$_2$(CH_2)(IMes) complex, the positive charge on Ru (E = S: +0.67; E = O: +0.69) and negative charge on the py nitrogen (-0.52 for both) are essentially identical in the two Ru(NCE-κ*N*)$_2$(py) models (Figure 9). Significant differences, however, are found in polarization of the atoms within the $(NCE)^-$ ligands. For the isothiocyanate ligand, the negative charge on the nitrogen donor atom is ca. 30% lower, and the positive charge on carbon ca. 4× lower, than the corresponding charges in the $(NCO)^-$ ligand (–0.66 vs. –0.84, and +0.18 vs. +0.80). The charges on the nitrogen and carbon atoms of the $(NCE)^-$ ligands interact with the positively charged (+0.22) ortho protons of the pyridine ligand, the magnitude of the interaction being proportional to both the charge and inter-nuclear distance between the atoms. Attraction between the opposite charges on the $(NCE)^-$ nitrogen and pyridine ortho protons are countered by repulsion between the latter and the positively charged $(NCE)^-$ carbon (Figure 9; Table 4).

For the isocyanate complex, the attractive and repulsive energy are very nearly balanced (0.14 e^- Å^{-1} and 0.12 e^- Å^{-1} respectively), resulting in a weak net attraction. In the isothiocyanate complex, the attractive interaction is slightly weaker (0.12 e^- Å^{-1}) due to the lower charge on the isothiocyanate nitrogen atom, but the much lower charge on the isothiocyanate carbon atom leads to a 4× weaker C...H repulsion (0.029 e^- Å^{-1}). The net result is a much stronger electrostatic attraction between the isothiocyanate ligand and

pyridine (0.091 e^- $Å^{-1}$) relative to the isocyanate complex, and this accounts for the low lability of the pyridine ligand in **Ru-12a**.

Bending of the $(NCS)^-$ ligands toward the pyridine ligand provides additional experimental evidence for the presence of a stronger interligand attraction in the isothiocyanate complex. In the isocyanate complex, in contrast, the $(NCO)^-$ ligands are oriented in different directions, one pointing toward and the other away from the pyridine ligand. Consequently, the shortest C...H distance of 2.76 Å for the isocyanate complex is slightly longer to that of 2.72 Å in the isothiocyanate complex (the shortest N...H distances are identical, at 2.46 Å in both complexes). That the N...H distances are not constrained by electrostatic interactions is evidenced from the negative correlation between this distance and the charges on the atoms involved. For example, the shortest N...H distance in both complexes is identical despite the $0.18e^-$ lower negative charge on the isothiocyanate nitrogen atom.

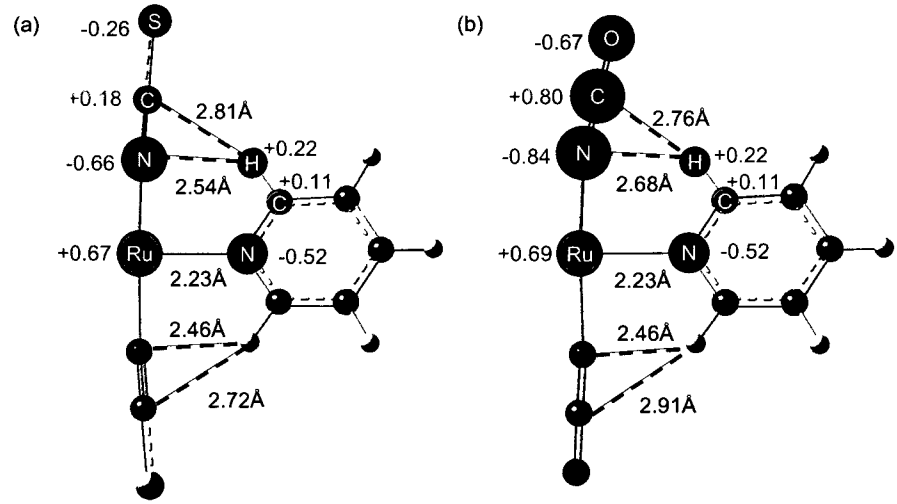

Figure 9. Charge distribution and internuclear distances for (a) Ru(NCS-κ*N*)$_2$(py) and (b) Ru(NCO-κ*N*)$_2$(py). The charge distribution on the two $(NCE)^-$ ligands within each complex is identical. The size of the atoms is proportional to their charge. Positively charged atoms are shown in red with negatively charged atoms in blue.

Ultimately, the stronger electrostatic attraction between the pyridine and $(NCS)^-$ ligands in **Ru-12a** is the major contributor (55%) of the 3.6 kcal mol^{-1} higher in the Ru-py binding energy relative to **Ru-12b**. The remainder is due to vibrational and orbital contributions (16% each) and structural relaxation (13%).

Table 4. Calculated electrostatic interaction energies between each $(NCE)^-$ ligand and the pyridine ortho protons.

E	Total attractive energy ($e^- Å^{-1}$)[a]	Total repulsive energy ($e^- Å^{-1}$)[a]	Total ($e^- Å^{-1}$)
S	0.12	0.029	0.091
O	0.14	0.12	0.020

[a] Calculated by $E = Q_1Q_2/R$; where Q is the charge and R is the internuclear distance between nuclei.

5.7 Conclusions

The work described in this Chapter builds on the knowledge gained from the catecholate catalysts described in Chapter 4. The goal of synthesizing "second-generation" *N*-bound pseudohalide metathesis catalysts in high yields was accomplished. Of great interest from a catalyst design perspective, the seemingly inconsequential change from an isocyanate to an isothiocyanate ligand has a dramatic effect on metathesis activity; consistently much higher reactivity being found for the isocyanate complex **Ru-12b**. This catalyst proved remarkably reactive for both ROMP and RCM, even at room temperature. In comparison, isothiocyanate **Ru-12a** was poorly reactive even for ROMP of a strained norbornene monomer. Experimental and computational analyses revealed that the dramatically reduced activity of **Ru-12a** reflects the low lability of its pyridine ligands, the origin of which was traced to a strong electrostatic attraction between pyridine and the isothiocyanate ligand of **Ru-12a**. Key to the rapid initiation characteristic of **Ru-12b** is the high positive charge on the isocyanate carbon, which limits electrostatic attraction between the isocyanate ligand and pyridine. Subsequent modification of the isocyanate platform should therefore be focused on maximizing the positive charge of the atom linked to the nitrogen donor. Particularly interesting in this context is the introduction of the phosphinimide $(N=PR_3)^-$ ligand,[92,93] for which the formal +5 charge on the phosphorus atom may lead to unprecedented initiation rates for a pseudohalide catalysts.

More generally, an electrostatic attraction between the $(NCS)^-$ and the styrenyl ether ligands may cause the low ROMP reactivity of Buchmeiser isothiocyanate complexes described above (**C**; Chart 1). However, no crystallographic analyses were provided for

isothiocyanate complexes **C**, which precludes the comparison of these internuclear N...H and C...H distances between **C** and **D**. Thus, future work should investigate whether the electrostatic interaction found for iso(thio)cyanate **Ru-12a/b** could be applicable to other catalyst system.

The high metathesis activity of **Ru-12b** is undoubtedly the most prominent discovery of this chapter. This catalyst allowed preparation of ROMP polymers with a high degree of control over the chain length, a task that has so far eluded the aryloxide and catecholate catalysts. Importantly, this also opens the door for investigation of this catalyst for tandem ROMP-hydrogenation or other tandem processes. Future work should focus on the application of **Ru-12b** to ROMP monomers relevant to advanced materials (e.g. tissue engineering).[76,94] As stated above, isocyanate **Ru-12b** may also be easily separated from the organic products, which would give this catalyst a clear advantage over its parent dichloride **Ru-6a** where much lengthier efforts are required to remove this catalyst.

5.8 References

(1) Samojlowicz, C.; Bieniek, M.; Grela, K., *Chem. Rev.* **2009**, *109*, 3708-3742.
(2) Vougioukalakis, G. C.; Grubbs, R. H., *Chem. Rev.* **2010**, *110*, 1746-1787.
(3) Monfette, S.; Camm, K. D.; Gorelsky, S. I.; Fogg, D. E., *Organometallics* **2009**, *28*, 944-946.
(4) Dias, E. L.; Nguyen, S. T.; Grubbs, R. H., *J. Am. Chem. Soc.* **1997**, *119*, 3887-3897.
(5) Occhipinti, G.; Bjorsvik, H.-R.; Jensen, V. R., *J. Am. Chem. Soc.* **2006**, *128*, 6952-6964.
(6) Monfette, S.; Fogg, D. E., *Organometallics* **2006**, *25*, 1940-1944.
(7) Blacquiere, J. M.; McDonald, R.; Fogg, D. E., *Angew. Chem., Int. Ed.* **2010**, *49*, 3807-3810.
(8) Conrad, J. C.; Amoroso, D.; Czechura, P.; Yap, G. P. A.; Fogg, D. E., *Organometallics* **2003**, *22*, 3634-3636.
(9) Conrad, J. C.; Parnas, H. H.; Snelgrove, J. L.; Fogg, D. E., *J. Am. Chem. Soc.* **2005**, *127*, 11882-11883.
(10) Braddock, D. C.; Tanaka, K.; Chadwick, D.; Boehm, V. P. W.; Roeper, M., *Tetrahedron Lett.* **2007**, *48*, 5301-5303.
(11) Zhang, W.; Liu, P.; Jin, K.; He, R., *J. Mol. Catal. A* **2007**, *275*, 194-199.
(12) Gawin, R.; Makal, A.; Wozniak, K.; Mauduit, M.; Grela, K., *Angew. Chem., Int. Ed.* **2007**, *46*, 7206-7209.
(13) Halbach, T. S.; Mix, S.; Fischer, D.; Maechling, S.; Krause, J. O.; Sievers, C.; Blechert, S.; Nuyken, O.; Buchmeiser, M. R., *J. Org. Chem.* **2005**, *70*, 4687-4694.
(14) Samee, J. S. M.; Grubbs, R. H., *Chem. Eur. J.* **2008**, *14*, 2686-2692.
(15) Gawin, R.; Czarnecka, P.; Grela, K., *Tetrahedron* **2010**, *66*, 1051-1056.
(16) Krause, J. O.; Nuyken, O.; Wurst, K.; Buchmeiser, M. R., *Chem. Eur. J.* **2004**, *10*, 777-784.

(17) Jordaan, M.; Vosloo, H. C. M., *Adv. Synth. Catal.* **2007**, *349*, 184-192.
(18) Denk, K.; Fridgen, J.; Herrmann, W. A., *Adv. Synth. Catal.* **2002**, *344*, 666-670.
(19) Snelgrove, J. L.; Conrad, J. C.; Moriarty, M. M.; Yap, G. P. A.; Fogg, D. E., *Organometallics* **2005**, *24*, 103-109.
(20) Snelgrove, J. L.; Conrad, J. C.; Yap, G. P. A.; Fogg, D. E., *Inorg. Chim. Acta* **2003**, *345*, 268-278.
(21) Barbasiewicz, M.; Szadkowska, A.; Bujok, R.; Grela, K., *Organometallics* **2006**, *25*, 3599-3604.
(22) Ung, T.; Hejl, A.; Grubbs, R. H.; Schrodi, Y., *Organometallics* **2004**, *23*, 5399-5401.
(23) Benitez, D.; Goddard, W. A., III, *J. Am. Chem. Soc.* **2005**, *127*, 12218-12219.
(24) Bieniek, M.; Michrowska, A.; Usanov, D. L.; Grela, K., *Chem. Eur. J.* **2008**, *14*, 806-818.
(25) Gradillas, A.; Perez-Castells, J., *Angew. Chem., Int. Ed.* **2006**, *45*, 6086-6101.
(26) Lysenko, Z.; Maughon, B. R.; Mokhtar-Zadeh, T.; Tulchinsky, M. L., *J. Organomet. Chem.* **2006**, *691*, 5197-5203.
(27) Ulman, M.; Grubbs, R. H., *J. Org. Chem.* **1999**, *64*, 7202-7207.
(28) Hong, S. H.; Wenzel, A. G.; Salguero, T. T.; Day, M. W.; Grubbs, R. H., *J. Am. Chem. Soc.* **2007**, *129*, 7961-7968.
(29) Szadkowska, A.; Grela, K., *Curr. Org. Chem.* **2008**, *12*, 1631-1647.
(30) Drouin, S. D.; Foucault, H. M.; Yap, G. P. A.; Fogg, D. E., *Can. J. Chem.* **2005**, *83*, 748-754.
(31) Jung, S.; Ilg, K.; Brandt, C. D.; Wolf, J.; Werner, H., *Eur. J. Inorg. Chem.* **2004**, 469-480.
(32) Kumar, P. S.; Wurst, K.; Buchmeiser, M. R., *Chem. Asian J.* **2009**, *4*, 1275-1283.
(33) Interestingly, π-complexation of the $(NCS)^-$ anion with large cations such as Rb^+ is possible. See: Tchertanov, L. *Supramol. Chem.* **2000**, *12*, 67-91.
(34) Ritter, T.; Hejl, A.; Wenzel, A. G.; Funk, T. W.; Grubbs, R. H., *Organometallics* **2006**, *25*, 5740-5745.
(35) Conrad, J. C.; Camm, K. D.; Fogg, D. E., *Inorg. Chim. Acta* **2006**, *359*, 1967-1973.
(36) Danopoulos, A. A.; Wilkinson, G.; Sweet, T. K. N.; Hursthouse, M. B., *Polyhedron* **1994**, *13*, 2899-2905.
(37) The DFT-calculated frequency of the ν_{CN} vibration for the free $(NCO)^-$ anion is 2219 cm^{-1}, with a C-N bond order of 2.71. For the $(NCS)^-$ anion, ν_{CN} is calculated as 2148 cm^{-1}, with a C-N bond order of 2.76.
(38) Arduengo, A. J., III; Dias, H. V. R.; Calabrese, J. C.; Davidson, F., *Organometallics* **1993**, *12*, 3405-3409.
(39) Fox, M. A.; Mahon, M. F.; Patmore, N. J.; Weller, A. S., *Inorg. Chem.* **2002**, *41*, 4567-4573.
(40) De Fremont, P.; Scott, N. M.; Stevens, E. D.; Ramnial, T.; Lightbody, O. C.; Macdonald, C. L. B.; Clyburne, J. A. C.; Abernethy, C. D.; Nolan, S. P., *Organometallics* **2005**, *24*, 6301-6309.
(41) Yu, X.-Y.; Patrick, B. O.; James, B. R., *Organometallics* **2006**, *25*, 2359-2363.
(42) Sentman, A. C.; Csihony, S.; Waymouth, R. M.; Hedrick, J. L., *J. Org. Chem.* **2005**, *70*, 2391-2393.
(43) Sanford, M. S.; Love, J. A.; Grubbs, R. H., *Organometallics* **2001**, *20*, 5314-5318.
(44) Burmeister, J. L., *Coord. Chem. Rev.* **1990**, *105*, 77-133.

References page 188

(45) Gould, R. O.; Gray, A. M.; Taylor, P.; Walkinshaw, M. D., *J. Am. Chem. Soc.* **1985**, *107*, 5921-5927.
(46) Fürstner, A.; Ackermann, L.; Gabor, B.; Goddard, R.; Lehmann, C. W.; Mynott, R.; Stelzer, F.; Thiel, O. R., *Chem. Eur. J.* **2001**, *7*, 3236-3253.
(47) Love, J. A.; Sanford, M. S.; Day, M. W.; Grubbs, R. H., *J. Am. Chem. Soc.* **2003**, *125*, 10103-10109.
(48) Ledoux, N.; Allaert, B.; Linden, A.; Van Der Voort, P.; Verpoort, F., *Organometallics* **2007**, *26*, 1052-1056.
(49) Ritter, T.; Day, M. W.; Grubbs, R. H., *J. Am. Chem. Soc.* **2006**, *128*, 11768-11769.
(50) Dinger, M. B.; Nieczypor, P.; Mol, J. C., *Organometallics* **2003**, *22*, 5291-5296.
(51) Leuthaeusser, S.; Schmidts, V.; Thiele, C. M.; Plenio, H., *Chem. Eur. J.* **2008**, *14*, 5465-5481.
(52) Kauffman, G. B., *Coord. Chem. Rev.* **1973**, *11*, 161-188.
(53) Cadierno, V.; Diez, J.; Garcia-Garrido, S. E.; Garcia-Granda, S.; Gimeno, J., *J. Chem. Soc., Dalton Trans.* **2002**, 1465-1472.
(54) Clough, C. R.; Mueller, P.; Cummins, C. C., *Dalton Trans.* **2008**, 4458-4463.
(55) Lense, S.; Hardcastle, K. I.; MacBeth, C. E., *Dalton Trans.* **2009**, 7396-7401.
(56) Homanen, P.; Haukka, M.; Pakkanen, T. A.; Pursiainen, J.; Laitinen, R. H., *Organometallics* **1996**, *15*, 4081-4084.
(57) Homanen, P.; Haukka, M.; Luukkanen, S.; Ahlgren, M.; Pakkanen, T. A., *Eur. J. Inorg. Chem.* **1999**, 101-106.
(58) Maroney, M. J.; Fey, E. O.; Baldwin, D. A.; Stenkamp, R. E.; Jensen, L. H.; Rose, N. J., *Inorg. Chem.* **1986**, *25*, 1409-1414.
(59) Lewis, J.; Nyholm, R. S.; Smith, P. W., *J. Chem. Soc.* **1961**, 4590-4599.
(60) Nakamoto, K., *Infrared and Raman Spectra of Inorganic and Coordination Compounds*. 3rd ed.; John Wiley & Sons: 1978; p 300.
(61) Bailey, R. A.; Kozak, S. L.; Michelsen, T. W.; Mills, W. N., *Coord. Chem. Rev.* **1971**, *6*, 407-445.
(62) Mitchell, P. C. H.; Williams, R. J. P., *J. Chem. Soc.* **1960**, 1912-1918.
(63) Sabatini, A.; Bertini, I., *Inorg. Chem.* **1965**, *4*, 1665-1667.
(64) Sabatini, A.; Bertini, I., *Inorg. Chem.* **1965**, *4*, 959-961.
(65) Love, J. A.; Morgan, J. P.; Trnka, T. M.; Grubbs, R. H., *Angew. Chem., Int. Ed.* **2002**, *41*, 4035-4037.
(66) Sanford, M. S.; Love, J. A.; Grubbs, R. H., *J. Am. Chem. Soc.* **2001**, *123*, 6543-6554.
(67) Conrad, J. C.; Eelman, M. D.; Duarte Silva, J. A.; Monfette, S.; Parnas, H. H.; Snelgrove, J. L.; Fogg, D. E., *J. Am. Chem. Soc.* **2007**, *129*, 1024-1025.
(68) Kamau, S. D.; Hodge, P.; Hall, A. J.; Dad, S.; Ben-Haida, A., *Polymer* **2007**, *48*, 6808-6822.
(69) Bazan, G. C.; Khosravi, E.; Schrock, R. R.; Feast, W. J.; Gibson, V. C.; O'Regan, M. B.; Thomas, J. K.; Davis, W. M., *J. Am. Chem. Soc.* **1990**, *112*, 8378-8387.
(70) Benedicto, A. D.; Claverie, J. P.; Grubbs, R. H., *Macromolecules* **1995**, *28*, 500-511.
(71) Ivin, K. J.; Mol, J. C., *Olefin Metathesis and Metathesis Polymerization*. Academic Press: New York, 1997.
(72) Six, C.; Beck, K.; Wegner, A.; Leitner, W., *Organometallics* **2000**, *19*, 4639-4642.
(73) Gstrein, X.; Burtscher, D.; Szadkowska, A.; Barbasiewicz, M.; Stelzer, F.; Grela, K.; Slugovc, C., *J. Polym. Sci., Part A* **2007**, *45*, 3494-3500.

(74) Nomura, K.; Sakai, I.; Imanishi, Y.; Fujiki, M.; Miyamoto, Y., *Macromol. Rapid Commun.* **2004**, *25*, 571-576.
(75) Fogg, D. E.; Foucault, H. M., Ring-Opening Metathesis Polymerization. In *Comprehensive Organometallic Chemistry III*, Crabtree, R. H.; Mingos, D. M. P., Eds. Elsevier: Oxford, 2007; Vol. 11, pp 623-652.
(76) Camm, K. D.; Castro, N. M.; Liu, Y.; Czechura, P.; Snelgrove, J. L.; Fogg, D. E., *J. Am. Chem. Soc.* **2007**, *129*, 4168-4169.
(77) Matson, J. B.; Grubbs, R. H., *Macromolecules* **2008**, *41*, 5626-5631.
(78) Choi, T.-L.; Grubbs, R. H., *Angew. Chem., Int. Ed.* **2003**, *42*, 1743-1746.
(79) Fogg, D. E.; dos Santos, E. N., *Coord. Chem. Rev.* **2004**, *248*, 2365-2379.
(80) Tuan, D. F. T.; Hoffmann, R., *Inorg. Chem.* **1985**, *24*, 871-876.
(81) Tuan, D. F. T.; Reed, J. W.; Hoffmann, R., *THEOCHEM* **1991**, *78*, 111-121.
(82) Schreiner, A. F.; Lin, S. W., *Inorg. Chim. Acta* **1971**, *5*, 290-294.
(83) Kitaura, K.; Morokuma, K., *Int. J. Quantum Chem.* **1976**, *10*, 325-340.
(84) Ziegler, T.; Rauk, A., *Theor. Chim. Acta* **1977**, *46*, 1-10.
(85) Frenking, G.; Wichmann, K.; Froehlich, N.; Grobe, J.; Golla, W.; Van, D. L.; Krebs, B.; Laege, M., *Organometallics* **2002**, *21*, 2921-2930.
(86) Frenking, G.; Wichmann, K.; Frohlich, N.; Loschen, C.; Lein, M.; Frunzke, J.; Rayon, V. M., *Coord. Chem. Rev.* **2003**, *238-239*, 55-82.
(87) Nemcsok, D.; Wichmann, K.; Frenking, G., *Organometallics* **2004**, *23*, 3640-3646.
(88) Lein, M.; Frenking, G., *Theory Appl. Comput. Chem.* **2005**, 291-372.
(89) Tonner, R.; Heydenrych, G.; Frenking, G., *Chem. Asian J.* **2007**, *2*, 1555-1567.
(90) Antonova, N. S.; Carbo, J. J.; Poblet, J. M., *Organometallics* **2009**, *28*, 4283-4287.
(91) Jacobsen, H.; Correa, A.; Poater, A.; Costabile, C.; Cavallo, L., *Coord. Chem. Rev.* **2009**, *253*, 687-703.
(92) Yue, N. L. S.; Stephan, D. W., *Organometallics* **2001**, *20*, 2303-2308.
(93) Stephan, D. W.; Stewart, J. C.; Guerin, F.; Spence, R. E. v. H.; Xu, W.; Harrison, D. G., *Organometallics* **1999**, *18*, 1116-1118.
(94) Merrett, K.; Liu, W.; Mitra, D.; Camm, K. D.; McLaughlin, C. R.; Liu, Y.; Watsky, M. A.; Li, F.; Griffith, M.; Fogg, D. E., *Biomaterials* **2009**, *30*, 5403–5408.

6. Getting RCM off the bench: transforming the assembly of large rings using a continuous-flow approach*

6.1 Introduction

RCM has now achieved an astonishing prominence in organic synthesis, and indeed is credited with having changed how chemists think about the assembly of cyclic structures.[1-3] This impact, however, is difficult to reconcile with its limited industrial use. Thirty years after the publication of the first RCM reactions by Villemin[4] and Tsuji,[5] and nearly twenty years following the report of the first Grubbs catalyst,[6] RCM remains almost exclusively confined to the research setting. In rare exceptions by two pharmaceutical concerns, RCM reactions have been scaled up (albeit to only multi-kilogram levels) by Boehringer-Ingelheim Ltd. (BI)[7-9] and GlaxoSmithKline Inc. (GSK).[10,11]

One of the major impediments to the industrial implementation of RCM methodologies is the high catalyst loading required for quantitative conversion to desired products. This imposes a very high catalyst cost on production scale (Chart 1), which is exacerbated by the laborious purification protocols required to lower the ruthenium content of organic products below the 5 ppm threshold set for pharmaceutical products.[12] Macrocyclic rings are particularly desirable from an industrial perspective, as evidenced by the reports of BI,[7-9,13] Merck,[14,15] Johnson & Johnson,[16] Pfizer[17] and Novartis.[18] Formation of such rings is complicated, however by the low effective molarity (EM) of the diene precursors.[1,19,20] While use of high dilutions and elevated temperatures can be employed to favor formation of the macrocyclic rings,[1] these conditions are highly detrimental to catalyst stability, and thus total productivity. Inefficient, wasteful[21] and uneconomical processes result.

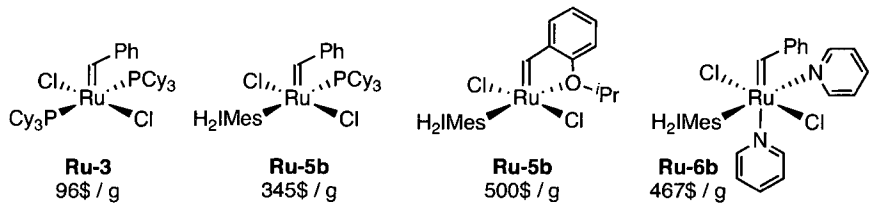

Chart 1. Market price of Grubbs catalysts in CAD (June, 2010; Aldrich Chemical Co.)

* Much of the work described in this Chapter has been published: Monfette, S.; Eyholzer, M.; Roberge, D. M.; Fogg, D. E., *Chem. Eur. J.* **2010**, *16*, 11720-11725.

Immobilization of the catalyst on a solid support represents one potentially attractive means of addressing the problems of catalyst cost and removal.[22-27] Supported catalysts can be utilized in high loadings if required, removed by filtration following reaction and (ideally) re-used in subsequent reactions. This approach is intended to limit costs both through recovery of the expensive catalysts, and facile purification of organic products. In practice, however, these goals are rarely met for RCM processes. Organic products with ruthenium content down to the sub-100 ppb level have been reported for high-EM substrates,[28] for which low catalyst loadings suffice, and metal leaching is therefore at a minimum. For more challenging RCM reactions (e.g. those involving sterically hindered olefins or formation of strained rings), the residual ruthenium content ranges from 500-5000 ppm despite use of supported catalysts.[29-31] The high catalysts loadings required for challenging transformations set a high bar for the robustness of anchoring. Further complications arise from the poorly understood chemistry leading to leaching of the ruthenium catalysts. While the relationship between leaching and catalyst decomposition has been little studied, loss of a "strongly binding" NHC ligand, or chlorination of an anionic ligand (for reactions in CH_2Cl_2), are readily envisaged as pathways by which the catalyst could be cleaved from the support.

Leaching problems, of course, affect any immobilized catalyst. A more fundamental challenge in achieving high performance in supported RCM processes is the impact of immobilization on catalyst lifetime (i.e. turnover number; TON). While intermolecular decomposition can be limited by anchoring, where sufficient separation between metal centers is achieved, intramolecular decomposition will be unaffected. Given the model studies suggesting that decomposition of the key Ru-methylidene propagating species occurs *primarily* by a unimolecular pathway for the homogeneous Grubbs catalysts,[32,33] it is remarkable that this issue has gone largely ignored in the "supported RCM" literature. If decomposition is indeed unimolecular, no benefits can be expected from immobilization of these catalysts. Of note, however, the model decomposition studies were conducted in the absence of substrate, clouding the relevance of the unimolecular deactivation pathway to real catalytic reactions.

Another issue arises from the increasingly common use of the bulky polymer supports, such as ROMP-derived polynorbornenes. As ligand C-H activation is thought to be a common decomposition route for the Grubbs catalysts (see Chapter 1, Section 1.2.5), such

"surface-as-ligand" supports may in fact be detrimental to catalyst lifetime. Consistent with this are the lower TONs commonly observed for the supported catalysts, relative to their homogeneous counterpart,[24] though steric inhibition (see next) may also play a part. A recent review[22] reports TONs on the order of 1,000 using various supported catalysts, with a maximum of 4,200 for the RCM of the high-EM tosylamine substrate **9a** (cf. >10,000 for the homogeneous second-generation catalyst **Ru-4b**).[34] Clearly, the supported Grubbs catalysts are generally less productive that their homogeneous counterparts, though it remains unclear whether this reduced productivity arises from shorter catalyst lifetime, slower reaction rates, or both.

While it is recognized that the steric demand of the solid support can impede reaction between catalyst and substrate, resulting in lower reaction rates,[24] insight into this point is limited by the paucity of turnover frequency (TOF) data in the supported metathesis catalyst literature.[22] Furthermore, the rare comparisons of TOF for homogeneous and supported catalysts tend to focus on model, high-EM substrates.[35,36] The negligible differences found in these cases may reflect the small size of the diene substrates employed. TOF studies utilizing larger dienes and/or polymerization reactions would be highly desirable. For immobilized RCM catalysts, two very important issues thus remain unaddressed: (1) the extent to which the solid support retards or promotes catalyst decomposition and (2) the impact of the support on metathesis rates.

Homogeneous metathesis catalysts are much more commonly used in industry, even for ROMP processes (e.g. those involving production of norbornene derivatives, including dicyclopentadiene).[37,38] This is also true for the kilogram-scale RCM syntheses reported by BI[7-9] and GSK,[10,11] which employ homogeneous Grubbs catalysts. Attractive features include commercial availability (in the case of **Ru-3-6**), as well as higher activity and lifetime. Indeed, remarkable TONs have been reported for RCM reactions catalyzed by second-generation Grubbs catalysts. As early as 2002, Mol and co-workers obtained >200,000 TON in neat diene, for RCM of **11a** (diethyl diallyl malonate) using **Ru-4b** (55 °C, [Ru]: **11a** ca. 1:1,000,000).[39] In closely related work at room temperature employing neat **11a**, as well as two other high-EM dienes, the Dorta group subsequently reported TON values approaching 20,000. The catalysts employed were naphthyl derivatives of **Ru-4b** (Chart 2b), at loadings of ca. 1:20,000 (50 ppm).[34]

While use of neat diene is attractive for the sake of such high TON values, it is not always feasible. (Indeed, for low-EM dienes, it is impossible: see Chapter 3). Where a solvent is required, however, lower TON values are invariably obtained. Thus, Grubbs reported a maximum TON of 2,000 for **Ru-4b** in RCM of **11a** in refluxing CH_2Cl_2. Fogg and co-workers reported that considerably higher TON values could be attained by replacing the chloride ligands with two perfluoroaryloxide ligands. Thus, up to 40,000 TON were achieved using catalyst **Ru-7a**,[40] as compared to 5,100 for the corresponding dichloride catalyst **Ru-6a**, and 17,000 for its PCy_3-stabilized analogue **Ru-4a** and (500 mM **11a** in $CDCl_3$, Δ, [Ru]: **11a** = 1:200,000).

Worth noting is the fact that the above high TON values were obtained using substrates that are particularly amenable to RCM. All the substrates investigated are structurally simple, high-EM dienes devoid of potentially problematic functionalities (e.g. allylic alcohols,[41-43] acrylates,[44-47] primary amines[48-50] and sulfides[51-54]) that could poison or decompose the catalysts. All of these factors limit the relevance of the above TON values to "real life" substrates. As a relevant example, the first-generation Grubbs-Hoveyda catalyst effected a maximum of 35 TON in the original BI synthesis of BILN 2061. After five years of optimization, including extensive screening of catalysts and protecting groups (the latter affecting the diene EM value),[9] the maximum TON was increased to only 330.[7]

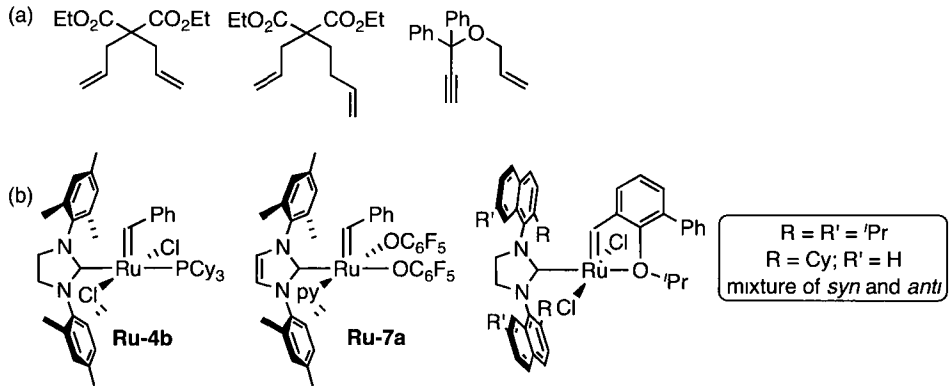

Chart 2. Substrates and catalysts for which >20,000 TON were achieved.[34]

Of great interest are alternative, less time-intensive, and potentially general paradigms that do not rely on catalyst design or substrate tuning. One potential solution considered in the present work asked a simple question: might RCM efficiency be artificially constrained by the reliance on conventional, batchwise RCM processes? The use of continuous-flow (CF)[55-

[57] reactors for RCM has been surprisingly little studied. To date, only two studies compare RCM yields obtained using different reactor types, and the findings are contradictory. Grela, Kirschning and co-workers reported poorer performance in CF-RCM of the high-EM diene **9a** via a ruthenium catalyst ionically bound to Raschig rings, vs. batch RCM with the same catalyst (Scheme 1).[36,56] In contrast, the Organ group found that CF-RCM was superior to batch reaction (likewise employing high-EM dienes; e.g. **7**) using the homogeneous catalyst **Ru-4b**.[58]

A detailed study was therefore undertaken to compare the RCM performance attainable in a batch reactor (BR) with that obtained using a plug-flow reactor (PFR) and a continuous stirred-tank reactor (CSTR), these representing the two dominant CF reactor configurations. To press the case, this investigation was deliberately performed using a challenging, low-EM substrate **1b** (the latter being the precursor to an important, macrocyclic perfumery agent),[59-61] in conjunction with the standard "off-the-shelf" (non-immobilized) catalyst **Ru-4b**. The results show that by matching the reactor design to the chemical problem, RCM macrocyclization can be made dramatically more efficient than the corresponding batch reaction, with significant advantages in terms of process and environmental costs.[21]

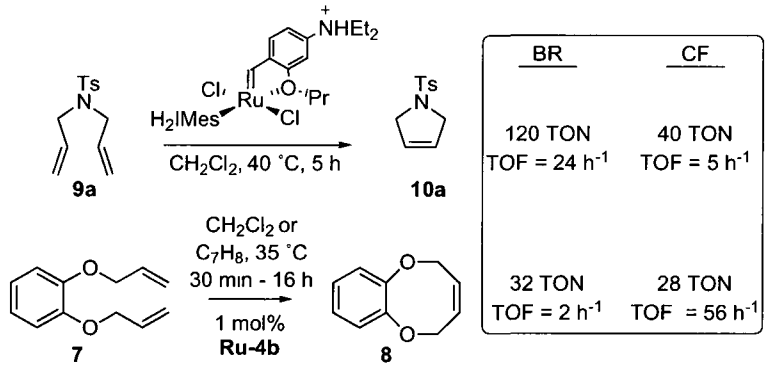

Scheme 1. Conflicting results reported in comparisons of batch vs. continuous-flow RCM.[36,56,58]

6.2 Methodology

Simplified reactor configurations and equipment are depicted in Figures 1-4, with pictures of the actual assembly for visual reference. The batch reactor (BR) consisted of a 0.5 L round-bottom flask equipped with a condenser and an argon inlet. The progress of RCM in

batch mode was monitored by periodically removing samples and quenching with Ktp (Ktp = potassium tris-pyrazolyl borate)[62] prior to GC-FID analysis.

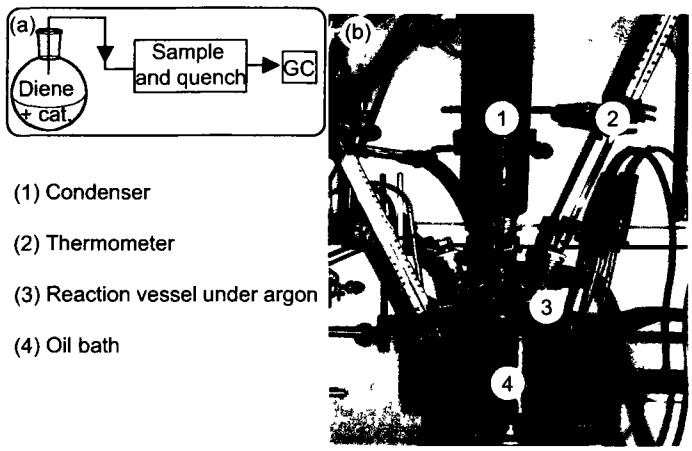

Figure 1. (a) Simplified BR setup. (b) Actual setup used in the experiments.

The PFR (Figures 2 and 3) consists of two Teledyne ISCO syringe pumps connected to a microstructured mixer (internal volume 25 μL) and a stainless steel coil (0.72 mm inner diameter, total volume 2.87 or 11 mL) immersed in a temperature-controlled (± 0.1 °C) oil bath. The syringe pumps drive catalyst and substrate into the micromixer, and the reactant stream through the coil. Offline quenching and GC analysis followed for each sample taken.

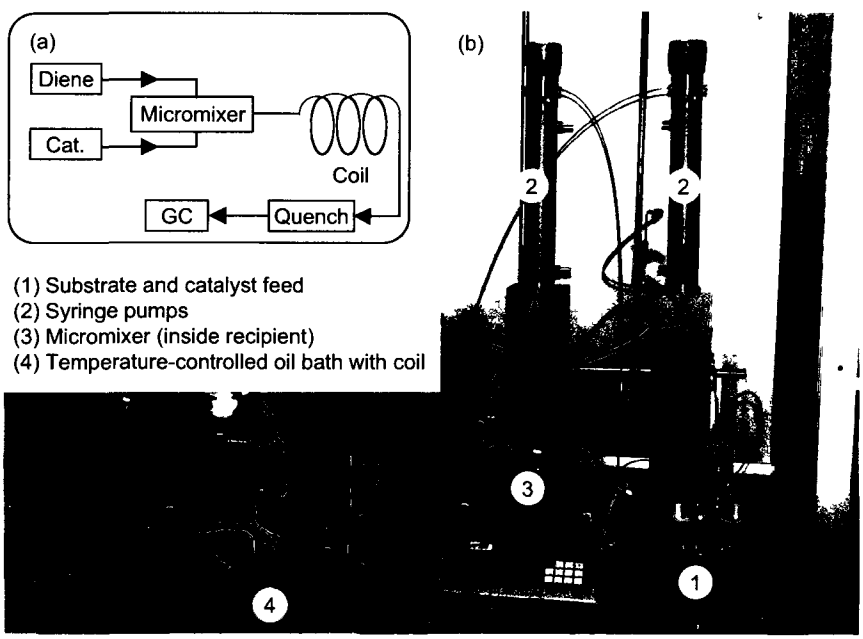

Figure 2. (a) Schematic representation of the PFR setup. (b) Actual assembly. The PFR was built in collaboration with Markus Eyholzer, technician at LONZA AG., Switzerland.

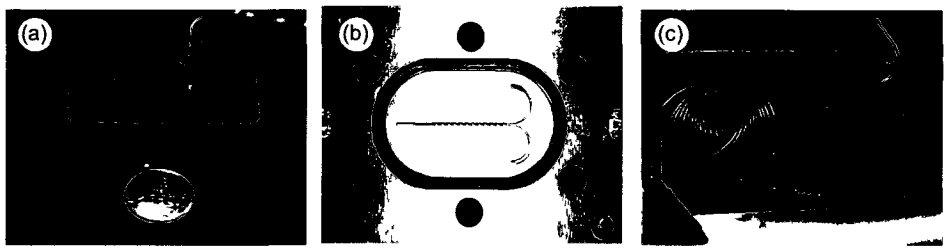

Figure 3. (a) Micromixer used in the CF study. (b) Internal structure of the micromixer. (c) Coils immersed in an oil bath.

Determination of time profiles for CF reactions is carried out by alteration of the residence time (reaction time) inside the coil (henceforth denoted as τ). The residence time can be calculated by dividing the volume of the coil used (mL) by the flow rate through the coil (mL min^{-1}). These were varied from 96 to 0.1 mL min^{-1}, which corresponds to τ of 0.03 to 60 min depending on the volume of the coil used (2.87 or 11 mL). Varying τ is accomplished simply by entering the desired flow rate value on the syringe pump console. The high precision of the Teledyne ISCO pumps (<1% for flow rates of 500 mL min^{-1} to 10 μL min^{-1}) enables highly-reproducible τ. The accuracy of the τ values requires immediate quenching of the catalyst in reaction aliquots. This was confirmed by a control experiment in which Ktp was charged along with the substrate feed. Null conversion to the RCM product was observed. Importantly, the minimal flow rate was set at 0.1 mL min^{-1} in order to avoid axial diffusion of the reactant plug through the coil, which would limit the reproducibility of τ. The minimal flow rate is not arbitrary: it is based on fluid dynamics calculations that take into account the viscosity of the solvent, the friction with the coil material and the diameter of the coil.

Another crucial aspect to recognize when working in CF is that fresh solutions of substrate and catalyst are constantly channeled into the system. Therefore, each data point in the time profile of a CF reaction corresponds to a new "experiment" where the fresh reactant stream was passed through the coil at a different flow rate. Avoiding contamination between data points is crucial for obtaining accurate, reproducible results. This is achieved by purging the micromixer and the coil with catalyst and substrate solutions for a period of 3τ (at the desired flow rate) for every variation in the flow rate. For each modification of the flow rate, a 10 sec period was allowed for the new flow rate to stabilize to the entered value before initiating the

References page 208

purge. Following completion of the purge time, samples were collected, quenched and analyzed by GC-FID as above.

Studies employing the CSTR (Figure 4) were carried out in a similar way as those using the PFR. Experiments were begun by infusing a solution of **1b** and **Ru-4b** (homogenized at 20 °C using the micromixer) into a 10 mL round-bottom flask containing 5 mL of toluene at 80 °C. A fine Teflon tube (1 m, internal volume = 247 μL; residence time in the tube ≤2.5 min) was used to limit the time required for transfer of the reactant stream from the mixer to the round-bottom "tank" portion. An exit piston pump ensured a constant volume of 5 mL by removing any volume of solution in excess of 5 mL. The speed of the piston pump was maintained at 40 mL min^{-1}, vs. a maximum of 5 mL min^{-1} for the upstream syringe pumps, to ensure a constant volume of 5 mL in the tank, and to minimize the time interval (maximum 5 sec) between removal from the tank, and addition to the quenching solution. This minimizes any run-on metathesis following exit from the tank, and has the added benefit of promoting exchange of the headspace gas. Product distributions were assayed once the tank content reached steady state (measured following a standard, arbitrary period of 10τ), as determined by GC analysis of the Ktp-quenched effluent.

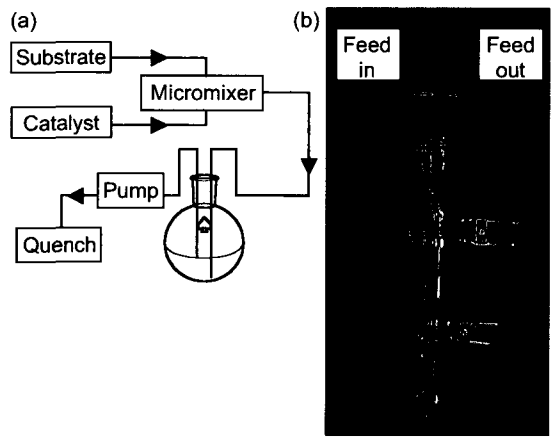

Figure 4. (a) Schematic representation of the CSTR setup. (b) Actual picture of the "tank" section. The CSTR was built in collaboration with Markus Eyholzer, technician at LONZA AG., Switzerland.

6.3 Optimization of RCM reactions using a plug-flow reactor

The efficiency of the macrolactonization of **1b** in the PFR, vs. a conventional BR, was assessed under conditions earlier established as optimal in batch mode (5 mM **1b**, 5 mol%

Ru-4b).[19] The sole change from reported batch reaction was the use of toluene as solvent in place of methylene chloride. The latter is undesirable in industrial practice: as well, its lower boiling point limits reaction rates and the thermodynamic driving force that controls selectivity in equilibrium RCM.[1] As a measure of the process efficiency, the criteria set forth by Boehringer-Ingelheim for improved commercial viability of the BILN 2061 process were employed: >90% yield, ≤1 h, ≤0.3 mol% [Ru].[7] While project-specific, these figures provide a useful point of comparison.

Rate profiles obtained using the BR and PFR reactors at 60 °C appear in Figure 5, with maximum conversions in Table 1, Entries 1/2. RCM rates are slightly but consistently lower in the PFR, probably owing to entrapment of the ethylene by-product. Closely comparable performance is expected for these homogeneous, kinetically-controlled reactions. The agreement was deemed sufficiently good to warrant deeper exploration. Three parameters were targeted for optimization: reaction temperature, catalyst loading, and feed concentration.

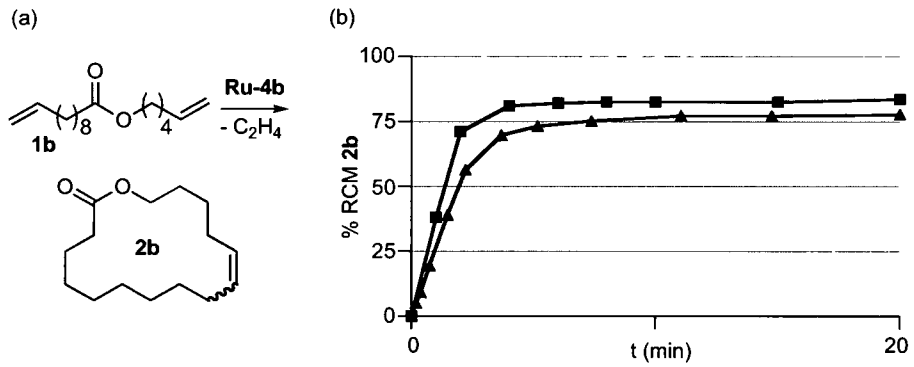

Figure 5. (a) RCM reaction studied in this Chapter. (b) Yields of **2b** vs. time in the RCM of **1b** by **Ru-4b**. BR (■) vs. PFR (▲). Conditions: 5 mM **1b** in C_7H_8, 60 °C, 5 mol% **Ru-4b**. Calibrated GC-FID analysis (±2% in replicate runs).

Temperature (Figure 6; Table 1, Entries 2-4). At 40 °C, RCM is slow, reaching only 17% after 0.5 h. The proportion of oligomers, initially high, declines over time as backbiting liberates cyclic **2b**. Thus, the selectivity for **2b** is 33% after 1 min, increasing to 55% at 30 min. At 60 °C, solely **2b** is observed, and conversion is considerably more rapid (79% RCM in 11 min), although limited by catalyst decomposition beyond 11 min. At 80 °C, 82% conversion is achieved in only 1.5 min. Again, conversions then plateau, but GC-FID analysis reveals no side-reactions (such as isomerization, thought to be mediated by catalyst

decomposition products).[63]

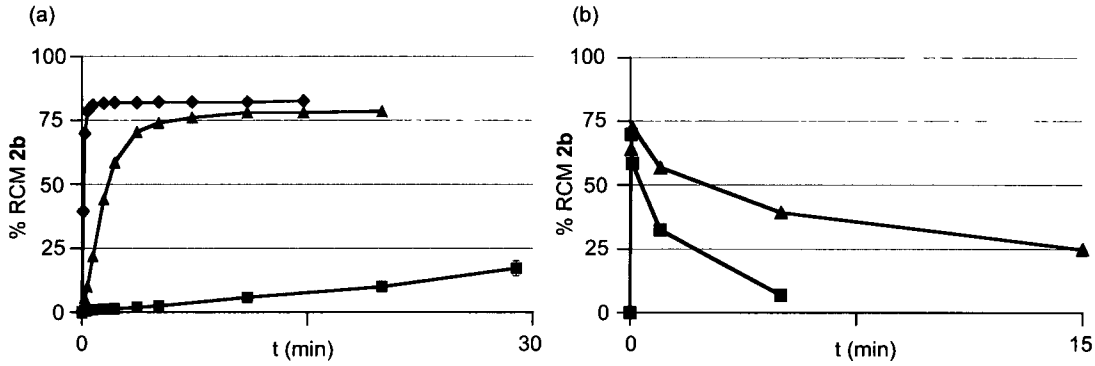

Figure 6. Yield of **2b** over time for different temperatures. (a) 80 °C (◆), 60 °C (▲), 40 °C (■); (b): 120 °C (▲), 150 °C (■). Conditions: 5 mM **1b** in C_7H_8, 5 mol% **Ru-4b**. Calibrated GC-FID analysis (±2% in replicate runs).

The results at 80 °C highlight the advantage of the fast dynamic response of the PFR, which allows reaction times to be reduced to a few minutes. In contrast, the much larger BR requires significantly longer to heat up, and thus cannot be operated for a few minutes at (e.g.) 80 °C. Of note, the rate of catalyst deactivation relative to RCM decreases in the PFR at higher temperatures. Maximum conversions are identical, within experimental error, at 60 and 80 °C, but are achieved 10× faster at 80 °C, without adversely affecting selectivity. In engineering terms, transferring operations from the BR to the PFR transforms a slow, unproductive ("Type C") reaction requiring hours into a highly intensified ("Type B") reaction requiring minutes.[64] This is of keen interest from a process engineering perspective, as the dramatically improved space-time yields will reduce reactor costs.

In an attempt to further increase space-time yields, the RCM of **1b** was investigated under superheated conditions. The term superheated refers to carrying out the reaction at a temperature above the normal boiling point of the solvent at ambient pressure (ca. 1 atm). These conditions necessarily require an elevated pressure within the system to maintain the solvent in the liquid phase. Simple calculations revealed that a pressure of 2.7 bar is sufficient to retain toluene in the liquid phase at a temperature of 150 °C. Increasing the pressure was accomplished by incorporating a fine PEEK (polyether ether ketone) capillary tube (length = 1-5 m; ID = 0.18 mm; internal volume = 25-127 μL) after the coil. The capillary tubing was chosen for its reduced diameter relative to that of the coil. Thus, a higher pressure on the liquid reagents is required from the syringe pump motors to maintain a

constant flow rate. Online pressure measurements at various points in the system were satisfactory (i.e. above the 2.7 bar threshold required), ranging from 10 bar at the syringe pumps down to 5 bar at the end of the coil. Such a pressure drop is typical in CF systems.

The rates of RCM at 120 °C and 150 °C are very high (Figure 6b). The maximum yields of **2b** (70-72%) were obtained in *less than five seconds* at both temperatures with complete selectivity for **2b**. Unexpectedly, however, a rapid decline in yield is observed as the reaction time is increased. At 120 °C, the yield of **2b** plummets from 72% at 4 sec to 28% at 1 min and 15% after 15 min. Likewise, at 150 °C, the initial yield of **2b** (70%) obtained after 4 sec drops to 29% at 20 sec. After 5 min, ≤5% **2b** was observed by GC-FID analysis. In all cases, GC-FID analysis confirms that the mass balance corresponds to starting **1b**.

This somewhat surprising regeneration of the starting diene **1b** is explained by the ring-opening of **2b**, followed by cross-metathesis with the entrapped ethylene (formed as co-product during RCM of **1b**; Scheme 2). The reports of Furstner[65] and Weiler,[66] using closely related macrocyclic substrates, attest to the feasibility of this reaction sequence. Unexpectedly, the results of the superheated reactions indicate that metathesis activity is retained for a longer period than at 80 °C. (Recall that metathesis stopped after about 90 sec at a temperature of 80 °C). This longer catalyst lifetime may reflect the higher stability of the alkylidene intermediate shown in Scheme 2. These mechanistic issues notwithstanding, a reaction temperature of 80 °C offers the best compromise in terms of yield and reaction time. Subsequent experiments in this Chapter were therefore carried out at this temperature.

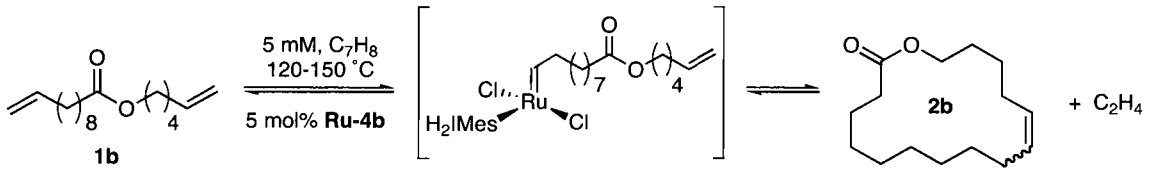

Scheme 2. Regeneration of **1b** by cross-metathesis of **2b** with ethylene.

Catalyst Loading (Figure 7a; Table 1, Entries 4-6). Decreasing the catalyst loadings from 5 mol% to 1 mol% has an unexpectedly low impact, maximum conversions dropping by only 12%. Catalyst lifetimes are also extended, with RCM being sustained over 11 min. Importantly, this implies that bimolecular deactivation dominates over unimolecular deactivation[32] under these process conditions (see discussion in section 6.1). Sustained consumption of **1b** is also observed at 10 mol% [Ru], but RCM ceases after only 1 min: that

is, non-metathetical reactions dominate.[63] Subsequent experiments were thus carried at ≤1 mol% [Ru].

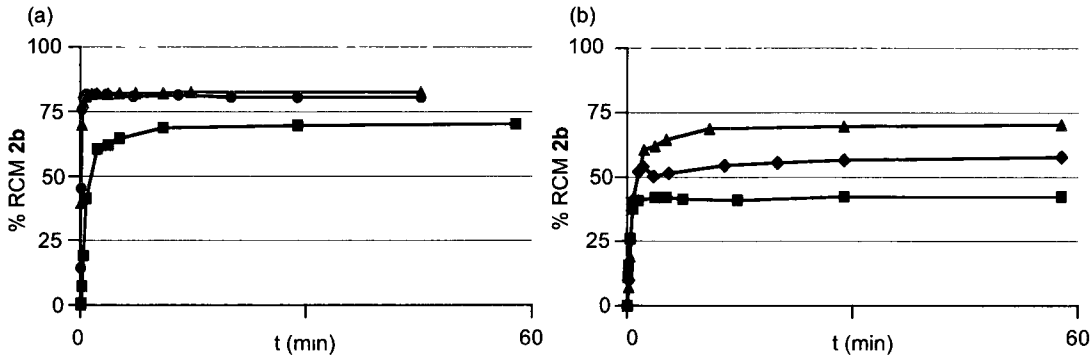

Figure 7. Yields of **2b** over time at (a) different loadings of **Ru-4b**: 5 mM **1b**: 10 mol% (●), 5 mol% (▲), 1 mol% (■); (b) different [**1b**]: 1 mol% **Ru-4b**: 20 mM (■), 10 mM (◆), 5 mM (▲). In both cases, the reaction was performed at 80 °C in C_7H_8. Calibrated GC-FID analysis (±2% in replicate runs).

Concentration (Figure 7b; Table 1, Entries 6-8). Because RCM macrocyclization of **1b** via **Ru-4b** proceeds under thermodynamic control,[1,19] high dilutions (5 mM **1b** in batch RCM) are essential to shift the concentration-dependent ring-chain equilibrium in favour of **2b**.[1,19,20] As expected, increasing the concentration of **1b** above 5 mM in the PFR increases rates of metathesis, but at the cost of selectivity for **2b**. Moreover, selectivity decreases over time, presumably owing to competing polymerization of **2b**, as reported by the Fürstner[67] and Yamamoto[68] groups for other macrocyclic targets.

Table 1. Overview of the RCM performance of **1b** via **Ru-4b**.[a]

	Reactor	mol% [Ru]	T (°C)	[**1b**] (mM)	τ end (min)[a]	% Conv. (Sel.)[b]	% Yield
1	BR	5	60	5	10	84 (*)	84
2	PFR	5	60	5	11	79 (*)	79
3	PFR	5	40	5	30	31 (55)	17
4	PFR	5	80	5	1.5	82 (*)	82
5	PFR	10	80	5	1	94 (86)[c]	81
6	PFR	1	80	5	11	70 (*)	70
7	PFR	1	80	10	2	72 (79)	57
8	PFR	1	80	20	1	84 (51)	43
9	CSTR	1	80	5	20	>99 (*)	>99
10	BR	1	80	5	10	82 (*)	82
11	CSTR	0.2	80	5	50[d]	>99 (*)	>99
12	CSTR	0.1	80	5	50[d]	76 (*)	76
13	CSTR	1	80	20	10	>99 (65)	65

[a] τ_{end} = reaction time at max. RCM yield (Figures 5-7), except for Entry 3 (terminated at 30 min). [b] Selectivity = % **2b** / % Conv. × 100; ≤±2 (Entry 5: ±3%). (*) = no observable by-products; [c] Isomerized and ring-contracted by-products observed; [d] τ unoptimized.

6.4 RCM reactions in a continuous stirred-tank reactor

The CSTR differs from the PFR and BR in its characteristically broad residence time distribution (RTD),[69] in consequence of which longer reaction times are required to reach comparable conversions. The high rates of RCM achieved in the PFR are thus an important prerequisite for transfer of this process to the CSTR. A compensating feature of great interest is the capacity of the CSTR to permit escape of ethylene and hence to limit non-productive metathesis and ethylene-mediated deactivation.[32,70] To facilitate the evolution of ethylene, the CSTR reactor was designed with a large headspace, which is continuously flushed with argon. The combination of this large head-space with the low solubility of ethylene in toluene (under 1 atm of C_2H_4; 8 mM at 40 °C and <1 mM above 45 °C)[71] should maintain sub-millimolar concentrations of ethylene in solution. As the broad RTD of the CSTR can limit selectivity if competitive reaction pathways are accessible, inhibiting oligomerization is critical. Therefore, the conditions of temperature and dilution established as optimal for selectivity in the PFR study were adopted. Additionally, the CSTR flow rate of 0.1 mL min^{-1} was chosen to maximize conversions. Under these conditions, the content of the tank, at steady-state, should consists primarily of cyclic **2b** and low concentrations of **1b** and **Ru-4b**.

Maximum RCM yields in the CSTR were significantly higher than in the optimized PFR or BR setups. Quantitative yields are obtained at 20 min when using 1 mol% **Ru-4b** at 80 °C and 5 mM **1b** (Figure 8a; Table 1, Entry 9: cf. Entries 6/10). Even on decreasing the catalyst loading five-fold, quantitative RCM was achieved at an unoptimized 50 min reaction time (Entry 11). At 0.1 mol% [Ru], however, 76% **2b** was obtained at the same stage (Entry 12). Use of the potentially more robust styrenyl ether analogue **Ru-5b** gave similar results. That is, in neither case was complete conversion effected within 1 h, which was set as the maximum tolerable duration of reaction to maintain space-time yields.

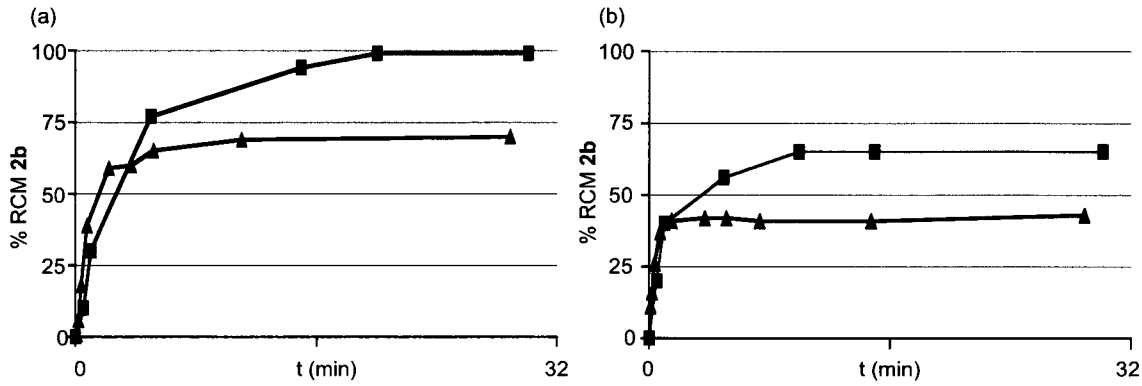

Figure 8. Yields of **2b** as function of time (C_7H_8, 80 °C, 1 mol% **Ru-4b**) at (a) 5 mM and (b) 20 mM. CSTR (■) vs. PFR (▲). Calibrated GC-FID analysis (±2% in replicate runs).

A key finding from Figure 8a is that although *initial* reaction is faster in the PFR (as predicted by theory; vide supra), it is rapidly outstripped by that in the CSTR. Moreover, RCM activity is sustained over a longer period in the CSTR. The beneficial impact of efficient removal of ethylene on catalyst lifetime and productivity has been noted in two earlier CF studies,[72,73] but this is the first delineation of its impact on the synthesis of a challenging, real-world RCM target. More unexpected is the slower deactivation in the CSTR relative to the BR implied by comparison of Entries 9 and 10. The simultaneous presence of fresh and "old" catalyst in the CSTR may be a factor contributing to this enhanced catalyst lifetime.

Increasing feed concentrations in the CSTR reduced selectivity, as expected, albeit to a lesser extent than in the PFR. At 20 mM **1b**, conversion was quantitative after 10 min using 1 mol% **Ru-4b**, but RCM yields reached only 65% (Entry 13; Figure 8b). Noteworthy, however, is the >20% improved yield of **2b** relative to that obtained in the PFR under

identical conditions (43%; Entry 8; Figure 8b). Operation in the CSTR thus appears to permit a slight increase in the diene concentration that can be tolerated in RCM macrocyclization. This may reflect the long "tail" in the RTD, which allows more time for backbiting, and hence establishment of equilibrium RCM yields.

The impact of these reactor configurations on catalyst productivity is highlighted in Figure 9, which depicts maximum turnover numbers (TON_{max}) and turnover frequencies (TOF_{max}) at 100% selectivity. Values of TON_{max} in the CSTR approach 800, an order of magnitude higher than in the PFR or BR (Figure 9a). Reactor throughputs show a less dramatic improvement, owing to the RTD issue noted above. Thus, TOF_{max} values of 15.2, 10.9 and 8.2 min^{-1} were observed for the CSTR, PFR and BR respectively (Figure 9b). The TOF_{max} of 15.2 min^{-1} obtained in the CSTR is a minimum figure, as the residence time was not optimized: that is, the minimum residence time was not explored. (Optimization is slower in the CSTR than the PFR, as the longer τ associated with the broad RTD means that time profiles take considerably longer to compile).

The unoptimized TOF_{max} attainable in the CSTR compares very favourably with the TOF of 1.5 min^{-1} reported by Ying and co-workers for the RCM of the much more readily-cyclized substrate diethyl diallyl malonate **11a**.[72] The Ying study employed a circulating packed-bed flow reactor in which a ruthenium catalyst was immobilized on mesoporous silica (50 mM substrate in CH_2Cl_2, 50 °C, 5 mol% [Ru]). Importantly, the reduced catalyst activity is not due to deactivation by retained ethylene, as an on-line degasser and an open reservoir were used to sweep ethylene out of the system. The higher efficiency attainable in the CSTR is due in part to the use of toluene as solvent, which enables a higher maximum operating temperature. The Ying group used CH_2Cl_2, rather than toluene, having observed higher conversions in the chlorinated solvent at 50 °C. Also a factor, however, may be the deleterious effect of immobilization on catalyst activity and/or lifetime. The much superior results obtained using the CSTR are important in emphasizing that CF processes do not require use of a supported catalyst, and in fact may be optimally conducted using homogeneous catalyst systems.

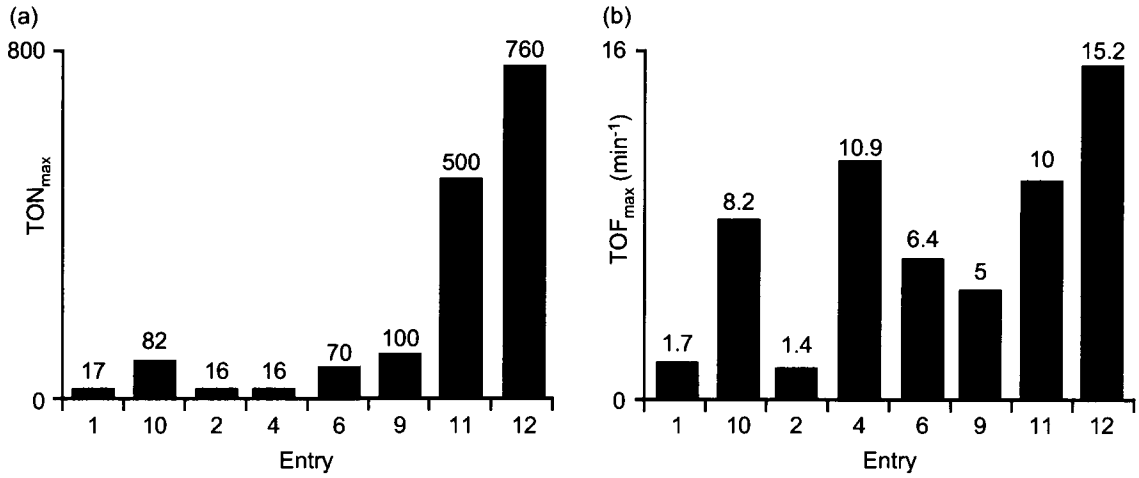

Figure 9. Comparison of (a) TON_{max} and (b) TOF_{max} for the BR (■), PFR (■) and CSTR (■). For conditions, see corresponding entry in Table 1.

It will be noted that at TOF_{max}, conversions are incomplete in all reactor configurations. Realization of quantitative conversion and selectivity is critical to minimizing purification requirements, with their deleterious economic and environmental impacts. A more relevant metric is thus TOF_{max} at quantitative conversion and 100% selectivity. In this respect the CSTR (with a value of 10 min^{-1}; see Entry 11) stands alone. Neither the PFR nor the BR permit full conversions under the optimized reaction conditions, even at 1 mol% [Ru] (BR) or 5 mol% [Ru] (PFR). Quantitative conversions were attained in the earlier work in the BR using refluxing CH_2Cl_2,[19] but only at a catalyst loading of 5 mol%.

The foregoing illustrates the complementary strengths and weaknesses of the PFR and CSTR. Consequently, these reactors provide a highly desirable degree of versatility for industrial applications. The importance of this flexibility becomes obvious when considering the various stages of pharmaceutical production. A key requirement during synthesis of fine chemicals for pre-clinical or clinical Phase I trials is speed. In Phase II and III trials, the emphasis shifts to product quality, while in commercial production, costs are of paramount importance.[64] The fast reaction rates obtained using the PFR may favour use of this reactor for RCM production of fine chemicals for Phase 1 trials. Conversely, the quantitative conversions observed, even at low catalyst loading, in the CSTR will facilitate product purification, rendering this reactor more suitable than the PFR for Phase II and III purposes.

References page 208

6.5 Conclusions

This chapter demonstrates that dramatic improvements in efficiency can be achieved in RCM of a challenging, low-EM diene, without recourse to catalyst or substrate tuning, by the use of an appropriate continuous-flow reactor. Quantitative RCM (i.e. full conversion and complete selectivity) of **1b** is achieved in the CSTR at 0.2 mol% [Ru], a catalyst loading 25× lower than that required for comparable performance in batch mode.[19] Operation in the PFR can reduce reaction times further, but at the cost of yields and selectivity. Continuous-flow methodologies that permit removal of ethylene thus show great potential to facilitate uptake of RCM into industrial practice

Notwithstanding the advantages of the PFR and CSTR described above, high selectivity for macrocyclic **2b** still requires dilute conditions. Of great interest in this context is the elevated selectivity obtained using the CSTR at higher diene concentrations. The implied potential of the CSTR to limit solvent costs renders this reactor even more interesting from an industrial perspective. Further improvements in selectivity may come from additional modifications to the reactor. Also of interest is the use of super-critical CO_2 ($scCO_2$) as reaction "solvent".[65] Incorporation of $scCO_2$ is particularly straightforward for the PFR reactor, which can readily be pressurized. Additional benefits, beyond selectivity, may stem from a potentially higher catalyst lifetime using $scCO_2$, owing to dilution of the generated ethylene.

6.6 References

(1) Monfette, S.; Fogg, D. E., *Chem. Rev.* **2009**, *109*, 3783–3816.
(2) Monfette, S.; Fogg, D. E., Ring-Closing Metathesis in the Synthesis of Medium and Large Rings: Challenges and Implications for Sustainable Synthesis. In *Green Metathesis Chemistry, NATO Science Series II*, Dragutan, V.; Demonceau, A.; Dragutan, I.; Finkelshtein, E. S., Eds. Springer Verlag: 2009.
(3) Gradillas, A.; Perez-Castells, J., *Angew. Chem., Int. Ed.* **2006**, *45*, 6086-6101.
(4) Villemin, D., *Tetrahedron Lett.* **1980**, *21*, 1715-1718.
(5) Tsuji, J.; Hashiguchi, S., *Tetrahedron Lett.* **1980**, *21*, 2955-2958.
(6) Nguyen, S. T.; Johnson, L. K.; Grubbs, R. H.; Ziller, J. W., *J. Am. Chem. Soc.* **1992**, *114*, 3974-3975.
(7) Farina, V.; Shu, C.; Zeng, X.; Wei, X.; Han, Z.; Yee, N. K.; Senanayake, C. H., *Org. Process Res. Dev.* **2009**, *13*, 250-254.
(8) Nicola, T.; Brenner, M.; Donsbach, K.; Kreye, P., *Org. Process Res. Dev.* **2005**, *9*, 513-515.
(9) Yee, N. K.; Farina, V.; Houpis, I. N.; Haddad, N.; Frutos, R. P.; Gallou, F.; Wang, X.-J.; Wei, X.; Simpson, R. D.; Feng, X.; Fuchs, V.; Xu, Y.; Tan, J.; Zhang, L.; Xu, J.; Smith-

Keenan, L. L.; Vitous, J.; Ridges, M. D.; Spinelli, E. M.; Johnson, M.; Donsbach, K.; Nicola, T.; Brenner, M.; Winter, E.; Kreye, P.; Samstag, W., *J. Org. Chem.* **2006**, *71*, 7133-7145.
(10) Wang, H.; Matsuhashi, H.; Doan, B. D.; Goodman, S. N.; Ouyang, X.; Clark, W. M., *Tetrahedron* **2009**, *65*, 6291-6303.
(11) Wang, H.; Goodman, S. N.; Dai, Q.; Stockdale, G. W.; Clark, W. M., *Org. Process Res. Dev.* **2008**, *12*, 226-234.
(12) Garrett, C. E.; Prasad, K., *Adv. Synth. Catal.* **2004**, *346*, 889-900.
(13) Faucher, A. M.; Bailey, M. D.; Beaulieu, P. L.; Brochu, C.; Duceppe, J. S.; Ferland, J. M.; Ghiro, E.; Gorys, V.; Halmos, T.; Kawai, S. H.; Poirier, M.; Simoneau, B.; Tsantrizos, Y. S.; Llinas-Brunet, M., *Org. Lett.* **2004**, *6*, 2901-2904.
(14) Liverton, N. J.; Holloway, M. K.; McCauley, J. A.; Rudd, M. T.; Butcher, J. W.; Carroll, S. S.; DiMuzio, J.; Fandozzi, C.; Gilbert, K. F.; Mao, S.-S.; McIntyre, C. J.; Nguyen, K. T.; Romano, J. J.; Stahlhut, M.; Wan, B.-L.; Olsen, D. B.; Vacca, J. P., *J. Am. Chem. Soc.* **2008**, *130*, 4607-4609.
(15) McCauley, J. A.; Rudd, M. T.; Nguyen, K. T.; McIntyre, C. J.; Romano, J. J.; Bush, K. J.; Varga, S. L.; Ross, C. W., III; Carroll, S. S.; DiMuzio, J.; Stahlhut, M. W.; Olsen, D. B.; Lyle, T. A.; Vacca, J. P.; Liverton, N. J., *Angew. Chem., Int. Ed.* **2008**, *47*, 9104-9107.
(16) Wilson, L. J.; Malaviya, R.; Yang, C.; Argentieri, R.; Wang, B.; Chen, X.; Murray, W. V.; Cavender, D., *Bioorg. Med. Chem. Lett.* **2009**, *19*, 3333-3338.
(17) Content, S.; Dutton, C. J.; Roberts, L., *Bioorg. Med. Chem. Lett.* **2003**, *13*, 321-325.
(18) Machauer, R.; Veenstra, S.; Rondeau, J.-M.; Tintelnot-Blomley, M.; Betschart, C.; Neumann, U.; Paganetti, P., *Bioorg. Med. Chem. Lett.* **2009**, *19*, 1361-1365.
(19) Conrad, J. C.; Eelman, M. D.; Duarte Silva, J. A.; Monfette, S.; Parnas, H. H.; Snelgrove, J. L.; Fogg, D. E., *J. Am. Chem. Soc.* **2007**, *129*, 1024-1025.
(20) Conrad, J. C.; Fogg, D. E., *Curr. Org. Chem.* **2006**, *10*, 185-202.
(21) Sheldon, R. A., *Green Chem.* **2007**, *9*, 1273-1283.
(22) Buchmeiser, M. R., *Chem. Rev.* **2009**, *109*, 303-321.
(23) Barrett, A. G. M.; Hopkins, B. T.; Koebberling, J., *Chem. Rev.* **2002**, *102*, 3301-3323.
(24) Dragutan, I.; Dragutan, V., *Platinum Met. Rev.* **2008**, *52*, 71-82.
(25) Clavier, H.; Grela, K.; Kirschning, A.; Mauduit, M.; Nolan, S. P., *Angew. Chem., Int. Ed.* **2007**, *46*, 6786-6801.
(26) Dragutan, I.; Dragutan, V., *Platinum Met. Rev.* **2008**, *52*, 157-162.
(27) Coperet, C.; Basset, J. M., *Adv. Synth. Catal.* **2007**, *349*, 78-92.
(28) Halbach, T. S.; Mix, S.; Fischer, D.; Maechling, S.; Krause, J. O.; Sievers, C.; Blechert, S.; Nuyken, O.; Buchmeiser, M. R., *J. Org. Chem.* **2005**, *70*, 4687-4694.
(29) Grela, K.; Tryznowski, M.; Bieniek, M., *Tetrahedron Lett.* **2002**, *43*, 9055-9059.
(30) Nieczypor, P.; Buchowicz, W.; Meester, W. J. N.; Rutjes, F.; Mol, J. C., *Tetrahedron Lett.* **2001**, *42*, 7103-7105.
(31) Michalek, F.; Maedge, D.; Ruehe, J.; Bannwarth, W., *J. Organomet. Chem.* **2006**, *691*, 5172-5180.
(32) Ulman, M.; Grubbs, R. H., *J. Org. Chem.* **1999**, *64*, 7202-7207.
(33) Hong, S. H.; Wenzel, A. G.; Salguero, T. T.; Day, M. W.; Grubbs, R. H., *J. Am. Chem. Soc.* **2007**, *129*, 7961-7968.
(34) Gatti, M.; Vieille-Petit, L.; Luan, X.; Mariz, R.; Drinkel, E.; Linden, A.; Dorta, R., *J. Am. Chem. Soc.* **2009**, *131*, 9498–9499.
(35) Mayr, M.; Mayr, B.; Buchmeiser, M. R., *Angew. Chem., Int. Ed.* **2001**, *40*, 3839-3842.

(36) Michrowska, A.; Mennecke, K.; Kunz, U.; Kirschning, A.; Grela, K., *J. Am. Chem. Soc.* **2006**, *128*, 13261-13267.
(37) Mol, J. C., *J. Mol. Catal. A* **2004**, *213*, 39-45.
(38) Frenzel, U.; Muller, B. K. M.; Nuyken, O., Metathesis Polymerization of Cycloolefins. In *Handbook of Polymer Synthesis*, 2nd ed.; Swift, G.; Kricheldorf, H. R.; Nuyken, O., Eds. Marcel Dekker: New York, 2005; pp 381-426.
(39) Dinger, M. B.; Mol, J. C., *Adv. Synth. Catal.* **2002**, *344*, 671-677.
(40) Conrad, J. C.; Amoroso, D.; Czechura, P.; Yap, G. P. A.; Fogg, D. E., *Organometallics* **2003**, *22*, 3634-3636.
(41) Werner, H.; Grunwald, C.; Stuer, W.; Wolf, J., *Organometallics* **2003**, *22*, 1558-1560.
(42) Caggiano, L.; Castoldi, D.; Beumer, R.; Bayon, P.; Tesler, J.; Gennari, C., *Tetrahedron Lett.* **2003**, *44*, 7913-7919.
(43) Gurjar, M. K.; Yakambram, P., *Tetrahedron Lett.* **2001**, *42*, 3633-3636.
(44) Fürstner, A.; Langemann, K., *J. Am. Chem. Soc.* **1997**, *119*, 9130-9136.
(45) Li, Y.; Zhang, T.; Li, Y.-L., *Tetrahedron Lett.* **2007**, *48*, 1503-1505.
(46) Selvakumar, N.; Kumar, P. K.; Reddy, K. C. S.; Chary, B. C., *Tetrahedron Lett.* **2007**, *48*, 2021-2024.
(47) Chen, X.; Wiemer, D. F., *J. Org. Chem.* **2003**, *68*, 6597-6604.
(48) Yang, Q.; Xiao, W.-J.; Yu, Z., *Org. Lett.* **2005**, *7*, 871-874.
(49) Fu, G. C.; Nguyen, S. T.; Grubbs, R. H., *J. Am. Chem. Soc.* **1993**, *115*, 9856-9857.
(50) Wilson, G. O.; Porter, K. A.; Weissman, H.; White, S. R.; Sottos, N. R.; Moore, J. S., *Adv. Synth. Catal.* **2009**, *351*, 1817-1825.
(51) Armstrong, S. K., *J. Chem. Soc., Perkin Trans.* **1998**, 371-388.
(52) Slugovc, C.; Demel, S.; Stelzer, F., *Chem. Commun.* **2002**, 2572-2573.
(53) Spagnol, G.; Heck, M.-P.; Nolan, S. P.; Mioskowski, C., *Org. Lett.* **2002**, *4*, 1767-1770.
(54) Schrock, R. R.; Hoveyda, A. H., *Angew. Chem., Int. Ed.* **2003**, *42*, 4592-4633.
(55) Mason, B. P.; Price, K. E.; Steinbacher, J. L.; Bogdan, A. R.; McQuade, D. T., *Chem. Rev.* **2007**, *107*, 2300-2318.
(56) Kirschning, A.; Solodenko, W.; Mennecke, K., *Chem. Eur. J.* **2006**, *12*, 5972-5990.
(57) Singh, B. K.; Kaval, N.; Tomar, S.; Van der Eycken, E.; Parmar, V. S., *Org. Process Res. Dev.* **2008**, *12*, 468-474.
(58) Comer, E.; Organ, M. G., *J. Am. Chem. Soc.* **2005**, *127*, 8160-8167.
(59) Kraft, P., Aroma Chemicals IV: Musks. In *Chemistry and Technology of Flavors and Fragrances*, Rowe, D. J., Ed. CRC Press: Boca Raton, 2005; pp 143-168.
(60) Fürstner, A.; Krause, H.; Ackermann, L.; Lehmann, C. W., *Chem. Commun.* **2001**, 2240-2241.
(61) Ackermann, L.; Fürstner, A.; Weskamp, T.; Kohl, F. J.; Herrmann, W. A., *Tetrahedron Lett.* **1999**, *40*, 4787-4790.
(62) Blacquiere, J. M.; Jurca, T.; Weiss, J.; Fogg, D. E., *Adv. Synth. Catal.* **2008**, *350*, 2849-2855.
(63) Alcaide, B.; Almendros, P.; Luna, A., *Chem. Rev.* **2009**, *109*, 3817-3858.
(64) Roberge, D. M.; Ducry, L.; Bieler, N.; Cretton, P.; Zimmermann, B., *Chem. Eng. Technol.* **2005**, *28*, 318-323.
(65) Fürstner, A.; Ackermann, L.; Beck, K.; Hori, H.; Koch, D.; Langemann, K.; Liebl, M.; Six, C.; Leitner, W., *J. Am. Chem. Soc.* **2001**, *123*, 9000-9006.
(66) Goldring, W. P. D.; Hodder, A. S.; Weiler, L., *Tetrahedron Lett.* **1998**, *39*, 4955-4958.

(67) Fürstner, A.; Thiel, O. R.; Ackermann, L., *Org. Lett.* **2001**, *3*, 449-451.
(68) Yamamoto, K.; Biswas, K.; Gaul, C.; Danishefsky, S. J., *Tetrahedron Lett.* **2003**, *44*, 3297-3299.
(69) Nauman, E. B., Residence Time Distribution. In *Handbook of Industrial Mixing - Science and Practice*, Paul, E. L.; Atiemo-Obeng, V. A.; Kresta, S. M., Eds. John Wiley & Sons: Hoboken, 2004; pp 1-17.
(70) Burdett, K. A.; Harris, L. D.; Margl, P.; Maughon, B. R.; Mokhtar-Zadeh, T.; Saucier, P. C.; Wasserman, E. P., *Organometallics* **2004**, *23*, 2027-2047.
(71) Lee, L.-S.; Ou, H.-J.; Hsu, H.-L., *Fluid Phase Equilib.* **2005**, *231*, 221-230.
(72) Lim, J.; Lee, S. S.; Ying, J. Y., *Chem. Commun.* **2010**, *46*, 806-808.
(73) Lysenko, Z.; Maughon, B. R.; Mokhtar-Zadeh, T.; Tulchinsky, M. L., *J. Organomet. Chem.* **2006**, *691*, 5197-5203.

7. Conclusions and future directions

The work described in this thesis was motivated by the prospect of "greener" use of the olefin metathesis reaction in both academia and industry. To that end, solutions to the problems of low catalyst lifetime and selectivity of the Grubbs catalysts were sought using a three-fold approach. First, mechanistic investigations of the RCM macrocyclization reaction were performed in order to evaluate the participation of the various Grubbs catalysts in the ring-chain equilibrium. Secondly, a systematic evaluation of the electronic properties of the anionic ligand was undertaken to elucidate the optimum properties of these ligands for metathesis activity. Third, the knowledge acquired regarding the RCM reaction was interfaced with chemical engineering concepts to evaluate the feasibility of RCM macrocyclization in industrial context. The combination of these approaches culminated in the rational design of catalysts and the judicious choice of reaction conditions and protocols for maximizing the efficiency of RCM. The results presented in this thesis highlight the transformation of performance that can be attained by careful understanding of the key factors governing reactivity of the Grubbs or pseudohalide catalysts.

The examination of the decomposition products of the Grubbs catalysts revealed that the ubiquitous chloride ligands within these catalysts are implicated in the deactivation process. Consequently, replacement of the chloride ligands by a more versatile framework could fulfill the long-sought goal of a selective, long-lived metathesis catalyst. Surprisingly, however, little was known about how the electronic properties of the anionic ligands affect metathesis activity. The few studies that had examined this point were clouded by the concomitant increase in steric demand of the ligands. The choice of a catecholate platform was instrumental in enabling, for the first time, the direct examination of electronic parameters while excluding any potential steric effects. The catalytic results obtained with the catecholate catalysts indicate that maximum metathesis activity is obtained when the anionic ligands donate the most electron density to the Ru center.

Building on the knowledge acquired from the catecholate study, "second-generation" pseudohalide catalysts bearing isocyanate and isothiocyanate ligands were successfully prepared. Of particular interest is the significantly improved catalytic activity of the isocyanate catalyst over that of the catecholate catalysts. Moreover, the enhanced lability of

the pyridine ligands in the former also allowed for the synthesis of polymers of low polydispersity and controlled chain length, a task that has so far eluded *all* the oxygen-bound Ru-pseudohalide catalysts. Thus, use of the isocyanate catalyst towards tandem ROMP-hydrogenation or other tandem processes is definitely worth investigating. Application of the new isocyanate catalyst to monomers relevant to advanced materials would be very interesting. Additionally, as the polarity within the isocyanate ligand could facilitate separation of the catalyst from the reaction products, studies regarding the removal of this new catalyst would definitively be worthwhile.

From a catalyst design perspective, the far superior reactivity of the isocyanate catalyst relative to its isothiocyanate counterpart was traced back to a potentially general inter-ligand electrostatic repulsion; the latter is driven by the high positive charge on the isocyanate carbon atom. Maximizing the charge on this atom thus appears to be key in facilitating initiation for such pseudohalide catalysts. The phosphinimides $(N{=}PR_3)^-$ ligands are particularly attractive in this context as the +5 formal charge on the phosphorus atom could lead to unprecedented levels of initiation, and perhaps activity, for a pseudohalide catalyst. Synthesis of chiral catalysts by incorporation of asymmetric phosphinimide ligands could also prove worthwhile to explore. Moreover, the phosphinimides, also termed "super-bases", could replace the ubiquitous NHC ligands within the Grubbs catalysts, when added in their neutral form. The difference in electronic properties between NHC and phosphinimide ligands could lead to unexpected reactivity.

Identification of the deactivation product(s) of the pseudohalide catalysts could provide invaluable insight for future catalyst design. Preliminary investigations into this matter, using perhaloaryloxide catalysts, reveal that the first step towards decomposition may involves halogen abstraction from the pendant aryloxide ring, which regenerates the starting Ru-halogen bond. The pseudohalide catalysts may then follow similar deactivation pathways as the Grubbs complexes. Alternatively, formation of carbynes through HX elimination is also possible.

Amidst the survey of various catalysts (Grubbs and pseudohalides) for RCM macrocyclization, the interplay between reaction mechanism, reaction conditions and protocol was deconvoluted. The long-standing questions of – Which catalyst should I use? How should I carry out my reaction? – have now been answered. The partitioning of the

Grubbs catalysts into kinetically- and thermodynamically-controlled has been studied in detail. All of the second-generation, thermodynamically-controlled Grubbs catalyst show a tendency towards oligomerization of long, flexible α,ω-dienes. In contrast, the first-generation catalyst shows a bias towards cyclization of the same substrate, and is then classified as kinetically-controlled. Perhaps one of the most important discoveries made in this context is that the selectivity for the RCM product can be altered by changing the structure of the catalyst. Indeed, under identical conditions, perbromophenoxide catalyst **Ru-7b** shows higher RCM yield relative to its dichloride parent for RCM macrocyclization. As preliminary investigations reveal that the origin of this preference for cyclization is electronic in origin, examination of the macrocyclization profiles with other pseudohalide catalysts may prove worthwhile. Deeper kinetic investigations are also warranted in order to determine the extent of participation of the pseudohalide catalysts in the ring-chain equilibrium. Mechanistic issues notwithstanding, the most exciting aspect of this chemistry remains that the pseudohalide catalysts display higher reactivity over a far larger substrate scope relative to the first-generation catalyst while retaining the tendency of this catalyst towards cyclization. The short lifetime of the perbromoaryloxide catalyst will need to be addressed, however, before any large-scale applications of this catalyst can be envisioned. Nevertheless, the key advantage of the pseudohalide ligands is their inherent high tunability. Thus, judicious modulation of the ligands may hold the solution to their high sensitivity. Also of interest is the incorporation of large neutral donors in place of (e.g) PCy_3 or NHC ligands. Such ligands may have unexpected effects on the conformation of the cyclization/oligomerization transition state for RCM macrocyclization. The large diversity of phosphine ligands commercially available for (e.g.) Pd-catalyzed cross-coupling reaction might be a good starting point.

Often neglected in academia is the importance that the reactor may have on the efficiency of a given reaction. This is also true in context of RCM; little was known about the influence of the reactor on cyclization yield. An evaluation of both traditional batch as well as continuous-flow reactors was thus undertaken. This study revealed that a sealed plug-flow reactor allowed for extremely rapid reaction kinetics, but comes at a cost in term of product yield relative to the traditional batch reaction. The decisive factor is the entrapment of the ethylene co-product in the continuous plug-flow reactor (PFR), which promotes catalyst

deactivation. By designing a continuous stirred-tank reactor (CSTR), which allows rapid release of ethylene, dramatically enhanced efficiency was obtained. The levels of productivity attained with this reactor are independent of catalyst design and substrate tuning, which is of great interest for a broad applicability. Unexpectedly, a significant effect of the CSTR on product selectivity was also noticed. This implies that elevated diene concentrations can be employed in this reactor, without adversely affecting product yields by competing oligomerization. The relationship between reactor and RCM efficiency shows great promise, and may provide a stepping stone for future industrial application of RCM.

Future modifications of the continuous-flow setups described herein are plentiful. For instance, increasing the workable reaction concentrations, without sacrificing yields, could be achieved by incorporation of super-critical CO_2 "diluent" ($scCO_2$) into the systems. Introduction of this solvent is particularly amenable to the PFR, as this reactor can be readily operated under pressure (a requirement for this methodology). Notably, $scCO_2$ could potentially serve to dilute the ethylene formed during reaction. Therefore, an additional benefit in terms of catalyst lifetime could be witnessed. The expanding applications of membranes in various fields of chemistry and engineering could also prove valuable for continuous-flow RCM. Introduction of gas-permeable membranes within the reactor could be envisioned to favor volatilization and sequestration of ethylene, even in the sealed PFR. As reaction scale-up often requires significant time and resources, the ease with which such a transformation can be effected using the PFR reactor is highly attractive.

Of the utmost importance, is to keep an open mind. "Every great advance in science has issued from a new audacity of imagination" - *John Dewey*

Appendix A. Catalytic data

Chapter 3.

(a) Numerical data for Figure 7:

Table A-1. Consumption of diene **1a** over time for each catalyst.

Time	% **1a**			
(h)	**Ru-3**	**Ru-4a**	**Ru-4b**	**Ru-5b**
0	100	100	100	100
0.25	24	28	19	22
0.5	21	21	18	19
0.75	19	19	18	18
1	21	18	18	18
1.5	18	16	17	17
2	19	16	16	16
3	18	15	17	15.
5	18	15	14	15

Conditions: 5 mM **1b** in CH_2Cl_2, 40 °C, 5 mol% [Ru].

Table A-2. Yield of **2a** over time for each catalyst.

Time	% **2a**			
(h)	**Ru-3**	**Ru-4a**	**Ru-4b**	**Ru-5b**
0	0	0	0	0
0.25	57	46	58	55
0.5	57	52	57	56
0.75	58	54	56	57
1	57	55	56	57
1.5	58	55	57	57
2	57	55	57	57
3	57	54	56	57
5	57	52	55	57

Conditions: 5 mM **1b** in CH_2Cl_2, 40 °C, 5 mol% [Ru].

Table A-3. Proportion of oligomeric species formed over time during the RCM of **1a** for each catalyst.

Time	% Oligomers			
(h)	**Ru-3**	**Ru-4a**	**Ru-4b**	**Ru-5b**
0	0	0	0	0
0.25	19	26	23	23
0.5	22	27	25	24
0.75	23	27	26	25
1	22	27	26	25
1.5	24	28	26	26
2	24	29	27	27
3	24	31	27	28
5	25	33	31	28

Conditions: 5 mM **1b** in CH_2Cl_2, 40 °C, 5 mol% [Ru].

(b) Numerical data for Figure 8:

Table A-4. Consumption of diene **1a** over time for each catalyst.

Time	% **1a**						
(min)	**Ru-3**	**Ru-4a**	**Ru-4b**	**Ru-5a**	**Ru-5b**	**Ru-5c**	**Ru-6a**
0	100	100	100	100	100	100	100
0.5	87	-	-	-	-	88	94
1	82	90	84	91	89	81	93
2	-	-	86	-	88	76	91
5	57	-	85	-	85	69	89
15	32	90	82	88	80	57	85
30	-	-	79	87	77	49	79
45	-	88	76	85	74	44	76
60	3	84	-	83	72	40	73

Conditions: 5 mM **1a** in CH_2Cl_2, 20 °C, 5 mol% [Ru].

Table A-5. Yield of **2a** over time for each catalyst.

Time	% **2a**						
(min)	**Ru-3**	**Ru-4a**	**Ru-4b**	**Ru-5a**	**Ru-5b**	**Ru-5c**	**Ru-6a**
0	0	0	0	0	0	0	0
0.5	7	-	-	-	-	3	0
1	10	0	0	2	2	7	1
2	-	-	0	-	2	10	1
5	25	-	1	-	4	16	3
15	44	1	3	4	7	24	6
30	-	-	5	5	10	31	9
45	-	1	7	7	12	35	11
60	70	2	-	7	14	37	13

Conditions: 5 mM **1a** in CH_2Cl_2, 20 °C, 5 mol% [Ru].

Table A-6. Proportion of oligomeric species formed over time during the RCM of **1a** for each catalyst.

Time	% Oligomers						
(min)	**Ru-3**	**Ru-4a**	**Ru-4b**	**Ru-5a**	**Ru-5b**	**Ru-5c**	**Ru-6a**
0	0	0	0	0	0	0	0
0.5	6	-	-	-	-	9	5
1	9	10	16	7	10	13	7
2	-	-	15	-	10	14	7
5	18	-	14	-	11	16	8
15	24	10	15	8	13	19	10
30	-	-	17	8	13	20	12
45	-	11	18	9	14	22	13
60	28	14	-	11	14	23	15

Conditions: 5 mM **1a** in CH_2Cl_2, 20 °C, 5 mol% [Ru].

Table A-7. Consumption of diene **1b** over time for each catalyst.

Time	% **1b**						
(min)	**Ru-3**	**Ru-4a**	**Ru-4b**	**Ru-5a**	**Ru-5b**	**Ru-5c**	**Ru-6a**
0	100	100	100	100	100	100	100
0.5	85	-	-	-	-	85	-
1	77	94	89	96	85	73	-
2	68	-	87	96	84	65	90
5	51	-	84	-	79	51	86
15	22	-	77	85	72	32	77
30	10	91	70	80	64	22	69
45	6	89	64	76	-	17	65
60	3	88	-	74	51	13	62

Conditions: 5 mM **1b** in CH_2Cl_2, 20 °C, 5 mol% [Ru].

Table A-8. Yield of **2b** over time for each catalyst.

Time	% **2b**						
(min)	**Ru-3**	**Ru-4a**	**Ru-4b**	**Ru-5a**	**Ru-5b**	**Ru-5c**	**Ru-6a**
0	0	0	0	0	0	0	0
0.5	11	-	-	-	-	8	-
1	18	0	0	0	0	17	-
2	25	-	1	0	2	25	3
5	40	-	4	-	8	40	7
15	69	-	11	8	18	61	16
30	86	1	17	13	25	73	24
45	92	2	22	17	-	79	29
60	96	4	-	20	33	84	32

Conditions: 5 mM **1b** in CH_2Cl_2, 20 °C, 5 mol% [Ru].

Table A-9. Proportion of oligomeric species formed over time during RCM of **1b** for each catalyst.

Time	% Oligomers						
(min)	**Ru-3**	**Ru-4a**	**Ru-4b**	**Ru-5a**	**Ru-5b**	**Ru-5c**	**Ru-6a**
0	0	0	0	0	0	0	0
0.5	4	-	-	-	-	7	-
1	6	7	11	4	15	10	-
2	7	-	12	4	14	10	7
5	9	-	12	-	13	9	7
15	9	-	12	6	11	7	7
30	5	8	13	7	11	5	7
45	2	9	14	7	-	4	7
60	1	7	-	6	16	3	6

Conditions: 5 mM **1b** in CH_2Cl_2, 20 °C, 5 mol% [Ru].

(c) Conversion profiles for **1a-c** and **3a/b**:

Table A-10. Consumption of diene **1a** over time for each catalyst.

Time	% **1a**								
(h)	**Ru-3**	**Ru-4a**	**Ru-4b**	**Ru-5a**	**Ru-5b**	**Ru-5c**	**Ru-6a**	**Ru-7a**	**Ru-7b**
0	100	100	100	100	100	100	100	100	100
0.25	7	0	1	4	8	3	3	98	87
0.5	4	0	0	3	3	1	1	94	59
0.75	3	0	0	2	3	0	1	-	30
1	4	0	0	2	2	0	1	91	17
1.5	4	0	0	2	0	0	0	-	6
2	4	0	0	2	0	0	0	-	-
3	0	0	0	2	0	0	0	34	3
4	-	-	-	-	-	-	-	12	-
5	-	-	-	-	-	-	-	1	0
6	-	-	-	-	-	-	-	0	-

Conditions: 5 mM **1a** in CH_2Cl_2, Δ, 5 mol% [Ru]; 20 mol% for **Ru-7b**.

Table A-11. Yield of **2a** over time for each catalyst.

Time	% **2a**								
(h)	**Ru-3**	**Ru-4a**	**Ru-4b**	**Ru-5a**	**Ru-5b**	**Ru-5c**	**Ru-6a**	**Ru-7a**	**Ru-7b**
0	0	0	0	0	0	0	0	0	0
0.25	72	13	5	9	8	32	6	0	4
0.5	80	26	18	13	23	53	42	1	21
0.75	83	-	27	13	32	56	47	-	38
1	83	35	35	15	37	57	49	3	51
1.5	87	41	41	15	47	63	54	-	63
2	90	50	50	15	52	61	54	-	-
3	94	50	54	15	54	57	53	31	68
4	-	-	-	-	-	-	-	52	-
5	-	-	-	-	-	-	-	60	68
6	-	-	-	-	-	-	-	62	-

Conditions: 5 mM **1a** in CH_2Cl_2, Δ, 5 mol% [Ru]; 20 mol% for **Ru-7b**.

Table A-12. Proportion of oligomeric species formed over time during the RCM of **1a** for each catalyst.

Time	% Oligomers								
(h)	**Ru-3**	**Ru-4a**	**Ru-4b**	**Ru-5a**	**Ru-5b**	**Ru-5c**	**Ru-6a**	**Ru-7a**	**Ru-7b**
0	0	0	0	0	0	0	0	0	0
0.25	22	87	94	87	84	64	91	3	9
0.5	16	75	82	84	73	46	57	5	20
0.75	14	-	73	84	71	44	53	-	32
1	13	65	65	83	61	41	50	7	32
1.5	9	60	59	83	53	37	45	-	31
2	7	50	50	83	48	39	45	-	-
3	5	50	46	83	46	43	46	35	30
4	-	-	-	-	-	-	-	36	-
5	-	-	-	-	-	-	-	35	29
6	-	-	-	-	-	-	-	32	-

Conditions: 5 mM **1a** in CH_2Cl_2, Δ, 5 mol% [Ru]; 20 mol% for **Ru-7b**.

Table A-13. Consumption of diene **1b** over time for each catalyst.

Time	% **1b**						
(h)	**Ru-3**	**Ru-4a**	**Ru-4b**	**Ru-5a**	**Ru-5b**	**Ru-5c**	**Ru-6a**
0	100	100	100	100	100	100	100
0.25	5	12	1	7	8	1	18
0.5	0	2	0	1	0	0	4
0.75	0	0	0	1	0	0	0
1	0	0	0	0	0	0	0
1.5	0	0	0	0	0	0	0
2	0	0	0	0	0	0	0
3	0	0	0	0	0	0	0

Conditions: 5 mM **1b** in CH_2Cl_2, Δ, 5 mol% [Ru].

Table A-14. Yield of **2b** over time for each catalyst.

Time	% **2b**						
(h)	**Ru-3**	**Ru-4a**	**Ru-4b**	**Ru-5a**	**Ru-5b**	**Ru-5c**	**Ru-6a**
0	0	0	0	0	0	0	0
0.25	90	37	47	49	45	64	23
0.5	>99	59	65	75	78	87	84
0.75	>99	75	83	85	85	92	89
1	>99	80	86	88	85	96	96
1.5	>99	88	87	94	91	>99	97
2	>99	96	96	97	97	>99	>99
3	>99	>99	>99	>99	>99	>99	>99

Conditions: 5 mM **1b** in CH_2Cl_2, Δ, 5 mol% [Ru].

Table A-15. Proportion of oligomeric species formed over time during the RCM of **1b** for each catalyst.

Time	% Oligomers						
(h)	**Ru-3**	**Ru-4a**	**Ru-4b**	**Ru-5a**	**Ru-5b**	**Ru-5c**	**Ru-6a**
0	0	0	0	0	0	0	0
0.25	6	51	53	44	47	35	60
0.5	1	39	35	24	22	14	13
0.75	1	25	17	15	15	8	11
1	0	20	14	13	15	4	4
1.5	0	12	13	7	9	0	3
2	0	4	4	4	3	0	0
3	0	1	1	0	0	0	0

Conditions: 5 mM **1b** in CH_2Cl_2, Δ, 5 mol% [Ru].

Table A-16. Consumption of diene **1c** over time for each catalyst.

Time	% **1c**						
(h)	**Ru-3**	**Ru-4a**	**Ru-4b**	**Ru-5a**	**Ru-5b**	**Ru-5c**	**Ru-6a**
0	100	100	100	100	100	100	100
0.25	33	8	1	7	3	1	18
0.5	13	6	3	1	1	0	4
0.75	5	6	3	1	0	0	3
1	1	2	2	1	0	0	2
1.5	0	0	0	0	0	0	0
2	0	0	0	0	0	0	0
3	0	0	0	0	0	0	0

Conditions: 5 mM **1c** in CH_2Cl_2, Δ, 5 mol% [Ru].

Table A-17. Yield of **2c** over time for each catalyst.

Time	% **2c**						
(h)	**Ru-3**	**Ru-4a**	**Ru-4b**	**Ru-5a**	**Ru-5b**	**Ru-5c**	**Ru-6a**
0	0	0	0	0	0	0	0
0.25	46	53	47	43	38	53	43
0.5	66	68	61	38	65	79	84
0.75	75	72	65	53	77	85	823
1	77	78	70	63	81	85	85
1.5	75	82	74	75	82	86	82
2	77	86	76	79	86	85	83
3	76	85	84	83	87	86	84

Conditions: 5 mM **1c** in CH_2Cl_2, Δ, 5 mol% [Ru].

Table A-18. Proportion of oligomeric species formed over time during the RCM of **1c** for each catalyst.

Time	% Oligomers						
(h)	**Ru-3**	**Ru-4a**	**Ru-4b**	**Ru-5a**	**Ru-5b**	**Ru-5c**	**Ru-6a**
0	0	0	0	0	0	0	0
0.25	22	39	53	50	59	46	39
0.5	21	26	36	62	34	21	13
0.75	20	22	32	60	23	16	14
1	19	18	28	59	19	15	13
1.5	20	14	24	58	18	14	14
2	20	11	22	58	14	15	13
3	20	11	23	56	13	14	12

Conditions: 5 mM **1c** in CH_2Cl_2, Δ, 5 mol% [Ru].

Table A-19. Consumption of diene **3b** over time for each catalyst.

Time	% **3b**						
(h)	**Ru-3**	**Ru-4a**	**Ru-4b**	**Ru-5a**	**Ru-5b**	**Ru-5c**	**Ru-6a**
0	100	100	100	100	100	100	100
0.25	39	60	3	88	98	79	32
0.5	22	26	0	76	84	30	20
0.75	14	7	0	62	68	18	15
1	9	1	0	49	58	13	10
1.5	2	0	0	27	36	8	7
2	0	0	0	7	5	5	3
3	0	0	0	0	0	0	0

Conditions: 0.5 mM **3b** in CH_2Cl_2, Δ, 5 mol% [Ru].

Table A-20. Yield of **4b** over time for each catalyst.

Time	% **4b**						
(h)	**Ru-3**	**Ru-4a**	**Ru-4b**	**Ru-5a**	**Ru-5b**	**Ru-5c**	**Ru-6a**
0	0	0	0	0	0	0	0
0.25	55	33	63	12	1	13	50
0.5	74	57	61	21	21	50	50
0.75	85	67	59	33	33	57	50
1	92	67	58	48	40	60	51
1.5	98	66	57	59	56	61	51
2	>99	63	57	60	67	61	52
3	>99	62	57	59	61	61	56

Conditions: 0.5 mM **3b** in CH_2Cl_2, Δ, 5 mol% [Ru].

Table A-21. Proportion of oligomeric species formed over time during the RCM of **3b** for each catalyst.

Time	% Oligomers						
(h)	**Ru-3**	**Ru-4a**	**Ru-4b**	**Ru-5a**	**Ru-5b**	**Ru-5c**	**Ru-6a**
0	0	0	0	0	0	0	0
0.25	6	7	35	0	0	8	19
0.5	4	17	39	3	0	19	21
0.75	1	26	41	5	0	26	35
1	0	32	43	7	2	28	38
1.5	0	34	43	14	7	32	42
2	0	37	43	31	28	33	44
3	0	39	43	41	39	38	44

Conditions: 0.5 mM **3b** in CH_2Cl_2, Δ, 5 mol% [Ru].

Table A-22. Consumption of diene **3a** over time for each catalyst.

Time	% **3a**						
(h)	**Ru-3**	**Ru-4a**	**Ru-4b**	**Ru-5a**	**Ru-5b**	**Ru-5c**	**Ru-6a**
0	100	100	100	100	100	100	100
0.25	82	88	43	94	91	81	66
0.5	72	0	0	59	33	20	41
0.75	69	0	0	29	26	12	20
1	67	0	0	15	22	4	14
1.5	61	0	0	8	13	1	9
2	61	0	0	6	4	0	3
3	60	0	0	0	0	0	0

Conditions: 0.5 mM **3a** in CH_2Cl_2, Δ, 5 mol% [Ru].

Table A-23. Yield of **4a** over time for each catalyst.

Time	% **4a**						
(h)	**Ru-3**	**Ru-4a**	**Ru-4b**	**Ru-5a**	**Ru-5b**	**Ru-5c**	**Ru-6a**
0	0	0	0	0	0	0	0
0.25	0	0	31	0	4	8	27
0.5	0	57	66	25	43	67	50
0.75	0	61	67	45	56	74	55
1	0	62	66	55	63	73	59
1.5	0	63	66	62	65	70	62
2	0	63	67	62	66	68	67
3	0	63	68	67	66	67	68

Conditions: 0.5 mM **3a** in CH_2Cl_2, Δ, 5 mol% [Ru].

Table A-24. Proportion of oligomeric species formed over time during the RCM of **3a** for each catalyst.

Time	% Oligomers						
(h)	**Ru-3**	**Ru-4a**	**Ru-4b**	**Ru-5a**	**Ru-5b**	**Ru-5c**	**Ru-6a**
0	0	0	0	0	0	0	0
0.25	18	12	26	6	4	11	7
0.5	28	22	32	16	24	13	9
0.75	31	25	33	26	19	14	24
1	33	23	33	30	15	23	27
1.5	39	22	33	30	21	29	29
2	39	23	36	32	30	32	29
3	40	24	36	33	34	33	32

Conditions: 0.5 mM **3a** in CH_2Cl_2, Δ, 5 mol% [Ru].

(d) Numerical data for Figure 10:

Table A-25. Yield of **2a** over time. Perturbation at 3 h.

Time	% **2a**		
(h)	(a)	(b)	(c)
0	0	0	0
0.75	6	7	6
1.5	42	47	44
2.25	47	49	49
3	49	52	54
3.25	-	19	75
3.5	-	39	85
3.75	-	-	92
4	54	48	96
4.5	-	52	-
5	53	53	96

Conditions: CH_2Cl_2, Δ, 5 mol% **Ru-4b**, (a) 5 mM **1a**, (b) 5 mM **1a** and addition of fresh **Ru-4b** at 3 h, and (c) 5 mM **1a** then dilution to 0.5 mM after 3 hour. Calibrated GC-FID analysis (±1% in replicate runs).

(e) Numerical data for Figure 12:

Table A-26. Z:E isomer ratio within **4b** over time.

Time	Z:E ratio						
(h)	**Ru-3**	**Ru-4a**	**Ru-4b**	**Ru-5a**	**Ru-5b**	**Ru-5c**	**Ru-6a**
0	-	-	-	-	-	-	-
0.25	3	22	20	20	19	25	21
0.5	3	21	20	22	23	24	22
0.75	3	21	21	21	21	23	21
1	3	22	21	22	21	22	22
1.5	3	22	21	22	21	22	-
2	4	21	21	21	21	22	-
3	4	21	21	21	21	22	21

Conditions: 0.5 mM **3b** in CH_2Cl_2, Δ, 5 mol% [Ru]. Calibrated GC-FID analysis (±1% in replicate runs).

(f) Numerical data for Figure 15:

Table A-27. Yield of **4b** from $[\mathbf{4b}]_2$ over time.

Time (h)	% **4b**			
	Ru-3	**Ru-4b**	**Ru-5b**	**Ru-5c**
0	0	0	0	0
0.25	0	45	18	27
0.5	0	52	20	34
0.75	0	52	-	38
1	0	53	23	41
1.5	0	52	-	-
2	0	52	-	48
3	0	52	31	51
8	-	-	-	55
18	-	-	55	-

Conditions: 0.5 mM $[\mathbf{4b}]_2$ in CH_2Cl_2, Δ, 5 mol% [Ru]. Calibrated GC-FID analysis (±1% in replicate runs).

Chapter 4.

Table A-28. Conversion of **Ru-6a** to **Ru-9a** using **40**.[a]

Time (h)	C_6D_6			THF		
	% **Ru-6a**	% **Ru-9a**	% decomp.[b]	% **Ru-6a**	% **Ru-9a**	% decomp.[b]
0	100	0	0	100	0	0
2	99	1	0	75	25	0
6	90	5	5	59	38	3
12	74	11	15	39	41	20
24	54	21	25	28	43	29

[a] Determined by ^{1}H NMR spectroscopy using 1,3,5-trimethoxybenzene as internal standard (±2% in replicate runs). [b] Determined by difference.

Table A-29. Numerical data for Figure 12 of Chapter 4.

Substrate / Catalyst	**Ru-8a**	**Ru-9a**	**Ru-8b**	**Ru-8c**	**Ru-9b**	**Ru-9c**	**Ru-9d**
9a	100	92	78	93	68	71	65
11a	100	100	100	100	76	34	26
13	100	100	96	76	23	15	25
15	100	100	100	100	56	32	28
17	100	100	100	80	15	20	17
7	43	20	12	8	5	4	1
19	6	2	0	1	6	4	2

Conditions: 50 mM diene in CH_2Cl_2, Δ, 3 h, 0.5 mol% [Ru]. Calibrated GC-FID analysis (±3% in replicate runs).

Table A-30. Conversion profiles for the RCM of **11a** catalyzed by **Ru-8/9**.

Time (h)	**Ru-8a**	**Ru-9a**	**Ru-8b**	**Ru-8c**	**Ru-9b**	**Ru-9c**	**Ru-9d**
0	0	0	0	0	0	0	0
0.25	7	2	2	1	1	0	0
0.5	18	7	4	3	4	0	0
0.75	29	11	8	5	5	0	0
1	37	17	13	7	5	0	0
1.5	48	23	16	9	5	0	0
2	56	27	19	12	5	0	0
3	68	33	23	15	5	2	0
5	78	41	24	17	6	3	0

Conditions: 5 mM **11a** in C_7H_8, 60 °C, 0.5 mol% [Ru]. Calibrated GC-FID analysis (±3% in replicate runs).

Table A-31. Conversion profiles for the RCM of **9a** catalyzed by **Ru-8/9**.

Time (h)	**Ru-8a**	**Ru-9a**	**Ru-8b**	**Ru-8c**	**Ru-9b**	**Ru-9c**	**Ru-9d**
0	0	0	0	0	0	0	0
0.25	5	3	2	2	1	0	0
0.5	15	6	4	3	1	1	0
0.75	23	12	6	4	1	2	0
1	30	16	8	5	2	2	1
1.5	37	20	12	7	2	3	1
2	40	23	16	9	4	3	1
3	47	26	17	9	4	3	1
5	50	27	18	10	5	3	1

Conditions: 5 mM **9a** in C_7H_8, 60 °C, 0.5 mol% [Ru]. Calibrated GC-FID analysis (±3% in replicate runs).

Table A-32. Conversion profiles for the ROMP of **21** catalyzed by **Ru-8/9** and **Ru-6a.**

Time (h)	**Ru-6a**	**Ru-8a**	**Ru-9a**	**Ru-8b**	**Ru-8c**	**Ru-9b**	**Ru-9c**	**Ru-9d**
0	0	0	0	0	0	0	0	0
0.08	93	30	16	-	-	7	-	-
0.16	100	55	30	-	-	12	-	-
0.33	100	70	47	23	17	21	-	-
0.5		80	60	47	38	30	-	-
0.66		86	77	-	-	38	-	-
0.83		92	78	-	-	47	-	-
1		96	83	69	61	55	4	0.4
1.33		100	91	79	75	69	-	-
1.66		100	95	-	85	79	-	-
2			98	92	91	85	-	-
3			100	97	97	96	10	1.1
4			100	100	99	99	-	-
5				100	100	100	16	-
6					100	100	-	6
7							22	-
9							35	16
15							96	80
17							100	-
19							100	100

Conditions: 100 mM **9a** in $CDCl_3$, 23 °C, 1 mol% [Ru]. ^1H NMR analysis (±1% in replicate runs).

Chapter 5.

Table A-33. Conversion for the ROMP of **21** or RCM of **9a/11a** catalyzed by **Ru-6a** and **Ru-12**.

Substrate / Catalyst	**Ru-6a**	**Ru-12a**	**Ru-12b**
9a	100	3	100
11a	100	0	100
21	100	20	100

Conditions: **21**: 100 mM in CH_2Cl_2, 24 °C, 1 mol% [Ru]; conversion to product at 5 min for **Ru-6a** and **Ru-12b**; at 24 h for **Ru-12a**. **9a/11a**: 100 mM in CH_2Cl_2, Δ, 0.5 mol% [Ru]; conversion to product at 15 min. ^{1}H NMR or calibrated GC-FID analysis (±1% in replicate runs).

Table A-34. Yield of **12a** over time obtained with **Ru-4b**, **Ru-6a** and **Ru-12b**.

Time (min)	**12a**		
	Ru-4b	**Ru-6a**	**Ru-12b**
0	0	0	0
5	6	51	12
10	11	64	24
15	16	71	34
20	21	76	41
30	29	81	54
45	39	85	66
60	47	86	70
90	58	86	75
180	71	87	75

Conditions: 5 mM **11a** in CH_2Cl_2, 24 °C, 1 mol% [Ru]. Calibrated GC-FID quantification (±1% in replicate runs).

Table A-35. Consumption of **1b** over time by **Ru-6a** and **Ru-12b**.

Time (min)	20 °C		Time (h)	Δ	
	Ru-6a	**Ru-12b**		**Ru-6a**	**Ru-12b**
0	100	100	0	100	100
2	90	-	0.25	18	69
5	86	-	0.5	4	48
15	77	93	0.75	0	-
30	69	91	1	0	40
45	65	90	1.5	0	-
60	62	89	2	0	36
			3	0	-

Conditions: 5 mM **1b** in CH_2Cl_2, 20 °C or Δ, 5 mol% [Ru]. Calibrated GC-FID quantification (±1% in replicate runs).

Table A-36. Yield of **2b** over time obtained with **Ru-6a** and **Ru-12b**.

Time (min)	20 °C		Time (h)	Δ	
	Ru-6a	**Ru-12b**		**Ru-6a**	**Ru-12b**
0	0	0	0	0	0
2	3	-	0.25	23	26
5	7	-	0.5	84	49
15	16	0	0.75	89	-
30	24	1	1	96	56
45	29	2	1.5	97	-
60	32	5	2	>99	60
			3	>99	-

Conditions: 5 mM **1b** in CH_2Cl_2, 20 °C or Δ, 5 mol% [Ru]. Calibrated GC-FID quantification (±1% in replicate runs).

Table A-37. Proportion of oligomers formed over time during RCM **1b** by **Ru-6a** and **Ru-12b**.

Time (min)	20 °C		Time (h)	Δ	
	Ru-6a	**Ru-12b**		**Ru-6a**	**Ru-12b**
0	0	0	0	0	0
2	7	-	0.25	60	5
5	7	-	0.5	13	3
15	7	7	0.75	11	-
30	7	7	1	4	4
45	7	8	1.5	3	-
60	6	6	2	0	4
			3	0	-

Conditions: 5 mM **1b** in CH_2Cl_2, 20 °C or Δ, 5 mol% [Ru]. Calibrated GC-FID quantification (±1% in replicate runs).

Chapter 6.

Table A-38. Conversion of **1b** and yield of **2b** over time in the BR and PFR.

Time (min)	Conv. (%) BR	Yield **2b** (%)	Time (min)	Conv. (%) PFR	Yield **2b** (%)
0	0	0	0	0	0
1	38	38	0.2	6	6
2	71	71	0.4	10	10
4	81	81	0.7	22	22
6	82	82	1.5	44	44
8	83	83	2.2	59	59
10	83	83	3.7	71	71
15	83	83	5.2	74	74
20	84	84	7.4	76	76
-	-	-	11	79	79
-	-	-	15	79	79
-	-	-	20	79	79

Conditions: 5 mM **1b** in C_7H_8, 60 °C, 5 mol% **Ru-4b**. Calibrated GC-FID quantification (±2% in replicate runs). Quantitative selectivity for **2b**. (-) Indicates no further measurements.

Table A-39. Conversion, selectivity and yield of **2b** over time at 40 °C.

Time (min)	Conversion (%)	Selectivity (%)	Yield **2b** (%)
0	0	0	0
0.2	2	34	1
0.4	3	33	1
0.7	3	31	1
1.5	4	31	1
2.2	4	33	1
3.7	6	33	2
5.2	8	32	3
11	16	36	6
20	23	42	10
29	31	55	17

Conditions: PFR, 5 mM **1b** in C_7H_8, 5 mol% **Ru-4b**. Calibrated GC-FID quantification (±2% in replicate runs).

Table A-40. Conversion of **1b**, selectivity and yield of **2b** over time at 60 °C.

Time (min)	Conversion (%)	Selectivity (%)	Yield **2b** (%)
0	0	0	0
0.2	6	93	6
0.4	10	92	9
0.7	22	89	20
1.5	44	89	39
2.2	59	96	57
3.7	71	>99	71
5.2	74	>99	74
7.4	76	>99	76
11	79	>99	79
15	79	>99	79
20	79	>99	79

Conditions: PFR, 5 mM **1b** in C_7H_8, 5 mol% **Ru-4b**. Calibrated GC-FID quantification (±2% in replicate runs).

Table A-41. Conversion of **1b**, selectivity and yield of **2b** over time at 80 °C.

Time (min)	Conversion (%)	Selectivity (%)	Yield **2b** (%)
0	0	0	0
0.1	39	79	31
0.2	70	84	59
0.4	78	96	75
0.7	81	95	77
1.5	82	>99	82
2.2	82	>99	82
3.7	82	>99	82
5.2	82	>99	82
7.4	82	>99	82
11	82	>99	82
15	82	>99	82
45	82	>99	82

Conditions: PFR, 5 mM **1b** in C_7H_8, 5 mol% **Ru-4b**. Calibrated GC-FID quantification (±2% in replicate runs).

Table A-42. Conversion of **1b** over time as a function of catalyst loading.

Time (min)	10 mol%	5 mol%	1 mol%
0	0	0	0
0.03	8	-	-
0.09	42	39	1
0.2	72	70	7
0.4	82	78	19
0.7	85	81	41
1.5	-	82	-
2.1	87	-	-
2.2	-	82	61
3.5	89	-	-
3.7	-	82	62
5.2	-	82	65
7	91	-	-
7.4	-	82	-
8	-	-	-
11	-	82	69
13	93	-	-
15	-	83	-
20	94	-	-
29	94	-	70
43	-	-	-
45	94	83	-
58	-	-	70

Conditions: PFR, 5 mM **1b** in C_7H_8, 80 °C. Calibrated GC-FID quantification (±3% in replicate runs). (-) Indicates that no sample was withdrawn at this residence time.

Table A-43. Selectivity for **2b** over time as a function of catalyst loading.

Time (min)	10 mol%	5 mol%	1 mol%
0	0	0	0
0.03	70	-	-
0.09	80	79	>99
0.2	81	84	>99
0.4	76	96	>99
0.7	95	95	>99
1.5	-	>99	-
2.1	93	-	-
2.2	-	>99	>99
3.5	91	-	-
3.7	-	>99	>99
5.2	-	>99	>99
7	89	-	-
7.4	-	>99	-
8	-	-	-
11	-	>99	>99
13	87	-	-
15	-	>99	-
20	86	-	-
29	86	-	>99
43	-	-	-
45	86	>99	-
58	-	-	>99

Conditions: PFR, 5 mM **1b** in C_7H_8, 80 °C. Calibrated GC-FID quantification (±3% in replicate runs). (-) Indicates that no sample was withdrawn at this residence time.

Table A-44. Yield of **2b** over time as a function of catalyst loading.

Time (min)	10 mol%	5 mol%	1 mol%
0	0	0	0
0.03	6	-	-
0.09	34	31	1
0.2	58	59	7
0.4	62	75	19
0.7	81	77	41
1.5	-	82	-
2.1	81	-	-
2.2	-	82	61
3.5	81	-	-
3.7	-	82	62
5.2	-	82	65
7	81	-	-
7.4	-	82	-
8	-	-	-
11	-	82	70
13	81	-	-
15	-	82	-
20	81	-	-
29	81	-	70
43	-	-	-
45	81	82	-
58	-	-	70

Conditions: PFR, 5 mM **1b** in C_7H_8, 80 °C. Calibrated GC-FID quantification (±3% in replicate runs). (-) Indicates that no sample was withdrawn at this residence time.

Table A-45. Conversion of **1b** over time as a function of the concentration of **1b**.

Time (min)	5 mM	10 mM	20 mM
0	0	0	0
0.1	1	5	21
0.2	7	10	29
0.4	19	25	43
0.7	41	44	60
1.5	-	58	70
2.1	-	72	84
2.2	61	-	-
3.5	-	73	-
3.7	62	-	83
5.2	65	-	84
5.5	-	71	-
7.4	-	-	84
11	70	-	-
13	-	72	-
15	-	-	82
20	-	73	-
29	70	73	84
58	70	72	84

Conditions: PFR, C_7H_8, 80 °C, 1 mol% **Ru-4b**. Calibrated GC-FID quantification (±2% in replicate runs). (-) Indicates that no sample was withdrawn at this residence time.

Table A-46. Selectivity for **2b** over time as a function of the concentration of **1b**.

Time (min)	5 mM	10 mM	20 mM
0	0	0	0
0.1	>99	>99	51
0.2	>99	>99	55
0.4	>99	93	61
0.7	>99	90	62
1.5	-	87	59
2.1	-	79	51
2.2	>99	-	-
3.5	-	78	-
3.7	>99	-	52
5.2	>99	-	51
5.5	-	79	-
7.4	-	-	53
11	>99	-	-
13	-	79	-
15	-	-	51
20	-	79	-
29	>99	79	51
58	>99	79	51

Conditions: PFR, C_7H_8, 80 °C, 1 mol% **Ru-4b**. Calibrated GC-FID quantification (±2% in replicate runs). (-) Indicates that no sample was withdrawn at this residence time.

Table A-47. Yield of **2b** over time as a function of the concentration of **1b**.

Time (min)	5 mM	10 mM	20 mM
0	0	0	0
0.1	1	5	11
0.2	7	10	16
0.4	19	23	26
0.7	41	40	43
1.5	-	50	43
2.1	-	57	43
2.2	61	-	-
3.5	-	57	-
3.7	62	-	44
5.2	65	-	43
5.5	-	56	-
7.4	-	-	43
11	70	-	-
13	-	57	-
15	-	-	43
20	-	58	-
29	70	57	43
58	70	57	44

Conditions: PFR, C_7H_8, 80 °C, 1 mol% **Ru-4b**. Calibrated GC-FID quantification (±2% in replicate runs). (-) Indicates that no sample was withdrawn at this residence time.

Table A-48. Conversion of **1b**, selectivity and yield of **2b** over time using the PFR and the CSTR.

PFR				CSTR			
Time (min)	Conv. (%)	Sel. (%)	Yield (%)	Time (min)	Conv. (%)	Sel. (%)	Yield (%)
0	0	0	0	0	0	0	
0.1	1	79	1	0.5	10	>99	10
0.2	7	84	6	1	30	>99	30
0.4	19	96	18	5	77	>99	77
0.7	41	95	39	15	94	>99	94
2.2	61	96	59	20	>99	>99	>99
3.7	62	97	60	30	>99	>99	>99
5.2	65	>99	65	-	-	-	-
11	70	>99	70	-	-	-	-
29	70	>99	70	-	-	-	-

Conditions: 5 mM **1b** in C_7H_8, 80 °C, 1 mol% **Ru-4b**. Calibrated GC-FID quantification (±2% in replicate runs). (-) Indicates no further measurements.

Table A-49. Conversion of **1b**, selectivity and yield of **2b** as a function of diene concentration using the CSTR.

5 mM **1b**				20 mM **1b**			
Time (min)	Conv. (%)	Sel. (%)	Yield (%)	Time (min)	Conv. (%)	Sel. (%)	Yield (%)
0	0	0		0	0	0	0
0.5	10	>99	10	0.5	32	64	20
1	30	>99	30	1	65	61	40
5	77	>99	77	5	92	61	56
15	94	>99	94	10	>99	65	65
20	>99	>99	>99	15	>99	65	65
30	>99	>99	>99	30	>99	65	65

Conditions: CSTR, C_7H_8, 80°C, 1 mol% **Ru-4b**. Calibrated GC-FID quantification (±2% in replicate runs).

Appendix B. Crystallographic data

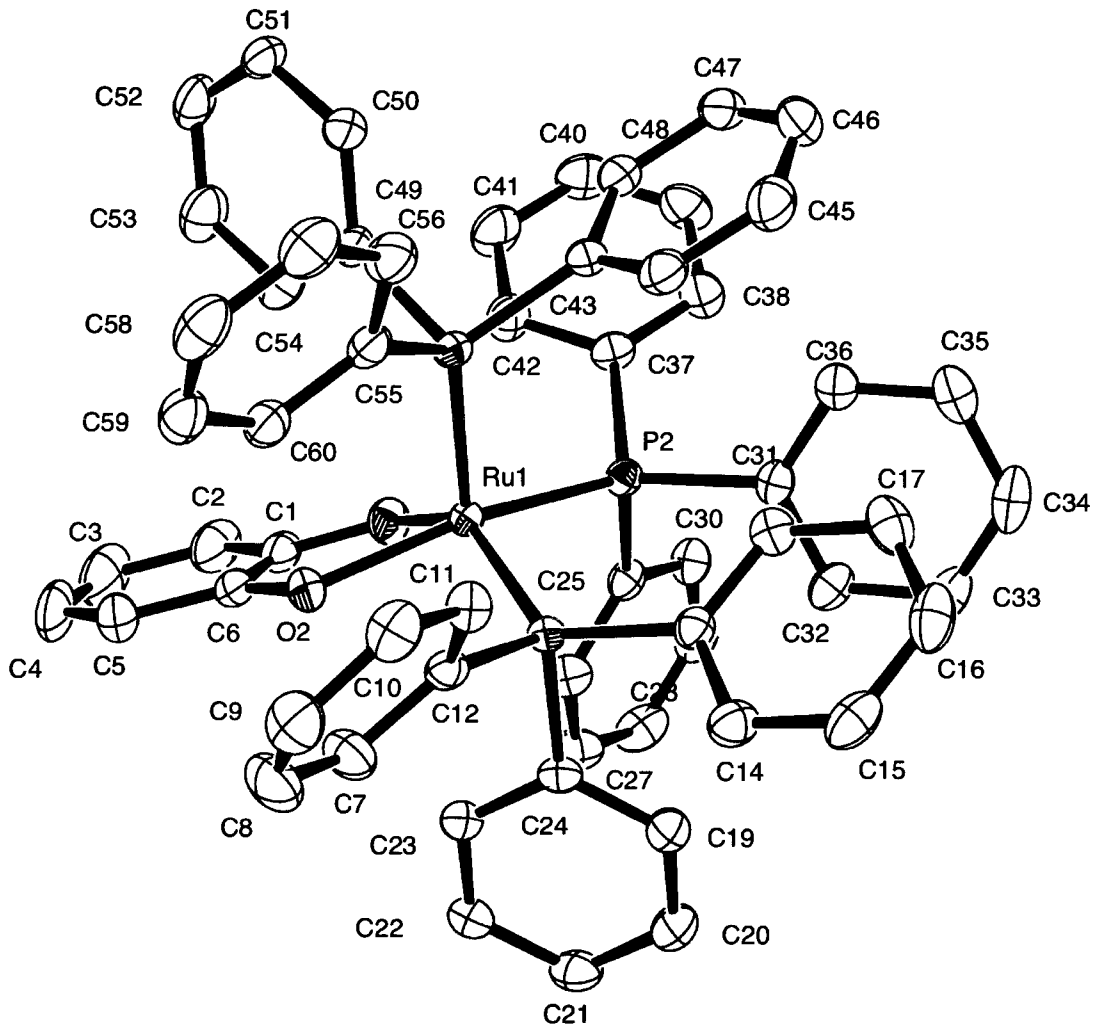

Figure A-1. ORTEP representation of **Ru-2a**. Thermal ellipsoids are shown at 30% probability. Hydrogen atoms and benzene solvate are omitted for clarity.

Table A-50. Crystal data and structure refinement for **Ru-2a**.

CCDC #	689209	
Formula	$C_{66}H_{55}O_2P_3Ru$	
Formula weight	1074.08	
Size	0.6 × 0.44 × 0.42 mm	
Crystal morphology	Blue Block	
Temperature	173(2) K	
Wavelength	0.71073 Å	
Crystal system	Monoclinic	
Space group	$P2_1/c$	
Unit cell dimensions	a = 13.3727(13) Å	$\alpha = 90°$
	b = 17.1572(18) Å	$\beta = 94.653(3)°$
	c = 23.022(2) Å	$\gamma = 90°$
Volume	5264.7(9) Å^3	
Z	4	
Density (calculated)	1.355 mg/m^3	
Absorption coefficient	0.435 mm^{-1}	
F(000)	2224	
Data collection range	$1.48 \le \theta \le 27.07°$	
Index ranges	$-17 \le h \le 12$, $-17 \le k \le 21$, $-22 \le l \le 28$	
Reflections collected	21831	
Independent reflections	10952 [R(int) = 0.0224]	
Observed reflections	9287 [$I > 2\sigma(I)$]	
Absorption correction	multi-scan	
Max. and min. transmission	0.8383 and 0.7802	
Refinement method	Full	
Data / restraints / parameters	10952 / 0 / 649	
Goodness of fit	1.032	
Final R indices [$I > 2\sigma(I)$]	R_1 = 0.0286, wR_2 = 0.0716	
R indices (all data)	R_1 = 0.0375, wR_2 = 0.075	
Largest diff. peak and hole	0.558 and -0.279 e Å^{-3}	

Table A-51. Interatomic distances (Å) with s.u.s in parentheses.

Ru(1)-O(1)	2.0294(12)	Ru(1)-O(2)	2.0698(13)
Ru(1)-P(3)	2.2527(5)	Ru(1)-P(1)	2.2954(5)
Ru(1)-P(2)	2.3496(5)	P(1)-C(13)	1.8402(18)
P(1)-C(24)	1.8477(18)	P(1)-C(12)	1.8524(19)
P(2)-C(31)	1.8393(18)	P(2)-C(25)	1.8533(18)
P(2)-C(37)	1.8557(17)	P(3)-C(43)	1.8422(18)
P(3)-C(55)	1.8550(19)	P(3)-C(49)	1.8563(18)
O(1)-C(1)	1.350(2)	O(2)-C(6)	1.345(2)
C(1)-C(2)	1.397(3)	C(1)-C(6)	1.406(3)
C(2)-C(3)	1.387(4)	C(3)-C(4)	1.372(4)
C(4)-C(5)	1.407(4)	C(5)-C(6)	1.397(3)
C(7)-C(12)	1.391(3)	C(7)-C(8)	1.393(3)
C(8)-C(9)	1.383(3)	C(9)-C(10)	1.381(3)
C(10)-C(11)	1.389(3)	C(11)-C(12)	1.393(2)
C(13)-C(18)	1.384(2)	C(13)-C(14)	1.405(2)
C(14)-C(15)	1.387(3)	C(15)-C(16)	1.390(3)
C(16)-C(17)	1.369(3)	C(17)-C(18)	1.396(3)
C(19)-C(20)	1.386(3)	C(19)-C(24)	1.399(3)
C(20)-C(21)	1.387(3)	C(21)-C(22)	1.388(3)
C(22)-C(23)	1.388(3)	C(23)-C(24)	1.405(2)
C(25)-C(26)	1.393(3)	C(25)-C(30)	1.398(3)
C(26)-C(27)	1.387(3)	C(27)-C(28)	1.385(3)
C(28)-C(29)	1.387(3)	C(29)-C(30)	1.387(3)
C(31)-C(36)	1.400(3)	C(31)-C(32)	1.404(3)
C(32)-C(33)	1.396(3)	C(33)-C(34)	1.384(3)
C(34)-C(35)	1.383(3)	C(35)-C(36)	1.395(3)
C(37)-C(38)	1.391(3)	C(37)-C(42)	1.394(3)
C(38)-C(39)	1.397(3)	C(39)-C(40)	1.379(3)
C(40)-C(41)	1.381(3)	C(41)-C(42)	1.390(3)
C(43)-C(44)	1.401(3)	C(43)-C(48)	1.403(3)
C(44)-C(45)	1.393(3)	C(45)-C(46)	1.387(3)
C(46)-C(47)	1.389(3)	C(47)-C(48)	1.394(3)
C(49)-C(54)	1.389(3)	C(49)-C(50)	1.399(3)
C(50)-C(51)	1.391(3)	C(51)-C(52)	1.383(3)
C(52)-C(53)	1.377(3)	C(53)-C(54)	1.396(3)
C(55)-C(56)	1.398(3)	C(55)-C(60)	1.401(3)
C(56)-C(57)	1.390(3)	C(57)-C(58)	1.381(3)
C(58)-C(59)	1.381(3)	C(59)-C(60)	1.393(3)
C(61)-C(66)	1.376(4)	C(61)-C(62)	1.381(4)
C(62)-C(63)	1.384(3)	C(63)-C(64)	1.371(3)
C(64)-C(65)	1.385(3)	C(65)-C(66)	1.377(3)

Table A-52. Angles (°) between interatomic vectors with s.u.s in parentheses.

O(1)-Ru(1)-O(2)	79.40(5)	O(1)-Ru(1)-P(3)	116.13(4)
O(2)-Ru(1)-P(3)	98.45(4)	O(1)-Ru(1)-P(1)	144.61(4)
O(2)-Ru(1)-P(1)	86.17(4)	P(3)-Ru(1)-P(1)	97.766(17)
O(1)-Ru(1)-P(2)	82.23(4)	O(2)-Ru(1)-P(2)	158.53(4)
P(3)-Ru(1)-P(2)	99.561(17)	P(1)-Ru(1)-P(2)	102.819(17)
C(13)-P(1)-C(24)	101.09(8)	C(13)-P(1)-C(12)	97.63(8)
C(24)-P(1)-C(12)	104.31(8)	C(13)-P(1)-Ru(1)	131.93(6)
C(24)-P(1)-Ru(1)	101.99(6)	C(12)-P(1)-Ru(1)	116.37(6)
C(31)-P(2)-C(25)	98.90(8)	C(31)-P(2)-C(37)	104.04(8)
C(25)-P(2)-C(37)	100.07(8)	C(31)-P(2)-Ru(1)	125.29(6)
C(25)-P(2)-Ru(1)	108.18(6)	C(37)-P(2)-Ru(1)	116.24(6)
C(43)-P(3)-C(55)	104.25(9)	C(43)-P(3)-C(49)	101.77(8)
C(55)-P(3)-C(49)	95.25(8)	C(43)-P(3)-Ru(1)	120.99(6)
C(55)-P(3)-Ru(1)	117.96(6)	C(49)-P(3)-Ru(1)	112.57(6)
C(1)-O(1)-Ru(1)	114.07(12)	C(6)-O(2)-Ru(1)	112.44(12)
O(1)-C(1)-C(2)	122.6(2)	O(1)-C(1)-C(6)	116.37(16)
C(2)-C(1)-C(6)	121.0(2)	C(3)-C(2)-C(1)	119.2(3)
C(4)-C(3)-C(2)	120.2(2)	C(3)-C(4)-C(5)	121.7(2)
C(6)-C(5)-C(4)	118.5(3)	O(2)-C(6)-C(5)	123.5(2)
O(2)-C(6)-C(1)	117.12(17)	C(5)-C(6)-C(1)	119.4(2)
C(12)-C(7)-C(8)	120.56(19)	C(9)-C(8)-C(7)	120.6(2)
C(10)-C(9)-C(8)	119.46(19)	C(9)-C(10)-C(11)	119.95(19)
C(10)-C(11)-C(12)	121.36(18)	C(7)-C(12)-C(11)	118.05(18)
C(7)-C(12)-P(1)	124.29(14)	C(11)-C(12)-P(1)	117.66(13)
C(18)-C(13)-C(14)	118.70(17)	C(18)-C(13)-P(1)	120.71(13)
C(14)-C(13)-P(1)	120.59(14)	C(15)-C(14)-C(13)	120.24(18)
C(14)-C(15)-C(16)	120.07(19)	C(17)-C(16)-C(15)	120.07(18)
C(16)-C(17)-C(18)	120.24(19)	C(13)-C(18)-C(17)	120.65(18)
C(20)-C(19)-C(24)	120.76(17)	C(19)-C(20)-C(21)	120.63(19)
C(20)-C(21)-C(22)	119.49(18)	C(23)-C(22)-C(21)	120.12(17)
C(22)-C(23)-C(24)	120.96(17)	C(19)-C(24)-C(23)	117.99(16)
C(19)-C(24)-P(1)	122.22(13)	C(23)-C(24)-P(1)	119.56(14)
C(26)-C(25)-C(30)	118.56(17)	C(26)-C(25)-P(2)	121.21(14)
C(30)-C(25)-P(2)	120.17(14)	C(27)-C(26)-C(25)	120.78(19)
C(28)-C(27)-C(26)	120.2(2)	C(27)-C(28)-C(29)	119.69(19)
C(30)-C(29)-C(28)	120.24(19)	C(29)-C(30)-C(25)	120.55(19)
C(36)-C(31)-C(32)	118.37(17)	C(36)-C(31)-P(2)	122.68(14)
C(32)-C(31)-P(2)	118.83(14)	C(33)-C(32)-C(31)	120.39(19)
C(34)-C(33)-C(32)	120.4(2)	C(35)-C(34)-C(33)	119.80(19)
C(34)-C(35)-C(36)	120.36(19)	C(35)-C(36)-C(31)	120.61(19)
C(38)-C(37)-C(42)	118.27(16)	C(38)-C(37)-P(2)	124.39(14)
C(42)-C(37)-P(2)	117.26(14)	C(37)-C(38)-C(39)	120.88(19)
C(40)-C(39)-C(38)	120.1(2)	C(39)-C(40)-C(41)	119.55(18)

Table A-52. (continued)

C(40)-C(41)-C(42)	120.6(2)	C(41)-C(42)-C(37)	120.59(19)
C(44)-C(43)-C(48)	118.30(17)	C(44)-C(43)-P(3)	120.80(14)
C(48)-C(43)-P(3)	120.85(14)	C(45)-C(44)-C(43)	120.93(19)
C(46)-C(45)-C(44)	120.0(2)	C(45)-C(46)-C(47)	119.99(19)
C(46)-C(47)-C(48)	120.14(19)	C(47)-C(48)-C(43)	120.66(18)
C(54)-C(49)-C(50)	118.59(17)	C(54)-C(49)-P(3)	120.65(14)
C(50)-C(49)-P(3)	120.39(14)	C(51)-C(50)-C(49)	120.4(2)
C(52)-C(51)-C(50)	120.1(2)	C(53)-C(52)-C(51)	120.18(19)
C(52)-C(53)-C(54)	119.9(2)	C(49)-C(54)-C(53)	120.81(19)
C(56)-C(55)-C(60)	118.00(18)	C(56)-C(55)-P(3)	123.56(15)
C(60)-C(55)-P(3)	117.90(14)	C(57)-C(56)-C(55)	120.83(19)
C(58)-C(57)-C(56)	120.6(2)	C(59)-C(58)-C(57)	119.3(2)
C(58)-C(59)-C(60)	120.7(2)	C(59)-C(60)-C(55)	120.54(19)
C(66)-C(61)-C(62)	120.4(2)	C(61)-C(62)-C(63)	119.7(2)
C(64)-C(63)-C(62)	119.9(2)	C(63)-C(64)-C(65)	120.3(2)
C(66)-C(65)-C(64)	119.9(2)	C(61)-C(66)-C(65)	119.7(2)

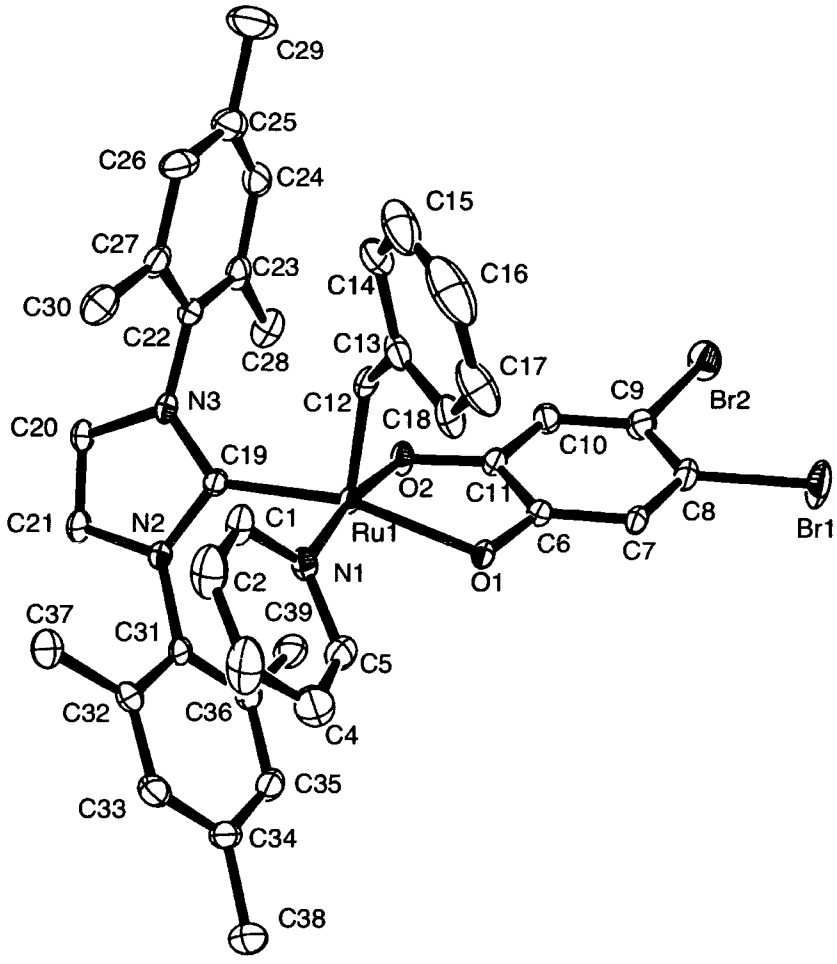

Figure A-2. ORTEP representation of **Ru-8c**. Thermal ellipsoids are shown at 30% probability. Hydrogen atoms are omitted for clarity.

Table A-53. Crystal data and structure refinement for **Ru-8c**.

Formula	$C_{39}H_{37}Br_2N_3O_2Ru$	
Formula weight	840.61	
Size	0.4 × 0.25 × 0.1 mm	
Crystal morphology	Orange Prism	
Temperature	173(2) K	
Wavelength	0.71073 Å	
Crystal system	Orthorhombic	
Space group	*Pbca*	
Unit cell dimensions	a = 15.957(6) Å	$\alpha = 90°$
	b = 16.591(4) Å	$\beta = 90°$
	c = 27.041(7) Å	$\gamma = 90°$
Volume	7159(4) Å^3	
Z	8	
Density (calculated)	1.56 mg/m^3	
Absorption coefficient	2.708 mm^{-1}	
F(000)	3376	
Data collection range	$1.92 \le \theta \le 27.09°$	
Index ranges	$-20 \le h \le 20$, $-20 \le k \le 21$, $-34 \le l \le 31$	
Reflections collected	46173	
Independent reflections	7861 [R(int) = 0.0694]	
Observed reflections	5589 [$I > 2\sigma(I)$]	
Absorption correction	multi-scan	
Max. and min. transmission	0.7734 and 0.4105	
Refinement method	Full	
Data / restraints / parameters	7861 / 0 / 430	
Goodness of fit	1.124	
Final R indices [$I > 2\sigma(I)$]	R_1 = 0.0619, wR_2 = 0.1387	
R indices (all data)	R_1 = 0.0966, wR_2 = 0.1538	
Largest diff. peak and hole	1.043 and -1.737 e Å^{-3}	

Table A-54. Interatomic distances (Å) with s.u.s in parentheses.

Ru(1)-C(12)	1.819(7)	Ru(1)-O(1)	2.033(4)
Ru(1)-O(2)	2.038(4)	Ru(1)-C(19)	2.045(5)
Ru(1)-N(1)	2.081(5)	Br(1)-C(8)	1.902(6)
Br(2)-C(9)	1.892(6)	O(1)-C(6)	1.341(7)
O(2)-C(11)	1.337(7)	N(1)-C(1)	1.338(8)
N(1)-C(5)	1.354(8)	N(2)-C(19)	1.356(7)
N(2)-C(21)	1.401(7)	N(2)-C(31)	1.446(8)
N(3)-C(19)	1.363(7)	N(3)-C(20)	1.400(7)
N(3)-C(22)	1.444(8)	C(1)-C(2)	1.365(10)
C(2)-C(3)	1.363(12)	C(3)-C(4)	1.380(13)
C(4)-C(5)	1.372(10)	C(6)-C(7)	1.394(7)
C(6)-C(11)	1.423(8)	C(7)-C(8)	1.396(9)
C(8)-C(9)	1.377(9)	C(9)-C(10)	1.400(8)
C(10)-C(11)	1.391(9)	C(12)-C(13)	1.468(10)
C(13)-C(14)	1.393(10)	C(13)-C(18)	1.401(10)
C(14)-C(15)	1.387(13)	C(15)-C(16)	1.351(16)
C(16)-C(17)	1.388(16)	C(17)-C(18)	1.376(11)
C(20)-C(21)	1.325(9)	C(22)-C(23)	1.383(9)
C(22)-C(27)	1.399(9)	C(23)-C(24)	1.396(10)
C(23)-C(28)	1.510(10)	C(24)-C(25)	1.367(11)
C(25)-C(26)	1.391(11)	C(25)-C(29)	1.508(11)
C(26)-C(27)	1.403(10)	C(27)-C(30)	1.490(10)
C(31)-C(32)	1.389(9)	C(31)-C(36)	1.398(8)
C(32)-C(33)	1.397(9)	C(32)-C(37)	1.509(9)
C(33)-C(34)	1.376(10)	C(34)-C(35)	1.379(10)
C(34)-C(38)	1.514(9)	C(35)-C(36)	1.392(9)
C(36)-C(39)	1.506(10)		

Table A-55. Angles (°) between interatomic vectors with s.u.s in parentheses.

C(12)-Ru(1)-O(1)	101.1(2)	C(12)-Ru(1)-O(2)	90.2(3)
O(1)-Ru(1)-O(2)	81.32(16)	C(12)-Ru(1)-C(19)	97.2(2)
O(1)-Ru(1)-C(19)	160.4(2)	O(2)-Ru(1)-C(19)	91.8(2)
C(12)-Ru(1)-N(1)	96.0(3)	O(1)-Ru(1)-N(1)	91.91(17)
O(2)-Ru(1)-N(1)	171.56(18)	C(19)-Ru(1)-N(1)	93.0(2)
C(6)-O(1)-Ru(1)	109.9(3)	C(11)-O(2)-Ru(1)	109.9(4)
C(1)-N(1)-C(5)	117.0(6)	C(1)-N(1)-Ru(1)	124.6(4)
C(5)-N(1)-Ru(1)	118.4(4)	C(19)-N(2)-C(21)	111.2(5)
C(19)-N(2)-C(31)	124.9(5)	C(21)-N(2)-C(31)	123.8(5)
C(19)-N(3)-C(20)	110.8(5)	C(19)-N(3)-C(22)	127.8(5)
C(20)-N(3)-C(22)	121.3(5)	N(1)-C(1)-C(2)	122.6(7)
C(3)-C(2)-C(1)	120.4(8)	C(2)-C(3)-C(4)	118.0(8)
C(5)-C(4)-C(3)	119.2(8)	N(1)-C(5)-C(4)	122.7(7)
O(1)-C(6)-C(7)	123.5(5)	O(1)-C(6)-C(11)	117.4(5)
C(7)-C(6)-C(11)	119.2(6)	C(6)-C(7)-C(8)	119.7(5)
C(9)-C(8)-C(7)	121.3(5)	C(9)-C(8)-Br(1)	121.4(5)
C(7)-C(8)-Br(1)	117.2(5)	C(8)-C(9)-C(10)	119.8(6)
C(8)-C(9)-Br(2)	122.2(5)	C(10)-C(9)-Br(2)	117.9(5)
C(11)-C(10)-C(9)	119.9(6)	O(2)-C(11)-C(10)	122.7(5)
O(2)-C(11)-C(6)	117.3(5)	C(10)-C(11)-C(6)	120.0(5)
C(13)-C(12)-Ru(1)	128.1(5)	C(14)-C(13)-C(18)	119.0(7)
C(14)-C(13)-C(12)	119.8(7)	C(18)-C(13)-C(12)	121.2(6)
C(15)-C(14)-C(13)	119.6(9)	C(16)-C(15)-C(14)	121.0(10)
C(15)-C(16)-C(17)	120.2(9)	C(18)-C(17)-C(16)	120.1(10)
C(17)-C(18)-C(13)	120.0(8)	N(2)-C(19)-N(3)	104.0(5)
N(2)-C(19)-Ru(1)	121.6(4)	N(3)-C(19)-Ru(1)	134.0(4)
C(21)-C(20)-N(3)	107.1(5)	C(20)-C(21)-N(2)	106.8(5)
C(23)-C(22)-C(27)	123.3(6)	C(23)-C(22)-N(3)	119.3(6)
C(27)-C(22)-N(3)	117.3(6)	C(22)-C(23)-C(24)	117.2(7)
C(22)-C(23)-C(28)	121.0(6)	C(24)-C(23)-C(28)	121.8(7)
C(25)-C(24)-C(23)	122.1(7)	C(24)-C(25)-C(26)	119.3(7)
C(24)-C(25)-C(29)	121.1(8)	C(26)-C(25)-C(29)	119.6(8)
C(25)-C(26)-C(27)	121.4(7)	C(22)-C(27)-C(26)	116.7(7)
C(22)-C(27)-C(30)	123.2(6)	C(26)-C(27)-C(30)	120.1(7)
C(32)-C(31)-C(36)	122.4(6)	C(32)-C(31)-N(2)	119.1(5)
C(36)-C(31)-N(2)	118.5(6)	C(31)-C(32)-C(33)	117.5(6)
C(31)-C(32)-C(37)	121.6(6)	C(33)-C(32)-C(37)	120.9(7)
C(34)-C(33)-C(32)	122.1(7)	C(33)-C(34)-C(35)	118.4(6)
C(33)-C(34)-C(38)	119.8(7)	C(35)-C(34)-C(38)	121.7(7)
C(34)-C(35)-C(36)	122.6(6)	C(35)-C(36)-C(31)	116.9(6)
C(35)-C(36)-C(39)	120.1(6)	C(31)-C(36)-C(39)	122.8(6)

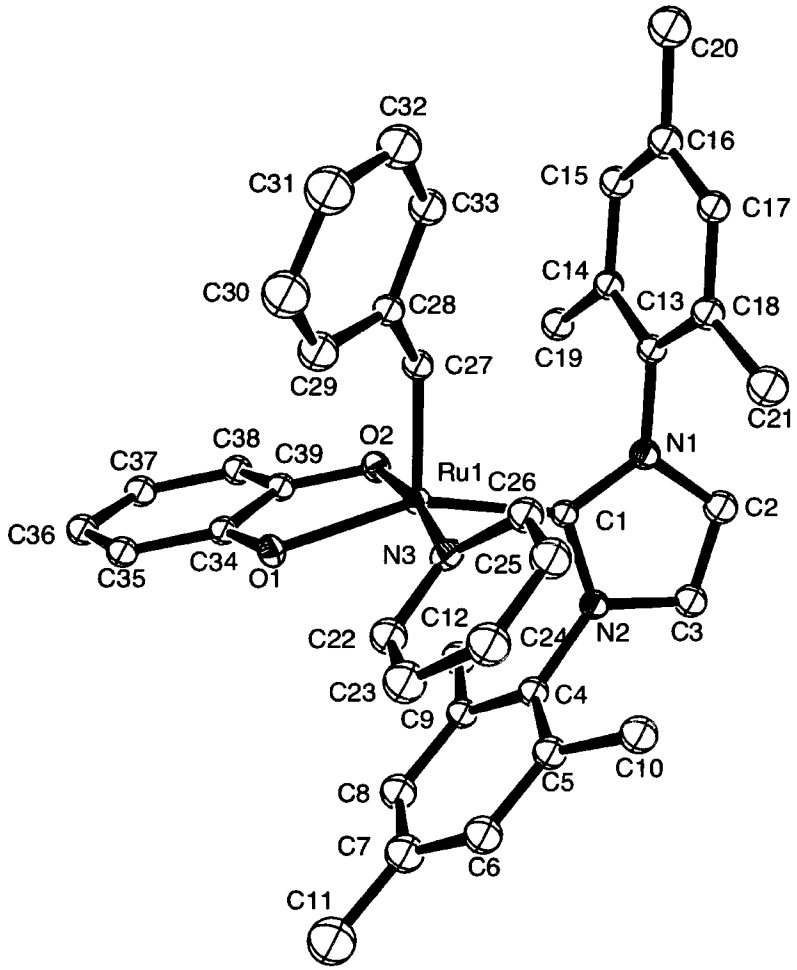

Figure A-3. ORTEP representation of **Ru-9a**. Thermal ellipsoids are shown at 30% probability. Hydrogen atoms are omitted for clarity.

Table A-56. Crystal data and structure refinement for **Ru-9a**.

Formula	$C_{39}H_{38}BrN_3O_2Ru$	
Formula weight	761.7	
Size	0.2 × 0.11 × 0.07 mm	
Crystal morphology	Dark green prism	
Temperature	173(2) K	
Wavelength	0.71073 Å	
Crystal system	Monoclinic	
Space group	$P2_1$	
Unit cell dimensions	a = 9.1238(12) Å	$\alpha = 90°$
	b = 17.399(2) Å	$\beta = 98.714(4)°$
	c = 11.2246(14) Å	$\gamma = 90°$
Volume	1761.3(4) Å^3	
Z	2	
Density (calculated)	1.436 mg/m^3	
Absorption coefficient	1.617 mm^{-1}	
F(000)	776	
Data collection range	$1.84 \le \theta \le 27.16°$	
Index ranges	$-11 \le h \le 11$, $-14 \le k \le 22$, $-13 \le l \le 14$	
Reflections collected	9441	
Independent reflections	5782 [R(int) = 0.0223]	
Observed reflections	5424 [$I > 2\sigma(I)$]	
Absorption correction	multi-scan	
Max. and min. transmission	0.8952 and 0.7381	
Refinement method	Full	
Data / restraints / parameters	5782 / 1 / 216	
Goodness of fit	0.741	
Final R indices [$I > 2\sigma(I)$]	R_1 = 0.0371, wR_2 = 0.0929	
R indices (all data)	R_1 = 0.0408, wR_2 = 0.0968	
Largest diff. peak and hole	0.848 and -0.56 e Å^{-3}	

Table A-57. Interatomic distances (Å) with s.u.s in parentheses.

Ru(1)-C(27)	1.843(4)	Ru(1)-O(1)	2.014(3)
Ru(1)-O(2)	2.053(3)	Ru(1)-C(1)	2.056(4)
Ru(1)-N(3)	2.082(4)	Br(1)-C(25)	1.907(6)
O(1)-C(34)	1.367(5)	O(2)-C(39)	1.337(5)
N(1)-C(1)	1.362(6)	N(1)-C(2)	1.377(6)
N(1)-C(13)	1.445(6)	N(2)-C(1)	1.364(5)
N(2)-C(3)	1.401(6)	N(2)-C(4)	1.442(6)
N(3)-C(22)	1.348(7)	N(3)-C(26)	1.354(6)
C(2)-C(3)	1.344(7)	C(4)-C(5)	1.394(7)
C(4)-C(9)	1.417(6)	C(5)-C(6)	1.393(8)
C(5)-C(10)	1.510(7)	C(6)-C(7)	1.396(7)
C(7)-C(8)	1.388(8)	C(7)-C(11)	1.514(10)
C(8)-C(9)	1.400(7)	C(9)-C(12)	1.498(7)
C(13)-C(18)	1.401(6)	C(13)-C(14)	1.404(6)
C(14)-C(15)	1.404(7)	C(14)-C(19)	1.503(6)
C(15)-C(16)	1.394(7)	C(16)-C(17)	1.399(7)
C(16)-C(20)	1.516(8)	C(17)-C(18)	1.393(7)
C(18)-C(21)	1.514(7)	C(22)-C(23)	1.379(8)
C(23)-C(24)	1.373(8)	C(24)-C(25)	1.384(9)
C(25)-C(26)	1.380(8)	C(27)-C(28)	1.471(6)
C(28)-C(29)	1.387(7)	C(28)-C(33)	1.408(6)
C(29)-C(30)	1.380(9)	C(30)-C(31)	1.388(10)
C(31)-C(32)	1.356(9)	C(32)-C(33)	1.421(8)
C(34)-C(35)	1.394(6)	C(34)-C(39)	1.423(6)
C(35)-C(36)	1.414(7)	C(36)-C(37)	1.375(7)
C(37)-C(38)	1.395(6)	C(38)-C(39)	1.408(6)

Table A-58. Angles (°) between interatomic vectors with s.u.s in parentheses.

C(27)-Ru(1)-O(1)	108.15(16)	C(27)-Ru(1)-O(2)	90.71(17)
O(1)-Ru(1)-O(2)	82.57(13)	C(27)-Ru(1)-C(1)	98.33(17)
O(1)-Ru(1)-C(1)	152.60(14)	O(2)-Ru(1)-C(1)	90.33(15)
C(27)-Ru(1)-N(3)	95.27(18)	O(1)-Ru(1)-N(3)	90.60(14)
O(2)-Ru(1)-N(3)	172.06(14)	C(1)-Ru(1)-N(3)	93.95(16)
C(34)-O(1)-Ru(1)	111.5(3)	C(39)-O(2)-Ru(1)	110.2(3)
C(1)-N(1)-C(2)	111.1(4)	C(1)-N(1)-C(13)	125.9(4)
C(2)-N(1)-C(13)	122.9(4)	C(1)-N(2)-C(3)	111.6(4)
C(1)-N(2)-C(4)	121.2(3)	C(3)-N(2)-C(4)	126.9(4)
C(22)-N(3)-C(26)	117.2(4)	C(22)-N(3)-Ru(1)	119.5(3)
C(26)-N(3)-Ru(1)	123.3(3)	N(1)-C(1)-N(2)	103.8(3)
N(1)-C(1)-Ru(1)	138.8(3)	N(2)-C(1)-Ru(1)	117.2(3)
C(3)-C(2)-N(1)	108.1(4)	C(2)-C(3)-N(2)	105.4(4)
C(5)-C(4)-C(9)	122.8(4)	C(5)-C(4)-N(2)	117.8(4)
C(9)-C(4)-N(2)	119.4(4)	C(4)-C(5)-C(6)	117.9(4)
C(4)-C(5)-C(10)	121.8(5)	C(6)-C(5)-C(10)	120.3(5)
C(7)-C(6)-C(5)	121.9(5)	C(6)-C(7)-C(8)	118.1(5)
C(6)-C(7)-C(11)	120.0(6)	C(8)-C(7)-C(11)	121.9(6)
C(7)-C(8)-C(9)	123.4(5)	C(8)-C(9)-C(4)	115.7(4)
C(8)-C(9)-C(12)	122.7(4)	C(4)-C(9)-C(12)	121.6(4)
C(18)-C(13)-C(14)	121.9(4)	C(18)-C(13)-N(1)	119.9(4)
C(14)-C(13)-N(1)	118.1(4)	C(15)-C(14)-C(13)	117.9(4)
C(15)-C(14)-C(19)	121.1(4)	C(13)-C(14)-C(19)	121.0(4)
C(16)-C(15)-C(14)	121.2(5)	C(15)-C(16)-C(17)	119.3(5)
C(15)-C(16)-C(20)	120.2(5)	C(17)-C(16)-C(20)	120.5(5)
C(18)-C(17)-C(16)	121.1(4)	C(17)-C(18)-C(13)	118.4(4)
C(17)-C(18)-C(21)	120.5(4)	C(13)-C(18)-C(21)	121.1(4)
N(3)-C(22)-C(23)	122.8(5)	C(22)-C(23)-C(24)	120.2(6)
C(23)-C(24)-C(25)	117.3(6)	C(26)-C(25)-C(24)	120.6(5)
C(26)-C(25)-Br(1)	118.5(4)	C(24)-C(25)-Br(1)	121.0(5)
N(3)-C(26)-C(25)	121.9(5)	C(28)-C(27)-Ru(1)	130.2(3)
C(29)-C(28)-C(33)	117.9(4)	C(29)-C(28)-C(27)	122.9(4)
C(33)-C(28)-C(27)	119.1(4)	C(30)-C(29)-C(28)	122.1(6)
C(29)-C(30)-C(31)	119.1(7)	C(32)-C(31)-C(30)	121.2(7)
C(31)-C(32)-C(33)	119.9(6)	C(28)-C(33)-C(32)	119.7(5)
O(1)-C(34)-C(35)	123.1(4)	O(1)-C(34)-C(39)	116.7(3)
C(35)-C(34)-C(39)	120.3(4)	C(34)-C(35)-C(36)	119.3(4)
C(37)-C(36)-C(35)	120.8(4)	C(36)-C(37)-C(38)	120.5(4)
C(37)-C(38)-C(39)	120.2(4)	O(2)-C(39)-C(38)	122.1(4)
O(2)-C(39)-C(34)	118.9(4)	C(38)-C(39)-C(34)	118.9(4)

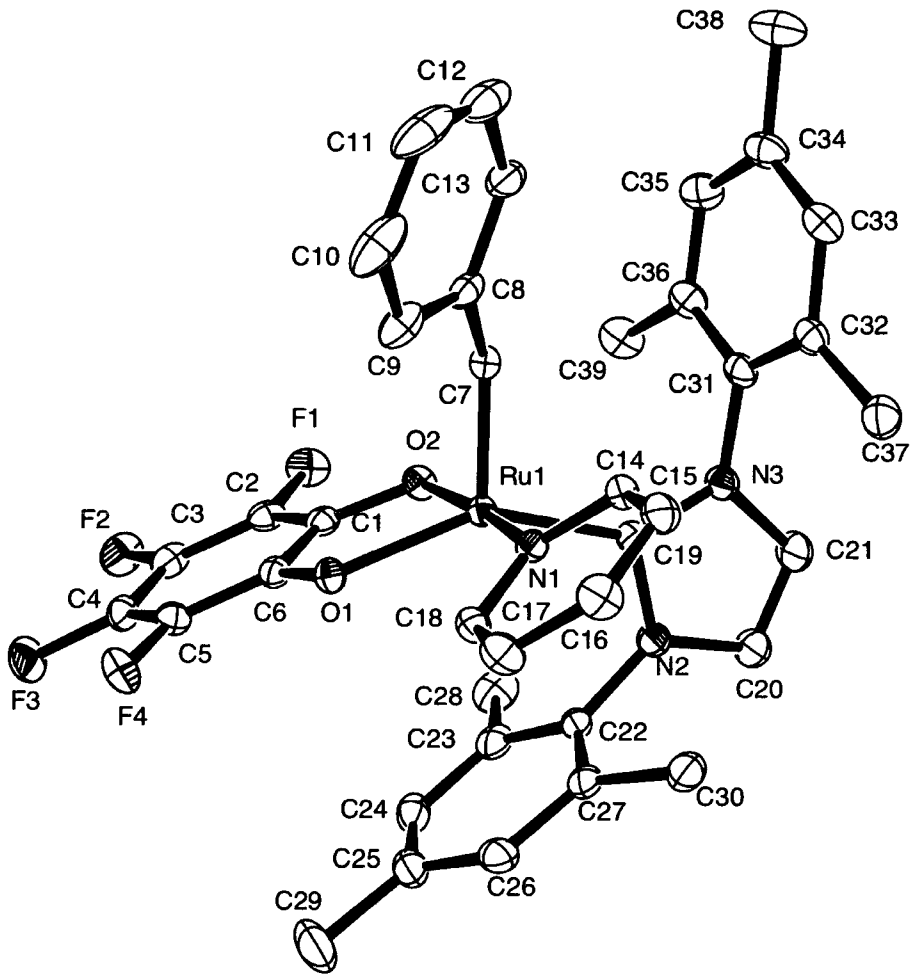

Figure A-4. ORTEP representation of **Ru-9b**. Thermal ellipsoids are shown at 30% probability. Hydrogen atoms are omitted for clarity.

Table A-59. Crystal data and structure refinement for **Ru-9b**.

Formula	$C_{39}H_{35}F_4N_3O_2Ru$	
Formula weight	754.77	
Size	0.35 × 0.22 × 0.21 mm	
Crystal morphology	Orange Prism	
Temperature	173(2) K	
Wavelength	0.71073 Å	
Crystal system	Monoclinic	
Space group	$P2_1/c$	
Unit cell dimensions	a = 8.1640(10) Å	α = 90°
	b = 20.642(3) Å	β = 93.364(4)°
	c = 20.137(3) Å	γ = 90°
Volume	3387.6(7) Å^3	
Z	4	
Density (calculated)	1.48 mg/m^3	
Absorption coefficient	0.524 mm^{-1}	
F(000)	1544	
Data collection range	$1.41 \le \theta \le 27.12°$	
Index ranges	$-7 \le h \le 10$, $-26 \le k \le 25$, $-25 \le l \le 25$	
Reflections collected	24086	
Independent reflections	7450 [R(int) = 0.0311]	
Observed reflections	6168 [$I > 2\sigma(I)$]	
Absorption correction	multi-scan	
Max. and min. transmission	0.8979 and 0.8378	
Refinement method	Full	
Data / restraints / parameters	7450 / 0 / 448	
Goodness of fit	1.027	
Final R indices [$I > 2\sigma(I)$]	R_1 = 0.0314, wR_2 = 0.0722	
R indices (all data)	R_1 = 0.0426, wR_2 = 0.0767	
Largest diff. peak and hole	0.495 and -0.68 e Å^{-3}	

Table A-60. Interatomic distances (Å) with s.u.s in parentheses.

Ru(1)-C(7)	1.831(2)	Ru(1)-O(1)	2.0145(14)
Ru(1)-C(19)	2.031(2)	Ru(1)-O(2)	2.0742(15)
Ru(1)-N(1)	2.0752(17)	F(1)-C(2)	1.368(3)
F(2)-C(3)	1.365(3)	F(3)-C(4)	1.361(3)
F(4)-C(5)	1.360(3)	O(1)-C(6)	1.341(3)
O(2)-C(1)	1.327(3)	N(1)-C(18)	1.349(3)
N(1)-C(14)	1.351(3)	N(2)-C(19)	1.359(3)
N(2)-C(20)	1.392(3)	N(2)-C(22)	1.451(3)
N(3)-C(19)	1.364(3)	N(3)-C(21)	1.394(3)
N(3)-C(31)	1.442(3)	C(1)-C(2)	1.390(3)
C(1)-C(6)	1.416(3)	C(2)-C(3)	1.379(3)
C(3)-C(4)	1.370(4)	C(4)-C(5)	1.384(3)
C(5)-C(6)	1.391(3)	C(7)-C(8)	1.474(3)
C(8)-C(9)	1.397(3)	C(8)-C(13)	1.399(3)
C(9)-C(10)	1.398(4)	C(10)-C(11)	1.379(5)
C(11)-C(12)	1.359(5)	C(12)-C(13)	1.379(4)
C(14)-C(15)	1.378(3)	C(15)-C(16)	1.374(3)
C(16)-C(17)	1.387(3)	C(17)-C(18)	1.381(3)
C(20)-C(21)	1.339(3)	C(22)-C(27)	1.392(3)
C(22)-C(23)	1.402(3)	C(23)-C(24)	1.396(3)
C(23)-C(28)	1.503(4)	C(24)-C(25)	1.378(4)
C(25)-C(26)	1.389(4)	C(25)-C(29)	1.520(4)
C(26)-C(27)	1.395(3)	C(27)-C(30)	1.506(3)
C(31)-C(32)	1.389(3)	C(31)-C(36)	1.399(3)
C(32)-C(33)	1.396(3)	C(32)-C(37)	1.511(3)
C(33)-C(34)	1.382(4)	C(34)-C(35)	1.384(4)
C(34)-C(38)	1.513(3)	C(35)-C(36)	1.387(3)
C(36)-C(39)	1.510(3)		

Table A-61. Angles (°) between interatomic vectors with s.u.s in parentheses.

C(7)-Ru(1)-O(1)	112.83(8)	C(7)-Ru(1)-C(19)	100.92(9)
O(1)-Ru(1)-C(19)	145.43(7)	C(7)-Ru(1)-O(2)	87.70(8)
O(1)-Ru(1)-O(2)	82.28(6)	C(19)-Ru(1)-O(2)	92.13(7)
C(7)-Ru(1)-N(1)	93.72(8)	O(1)-Ru(1)-N(1)	92.01(6)
C(19)-Ru(1)-N(1)	93.10(8)	O(2)-Ru(1)-N(1)	174.22(6)
C(6)-O(1)-Ru(1)	111.01(13)	C(1)-O(2)-Ru(1)	109.53(13)
C(18)-N(1)-C(14)	117.41(18)	C(18)-N(1)-Ru(1)	120.07(14)
C(14)-N(1)-Ru(1)	122.50(14)	C(19)-N(2)-C(20)	111.72(18)
C(19)-N(2)-C(22)	119.93(17)	C(20)-N(2)-C(22)	128.32(19)
C(19)-N(3)-C(21)	110.80(19)	C(19)-N(3)-C(31)	124.11(18)
C(21)-N(3)-C(31)	124.87(19)	O(2)-C(1)-C(2)	123.1(2)
O(2)-C(1)-C(6)	118.65(19)	C(2)-C(1)-C(6)	118.2(2)
F(1)-C(2)-C(3)	118.8(2)	F(1)-C(2)-C(1)	119.3(2)
C(3)-C(2)-C(1)	122.0(2)	F(2)-C(3)-C(4)	119.8(2)
F(2)-C(3)-C(2)	120.3(2)	C(4)-C(3)-C(2)	119.8(2)
F(3)-C(4)-C(3)	120.1(2)	F(3)-C(4)-C(5)	120.2(2)
C(3)-C(4)-C(5)	119.7(2)	F(4)-C(5)-C(4)	119.0(2)
F(4)-C(5)-C(6)	119.4(2)	C(4)-C(5)-C(6)	121.6(2)
O(1)-C(6)-C(5)	123.0(2)	O(1)-C(6)-C(1)	118.36(18)
C(5)-C(6)-C(1)	118.6(2)	C(8)-C(7)-Ru(1)	130.85(17)
C(9)-C(8)-C(13)	118.3(2)	C(9)-C(8)-C(7)	122.6(2)
C(13)-C(8)-C(7)	118.9(2)	C(8)-C(9)-C(10)	119.6(3)
C(11)-C(10)-C(9)	120.6(3)	C(12)-C(11)-C(10)	119.9(3)
C(11)-C(12)-C(13)	120.7(3)	C(12)-C(13)-C(8)	120.9(3)
N(1)-C(14)-C(15)	123.0(2)	C(16)-C(15)-C(14)	119.4(2)
C(15)-C(16)-C(17)	118.3(2)	C(18)-C(17)-C(16)	119.7(2)
N(1)-C(18)-C(17)	122.2(2)	N(2)-C(19)-N(3)	103.89(18)
N(2)-C(19)-Ru(1)	115.22(14)	N(3)-C(19)-Ru(1)	140.71(16)
C(21)-C(20)-N(2)	106.3(2)	C(20)-C(21)-N(3)	107.3(2)
C(27)-C(22)-C(23)	122.5(2)	C(27)-C(22)-N(2)	118.5(2)
C(23)-C(22)-N(2)	118.9(2)	C(24)-C(23)-C(22)	116.8(2)
C(24)-C(23)-C(28)	121.1(2)	C(22)-C(23)-C(28)	122.0(2)
C(25)-C(24)-C(23)	122.4(2)	C(24)-C(25)-C(26)	118.8(2)
C(24)-C(25)-C(29)	121.4(3)	C(26)-C(25)-C(29)	119.8(3)
C(25)-C(26)-C(27)	121.6(3)	C(22)-C(27)-C(26)	117.6(2)
C(22)-C(27)-C(30)	122.1(2)	C(26)-C(27)-C(30)	120.2(2)
C(32)-C(31)-C(36)	122.4(2)	C(32)-C(31)-N(3)	118.7(2)
C(36)-C(31)-N(3)	118.9(2)	C(31)-C(32)-C(33)	117.7(2)
C(31)-C(32)-C(37)	122.2(2)	C(33)-C(32)-C(37)	120.0(2)
C(34)-C(33)-C(32)	121.7(2)	C(33)-C(34)-C(35)	118.6(2)
C(33)-C(34)-C(38)	120.0(2)	C(35)-C(34)-C(38)	121.4(3)
C(34)-C(35)-C(36)	122.3(2)	C(35)-C(36)-C(31)	117.2(2)
C(35)-C(36)-C(39)	121.4(2)	C(31)-C(36)-C(39)	121.4(2)

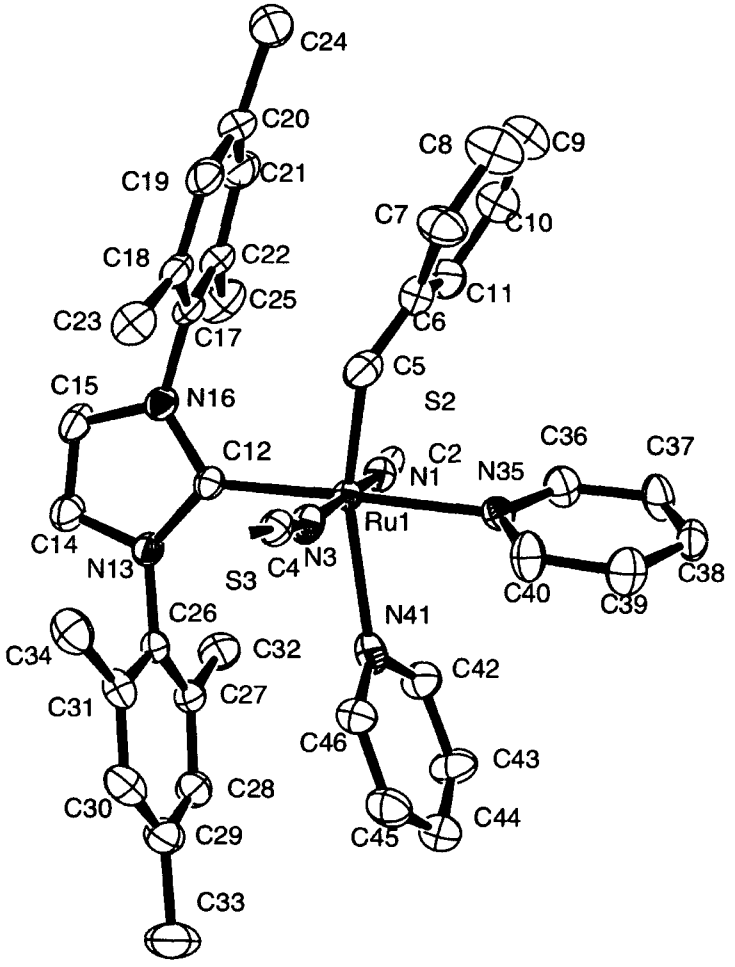

Figure A-5. ORTEP representation of **Ru-12a**. Thermal ellipsoids are shown at 30% probability. Hydrogen atoms and THF solvate are omitted for clarity. The crystals were grown by Jay Conrad.

Table A-62. Crystal data and structure refinement for **Ru-12a**.

CCDC #	791245	
Formula	$C_{42}H_{44}N_6O_{0.5}S_2Ru$	
Formula weight	806.02	
Size	0.40 × 0.20 × 0.08 mm	
Crystal morphology	Green blocks	
Temperature	208(2) K	
Wavelength	0.71073 Å	
Crystal system	Monoclinic	
Space group	C2/c	
Unit cell dimensions	a = 35.989(4) Å	α= 90°
	b = 10.5410(10) Å	β= 118.082(2)°
	c = 24.085(3) Å	γ = 90°
Volume	8061.2(15) Å^3	
Z	8	
Density (calculated)	1.328 mg/m^3	
Absorption coefficient	0.531 mm^{-1}	
F(000)	3344	
Data collection range	1.28 ≤ θ ≤ 26.37°	
Index ranges	-44 ≤ h ≤ 44, -13 ≤ k ≤ 13, -19 ≤ l ≤ 29	
Reflections collected	18700	
Independent reflections	8200 [R(int) = 0.0729]	
Observed reflections	5040	
Absorption correction	Semi-empirical from equivalents	
Max. and min. transmission	1.0 and 0.76	
Refinement method	Full	
Data / restraints / parameters	8200 / 9 / 467	
Goodness of fit	1.029	
Final R indices [I>2σ(I)]	R_1 = 0.0633, wR_2 = 0.1268	
R indices (all data)	R_1 = 0.1175, wR_2 = 0.1437	
Largest diff. peak and hole	0.689 and -0.653 e Å^{-3}	

Table A-63. Interatomic distances (Å) with s.u.s in parentheses.

Ru(1)-C(5)	1.901(6)	C(27)-C(32)	1.487(7)
Ru(1)-N(1)	2.042(4)	C(28)-C(29)	1.381(8)
Ru(1)-N(3)	2.050(4)	C(29)-C(30)	1.385(8)
Ru(1)-C(12)	2.068(4)	C(29)-C(33)	1.520(8)
Ru(1)-N(35)	2.191(4)	C(30)-C(31)	1.389(7)
Ru(1)-N(41)	2.331(4)	C(31)-C(34)	1.516(7)
N(1)-C(2)	1.161(6)	N(35)-C(36)	1.323(6)
C(2)-S(2)	1.631(5)	N(35)-C(40)	1.328(6)
N(3)-C(4)	1.156(6)	C(36)-C(37)	1.388(7)
C(4)-S(3)	1.627(5)	C(37)-C(38)	1.341(7)
C(5)-C(6)	1.357(8)	C(38)-C(39)	1.376(7)
C(6)-C(11)	1.357(8)	C(39)-C(40)	1.398(7)
C(6)-C(7)	1.463(8)	N(41)-C(46)	1.334(6)
C(7)-C(8)	1.342(9)	N(41)-C(42)	1.339(6)
C(8)-C(9)	1.351(9)	C(42)-C(43)	1.371(7)
C(9)-C(10)	1.379(9)	C(43)-C(44)	1.365(8)
C(10)-C(11)	1.388(8)	C(44)-C(45)	1.392(8)
C(12)-N(13)	1.362(6)	C(45)-C(46)	1.378(7)
C(12)-N(16)	1.390(6)	O(47)-O(47)#1	0.77(3)
N(13)-C(14)	1.375(6)	O(47)-C(51)#1	1.01(2)
N(13)-C(26)	1.440(6)	O(47)-C(48)	1.474(16)
C(14)-C(15)	1.324(7)	O(47)-C(51)	1.479(18)
C(15)-N(16)	1.376(6)	C(48)-C(51)#1	0.69(2)
N(16)-C(17)	1.444(6)	C(48)-C(50)#1	0.89(2)
C(17)-C(22)	1.368(7)	C(48)-C(49)	1.440(17)
C(17)-C(18)	1.420(6)	C(49)-C(50)#1	0.64(3)
C(18)-C(19)	1.391(7)	C(49)-C(49)#1	1.17(3)
C(18)-C(23)	1.483(7)	C(49)-C(50)	1.50(2)
C(19)-C(20)	1.391(8)	C(49)-C(51)#1	1.95(2)
C(20)-C(21)	1.385(8)	C(50)-C(49)#1	0.64(3)
C(20)-C(24)	1.502(9)	C(50)-C(48)#1	0.89(2)
C(20)-C(24B)	1.562(14)	C(50)-C(51)	1.464(18)
C(21)-C(22)	1.383(8)	C(50)-C(50)#1	1.87(4)
C(22)-C(25)	1.508(7)	C(51)-C(48)#1	0.69(2)
C(26)-C(31)	1.388(7)	C(51)-O(47)#1	1.01(2)
C(26)-C(27)	1.409(7)	C(51)-C(49)#1	1.95(2)
C(27)-C(28)	1.391(7)		

Table A-64. Angles (°) between interatomic vectors with s.u.s in parentheses.

C(5)-Ru(1)-N(1)	97.1(2)	C(17)-C(18)-C(23)	123.9(5)
C(5)-Ru(1)-N(3)	85.7(2)	C(18)-C(19)-C(20)	123.8(6)
N(1)-Ru(1)-N(3)	176.55(16)	C(21)-C(20)-C(19)	117.4(6)
C(5)-Ru(1)-C(12)	96.3(2)	C(21)-C(20)-C(24)	110.3(14)
N(1)-Ru(1)-C(12)	87.32(16)	C(19)-C(20)-C(24)	132.0(14)
N(3)-Ru(1)-C(12)	90.38(17)	C(21)-C(20)-C(24B)	131.6(13)
C(5)-Ru(1)-N(35)	86.15(19)	C(19)-C(20)-C(24B)	110.9(13)
N(1)-Ru(1)-N(35)	90.18(15)	C(24)-C(20)-C(24B)	23.38(16)
N(3)-Ru(1)-N(35)	92.02(15)	C(22)-C(21)-C(20)	122.1(6)
C(12)-Ru(1)-N(35)	176.67(16)	C(17)-C(22)-C(21)	118.3(5)
C(5)-Ru(1)-N(41)	161.54(18)	C(17)-C(22)-C(25)	121.5(5)
N(1)-Ru(1)-N(41)	89.96(15)	C(21)-C(22)-C(25)	120.2(5)
N(3)-Ru(1)-N(41)	87.97(15)	C(31)-C(26)-C(27)	122.3(5)
C(12)-Ru(1)-N(41)	101.03(16)	C(31)-C(26)-N(13)	118.7(5)
N(35)-Ru(1)-N(41)	76.75(14)	C(27)-C(26)-N(13)	118.7(5)
C(2)-N(1)-Ru(1)	173.2(4)	C(28)-C(27)-C(26)	117.1(5)
N(1)-C(2)-S(2)	178.1(5)	C(28)-C(27)-C(32)	121.6(5)
C(4)-N(3)-Ru(1)	170.2(4)	C(26)-C(27)-C(32)	121.2(5)
N(3)-C(4)-S(3)	178.4(5)	C(29)-C(28)-C(27)	121.9(5)
C(6)-C(5)-Ru(1)	138.2(5)	C(28)-C(29)-C(30)	119.1(6)
C(5)-C(6)-C(11)	125.3(6)	C(28)-C(29)-C(33)	120.3(6)
C(5)-C(6)-C(7)	117.0(6)	C(30)-C(29)-C(33)	120.7(6)
C(11)-C(6)-C(7)	117.8(6)	C(29)-C(30)-C(31)	121.8(6)
C(8)-C(7)-C(6)	117.8(6)	C(30)-C(31)-C(26)	117.7(5)
C(7)-C(8)-C(9)	125.3(7)	C(30)-C(31)-C(34)	120.8(5)
C(8)-C(9)-C(10)	116.4(7)	C(26)-C(31)-C(34)	121.6(5)
C(9)-C(10)-C(11)	122.2(7)	C(36)-N(35)-C(40)	116.9(4)
C(6)-C(11)-C(10)	120.5(6)	C(36)-N(35)-Ru(1)	122.2(3)
N(13)-C(12)-N(16)	102.4(4)	C(40)-N(35)-Ru(1)	120.9(3)
N(13)-C(12)-Ru(1)	129.7(3)	N(35)-C(36)-C(37)	123.1(5)
N(16)-C(12)-Ru(1)	127.6(3)	C(38)-C(37)-C(36)	120.2(5)
C(12)-N(13)-C(14)	112.0(4)	C(37)-C(38)-C(39)	118.1(5)
C(12)-N(13)-C(26)	127.9(4)	C(38)-C(39)-C(40)	118.7(5)
C(14)-N(13)-C(26)	119.7(4)	N(35)-C(40)-C(39)	123.1(5)
C(15)-C(14)-N(13)	107.2(5)	C(46)-N(41)-C(42)	116.2(5)
C(14)-C(15)-N(16)	107.5(5)	C(46)-N(41)-Ru(1)	121.5(3)
C(15)-N(16)-C(12)	110.8(4)	C(42)-N(41)-Ru(1)	120.0(4)
C(15)-N(16)-C(17)	120.8(4)	N(41)-C(42)-C(43)	123.5(5)
C(12)-N(16)-C(17)	128.2(4)	C(44)-C(43)-C(42)	120.3(6)
C(22)-C(17)-C(18)	123.3(5)	C(43)-C(44)-C(45)	117.1(6)
C(22)-C(17)-N(16)	119.2(4)	C(46)-C(45)-C(44)	119.2(6)
C(18)-C(17)-N(16)	117.3(5)	N(41)-C(46)-C(45)	123.7(5)
C(19)-C(18)-C(17)	114.9(5)	O(47)#1-O(47)-C(51)#1	113(3)
C(19)-C(18)-C(23)	121.2(5)	O(47)#1-O(47)-C(48)	118(2)

C(51)#1-O(47)-C(48)	23.7(15)	C(48)#1-C(50)-C(51)	18.6(19)
O(47)#1-O(47)-C(51)	39(2)	C(49)#1-C(50)-C(49)	48(3)
C(51)#1-O(47)-C(51)	122(2)	C(48)#1-C(50)-C(49)	124(2)
C(48)-O(47)-C(51)	110.3(14)	C(51)-C(50)-C(49)	105.3(10)
C(51)#1-C(48)-C(50)#1	137(4)	C(49)#1-C(50)-C(50)#1	46(2)
C(51)#1-C(48)-C(49)	130(2)	C(48)#1-C(50)-C(50)#1	112(2)
C(50)#1-C(48)-C(49)	17(2)	C(51)-C(50)-C(50)#1	94.9(9)
C(51)#1-C(48)-O(47)	36(2)	C(49)-C(50)-C(50)#1	18.1(9)
C(50)#1-C(48)-O(47)	118(2)	C(48)#1-C(51)-O(47)#1	120(4)
C(49)-C(48)-O(47)	103.5(11)	C(48)#1-C(51)-C(50)	24(2)
C(50)#1-C(49)-C(49)#1	108(4)	O(47)#1-C(51)-C(50)	110.1(18)
C(50)#1-C(49)-C(48)	23(2)	C(48)#1-C(51)-O(47)	124(2)
C(49)#1-C(49)-C(48)	108.6(17)	O(47)#1-C(51)-O(47)	28.6(19)
C(50)#1-C(49)-C(50)	116(3)	C(50)-C(51)-O(47)	104.2(11)
C(49)#1-C(49)-C(50)	24.0(15)	C(48)#1-C(51)-C(49)#1	34.2(15)
C(48)-C(49)-C(50)	105.9(10)	O(47)#1-C(51)-C(49)#1	96.0(18)
C(50)#1-C(49)-C(51)#1	33.9(18)	C(50)-C(51)-C(49)#1	14.2(11)
C(49)#1-C(49)-C(51)#1	94.7(13)	O(47)-C(51)-C(49)#1	91.3(11)
C(48)-C(49)-C(51)#1	15.5(8)		
C(50)-C(49)-C(51)#1	90.4(11)		
C(49)#1-C(50)-C(48)#1	140(4)		
C(49)#1-C(50)-C(51)	132(3)		

Symmetry transformations used to generate equivalent atoms: #1 -x+1,y,-z+3/2

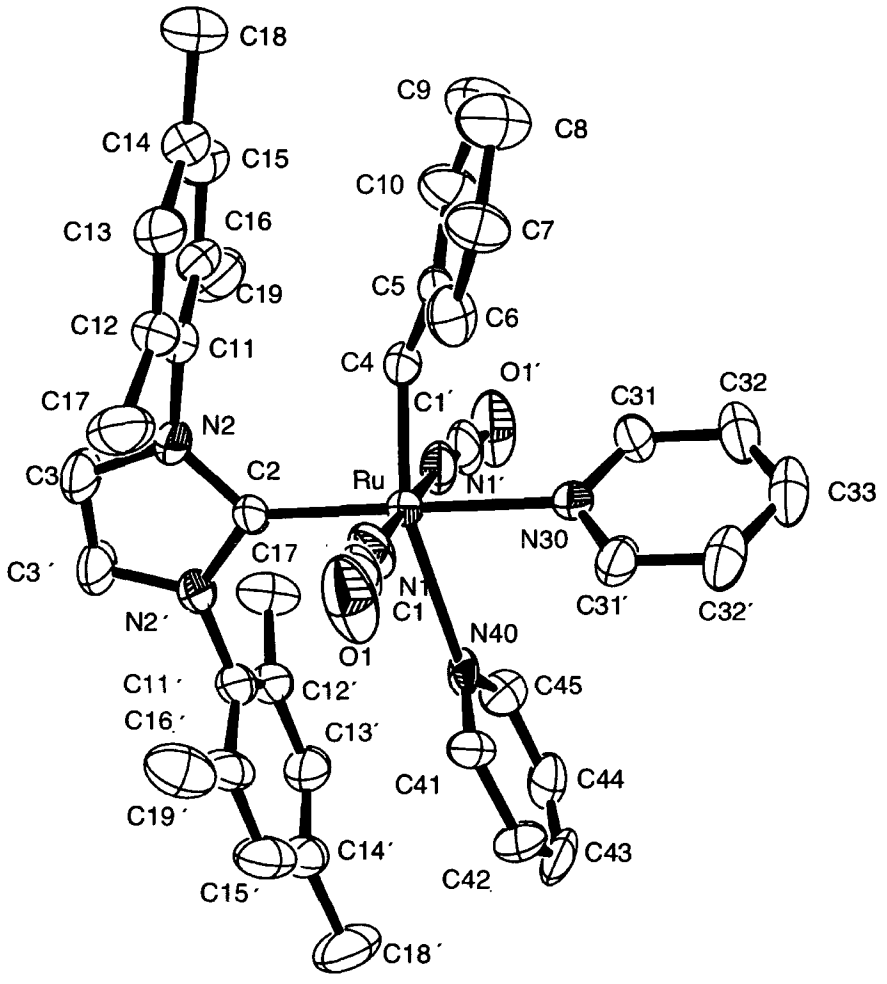

Figure A-6. ORTEP representation of **Ru-12b**. Thermal ellipsoids are shown at 30% probability. Hydrogen atoms are omitted for clarity.

Table A-65. Crystal data and structure refinement for **Ru-12b**.

CCDC #	791246	
Formula	$C_{40}H_{40}N_6O_2Ru$	
Formula weight	737.85	
Size	0.30 × 0.29 × 0.23 mm	
Crystal morphology	Green block	
Temperature	173(2) K	
Wavelength	0.71073 Å	
Crystal system	tetragonal	
Space group	$P4_12_12$ (No. 92)	
Unit cell parameters	a = 9.5752(8) Å	$\alpha = 90°$
	c = 39.106(3) Å	$\gamma = 90°$
Volume	3585.4(5) Å^3	
Z	4	
Density (calculated)	1.367 mg/m^3	
Absorption coefficient	0.481 mm^{-1}	
F(000)	1528	
Data collection range	$4.74° < 2\theta < 40.96°$	
Index ranges	$-11 \le h \le 11, -11 \le k \le 11, -47 \le l \le 47$	
Reflections collected	26313	
Independent reflections	3346 [R(int) = 0.0464]	
Observed reflections	3159 [$F_o^2 \ge 2\sigma(F_o^2)$]	
Absorption correction	Gaussian integration (face-indexed)	
Max. and min. transmission	0.8959–0.8708	
Refinement method	Full	
Data / restraints / parameters	3346 [$F_o^2 \ge -3\sigma(F_o^2)$] / 12 / 288	
Goodness of fit	1.185 [$F_o^2 \ge -3\sigma(F_o^2)$]	
Final R indices	R_1 = 0.0452, wR_2 = 0.1097	
Largest diff. peak and hole	0.917 and –0.507 e Å^{-3}	

Table A-66. Selected interatomic distances (Å) with s.u.s in parentheses.

Atom1-Atom2	Distance	Atom1-Atom2	Distance
Ru-N1	2.034(5)	C6-C7	1.376(11)
Ru-N1'	2.034(5)	C7-C8	1.380(10)
Ru-N30	2.195(5)	C8-C9	1.376(11)
Ru-N40	2.375(12)	C9-C10	1.372(11)
Ru-C2	2.050(6)	C11-C12	1.390(8)
Ru-C4	1.873(10)	C11-C16	1.366(8)
O1-C1	1.227(9)	C12-C13	1.396(7)
N1-C1	1.154(9)	C12-C17	1.509(8)
N2-C2	1.385(5)	C13-C14	1.412(9)
N2-C3	1.372(6)	C14-C15	1.358(9)
N2-C11	1.447(6)	C14-C18	1.532(8)
N2'-C2	1.385(5)	C15-C16	1.396(9)
N30-C31	1.339(6)	C16-C19	1.497(9)
N30-C31'	1.339(6)	C31-C32	1.347(7)
N40-C41	1.351(14)	C32-C33	1.354(7)
N40-C45	1.347(14)	C32-C33'	1.354(7)
C3-C3'	1.323(11)	C41-C42	1.372(12)
C4-C5	1.404(16)	C42-C43	1.365(13)
C5-C6	1.375(11)	C43-C44	1.365(13)
C5-C10	1.380(11)	C44-C45	1.366(12)

Primed atoms are related to unprimed ones via the crystallographic twofold axis ($x, x, {}^{1}/_{2}$).

Table A-67. Selected angles (°) between interatomic vectors with s.u.s in parentheses.

Atom1-Atom2-Atom3	Angle	Atom1-Atom2-Atom3	Angle
N1-Ru-N1'	178.8(3)	C4-C5-C6	120.0(12)
N1-Ru-N30	89.39(13)	C4-C5-C10	116.2(15)
N1-Ru-N40	85.5(3)	C6-C5-C10	123.7(17)
N1-Ru-C2	90.61(13)	C5-C6-C7	113.1(18)
N1-Ru-C4	76.9(4)	C6-C7-C8	125.6(17)
N1'-Ru-N30	89.39(13)	C7-C8-C9	118.6(18)
N1'-Ru-N40	94.2(3)	C8-C9-C10	118(2)
N1'-Ru-C2	90.61(13)	C5-C10-C9	120.6(17)
N1'-Ru-C4	103.0(4)	N2-C11-C12	117.4(5)
N30-Ru-N40	77.6(3)	N2-C11-C16	118.2(6)
N30-Ru-C2	180.0	C12-C11-C16	124.1(5)
N30-Ru-C4	87.9(3)	C11-C12-C13	118.0(6)
N40-Ru-C2	102.4(3)	C11-C12-C17	122.0(5)
N40-Ru-C4	157.4(4)	C13-C12-C17	119.9(6)
C2-Ru-C4	92.1(3)	C12-C13-C14	119.0(7)
Ru-N1-C1	174.0(5)	C13-C14-C15	119.6(6)
C2-N2-C3	113.1(4)	C13-C14-C18	118.3(7)
C2-N2-C11	127.2(4)	C15-C14-C18	122.2(6)
C3-N2-C11	119.6(4)	C14-C15-C16	123.0(7)
Ru-N30-C31	121.2(3)	C11-C16-C15	116.0(7)
Ru-N30-C31'	121.2(3)	C11-C16-C19	122.1(5)
C31-N30-C31'	117.6(6)	C15-C16-C19	121.9(6)
Ru-N40-C41	118.7(8)	N30-C31-C32	121.5(6)
Ru-N40-C45	125.7(11)	C31-C32-C33	121.2(6)
C41-N40-C45	114.9(15)	C32-C33-C32'	116.9(7)
O1-C1-N1	178.8(9)	N40-C41-C42	122.6(16)
Ru-C2-N2	130.0(2)	C41-C42-C43	122(2)
Ru-C2-N2'	130.0(2)	C42-C43-C44	116.0(18)
N2-C2-N2'	99.9(5)	C43-C44-C45	120.6(19)
N2-C3-C3'	106.9(3)	N40-C45-C44	124.1(19)
Ru-C4-C5	132.7(10)		

Primed atoms are related to unprimed ones via the crystallographic twofold axis ($x, x, {}^1/_2$).

List of contributions

Manuscripts published or accepted:

13- Monfette, S.; Blacquiere, J. M.; Fogg, D. E., *Organometallics* **2011**, accepted. (Invited contribution: special issue on the "Future of Organometallic Chemistry").

12- Monfette, S.; Conrad, J. C.; Camm, K. D.; Fogg, D. E., *Poly. Prepr.* **2010**, accepted.

11- Monfette, S.; Eyholzer, M.; Roberge, D. M.; Fogg, D. E., *Chem. Eur. J.* **2010**, *16*, 11720-11725.

10- Monfette, S.; Crane, A. K.; Duarte Silva, J. A.; Facey, G. A.; dos Santos, E. N.; Araujo, M. H.; Fogg, D. E., *Inorg. Chim. Acta* **2010**, *363*, 481-486.

9- Monfette, S.; Fogg, D. E., *Chem. Rev.* **2009**, *109*, 3783–3816.

8- Monfette, S.; Fogg, D. E., Ring-Closing Metathesis in the Synthesis of Medium and Large Rings: Challenges and Implications for Sustainable Synthesis. In *Green Metathesis Chemistry, NATO Science Series II*, Dragutan, V.; Demonceau, A.; Dragutan, I.; Finkelshtein, E. S., Eds. Springer Verlag: 2009.

7- Monfette, S.; Duarte Silva, J. A.; Gorelsky, S. I.; Dalgarno, S. J.; dos Santos, E. N.; Araujo, M. H.; Fogg, D. E., *Can. J. Chem.* **2009**, *87*, 361-367.

6- Monfette, S.; Camm, K. D.; Gorelsky, S. I.; Fogg, D. E., *Organometallics* **2009**, *28*, 944-946.

5- Monfette, S.; Blacquiere, J. M.; Conrad, J. C.; Beach, N. J.; Fogg, D. E., Ru-Aryloxide Catalysts for Olefin Metathesis. In *NATO Sci. Ser. II*, Imamoglu, Y.; Dragutan, V., Eds. Springer Verlag: Berlin, 2007; Vol. 243, pp 79-89.

4- Conrad, J. C.; Eelman, M. D.; Duarte Silva, J. A.; Monfette, S.; Parnas, H. H.; Snelgrove, J. L.; Fogg, D. E., *J. Am. Chem. Soc.* **2007**, *129*, 1024-1025.

3- Monfette, S.; Fogg, D. E., *Organometallics* **2006**, *25*, 1940-1944.

2- Jackson, S.M., Hughes, C.E., Monfette, S., Rosenberg, L., *Inorg. Chim. Acta* **2006**, *359*, 2966-2972.

1- Drouin, S. D.; Monfette, S.; Amoroso, D.; Yap, G. P. A.; Fogg, D. E., *Organometallics* **2005**, *24*, 4721-4728.

Manuscripts in preparation:

A- Monfette, S.; Conrad, J. C.; Gorelsky, S. I.; Moir, J. M.; Hogan, K.; McDonald, R.; Fogg, D. E., Highly-efficient Ru-pseudohalide metathesis catalysts bearing linear $(NCE)^-$ ligands.

B- Monfette, S.; Robinson, M. E.; Payne, P. R.; Fogg, D. E., Kinetic and thermodynamic partitioning of the Ru metathesis catalysts for RCM macrocyclization.

C- Kotyk, M. W.; Monfette, S.; Gorelsky, S. I.; Fogg, D. E., The influence of the neutral and anionic ligands on formation of the metallacyclobutane intermediate, a DFT study.

D- Monfette, S.; Reckling, A. M.; Fogg, D. E., Direct examination of the influence of anionic ligand disposition on metathesis rates. Synthesis of a four-coordinate Ru-catecholate complex.

E- Blacquiere, J. M.; Monfette, S.; Fogg, D. E., High-throughput methods for Ru-catalyzed olefin metathesis: hit or myth?